

Smart Mechanical Ventilators

Citation for published version (APA):

Reinders, J. M. F. (2022). *Smart Mechanical Ventilators: Learning for Monitoring and Control*. [Phd Thesis 1 (Research TU/e / Graduation TU/e), Mechanical Engineering]. Eindhoven University of Technology.

Document status and date:

Published: 02/02/2022

Document Version:

Publisher's PDF, also known as Version of Record (includes final page, issue and volume numbers)

Please check the document version of this publication:

- A submitted manuscript is the version of the article upon submission and before peer-review. There can be important differences between the submitted version and the official published version of record. People interested in the research are advised to contact the author for the final version of the publication, or visit the DOI to the publisher's website.
- The final author version and the galley proof are versions of the publication after peer review.
- The final published version features the final layout of the paper including the volume, issue and page numbers.

[Link to publication](#)

General rights

Copyright and moral rights for the publications made accessible in the public portal are retained by the authors and/or other copyright owners and it is a condition of accessing publications that users recognise and abide by the legal requirements associated with these rights.

- Users may download and print one copy of any publication from the public portal for the purpose of private study or research.
- You may not further distribute the material or use it for any profit-making activity or commercial gain
- You may freely distribute the URL identifying the publication in the public portal.

If the publication is distributed under the terms of Article 25fa of the Dutch Copyright Act, indicated by the "Taverne" license above, please follow below link for the End User Agreement:

www.tue.nl/taverne

Take down policy

If you believe that this document breaches copyright please contact us at:

openaccess@tue.nl

providing details and we will investigate your claim.

Smart Mechanical Ventilators

Learning for Monitoring and Control

Joey Reinders

disc

The author has successfully completed the educational program of the Graduate School of the Dutch Institute of Systems and Control (DISC).



DEMCON



**EINDHOVEN
UNIVERSITY OF
TECHNOLOGY**

This research is supported and funded by DEMCON Advanced Mechatronics, Best, The Netherlands.

A catalogue record is available from the Eindhoven University of Technology Library.
ISBN: 978-90-386-5441-6

Typeset by the author using L^AT_EX

Reproduction: Ipskamp Printing, Enschede, the Netherlands.

©2022 by J.M.F. Reinders. All rights reserved.

Smart Mechanical Ventilators

Learning for Monitoring and Control

PROEFSCHRIFT

ter verkrijging van de graad van doctor aan de
Technische Universiteit Eindhoven, op gezag van de
rector magnificus, prof.dr.ir. F.P.T. Baaijens, voor een
commissie aangewezen door het College voor
Promoties, in het openbaar te verdedigen
op woensdag 2 februari 2022 om 11.00 uur

door

Joey Martinus Franciscus Reinders

geboren te Helden

Dit proefschrift is goedgekeurd door de promotoren en de samenstelling van de promotiecommissie is als volgt:

voorzitter:	prof.dr.ir. W.P.M.H. Heemels
1 ^e promotor:	prof.dr.ir. N. van de Wouw
2 ^e promotor:	prof.dr.ir. T.A.E. Oomen
co-promotor:	dr.ir. B.G.B. Hunnekens (Demcon Advanced Mechatronics)
leden:	prof.dr. D.A.M.P.J. Gommers (Erasmus Medical Center)
	prof.dr. Y. Tan (University of Melbourne)
	prof.dr.ir. P.M.J. Van den Hof

Het onderzoek dat in dit proefschrift wordt beschreven is uitgevoerd in overeenstemming met de TU/e Gedragscode Wetenschapsbeoefening.

Contents

1	Introduction	1
1.1	Background	1
1.2	History of mechanical ventilation	2
1.3	Modern positive pressure ventilation	5
1.4	Challenges in mechanical ventilation	8
1.5	Research goals	10
1.6	Contributions of this thesis	15
1.7	Thesis outline	18
I	Improved control algorithms for ventilation	21
2	Adaptive control for mechanical ventilation for improved pressure support	23
2.1	Introduction	23
2.2	Control problem formulation	26
2.3	Patient-hose dynamics	29
2.4	Adaptive controller design and stability analysis	31
2.5	Simulation case study	38
2.6	Experimental case study	44
2.7	Conclusions and recommendations	51
2.A	Appendix	51
3	Accurate pressure tracking to support mechanically ventilated patients using an estimated nonlinear hose model and delay compensation	53
3.1	Introduction	53
3.2	Problem formulation	56
3.3	Proposed high-level control strategy	57
3.4	Linear closed-loop dynamics	59
3.5	Output delay compensation and linear estimator design	62

3.6	Quadratic hose resistance and estimator	67
3.7	Simulation case study	68
3.8	Experimental case study	71
3.9	Conclusions and future work	78
3.A	Appendix	78
4	Improving mechanical ventilation for patient care through repetitive control	85
4.1	Introduction	85
4.2	Control problem	87
4.3	Repetitive control	89
4.4	Repetitive control applied to mechanical ventilation scenarios	92
4.5	Conclusions	96
5	Linear repetitive control for a nonlinear mechanical ventilation system using feedback linearization	97
5.1	Introduction	97
5.2	Control problem	99
5.3	Nonlinear ventilation system dynamics	101
5.4	Feedback linearization for repetitive control	102
5.5	Simulation results	106
5.6	Experimental results	110
5.7	Conclusions	114
6	Repetitive control for Lur'e-type systems: application to mechanical ventilation	115
6.1	Introduction	115
6.2	Problem statement	117
6.3	Repetitive control of Lur'e-type systems	119
6.4	Application to mechanical ventilation	124
6.5	Conclusion and future work	135
7	Triggered repetitive control: application to mechanically ventilated patients	137
7.1	Introduction	137
7.2	Control problem formulation	139
7.3	Triggered repetitive control framework	143
7.4	Ventilation system and patient effort modeling	147
7.5	Triggered repetitive control applied to mechanical ventilation	152
7.6	Conclusions and future work	159
7.A	Appendix	159

II	Improved monitoring algorithms for ventilation	161
8	Noninvasive breathing effort estimation of mechanically ventilated patients using sparse optimization	163
8.1	Introduction	163
8.2	Patient and breathing effort modeling	165
8.3	Estimation goal	168
8.4	Sparse estimation	171
8.5	Simulation case study	172
8.6	Experimental case study	174
8.7	Conclusions and recommendations	178
9	Automatic patient-ventilator asynchrony detection and classification framework using objective asynchrony definitions	181
9.1	Introduction	181
9.2	PVA detection and classification framework	184
9.3	Patient-ventilator asynchrony definition	185
9.4	Synthetic PVA data generation	190
9.5	Detection and classification model	195
9.6	Performance evaluation	200
9.7	Conclusions and recommendations	209
10	Conclusions and recommendations	211
10.1	Conclusions	211
10.2	Recommendations	214
	Bibliography	219
	Summary	237
	Samenvatting	239
	Dankwoord	243
	List of publications	247
	Curriculum vitae	249

Chapter 1

Introduction

1.1 Background

In recent years, the workload for health workers and the costs of healthcare have increased consistently. Important drivers for the increase in workload are a lack of trained personnel, see Buchan and Aiken (2008); Duffield and O'Brien-Pallas (2003), and the aging Western world's population (Jakob and Rothen, 1997). This increasing workload has negative effects such as, for example, burnouts (Aiken et al., 2002; Holden et al., 2011; Leiter and Maslach, 2005; Portoghese et al., 2014), adverse events related to ventilation (Filho et al., 2011), increased mortality rates (Aiken et al., 2002; Ball et al., 2018; Neuraz et al., 2015; Tarnow-Mordi et al., 2000), increased chance of medication errors (Holden et al., 2011), and increased length of hospital stay (de Magalhães et al., 2017). Therefore, it is vital to reduce the workload in healthcare and therewith reducing costs.

This thesis focuses on improvements of the treatment and reducing the workload related to mechanical ventilation. Mechanical ventilation is a treatment used for patients that are unable to breathe sufficiently on their own. A mechanical ventilator supports or takes over the breathing of a critically ill patient. Especially on the Intensive Care Unit (ICU) ventilation has proven to be a life-saving treatment for many patients. Demand for ventilation has been increasing over the past decades (Needham et al., 2005). Especially during the flu-season or a pandemic, such as the COVID-19 pandemic, demand for mechanical ventilation is very high (Wells et al., 2020). Therefore, improving quality of mechanical ventilation and development of autonomous mechanical ventilators can potentially improve the treatment outcome, decrease the workload in the ICU, and reduce the costs of healthcare.

Modern mechanical ventilators are complex mechatronic systems that are used to support or take over a patient's breathing. Several ventilator manufacturers world-wide

aim at developing the best possible ventilator to assist the clinician. This has resulted in a large variety of ventilation modes, diagnostics tools, and estimated parameters that can aid the clinician's decision making. However, significant improvements can still be achieved by utilizing state-of-the-art techniques from engineering fields, such as, control engineering, system identification, and artificial intelligence.

In this thesis, two different aspects of technological development for ventilators are considered. Both aspects focus on improving the treatment and reducing the workload for the hospital staff. The first part of this thesis aims at improving pressure tracking performance of ventilators by using advanced learning control algorithms. Improved tracking performance ensures that the desired pressure levels are achieved more accurately, and undesired pressure peaks and oscillations are avoided. Therewith, harmful pressure peaks are avoided and the treatment is improved. The second part of this thesis aims at aiding the clinician's decision making by presenting clinically relevant information about the patient or the treatment. This information is retrieved by novel data-driven algorithms. Eventually, these algorithms can be used in the development of closed-loop autonomous ventilators. This results in a reduction of the workload and can potentially improve the treatment as well.

The remainder of this introduction contains a brief history of ventilation in Section 1.2. Thereafter, the ventilation system and modes considered in this thesis are explained in Section 1.3. The challenges in ventilation that are in scope of this thesis are presented and an overall research challenge for ventilation is formulated in Section 1.4. Next, in Section 1.5, the research goals of this thesis are formulated and the literature relevant to these research goals is briefly reviewed. Then, the contributions of this thesis are formulated in Section 1.6. Finally, the outline of the remainder of this thesis is presented in Section 1.7.

1.2 History of mechanical ventilation

Mechanical ventilators use mechanical means to assist or replace a patient's spontaneous breathing. The goal of ventilation is to ensure oxygenation and carbon dioxide elimination (Warner and Patel, 2013). The development of mechanical ventilation has a long history. It started in 1543, when Andreas Vesalius published his book *De Humani Corporis Fabrica* (On the Fabric of the Human Body), which likely contains the first reference to ventilation. In Vesalius (1543), he wrote: "*But that life may be restored to the animal, an opening must be attempted in the trunk of the trachea, into which a tube of reed or cane should be put; you will then blow into this, so that the lung may rise again and take air*". This essentially describes modern-day positive pressure ventilation with an endotracheal tube. However, this was forgotten and not incorporated into medical practice for several centuries.

In the late 19th century, *negative* pressure ventilators were developed. Negative pressure ventilators generate a subatmospheric pressure around the patient's body, causing the lungs to expand and air to flow into the patients. A picture of one of the first

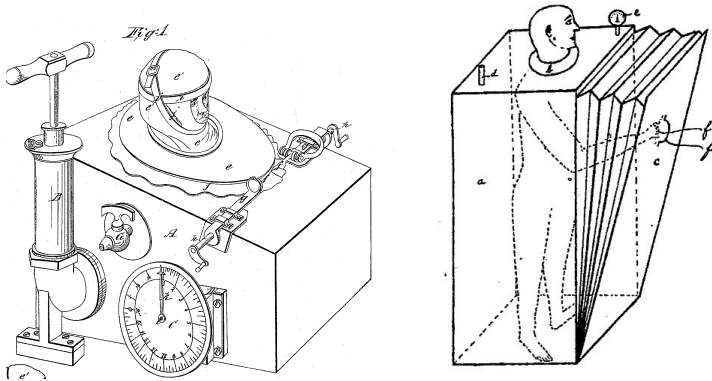
negative pressure ventilators, from Jone (1864), is shown in Fig. 1.1a. In Schwake (1927), a negative pressure ventilator is developed which allows for synchronization of the mechanical assisted breath and the patient's required breath, see Fig. 1.1b. In this ventilator, the patient can manually move the bellow to improve synchronization of the machine and patient breaths. A disadvantage of such ventilators is that proper treatment of the patient by the nursing staff is challenging, since, they cannot access the patient's body. To address this problem the respirator room, as shown in Fig. 1.1c, is proposed in Lord and Lord (1908). In this system, the entire room is pressurized, with the patient's body inside this room. The medical staff can enter the room through a door to tend to the patient. All these designs have their limitations and were not adopted widely.

The first negative pressure ventilator, named the "iron lung", that is adopted widely is proposed in Drinker and Shaw (1929), see Fig. 1.1d. This negative ventilator is first used on a human in 1928 to treat a patient with respiratory failure due to polio. Thereafter, designs with small improvements were developed and employed around the world. With long rows of iron lungs filled hospitals wards at the height of the polio outbreak in the 1940s and 1950s (Slutsky, 2015).

Eventually, the switch to *positive* pressure ventilation was made and the negative pressure ventilators have been replaced rapidly. In positive pressure ventilation an alternating positive pressure pattern is generated near the patient's airway. This alternating pattern results in flow in and out of the lung, which is a substitute for the patient's spontaneous breathing effort or an addition to its spontaneous effort. The main reason for this change is that during the polio pandemic in the 1950s positive pressure ventilation resulted in a significantly lower mortality rate (Lassen, 1953). Furthermore, nursing a patient attached to a positive pressure ventilator is much easier than nursing a patient inside an iron lung.

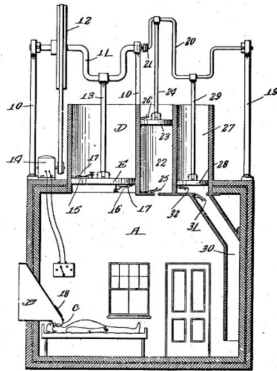
The first positive pressure "ventilators" were typically Non-Invasive Ventilation (NIV) machines. In NIV, the patient is not intubated but the interface between the patient and the ventilator is not invasive, e.g., using a ventilation mask. The first non-invasive positive pressure "ventilator" is introduced by Chaussier in 1780 according to Mushin et al. (1980). This system consisted of a bag, which was manually operated and a mask is used as an interface to the patient. Thereafter, in 1887 a system with bellows and a mask has been introduced by Fell. Then, in 1911 the Dräger Pulmotor has been introduced. This is a more sophisticated pneumatically operated positive pressure device. This device is credited with saving thousands of lives according to Mushin et al. (1980).

The invasive positive pressure ventilators, which are typically used in modern ICUs, became available in the 1940s and 1950s. The first systems are rather limited in functionality compared to modern ventilators. They only allowed volume-controlled modes and patient-triggered ventilation was not available. Typically, these old systems are driven by bellows, a piston, or compressed air. Furthermore, monitoring possibilities were rather limited.

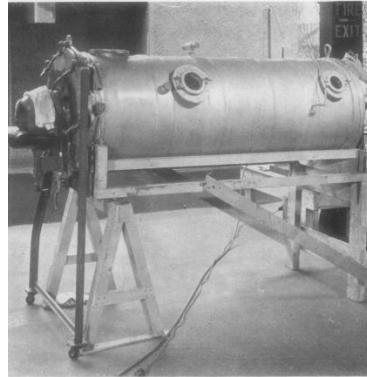


(a) One of the first negative pressure ventilators. Image from: Jones (1864).

(b) Negative pressure ventilator with synchronization. Image from: Schwake (1927).



(c) A respirator room to improve nursing possibilities. Image from: Lord and Lord (1908).



(d) An "iron lung", the first negative pressure ventilator that is widely adopted to treat polio patients. Image from: Drinker and Shaw (1929).

Fig. 1.1. History of various negative pressure ventilators.

The current ICU ventilators made significant steps compared to the first positive pressure systems, an example of a modern ICU ventilator is depicted in Fig. 1.2. One of the most important drivers of this change is the introduction of microprocessors, allowing significantly more monitoring and control possibilities. With extensive innovation and engineering contributions, modern ventilators have a large variety of ventilation modes, ventilation maneuvers, and monitoring possibilities. In the remainder of this thesis, such modern ICU ventilators are considered. More details on this type of ventilation are presented in the following section.



Fig. 1.2. The DemcAir ICU ventilator developed by DEMCON macawi respiratory systems.

1.3 Modern positive pressure ventilation

Nowadays, a variety of positive pressure ventilators and ventilation modes are available. In Section 1.3.1, different types of ventilators are briefly described. Thereafter, different ventilation modes are briefly described in Section 1.3.2. For both the ventilator type and ventilation modes, it is made explicit what is considered in this thesis.

1.3.1 Modern ventilators

Two features are used to distinguish the different types of ventilators. Firstly, a differentiation is made between blower-driven ventilators and ventilators using compressed air. Secondly, a differentiation is made between passive expiration leaks and active expiration valves.

A blower-driven ventilator is using a centrifugal blower to compress ambient air to achieve the desired flow or pressure at the ventilators outlet. Machines using compressed air are connected to an air source, i.e., bottles with compressed air or a wall outlet in the hospital. These ventilators are using valves to achieve the desired pressure or flow. Usually, both types of machines have the ability to include compressed oxygen as well. The compressed oxygen is mixed with air to improve oxygenation. In this thesis, blower-driven ventilators are considered. The main advantage of blower-driven ventilators is that they do not require an external air source. Especially during transportation of patients this saves weight and space.

The second differentiation in ventilation systems are active and passive expiration systems, as depicted schematically in Fig. 1.3a and 1.3b, respectively. In a passive expiration system, exhalation, i.e., flushing of exhaled CO_2 rich air, is done through an intended permanent hole in the hose. In a ventilator with an actively controlled expiration valve, a controlled expiration valve is used to ensure that the exhaled CO_2 -rich air flows out of the system, see Fig. 1.3b. An advantage of the active expiration

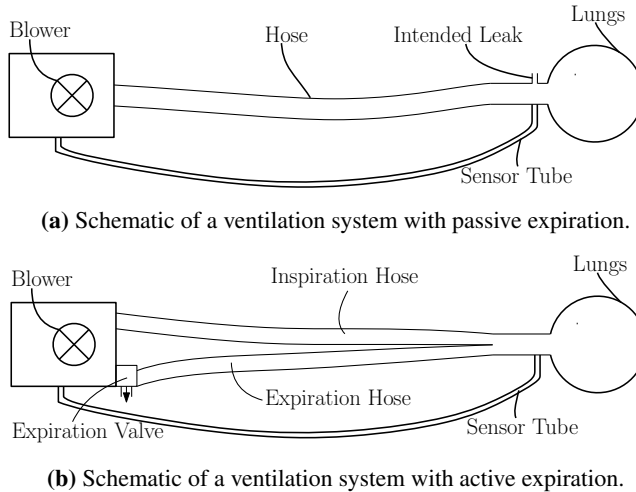


Fig. 1.3. Schematic of a ventilation system with passive expiration and a ventilation system with an actively controlled expiration valve.

system is that less supplemented O_2 is spilled because the expiration branch can be closed. A disadvantage of the active expiration system is that modeling and analysis is significantly more complex, making it less suitable for development. Therefore, a ventilation system with passive expiration is considered throughout this thesis.

1.3.2 Modern modes of ventilation

The ventilators presented in the previous section aim at moving a desired volume of air in and out of the lungs. This can be achieved in different ventilation modes. These modes can be divided into two main categories: pressure-controlled modes and volume-controlled modes. Within these two main categories, various ventilation modes have been developed that achieve a different level of synchronization between the patient and the ventilator. First, both main categories are addressed. Thereafter, the relevant pressure-controlled ventilation modes are summed up.

Pressure-controlled ventilation achieves ventilation by applying a certain desired pressure profile near the patient's airway. This pressure profile results in a flow in and out of the lungs. An example of a pressure-controlled profile and its resulting flow is depicted in Fig. 1.4a. The pressure profile has a Positive End Expiratory Pressure (PEEP), then it builds up to an Inspiratory Positive Airway Pressure (IPAP) to enable air to flow into the lungs.

Volume-controlled ventilation achieves ventilation by forcing a desired volume profile into the patient's lungs. In volume-controlled ventilation a desired flow profile is applied, resulting in a corresponding pressure in front of the patient's mouth. An exam-

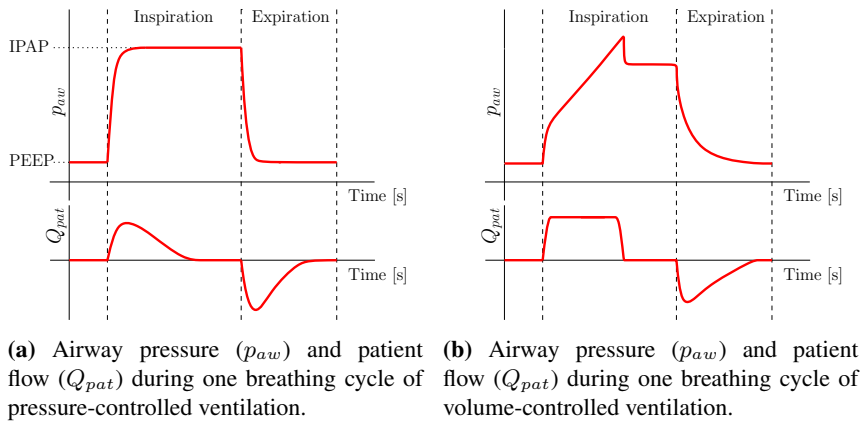


Fig. 1.4. Schematic pressure and flow curves for a pressure and volume-controlled ventilation mode. Showing the airway pressure and the flow into the patient's lungs.

ple of a volume-controlled flow profile and its resulting pressure is depicted in Fig. 1.4b. The figure shows a constant volume flow during inspiration. The required airway pressure increases, since the pressure in the lung increases. When the flow of air stops, we see a drop in the airway pressure, this pressure drop is caused by the resistance of the patient's airway.

Both pressure- and volume-controlled ventilation have advantages and disadvantages. However, there is no consensus on which one is better in general. Typically, it depends on the region, hospital, and hospital staff which mode is preferred.

In both pressure- and volume-controlled ventilation, different modes of ventilation are available. In the past decades an abundance of modes has been developed. These different modes allow a varying level of synchronization between the patient and the ventilator. A synchronized mode aims to respond to the demand of the patient, if a patient starts a breath the ventilator assists the patient. In modes without synchronization, a breath is forced on fixed intervals.

Several relevant ventilation modes are Continuous Mandatory Ventilation (CMV), Pressure Controlled - Assist Control Ventilation (PC-ACV), Pressure Support Ventilation (PSV), and Continuous Positive Airway Pressure (CPAP). All of these ventilation modes allow a different level of synchronization and are used in a different phase of a patient's treatment. Note that naming of ventilation modes throughout literature is inconsistent, i.e., several names are used for one mode. The naming used in this section is adopted throughout this thesis.

Concluding, in this thesis a blower-driven ventilation system with passive expiration, as depicted in Fig. 1.3a, is considered. Furthermore, only pressure-controlled ventilation modes are considered and the exact ventilation mode depends on the specific chapter and use-case. The exact ventilation mode that is considered for every technique

is clearly described in the specific chapter. Note that the presented techniques can be extended, potentially with some minor changes, to different ventilation modes and a ventilation system with an active expiration valve.

1.4 Challenges in mechanical ventilation

In the past decade mechanical ventilation has evolved and improved significantly, saving many lives. However, several open challenges that should be tackled to further improve mechanical ventilation can be identified. In this section, several mechanical ventilation-related challenges are presented and an overall research challenge is formulated. Thereafter, currently available systems that aim to solve this challenge are presented.

Mechanical ventilation has proven to be a life-saving treatment. However, it can also cause damage to a patient's lungs, referred to as Ventilator-Induced Lung Injury (VILI) (Slutsky and Ranieri, 2013). This VILI has many potential causes, a few examples are high pressure peaks, low PEEP, and large tidal volumes. Significant effort has been made in literature to avoid VILI by choosing the optimal ventilator settings, e.g., PEEP and IPAP levels, for example in Amato et al. (2015); Brochard et al. (1998); Determann et al. (2010); Lachmann (1992); Rittayamai and Brochard (2015); Rouby et al. (2002). Because the optimal settings are highly dependent on the patient, the settings that are used in practice are still subject to the specific clinician's expertise.

Ventilation becomes even more challenging in case of partially spontaneously breathing patients. Spontaneous breathing effort of the patient has several benefits; it prevents muscle atrophy, avoids paralysis, and decreases sedation needs (Goligher et al., 2015; Mauri et al., 2017). However, uncontrolled spontaneous effort also has serious disadvantages. Firstly, this spontaneous effort is typically not measured and unknown. When this effort is not taken into account when choosing the ventilator settings this might damage the lungs (Mauri et al., 2017; Yoshida et al., 2012), excessive effort might even damage the diaphragm (Goligher et al., 2015). Secondly, spontaneous effort of the patient may result in asynchrony between the ventilator and the patient. According to Holanda et al. (2018), asynchrony can refer to a mismatch between the patient's demand and the ventilators delivery regarding time, flow, volume, or pressures. According to Thille et al. (2006) up to 24 % and according to Vignaux et al. (2009) up to 43 % of the ventilated patients experience severe levels of asynchrony. According to Blanch et al. (2015); Epstein (2011); Thille et al. (2006), patient-ventilator asynchrony is associated with various negative treatment outcomes, such as prolonged ICU stay and even increased mortality rates.

Other challenges in ventilation are the earlier mentioned shortage of nursing staff and the high costs of a mechanically ventilated patient on the ICU. According to Aiken et al. (2002); Rafferty et al. (2007); Verdon et al. (2008), the shortage in staffing is related to higher mortality rates and burnout rates. Furthermore, the costs of a mechanically ventilated patient on the ICU are very high (Cox et al., 2007; Dasta et al.,

2005).

Considering these challenges, the overall Research Challenge for mechanical ventilation is formulated:

Research Challenge: *Reduce the mechanical ventilation-related workload and costs, while simultaneously improving the treatment for the ventilated patient.*

This Research Challenge requires changes and innovations in different fields of expertise, such as, regulatory affairs, medical innovations, and technological developments. The aim of this thesis, is to tackle the Research Challenge with technological developments. To accomplish the Research Challenge, through technological innovations, a tremendous joint effort of researchers, engineers, and clinicians is required. In the following section, existing approaches towards solving the Research Challenge, with technological developments, are presented. This literature focuses on developing closed-loop ventilation systems.

1.4.1 Closed-loop ventilation systems

Several closed-loop ventilation systems are already available and according to Lellouche and Brochard (2009) the importance of such systems will increase in the future. Such closed-loop ventilation systems automatically adjust ventilation settings using an algorithm to achieve a particular goal, e.g., blood saturation levels. In theory, these algorithms are able to decrease the required number of staff interventions and improve the treatment. Different closed-loop ventilation systems are described in literature; overviews of such systems are presented in Chatburn (2004); Wysocki et al. (2013). These systems typically use measured data, some clinician-set parameters, and algorithms to improve certain aspects of ventilation, e.g., synchrony and/or automate (parts of) ventilation. Next, several commercially available closed-loop ventilation systems are briefly presented.

Proportional Assist Ventilation (PAV) is a ventilation mode for spontaneously breathing patients. The ventilator pressure is generated in proportion to the patient's spontaneous breathing effort (Younes, 2003). A clinical trial in Younes et al. (1992) has shown that PAV is a feasible ventilation mode for spontaneously breathing patients. Furthermore, it can be implemented at lower peak pressures, potentially reducing VILI. According to Grasso and Ranieri (2001), PAV can potentially improve the patient's control over ventilation.

SmartCare is an automated protocol that automatically lowers the ventilatory support with the goal to wean a patient from the ventilator, i.e., lowering the ventilator assist with the goal of detaching the ventilator. SmartCare aims at keeping the patient's spontaneous effort in a certain comfortable zone and gradually lowers the ventilator support. In Lellouche et al. (2006) and Bouadma et al. (2005), it is shown that ventilation, weaning, and ICU time is significantly reduced by the SmartCare automated weaning protocol compared to a standardized weaning protocol executed by a clinician. However, in Rose et al. (2008), SmartCare showed no benefits over weaning conducted by

well-trained ICU staff in a one-to-one patient-to-nurse ratio. However, it is potentially beneficial in settings with lower staffing and training levels.

Adaptive Support Ventilation (ASV) is a ventilation mode that automatically adjust the respiratory rates, tidal volume, and inspiratory time. These settings are adjusted based on the patient's lung mechanics and the spontaneous breathing effort. ASV aims to maintain a operator-set minute volume and determines the ventilator settings based on the minimal work of breathing principle as described in Otis (1954). ASV is successfully used in several studies, e.g., Chen et al. (2011); Gruber et al. (2008); Kirakli et al. (2011); Petter et al. (2003); Tassaux et al. (2002). These studies showed several benefits, such as improved patient-ventilator synchrony, decreased weaning duration, earlier extubation, fewer manual adjustments, and fewer alarms.

Neurally Adjusted Ventilatory Assist (NAVA) is an automated ventilation mode that uses measurements of the electrical activity of the diaphragm using a sensor attached to an esophagus catheter. The information about the diaphragm activity is used to achieve faster triggering and to adjust the level of ventilator assistance. NAVA has been implemented successfully in Kacmarek et al. (2020); Kallio et al. (2015); Liu et al. (2020); Piquilloud et al. (2011); Yonis et al. (2015). These studies show several benefits over conventional ventilation, such as improved patient-ventilator synchrony, reduced sedation levels of the patient, earlier weaning, and shorter ventilation times.

Intellivent-ASV is a closed-loop ventilation system where the clinician has to choose targets for the end tidal CO_2 (the partial pressure of CO_2 at the end of an exhaled breath) and the oxygen saturation in the patient's blood. These values are measured using two additional sensors. The ventilator determines the optimal PEEP level, supplemental O_2 level, and target minute volume using results from literature and the measured data. Then, the ASV algorithm determines the required tidal volume and respiratory rate. Furthermore, Intellivent-ASV has an automated weaning protocol that decreases the ventilators assist if possible. Intellivent-ASV has been successfully implemented in several studies, e.g., Arnal et al. (2013, 2012); Beijers et al. (2014); Fot et al. (2017); Lellouche et al. (2013). These studies show that Intellivent-ASV is safe, uses lower pressures, keeps patient in an optimal ventilation zone, and requires fewer interventions by the hospital staff.

The available closed-loop systems have great potential in reducing the workload and improving the treatment, and therewith (partially) fulfilling the Research Challenge. However, several technological breakthroughs are required to fulfill the Research Challenge. The main challenges in developing such system is to make them insightful, such that the hospital staff knows why the system is making particular choices (Wysocki et al., 2013). This brings us to the first shortcoming of the presented systems. Namely, the available system are not insightful to the hospital staff. In other words, it is hard to deduce why the described systems adjust a particular setting. This insight is essential for acceptance of such systems in practice. The second shortcoming is that the more advanced systems presented in this section require additional sensing which is undesired. Adding additional sensors results in an increased workload, increased costs, and an increased risk of sensor failure. The third shortcoming is that further automation is

required, still clinicians or nurses have to intervene with the presented systems. Ideally, the ventilator requires no human interventions from intubation until extubation of the patient. Using this knowledge, two research goals are defined in the following section to further improve mechanical ventilation and make a significant step toward the Research Challenge.

1.5 Research goals

In the previous section, it is shown that significant steps towards solving the Research Challenge are already being made. However, there is still significant room for improvement. Therefore, in this thesis two research goals are addressed, which are formulated in Section 1.5.1. Thereafter, for both research goals the relevant literature is presented in Section 1.5.2.

1.5.1 Research goals

Based on the Research Challenge, two distinct research goals are addressed in this thesis. Both goals aim to improve ventilator performance and the treatment in a distinct way and are significant steps towards the overall Research Challenge. The first research goal, which is addressed in Part I of this thesis, is formulated as:

Research Goal I: *Improve the pressure tracking performance of mechanical ventilators to avoid pressure peaks and oscillations using self-learning control strategies that achieve superior tracking performance for a wide variety of patients and scenarios.*

Several benefits can be achieved if this research goal is accomplished. First, it can improve the treatment by avoiding overshoot and oscillations in the pressure and flow signals. Such overshoot and oscillations are potentially harmful to the patient's lungs and cause VILI as mentioned in Section 1.4. Furthermore, overshoot and oscillations might introduce auto triggering of the ventilator and therewith introduce patient-ventilator asynchrony. Also, control strategies that achieve superior performance on a wide variety of patients improve consistency of the treatment over varying patients and scenarios.

The second research goal, which is addressed in Part II of this thesis, is formulated as:

Research Goal II: *Improve the monitoring capabilities of mechanical ventilators using the available data and novel algorithms to retrieve real-time information about the patient's clinical condition and the ventilator's performance.*

The second research goal is mainly focused on assisting the hospital staff in choosing the optimal treatment for a specific patient. This helps to improve the treatment, reduce the workload, and reduce the costs. This is achieved by using the measured data to retrieve information about the patient's clinical condition and the ventilator's

performance. The focus of this thesis towards reaching this research goal is twofold, namely:

- (a) estimation of the spontaneous breathing effort and lung mechanics parameters of the patient;
- (b) detection and classification of patient-ventilator asynchrony.

It is envisioned that, in the near future, the retrieved information is presented to the hospital staff such that they can respond accordingly to improve the treatment outcome. Eventually, the retrieved information can be used in autonomous ventilators that use this information to change the ventilator settings automatically without human interventions.

1.5.2 Current state-of-the-art

Both research goals are a step towards fully closed-loop ventilation systems and therefore towards the Research Challenge. In this section, first, a literature review on the current state-of-the-art in achieving Research Goal I is presented. Thereafter, the relevant literature for Research Goal II is presented. The literature on Research Goal II is divided in two separate sections corresponding to the distinct focus areas within Research Goal II of this thesis.

State-of-the-art control strategies for improved tracking performance

The main challenge in control for mechanical ventilation is the wide variety of uncertainties, e.g., patient type, leakages, hose system, and patient effort. This challenge has spurred significant efforts to improve the tracking performance of mechanical ventilators using novel control strategies. An overview of control and modeling methods for mechanical ventilation is presented in Borrello (2005). Since then, a lot of new contributions to control for ventilation have been made that are also included in this section.

In Borrello (2002), a positive feedback loop is added in a flow controller for mechanical ventilation. This results in a system where the output appears to be a constant pressure source. A funnel-based control strategy is developed and applied in Pomprapa et al. (2015). A variable-gain controller is developed and implemented in Hunnekens et al. (2020); Van de Wouw et al. (2018). This variable-gain controller helps to overcome the conflicting goals of fast pressure rise times and limited overshoot. In Chellaboina et al. (2010), a model reference direct adaptive controller framework for a multi-compartmental patient model is developed and implemented. Model Predictive Control (MPC) using the model of Chellaboina et al. (2010) is applied to ventilation in Li and Haddad (2013). This method exploits the ability of MPC to include constraints and the repetitive nature of breathing by combining the method with repetitive control. Another model-based control approach is developed in Scheel et al. (2017). In

this work, a disturbance observer is used to estimate the patient's spontaneous breathing effort, which is then used to improve the control performance. In Borrello (2001) and Borrello (2018), adaptive control strategies are applied to ventilation. Adaptive control strategies adapt the control parameters during operation using measured signals and an update law. Other learning control strategies, that exploit the repetitive nature of breathing, are Iterative Learning Control (ILC) and Repetitive Control (RC). ILC has been applied to mechanical ventilation in De Castro and Tôrres (2019); Scheel et al. (2015); Hazarika and Swarup (2020), showing a significant potential in performance gain.

The presented literature has shown significant improvements in tracking control for mechanical ventilation. However, further improvements are desired to improve the safety, comfort, and accuracy of the treatment. Therefore, improvements in tracking performance for varieties of circumstances are achieved in this thesis by utilizing data-driven control techniques. Contribution I.a - Contribution I.f, presented in Section 1.6, aim at further improving control for mechanical ventilation using data-driven control techniques. Therewith, a significant step towards achieving Research Goal I is made.

State-of-the-art on estimation of breathing effort and lung mechanics

Estimation of lung mechanics parameters and spontaneous breathing effort requires simple and accurate lung and patient effort models. Therefore, different types of models that are developed in literature are addressed first. Thereafter, different estimation approaches of the parameters corresponding to these models are addressed.

A large overview of models for lung mechanics is presented in Bates (2009). The models in this work vary from linear one-compartmental to multi-compartmental models with nonlinear compliances and resistances. Furthermore, in Van Diepen et al. (2021) different patient models are presented that represent different types of clinical conditions, e.g., ARDS and COPD. Besides models of the lung mechanics, different methods to model the patient's spontaneous breathing effort are presented in literature. Most common is a method where the patient's effort is considered to be a disturbance to the pressure inside the lungs, caused by the movement of the diaphragm. This method is used in for example Navajas et al. (2000); Scheel et al. (2017); Vicario et al. (2015). Another method to model a patient's breathing effort is to model the patient's lung compliance as a time-varying parameter. This method is used in Chiew et al. (2015); Kim et al. (2017); Van Drunen et al. (2014).

For sedated patients, considering a particular patient model, parameter estimation is straightforward. In Avanzolini et al. (1997); Borrello (2001) patient parameters are estimated using recursive least squares algorithms. In Schranz et al. (2011), a hierarchical approach to estimate nonlinear patient model parameters is proposed.

When a patient is spontaneously breathing, performance of such algorithms deteriorates because the patient's breathing effort introduces a significant, unknown disturbance which has to be taken into account. Therefore, other approaches to estimate patient parameters and patient effort have been developed. In practice, methods such as

an esophageal pressure measurement or measurements of the Electromyography (EMG) signal of the diaphragm give an indication of the patient's spontaneous breathing effort. However, adding an additional sensor results in an increased workload. Therefore, algorithms to estimate the patient effort have been developed that use the signals that are already available in typical ventilation systems. In Dietz et al. (2003); Navajas et al. (2000), a method to estimate the respiratory parameters of spontaneously breathing patients is proposed. This method uses the assumption that the patient effort is the same over successive breaths. In Maes et al. (2014, 2017), another method to estimate the lung mechanics parameters of a spontaneously breathing patient is developed. In this method, the respiratory system is excited by applying a multisine pressure signal to the patient's airway. Using the measurements, a frequency-based analysis is used to determine the lung characteristics. In Kim et al. (2017), a method is proposed that estimates the patient's effort by considering a negative elasticity component of the lung that represents the patient effort. Another method is proposed in Vicario et al. (2015), this method uses a constraint optimization to obtain the lung parameters and the patient effort. Furthermore, in Scheel et al. (2017), a disturbance observer is used that assumes that the patient effort is a pure sine wave.

The presented estimation algorithms show significant potential in estimation of the patient's lung mechanics parameters and effort. However, all methods use either additional sensing, stringent assumptions on the patient effort, or adapt the excitation signal. Additional sensing is undesired because it increases the workload and is error prone, stringent assumptions on the patient's breathing effort results in unrealistic estimation results, and adaptations of the excitation signal interrupts the ventilation treatment which is undesired. Contribution II.a, presented in Section 1.6, aims at overcoming these shortcomings in the presented literature, which is a significant step towards achieving Research Goal II.

State-of-the-art on detection and classification of patient-ventilator asynchrony

As mentioned, patient-ventilator asynchrony is a major issue in mechanically ventilated patients. According to Colombo et al. (2011) physicians are unable to detect asynchrony accurately based on the measured waveforms. Therefore, researchers have worked on developing algorithms that can detect and classify patient-ventilatory asynchrony related to the timing of the patient's breath and the ventilator assisted breath.

Rule-based algorithms are developed to detect asynchrony in ventilated patients, for example, Adams et al. (2017); Blanch et al. (2012). More specifically, in Adams et al. (2017), parameters such as the tidal volume are used in a manually tuned rule based algorithm to detect different asynchrony types. In Blanch et al. (2012), an ideal expiration curve is compared to the measured expiration curve. If these curves deviate too much, it is concluded that an ineffective patient effort is present.

Besides these coded rule-based algorithms, more advanced algorithms are developed, using machine learning techniques. Several different techniques are used in practice. In Mulqueeney et al. (2009), a Bayes's rule was used to distinguish normal breaths

from ineffective efforts. In Rehm et al. (2018), an ensemble machine learning algorithm is developed that can detect double triggers and breath stacking. In Sottile et al. (2018), several algorithms are tested, such as random forest and Gaussian naive Bayes. In Gholami et al. (2018), a random forest is used to distinguish cycling asynchronies from normal breaths. The algorithms in this paragraph use breath-by-breath features, such as the tidal volume and the respiratory rate, as inputs for the algorithms. This requires a lot of signal processing, which is error-prone. Therefore, algorithms using the measured waveforms directly are presented next.

The use of raw data, instead of features has significant advantages. The first advantage is that it reduces the loss of information between data-acquisition and feeding it into the algorithm. The second advantage is that it reduces the required amount of data pre-processing, which is challenging to implement robustly and might require a lot of computation power and data storage capacity on the ventilator. In Loo et al. (2018), a convolutional neural network is used to distinguish between synchronous and asynchronous breaths. This is achieved by using a convolutional neural network to analyze images of the pressure and flow waveform. Furthermore, in Zhang et al. (2020), an Long Short-Term Memory (LSTM) network is used that uses the raw pressure and flow data from the mechanical ventilator. This algorithm distinguishes ineffective efforts, double triggering, and normal breaths. These algorithms make a significant step forwards in terms of loss of information. However, interpretation of the output of these algorithms remains challenging, i.e., the relation between data and output is a black box model. This makes acceptance by clinicians challenging. Therefore, Pan et al. (2021) developed an algorithm that indicates which part of the waveform is used to classify the breath. In this work, a convolutional neural network is used that gives an indication of the most relevant parts of the waveforms for classification. Another method that gives more insights in the decision is the work of Bakkes et al. (2020). In this work, a modified version of the U-net, from Ronneberger et al. (2015), is used to detect the start times of the patient's and ventilator's inspiration and expiration. These timings are used to determine which type of timing asynchrony is occurring, e.g., delayed triggering or premature cycling.

A challenge of all developed algorithms is gathering accurately labeled data, since manual labeling by a clinician is error-prone. Therefore, in Van Diepen et al. (2021), the algorithm developed in Bakkes et al. (2020) is tested on simulation based data. Using this simulation based data, the ground-truth labels are always correct. In this study, it is shown that the algorithm developed in Bakkes et al. (2020) works on this simulation data as well.

The presented asynchrony detection and classification algorithms show promising results in detection and classification of patient-ventilator asynchrony. However, the following open challenges are identified that, when addressed, will lead to a major breakthrough in patient-ventilator asynchrony detection and classification:

- development of a clear framework that distinguishes the different types of asynchrony;

- the presented algorithms focus on a detecting and/or classifying a limited number of asynchrony types; an algorithm or a combination of algorithms should be able to detect all types of asynchrony;
- the presented algorithms require some form of a data pre-processing step, e.g., extracting features and/or dividing the data in separate breaths; this is error-prone and challenging to implement robustly;
- the ground-truth labeling of real ICU data by clinicians is error-prone and time consuming, which limits the achievable performance of the algorithms.

Contribution II.b, presented in Section 1.6, aims at overcoming these gaps in the presented literature. Therewith, a significant step towards achieving Research Goal II is made.

1.6 Contributions of this thesis

In this section, the contributions of this thesis are summed up. The contributions are divided by the specific research goals that they aim to accomplish. More specifically, the contributions of this thesis that are related to Research Goal I are described in Section 1.6.1. Thereafter, the contributions that are related to Research Goal II are described in Section 1.6.2.

1.6.1 Contributions to Research Goal I

This thesis considers several data-driven control strategies to further improve pressure tracking control in mechanical ventilation. These techniques achieve accurate tracking of the target pressure.

To control the airway pressure accurately, the pressure drop over the hose should be compensated. Using a model of the hose resistance in a feedback loop and estimating its linear resistance parameter led to the first contribution.

Contribution Ia: *An adaptive control strategy using a linear hose model to compensate the pressure drop over the hose, for both fully sedated and spontaneously breathing patients.*

The proposed control strategy in the first contribution led to a significant improvement in tracking performance. However, the assumption that the hose resistance is linear and that the system has no (measurement) delays still limits the actual achievable performance. This insight led to the second contribution of this thesis.

Contribution Ib: *An adaptive control strategy using an estimated non-linear hose model to compensate the pressure drop over the hose, taking into account the measurement delay during estimation, for both fully sedated and spontaneously breathing patients.*

The control strategy in the second contribution has further improved pressure tracking performance in a variety of patients and ventilation modes. However, the tracking performance can be improved even further.

Breathing is a repetitive process, especially in the case of mandatory ventilation of sedated patients. Exploiting this fact, a learning control approach, that learns from errors during previous breaths, has been designed and implemented in ventilation. This led to the third contribution of this thesis.

Contribution I.c: *A linear control strategy designed for and applied to ventilation of fully sedated patients.*

The experimental results achieved with the control strategy of the third contribution led to perfect tracking in a wide variety of patients during continuous mandatory ventilation. Since the stability proof of repetitive control assumes linear models, a feedback linearization technique has been used to formally guarantee stability, this led to the fourth contribution of this thesis.

Contribution I.d: *Feedback linearization to guarantee stability of linear repetitive control applied to fully sedated patients in ventilators with nonlinear hose characteristics.*

This led to perfect tracking with a formal stability guarantee. However, the stability proof relies on exact estimation of the nonlinear hose resistance. Therefore, a repetitive control strategy that guarantees stability of the nonlinear system for a set of nonlinear hose characteristics is developed. This led to the fifth contribution of this thesis.

Contribution I.e: *A repetitive control strategy applied to fully sedated patients with a stability guarantee for a set of nonlinear hose characteristics.*

This contribution led to significantly improved tracking performance with a formal stability guarantee, with significantly better robustness against an estimation error in the nonlinearity of the hose resistance. However, performance of the strategy proposed in the third, fourth, and fifth contribution degrades in ventilation modes for spontaneously breathing patients. Therefore, a learning control strategy that can handle triggering of repetitive tasks on a varying interval has been developed. This led to the sixth contribution of this thesis.

Contribution I.f: *A triggered repetitive control framework is developed and applied to spontaneously breathing patients.*

The developed control framework in the sixth contribution has been applied to spontaneously breathing patients, resulting in a significant improvement in tracking performance compared to existing techniques for spontaneously breathing patients.

Concluding, Contribution I.a - Contribution I.f significantly improve pressure tracking performance in a wide variety of mechanical ventilation scenarios. Therewith, they make a substantial contribution to Research Goal I.

1.6.2 Contributions to Research Goal II

The last two contribution of this thesis focus on assisting the clinician to choose the optimal ventilator settings. This is achieved by using data-driven algorithms that estimate or detect relevant information about the patient and/or the treatment.

From Section 1.5.2, it is concluded that the spontaneous breathing effort and the lung mechanics of a spontaneously breathing patient are very valuable information. The desire to accurately retrieve this information led to the seventh contribution of this thesis.

Contribution II.a: *A non-invasive estimation algorithm using sparse estimation techniques to estimate the spontaneous breathing effort and lung mechanics parameters during ventilation.*

In experiments it is shown that the developed algorithm retrieves accurate and useful estimates of the patient effort and lung mechanics. Furthermore, it does not interfere with the patient's treatment.

In Section 1.5.2, it is concluded that accurate information about patient-ventilator asynchrony is important to further improve ventilation and a patient's treatment in general. The desire for information about patient-ventilation asynchrony has led to the eight contribution of this thesis.

Contribution II.b: *A framework, based on a supervised learning approach and using the typically available sensor data, to detect and classify timing asynchronies in ventilated patients.*

It is shown that by generating augmented data using a simulation environment, accurate classification algorithms for patient-ventilator asynchrony can be developed. The developed algorithm has been validated in a lab environment, showing that it can accurately detect and classify a wide variety of patient-ventilator asynchronies.

Concluding, Contribution II.a and Contribution II.b can significantly improve the monitoring capabilities of modern ventilators. Therewith, they significantly contribute to achieving Research Goal II.

1.7 Thesis outline

The organization of the remainder of this thesis is presented in Fig. 1.5. The thesis is divided into two parts, corresponding to research Goal I and research Goal II. Each chapter of this thesis corresponds to one of the contributions of this thesis. Besides the organization of this thesis, Fig. 1.5 also shows how the different contributions interact with the ventilator, patient, and clinician. More specifically, Contribution I.a-Contribution I.f are in the low-level control loop to improve the target pressure tracking. Contribution II.a-Contribution II.b are helping the clinician to determine the optimal target pressure profile, in other words, the optimal ventilation strategy. Finally, the main conclusions of this thesis and recommendations for future work are accumulated in Chapter 10. All

chapters are based on research papers and are self-contained, hence, every chapter can be read independently. A full list of the author's relevant publications is included at the end of this thesis. In a footnote at the start of every chapter it is indicated which research paper is the basis of the particular chapter.

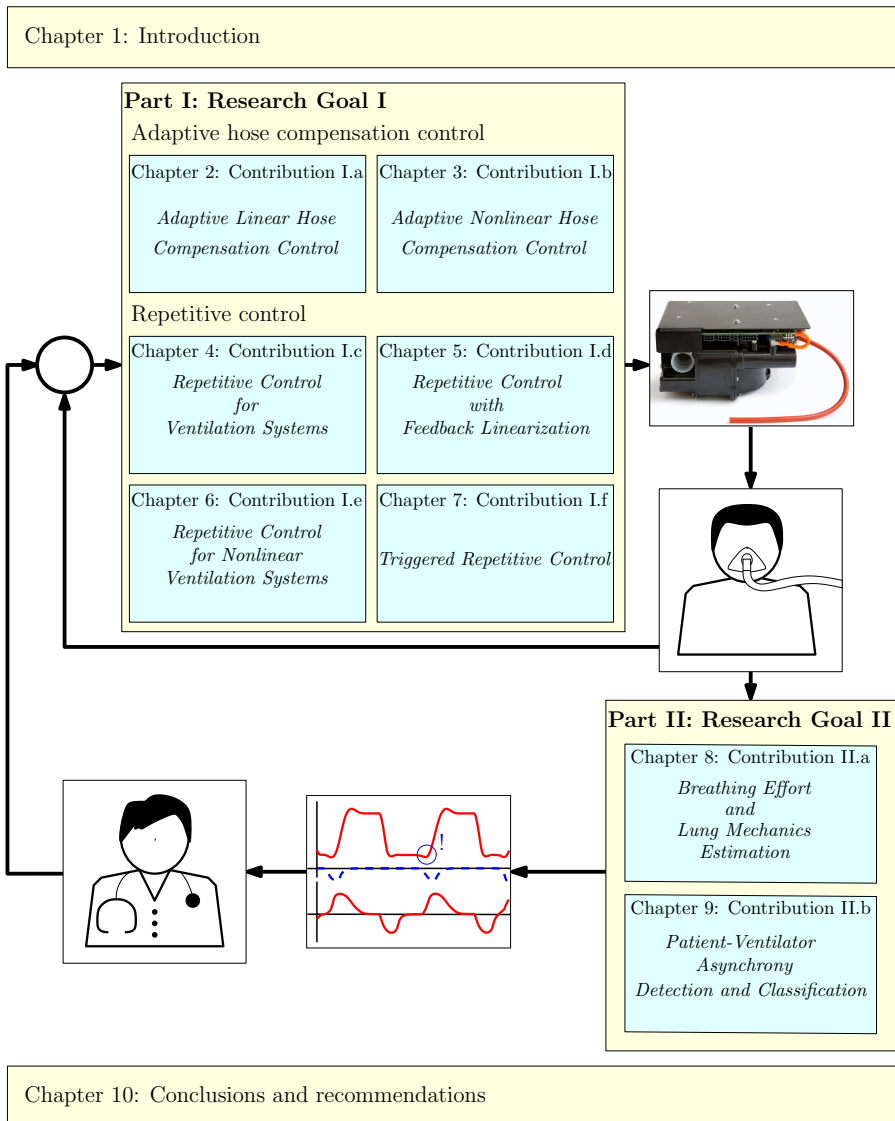


Fig. 1.5. Organization of this thesis.

Part I

Improved control algorithms for ventilation

Chapter 2

Adaptive control for mechanical ventilation for improved pressure support

Abstract – Respiratory modules are medical devices used to assist patients to breathe. The aim of this chapter is to develop a control method that achieves exact tracking of a time-varying target pressure, for unknown patient-hose-leak parameters and in presence of patient breathing effort. This is achieved by an online estimation of the hose characteristics that enables compensation for the pressure drop over the hose. Stability of the closed-loop system is proved and the performance improvement compared to existing control strategies is demonstrated by simulation and experimental case studies.

2.1 Introduction

Mechanical ventilation is commonly used in Intensive Care Units (ICUs) to assist patients who need support to breathe sufficiently. The main goals of mechanical ventilation are to ensure oxygenation and carbon dioxide elimination (Warner and Patel, 2013). A large number of patients requires mechanical ventilation. According to Needham et al. (2005), 19,186 people required mechanical ventilation in Ontario, Canada, in 2000. Therefore, improvements of ventilation benefit a large population worldwide.

The goal of mechanical ventilation is achieved using a mechatronic system, the mechanical ventilator. A schematic overview of a mechanical ventilator, with a single-hose setup and a patient, is depicted in Fig. 2.1. In this chapter, blower-driven Pressure Controlled Ventilation (PCV) of sedated patients and Continuous Positive Airway Pressure (CPAP) ventilation of spontaneously breathing patients is considered.

The contents of this chapter are published in Reinders et al. (2021b), preliminary results are presented in Reinders et al. (2019).

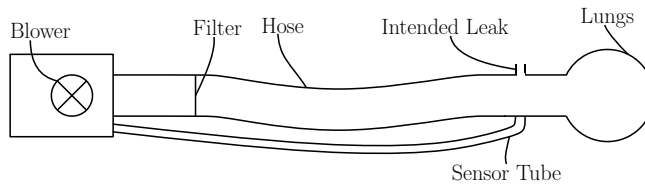


Fig. 2.1. Schematic representation of the blower-hose-patient system of the considered positive pressure ventilation system.

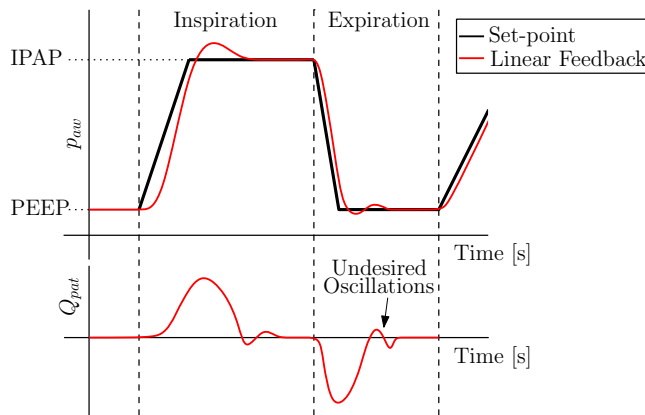


Fig. 2.2. Airway pressure and patient flow during one breathing cycle of pressure controlled ventilation (p_{ow} : airway pressure, Q_{pat} : flow into the patient's lungs, see also Fig. 2.5).

In PCV, the blower compresses ambient air to achieve the desired pressure profile, see Fig. 2.2, near the patient's mouth. The blower is increasing the airway pressure during inspiration, to achieve the Inspiratory Positive Airway Pressure (IPAP), filling the patient's lungs with air. After a preset amount of time has passed, the blower decreases the pressure to the Positive End-Expiratory Pressure (PEEP), such that the lungs are emptied.

In CPAP, the goal is to achieve a continuous airway pressure, while the patient breaths through this profile. A substantial amount of research has been conducted to obtain the optimal ventilator settings and modes, e.g., Lachmann (1992), Amato et al. (1998), and Amato et al. (2015), which focuses on the design of the pressure set-point.

Accurate tracking of the target pressure is important to achieve sufficient support for the patient, especially in cases of large flows, as a result of large lungs and/or unintentional leaks, e.g., in non-invasive ventilation. Furthermore, accurate pressure tracking results in better patient-ventilator synchrony; in Van de Wouw et al. (2018) and Hunnekens et al. (2020), it is argued that better tracking prevents false triggers, improving

patient-ventilator synchrony. Asynchrony between patient and machine is even associated with high mortality (Blanch et al., 2015). Finally, for more complex ventilation modes, allowing for patient effort, exact tracking is essential to deliver the required level of assistance more accurately.

Traditionally, these ventilators are controlled using linear time-invariant feedback controllers. This results in unsatisfactory tracking performance in terms of overshoot and settling time, as shown in Fig. 2.2. The main cause for such unsatisfactory performance is the large variation of plants for which the linear feedback controller should be robust. Indeed, the controller should ensure robust performance for a broad spectrum of patients, from infants to adults, varying disposable hose-filter systems, unknown leakage, and possibly unknown patient activity.

Different control strategies have been investigated to improve the mechanical ventilators. In Borrello (2005), an overview of modelling and control techniques for mechanical ventilation is presented. Variable-gain control is proposed in Van de Wouw et al. (2018) and Hunnekens et al. (2020), which aims to achieve pressure tracking while reducing the overshoot in patient flow, preventing false triggering. This work shows a clear reduction in patient flow overshoot. However, still some overshoot is present and the patient flow is used in the control strategy, which is typically not available. In Borrello (2001), an adaptive feedback control approach is applied which is estimating the patient model and using this to adaptively tune a controller which achieves a desired closed-loop transfer function. In theory this works well, however, in practice it is complex to obtain an accurate patient model. Furthermore, in Borrello (2001) the hose resistance is neglected, while for large air flows, induced by large lungs and/or leakage, the hose-induced pressure drop cannot be neglected. Also funnel-based control (Pomprapa et al., 2015) is applied to mechanical ventilation, however, the obtained gain in tracking performance is limited. In Scheel et al. (2017), a model-based control approach is used and in Li and Haddad (2012) a model predictive control approach is applied. These methods require accurate patient parameters which are typically not available in practice. Furthermore, iterative learning control (Scheel et al., 2015) is applied to mechanical ventilation. This work shows a significant improvement in tracking performance. A drawback of this approach is that it is limited to repeated sequences of the set-point and initial conditions. Therefore, performance of the iterative learning control framework proposed by Scheel et al. (2015) degrades when patients are breathing spontaneously.

Although previous research shows promising improvements in tracking performance, it does not achieve sufficiently accurate tracking of the target pressure, for the required range of patients, patient effort, hose-filter systems, and set-points. To achieve this, this chapter presents an adaptive control strategy that compensates for the pressure drop over the hose. A hose resistance estimate and the measured output flow are used to compensate for the pressure drop over the hose. Manual calibration of the hose-filter system to obtain the hose resistance is an undesired option, because of the already increasing demand of health care and the lack of trained personnel, see Needham et al. (2005) and Angus et al. (2000). Further, the hose resistance might change during venti-

lation, due to clogging of the filter. Therefore, an online Recursive Least Squares (RLS) estimator is developed to estimate the hose resistance automatically during ventilation.

In this work, an adaptive control scheme is considered instead of a robust scheme. First, the wide variety in patients and hose types leads to a situation where it is challenging to achieve adequate performance for every patient using one single robustly-tuned linear feedback controller. Second, manual calibrations are undesired because of the lack of time in a hospital setting; such calibration can be omitted by using an adaptive controller. Third, since the system parameters may vary over time, it is beneficial that an adaptive scheme allows to respond to such variations, thereby guaranteeing high performance under such changing circumstances.

The main difference with the adaptive control strategy in Borrello (2001) is that in the proposed control strategy only the hose-resistance model is estimated and used in the feedback loop. The patient parameters are not estimated, which is typically challenging because of the wide variety of patients and the model uncertainty concerning the structure of the patient model. Therewith, the method proposed in this work is invariant to the patient model, which is a significant advantage over the adaptive control scheme in Borrello (2001).

The main contribution of this chapter is the design of a control strategy for mechanical ventilation which ensures exact tracking of the airway pressure independent of the patient, hose, leakage, patient effort, and set-point. Key advantages of the proposed approach include that it

- allows for a fast and accurate pressure response, even for large lungs and big leaks;
- prevents overshoot in the patient flow and therewith prevents false triggering; and
- is not using direct feedback on the patient airway pressure, improving robustness, since the patient airway sensor tube might detach;

The first subcontribution is a stability proof of the resulting closed-loop system, ensuring exponential convergence of the estimation and tracking errors to zero. As a second subcontribution, a significant improvement in tracking performance in comparison to state-of-practice control strategies is shown through a simulation case study. The third subcontribution, is an experimental case study that shows the practical applicability of the controller and improvement over the state-of-practice control strategies.

The outline of this chapter is as follows. In Section 2.2, the control problem and high-level control approach are described. In section 2.3, a mathematical model of the patient-hose system is presented. In Section 2.4, the developed control strategy is described and a stability analysis is presented. A model-based simulation study is presented in Section 2.5, comparing state-of-practice control strategies to the developed adaptive controller. In Section 2.6, the adaptive controller is compared to state-of-practice control strategies in an experimental case study. Finally, the conclusions and recommendations are presented in Section 2.7.

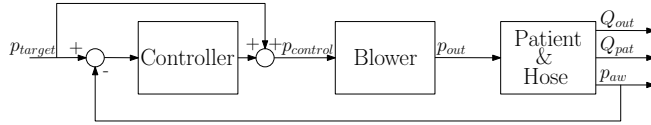


Fig. 2.3. State-of-practice control scheme with a linear feedback and unit feedforward controller that generate the controller output $p_{control}$. Furthermore, showing the plant that consists of a blower, which generates the blower outlet pressure p_{out} , and the patient-hose system with the outlet flow Q_{out} , the patient flow Q_{pat} , and the airway pressure p_{aw} .

2.2 Control problem formulation

In this section, the considered system is first presented. Thereafter, the control problem is formulated and the state-of-practice control approach is discussed in this context. Furthermore, a high-level description of the proposed control approach is given.

A schematic overview of the system, with the most important system components, is depicted in Fig. 2.1. The system is operated by the blower, which pressurizes ambient air in order to ventilate the patient. A hose is used to connect the respiratory module to the patient. The flow, which leaves the blower, runs through the hose towards the patient. The patient exhales partly back through the blower, and partly through a leak in the hose near the patient's mouth, see Fig. 2.1. This leak is used to refresh the air in the hose, to ensure that the patient does not inhale previously exhaled, low-oxygen, air.

2.2.1 Control problem and state-of-practice approach

In blower-driven respiratory systems, typically linear integral feedback controllers are used. Implementing a linear feedback controller results in a closed-loop system, as depicted in Fig. 2.3. In this closed-loop system the airway pressure p_{aw} is the variable to be controlled, i.e., it should track the target pressure p_{target} . The overall control goal is to minimize the tracking error, defined as

$$e := p_{target} - p_{aw}, \quad (2.1)$$

or ideally let it converge to zero asymptotically.

The blower is internally controlled by an accurate lookup table and an additional feedback controller using the blower error ($p_{control} - p_{out}$). This controller achieves a blower output pressure that is equal to the main controller output $p_{control}$, i.e., $p_{out} = p_{control}$. Combined, the lookup table and the feedback controller accurately achieve $p_{out} = p_{control}$ in the frequency domain of interest. Consequently, the unit feedforward in combination with the blower characteristic ensures that p_{out} is exactly tracking p_{target} . Therefore, in the remainder of this chapter, it is assumed that $p_{out} = p_{target}$.

Since unit feedforward achieves $p_{out} = p_{target}$, the feedback controller in Fig. 2.3 has to compensate for the pressure drop $\Delta p = p_{out} - p_{aw}$ along the hose. Note that it

is challenging to predict the pressure drop along the hose due to several factors:

- the type of lung attached, i.e., the patient, is in principle unknown. Although the pressure target is a priori known, the amount of flow entering a lung depends on the lung resistance and lung compliance and is therefore unknown. Therewith, also the flow through the hose, and thus the pressure drop Δp are unknown;
- the characteristic of the hose system attached is also unknown. Hence, the pressure drop along the hose is unknown;
- during (non-invasive) ventilation there can be leakage around the mask, which cannot be predicted and therefore results in an a priori unknown pressure drop;
- additionally, patients can have spontaneous breathing activity (resulting in a flow and therewith a pressure drop along the hose), which also cannot be predicted a priori.

Therefore, exact feedforward control cannot be used to compensate for the pressure drop Δp over the hose.

Alternatively, a linear feedback controller, typically a Proportional-Integral (PI) controller, is used to compensate for the pressure drop over the hose. A linear feedback controller has to be tuned for robustness over large plant variations. Therefore, it is unable to achieve accurate tracking for all considered patients. Furthermore, a feedback controller uses the measured airway pressure p_{aw} in the feedback loop. Feedback on p_{aw} is undesired, since the sensor tube might get detached in practice.

2.2.2 Proposed control strategy

Here, a control strategy is proposed that uses an estimated hose resistance model and the output flow Q_{out} , which is measured near the blower, to compensate for the pressure drop Δp over the hose, see Fig. 2.4. Because the hose resistance is unknown, an offline calibration could be conducted by hospital personnel to estimate the hose resistance prior to ventilation. This calibration requires extra time of the hospital staff, which is undesired because of the already existing lack of time for hospital staff, as mentioned in Section 2.1. Furthermore, the resistance may change over time.

Therefore, an adaptive control approach is developed, which is using an online Recursive Least Squares (RLS) estimator to estimate the hose resistance automatically during ventilation, see Fig. 2.4. Practically, this approach is considerably more reliable than the state-of-practice feedback method, which is using p_{aw} directly in the feedback loop. The proposed strategy is only using p_{aw} for updating the estimator. In practice, the sensor tube used to measure p_{aw} might get detached. In such a scenario, the proposed controller can keep running without updating the resistance, whereas the feedback controller fails and may cause a potentially dangerous situation.

Another advantage of this control strategy is that it compensates for the pressure drop Δp over the hose using the measured blower outlet flow Q_{out} . The pressure drop

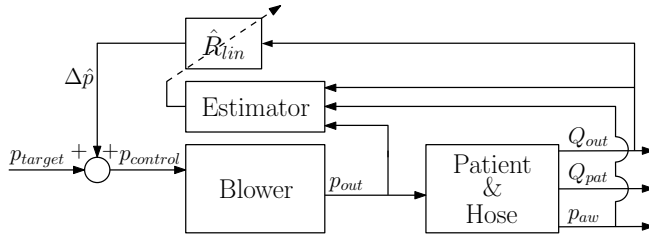


Fig. 2.4. Schematic representation of the proposed closed-loop system with a recursive least squares estimator for the hose resistance estimation.

over the hose Δp depends on the flow through the hose, which is equal to the blower outlet flow Q_{out} . Therefore, exact compensation of this pressure drop based on the measured flow allows for perfect tracking independent of the leak, patient dynamics, and patient effort. In the following section, a model of the patient-hose dynamics is presented.

2.3 Patient-hose dynamics

In this section, a description of the system parameters used in the model is given. Thereafter, the open-loop patient-hose dynamics are presented.

2.3.1 Patient-hose parameters

Before presenting the mathematical model, the system parameters and their physical meaning are discussed. Consider the schematic representation of the blower, hose, and patient depicted in Fig. 2.5. First, the blower compresses ambient air to the desired blower outlet pressure p_{out} . Note that all pressures are defined relative to the ambient pressure, i.e., $p_{amb} = 0$. This outlet pressure results in a flow Q_{out} through the hose, with resistance R_{lin} . Furthermore, the patient airway pressure p_{aw} is measured just in front of the patient's mouth, using the sensor tube. A leak is used to flush exhaled CO_2 -rich air from the hose system and is modeled using the leak resistance R_{leak} . The lung is modeled using a linear one-compartmental lung model as described in Bates (2009), with lung compliance C_{lung} and resistance R_{lung} . Note that all physical patient-hose parameters, i.e., R_{lin} , R_{leak} , R_{lung} , and C_{lung} , are strictly positive. Furthermore, Fig. 2.5 shows the patient's breathing effort p_{pat} , which is considered an exogenous disturbance on the lung pressure, caused by the patient's respiratory effort.

2.3.2 Patient-hose model

Using the parameters and models outlined above, a mathematical patient-hose model is derived. This model describes the relation between the blower outlet pressure p_{out} , the

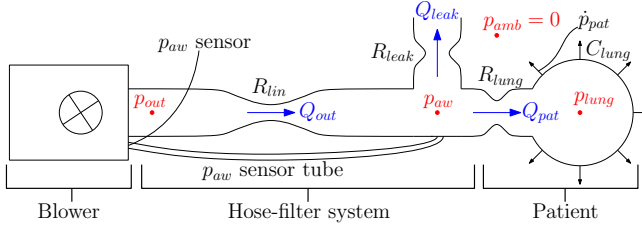


Fig. 2.5. Schematic representation of the blower-hose-patient system, with the corresponding resistances, lung compliance and patient effort.

disturbance \dot{p}_{pat} , the state p_{lung} , and the outputs p_{aw} and Q_{out} .

Using conservation of flow, the output flow Q_{out} , patient flow Q_{pat} , and leakage flow Q_{leak} are related by

$$Q_{pat} = Q_{out} - Q_{leak}. \quad (2.2)$$

The resistances are modeled using a linear resistance model, which is reasonably accurate for typical flows in ventilation. Using the linear resistances R_{lin} , R_{leak} , and R_{lung} , the pressures and flows are related as follows:

$$\begin{aligned} Q_{out} &= \frac{p_{out} - p_{aw}}{R_{lin}}, \\ Q_{leak} &= \frac{p_{aw}}{R_{leak}}, \\ Q_{pat} &= \frac{p_{aw} - p_{lung}}{R_{lung}}. \end{aligned} \quad (2.3)$$

The lung dynamics are governed by

$$p_{lung}(t) = \frac{1}{C_{lung}} \int_0^t Q_{pat} dt + p_{pat}(t) + p_{lung}(0) \quad (2.4)$$

with $p_{pat}(t)$ the (time-varying) patient effort. The patient effort is modeled as an unknown disturbance on the lung pressure, induced by the patient's respiratory efforts, e.g., diaphragm and/or abdominal muscle contractions. Furthermore, $p_{lung}(0)$ represents the initial lung pressure excluding the patient effort. The time derivative of the lung pressure then satisfies

$$\dot{p}_{lung}(t) = \frac{1}{C_{lung}} Q_{pat} + \dot{p}_{pat}. \quad (2.5)$$

Combining (2.3) and (2.5), the lung dynamics are described by

$$\dot{p}_{lung} = \frac{p_{aw} - p_{lung}}{C_{lung} R_{lung}} + \dot{p}_{pat}. \quad (2.6)$$

The following relation for the airway pressure is obtained from (2.2) and (2.3):

$$p_{aw} = \frac{R_{lin}R_{leak}p_{lung} + R_{leak}R_{lung}p_{out}}{\bar{R}} \quad (2.7)$$

with $\bar{R} := R_{lin}R_{leak} + R_{lin}R_{lung} + R_{leak}R_{lung}$. By substituting (2.7) into (2.6), a differential equation for the lung dynamics is obtained

$$\dot{p}_{lung} = \frac{-(R_{lin} + R_{leak})}{C_{lung}\bar{R}}p_{lung} + \frac{R_{leak}}{C_{lung}\bar{R}}p_{out} + \dot{p}_{pat}. \quad (2.8)$$

Given (2.8), (2.7), and (2.3), the patient-hose system dynamics can be written as a linear state-space system with input p_{out} , outputs p_{aw} and Q_{pat} , state p_{lung} , and disturbance \dot{p}_{pat} :

$$\begin{aligned} \dot{p}_{lung} &= \mathbf{A}_h p_{lung} + \mathbf{B}_h p_{out} + \dot{p}_{pat} \\ \begin{bmatrix} p_{aw} \\ Q_{pat} \end{bmatrix} &= \mathbf{C}_h p_{lung} + \mathbf{D}_h p_{out} \end{aligned} \quad (2.9)$$

with

$$\begin{aligned} \mathbf{A}_h &= -\frac{R_{lin} + R_{leak}}{C_{lung}\bar{R}}, \quad \mathbf{B}_h = \frac{R_{leak}}{C_{lung}\bar{R}}, \\ \mathbf{C}_h &= \left[\frac{R_{lin}R_{leak}}{\bar{R}} \quad -\frac{R_{lin}+R_{leak}}{\bar{R}} \right]^T, \\ \mathbf{D}_h &= \left[\frac{R_{leak}R_{lung}}{\bar{R}} \quad \frac{R_{leak}}{\bar{R}} \right]^T. \end{aligned} \quad (2.10)$$

Since all resistances and the compliance are strictly positive constants, \mathbf{A}_h is negative and hence the patient-hose system is inherently asymptotically stable. Note that \dot{p}_{pat} is considered to be an exogenous disturbance, whereas in practice it contains dynamics, i.e., the patient's breathing behavior.

2.4 Adaptive controller design and stability analysis

In this section, the proposed adaptive control approach is presented, leading to the main contribution of this work. In Section 2.4.1, the closed-loop dynamics resulting from the new control strategy are presented, for the case in which a constant estimate \hat{R}_{lin} of the hose resistance R_{lin} is used. In Section 2.4.2, the RLS estimator, used to estimate the hose resistance, is given. Finally, in Section 2.4.3, a stability analysis of the resulting closed-loop dynamics, including the estimator, is presented.

2.4.1 Closed-loop dynamics for a constant hose-resistance estimate

In this section, a state-space description of the closed-loop dynamics with a constant estimate \hat{R}_{lin} are derived. This state-space description is needed to analyze the performance and stability of the controlled system. In the closed-loop dynamics, a feedback controller on the blower outlet flow Q_{out} is included, as depicted in Fig. 2.4.

The constant feedback controller in Fig. 2.4 and the fact that the blower gain is 1 in the frequency domain of interest results in $p_{out} = p_{control} = \Delta\hat{p} + p_{target}$. Using $p_{out} = \Delta\hat{p} + p_{target}$ and (2.9) results in

$$\dot{p}_{lung} = \mathbf{A}_h p_{lung} + \mathbf{B}_h (p_{target} + \Delta\hat{p}) + \dot{p}_{pat}. \quad (2.11)$$

From Fig. 2.4, we know that the estimated pressure drop is given by $\Delta\hat{p} = \hat{R}_{lin} Q_{out}$. Using (2.2), (2.3), and (2.5) this pressure drop estimate can be rewritten to

$$\begin{aligned} \Delta\hat{p} &= \hat{R}_{lin} Q_{out} \\ &= \hat{R}_{lin} (Q_{pat} + Q_{leak}) \\ &= \hat{R}_{lin} \left(C_{lung} (\dot{p}_{lung} - \dot{p}_{pat}) + \frac{p_{aw}}{R_{leak}} \right). \end{aligned} \quad (2.12)$$

Note that $p_{control} = \Delta\hat{p} + p_{target}$ together with (2.12) essentially form the proposed feedback law that aims at compensating the pressure drop over the hose-filter system. Substituting the airway pressure, obtained from (2.6), into (2.12) gives

$$\Delta\hat{p} = \hat{R}_{lin} \left(C_{lung} \left(1 + \frac{R_{lung}}{R_{leak}} \right) (\dot{p}_{lung} - \dot{p}_{pat}) + \frac{p_{lung}}{R_{leak}} \right). \quad (2.13)$$

For notational purposes, the combined variable

$$R(e_{LS}) := e_{LS} (R_{leak} + R_{lung}) + R_{leak} R_{lung} \quad (2.14)$$

is defined with the estimation error

$$e_{LS} := R_{lin} - \hat{R}_{lin}. \quad (2.15)$$

Then, substitution of (2.13) in (2.11) gives

$$\dot{p}_{lung} = \frac{-R_{leak} - e_{LS}}{C_{lung} R(e_{LS})} p_{lung} + \frac{R_{leak}}{C_{lung} R(e_{LS})} p_{target} + \dot{p}_{pat}. \quad (2.16)$$

The variables p_{aw} , Q_{pat} , and Q_{out} are considered as outputs and the resulting closed-loop system is described as follows:

$$\begin{aligned} \dot{p}_{lung} &= \mathbf{A}(e_{LS}) p_{lung} + \mathbf{B}(e_{LS}) p_{target} + \dot{p}_{pat} \\ \begin{bmatrix} p_{aw} \\ Q_{pat} \\ Q_{out} \end{bmatrix} &= \mathbf{C}(e_{LS}) p_{lung} + \mathbf{D}(e_{LS}) p_{target} \end{aligned} \quad (2.17)$$

with

$$\begin{aligned} \mathbf{A}(e_{LS}) &= \frac{-R_{leak} - e_{LS}}{C_{lung} R(e_{LS})}, \quad \mathbf{B}(e_{LS}) = \frac{R_{leak}}{C_{lung} R(e_{LS})}, \\ \mathbf{C}(e_{LS}) &= \left[1 - \frac{(R_{leak} + e_{LS}) R_{lung}}{R(e_{LS})} \quad \frac{-R_{leak} - e_{LS}}{R(e_{LS})} \quad \frac{-R_{leak}}{R(e_{LS})} \right]^T, \\ \mathbf{D}(e_{LS}) &= \left[\frac{R_{leak} R_{lung}}{R(e_{LS})} \quad \frac{R_{leak}}{R(e_{LS})} \quad \frac{R_{leak} + R_{lung}}{R(e_{LS})} \right]^T. \end{aligned} \quad (2.18)$$

Note that the dynamics in (2.17) are in fact nonlinear in the estimation error e_{LS} because of the dependency of the system matrices on this estimation error. Next, the system is analyzed for a constant least-squares estimation error e_{LS} . In particular, we are interested in these linear dynamics for $e_{LS} = 0$ to understand the closed-loop system behavior, with hose pressure compensation once a perfect hose resistance estimate is available. This analysis is performed by means of the transfer function of the linear system with a constant estimation error. From this transfer function strong performance features of the closed-loop system are obtained.

Using the system dynamics in (2.17) and (2.18), the transfer function from the inputs p_{target} and \dot{p}_{pat} to the output p_{aw} is computed. Hereto, the closed-loop system is rewritten to the following form:

$$\dot{p}_{lung} = \bar{\mathbf{A}}p_{lung} + \bar{\mathbf{B}}u \quad (2.19)$$

$$p_{aw} = \bar{\mathbf{C}}p_{lung} + \bar{\mathbf{D}}u \quad (2.20)$$

with a combined input vector $u = [p_{target} \ \dot{p}_{pat}]^T$,

$$\bar{\mathbf{A}} = \mathbf{A}(e_{LS}), \quad \bar{\mathbf{B}} = [\mathbf{B}(e_{LS}) \ 1], \quad (2.21)$$

$$\bar{\mathbf{C}} = \mathbf{C}_1(e_{LS}), \quad \bar{\mathbf{D}} = [\mathbf{D}_1(e_{LS}) \ 0], \quad (2.22)$$

where $\mathbf{C}_1(e_{LS})$ and $\mathbf{D}_1(e_{LS})$ are the first elements in $\mathbf{C}(e_{LS})$ and $\mathbf{D}(e_{LS})$, respectively. Using this form of the closed-loop system, the transfer function from u to p_{aw} is obtained

$$\frac{p_{aw}(s)}{u(s)} = \bar{\mathbf{C}}(s - \bar{\mathbf{A}})^{-1}\bar{\mathbf{B}} + \bar{\mathbf{D}} \quad (2.23)$$

with $s \in \mathbb{C}$ the Laplace variable. Using this, an expression for p_{aw} is obtained

$$p_{aw}(s) = P_1 p_{target}(s) + P_2 \dot{p}_{pat}(s) \quad (2.24)$$

with

$$P_1 = \frac{R_{leak} + C_{lung}R_{leak}R_{lung}s}{R_{leak} + C_{lung}R_{leak}R_{lung}s + e_{LS}(1 + C_{lung}(R_{leak} + R_{lung})s)}$$

and

$$P_2 = \frac{C_{lung}e_{LS}R_{leak}}{R_{leak} + C_{lung}R_{leak}R_{lung}s + e_{LS}(1 + C_{lung}(R_{leak} + R_{lung})s)}.$$

Next, an exact estimate of the hose resistance is assumed, i.e., estimation error $e_{LS} = 0$. For an exact estimate of the hose resistance, the term P_1 in (2.24), i.e., the transfer function from p_{target} to p_{aw} , is one for all $s \in \mathbb{C}$. Further, the term P_2 , i.e., the transfer function from \dot{p}_{pat} to p_{aw} , is zero for all $s \in \mathbb{C}$. Therefore, the airway pressure of the closed-loop system is exactly the same as p_{target} . Furthermore, the

airway pressure is independent of the patient dynamics and the exogenous disturbance \dot{p}_{pat} related to the patient effort. This is a highly desirable property for a controlled system. A formal proof of these properties (zero tracking error independent of patient effort and patient dynamics) for the full nonlinear dynamics, i.e., with convergence of e_{LS} to zero, is presented in Section 2.4.3.

2.4.2 Recursive least squares estimation of the hose resistance

In the previous section, the equations describing the proposed controlled plant model are presented for a given (constant) hose resistance estimate \hat{R}_{lin} . Since the hose resistance is an unknown parameter, an RLS estimator that estimates the value of R_{lin} automatically during ventilation is proposed; hence no additional calibration steps are required in the hospital. In this particular application, an RLS algorithm with exponential forgetting factor β is used (Ioannou and Sun, 1996, p. 200), since data far in the past is considered less important than more recent data. A schematic representation of the system including the hose resistance estimator is depicted in Fig. 2.4.

The RLS estimator with forgetting factor is given by¹:

$$\dot{\hat{R}}_{lin} = P \frac{\Delta p - \hat{R}_{lin} Q_{out}}{m^2} Q_{out}, \quad (2.25)$$

$$\dot{P} = \beta P - P^2 \frac{Q_{out}^2}{m^2}, \quad (2.26)$$

where Q_{out} is the exciting variable, $P(t)$ is called the covariance, and $\frac{\Delta p - \hat{R}_{lin} Q_{out}}{m^2}$ represents the normalized estimation error of the pressure drop, with $m^2 > 0$ a constant normalization parameter. Since $\Delta p = R_{lin} Q_{out}$, $e_{LS}(t) = R_{lin} - \hat{R}_{lin}(t)$, and R_{lin} is a constant, the least squares error dynamics are written as follows:

$$\dot{e}_{LS} = -P \frac{Q_{out}^2}{m^2} e_{LS}. \quad (2.27)$$

The resulting closed-loop dynamics with estimator and hose compensation controller are given by (2.17), (2.18), (2.26), and (2.27).

The parameters β and $P(0)$ should be chosen such that convergence is sufficiently fast, i.e., within a couple of breaths. However, choosing β too high results in fast convergence but might also result in strong oscillations in the parameter due to measurement noise and effects that are not captured by the hose model. Furthermore, β and $P(0)$ should be positive to ensure stability as discussed in the following section. Additionally, in this chapter, the constant normalization parameter m is chosen to be one, i.e., $m = 1$, to reduce the number of tuning parameters.

¹The notation equivalents to the notation of (Ioannou and Sun, 1996, p. 200) are $R_{lin} = \theta^*$, $\hat{R}_{lin} = \theta$, $Q_{out} = \phi_0$, and $\Delta p = z$.

2.4.3 Stability analysis

The closed-loop system dynamics with the adaptive controller are given by (2.17), (2.18), (2.26), and (2.27). In this section, stability conditions for the closed-loop controlled system are derived. First, several auxiliary results are presented. Using these auxiliary results, Theorem 2.1 is presented below. Theorem 2.1 provides sufficient conditions for exponential convergence to zero of the tracking error $e(t)$ and of the estimation error $e_{LS}(t)$. Herein, we consider time-varying pressure targets $p_{target}(t)$, unknown patient effort $p_{pat}(t)$, and unknown patient-hose parameters, i.e., resistances and compliance. In support of the proofs, the auxiliary lemmas in the appendix are used.

First, a Persistently Exciting (PE) signal is defined.

Definition 2.1. *A piece-wise continuous scalar signal $\phi(t)$ is PE if there exist constants $\alpha_0, \alpha_1, T_0 \in \mathbb{R}_{>0}$ such that*

$$\alpha_1 \geq \frac{1}{T_0} \int_t^{t+T_0} \phi^2(\tau) d\tau \geq \alpha_0, \forall t \geq 0. \quad (2.28)$$

Furthermore, the RLS estimator in (2.26) and (2.27) is assumed to satisfy Assumption 2.1.

Assumption 2.1. *The RLS estimator in (2.26) and (2.27) is designed and initialized such that the following properties hold:*

- $P(0)$ is chosen to be positive, i.e., $P(0) > 0$.
- $\hat{R}_{lin}(0)$ is chosen such that the following inequalities hold (with $\epsilon > 0$ a small constant):

$$\begin{aligned} \hat{R}_{lin}(0) &< R_{lin} + R_{leak}, \\ \hat{R}_{lin}(0) &\leq R_{lin} + \frac{R_{leak}R_{lung}}{R_{leak} + R_{lung}} - \epsilon. \end{aligned}$$

- β is designed to be positive, i.e., $\beta > 0$.

Note that we can always design and initialize the RLS estimator such that Assumption 2.1 holds. Furthermore, choosing $\hat{R}_{lin}(0) = 0$ directly ensures the inequalities in Assumption 2.1, since all resistances are positive, though this may be a conservative initial estimate for the hose resistance.

Assumption 2.2 below states that the target pressure profile is always positive and bounded.

Assumption 2.2. *$p_{target}(t)$ is bounded and positive by design; in particular, $\epsilon_1 < p_{target}(t) < \infty$, $\forall t \geq 0$, with $\epsilon_1 > 0$ a positive constant.*

This is a valid assumption, since a positive and bounded target pressure is desired during positive pressure ventilation see Fig. 2.2, with PEEP > 0 .

Assumption 2.3 below states that the disturbance $\dot{p}_{pat}(t)$ is bounded.

Assumption 2.3. *The patient effort $p_{pat}(t)$ is a bounded signal. Furthermore, its time derivative $\dot{p}_{pat}(t)$ is a bounded signal as well.*

Assumption 2.3 is valid in practice, since a patient cannot generate unbounded pressure or derivatives in pressure.

Note that PE-conditions on the excitation signals are required to guarantee RLS estimators with a forgetting factor to converge, see Corollary 4.3.2 in Ioannou and Sun (1996). Here, the exciting variable $Q_{out}(p_{lung}(t), e_{LS}(t), p_{target}(t))$ is not an external signal, but a variable dependent on the states, see (2.17) and (2.18). This complicates the stability analysis and requires an analysis of the PE-properties of $Q_{out}(p_{lung}(t), e_{LS}(t), p_{target}(t))$ as in Lemma 2.1 below. Note that no additional excitations are induced to ensure the PE condition, i.e., Q_{out} is PE in the considered, common, ventilation scenarios.

Lemma 2.1. *Consider the closed-loop system dynamics defined by (2.17), (2.18), (2.26), and (2.27) and adopt Assumptions 2.1, 2.2, and 2.3. Then, $Q_{out}(p_{lung}(t), e_{LS}(t), p_{target}(t))$ is PE as defined in Definition 2.1.*

Proof. To ensure the existence of upper bound α_1 of the PE condition in Definition 2.1, Lemma 2.5 in the Appendix is invoked, which ensures that $Q_{out}(p_{lung}(t), e_{LS}(t), p_{target}(t))$ is bounded for all $t \geq 0$. Since $Q_{out}(p_{lung}(t), e_{LS}(t), p_{target}(t))$ is bounded, $\alpha_1 > 0$ indeed exists such that the upper bound in (2.28) is satisfied for $\phi(t) := Q_{out}(p_{lung}(t), e_{LS}(t), p_{target}(t))$.

Next, we have to show that the lower bound α_0 in the PE condition in (2.28) exists. For such lower bound to exist, the following equality should not hold for any $t^* \geq 0$ for some $T_0 \in \mathbb{R}_{>0}$:

$$Q_{out}(p_{lung}(t), e_{LS}(t), p_{target}(t)) = 0, \forall t \in [t^*, t^* + T_0]. \quad (2.29)$$

If there is no output flow, i.e., $Q_{out}(p_{lung}(t), e_{LS}(t), p_{target}(t)) = 0$, then from (2.2), $-Q_{leak} = Q_{pat}$. Furthermore, the pressure drop $p_{aw} - p_{out} = \Delta p = R_{lin}Q_{out}$ and the estimated pressure drop $\Delta \hat{p} = \hat{R}_{lin}Q_{out}$ are also zero under such condition. Using this and Assumption 2.2 gives $p_{aw}(t) = p_{out}(t) = p_{target}(t) > \epsilon_1, \forall t \in [t^*, t^* + T_0]$ if $Q_{out}(p_{lung}(t), e_{LS}(t), p_{target}(t)) = 0, \forall t \in [t^*, t^* + T_0]$. Moreover, $-Q_{leak} = Q_{pat}$ in combination with (2.3) gives

$$-\frac{p_{target}}{R_{leak}} = \frac{p_{target} - p_{lung}}{R_{lung}}, \quad (2.30)$$

which is rewritten to obtain

$$p_{lung}(t) = \frac{R_{lung}}{R_{leak}}p_{target}(t) + p_{target}(t), \forall t \in [t^*, t^* + T_0]. \quad (2.31)$$

Using (2.4) and (2.31) we obtain

$$\begin{aligned} & \frac{1}{C_{lung}} \int_{t^*}^t Q_{pat}(\tau) d\tau + p_{pat}(t) + p_{lung}(t^*) \\ &= \frac{R_{lung}}{R_{leak}} p_{target}(t) + p_{target}(t), \forall t \in [t^*, t^* + T_0], \end{aligned}$$

which is rewritten to

$$\begin{aligned} & -\frac{1}{C_{lung} R_{leak}} \int_{t^*}^t p_{target}(\tau) d\tau + p_{pat}(t) + p_{lung}(t^*) \\ &= \frac{R_{lung}}{R_{leak}} p_{target}(t) + p_{target}(t), \forall t \in [t^*, t^* + T_0], \end{aligned} \quad (2.32)$$

using $Q_{pat} = -\frac{p_{target}}{R_{leak}}$. We can choose a value $T_0 \in \mathbb{R}_{>0}$, such that this will not hold for any $t^* \geq 0$. If we take $T_0 \rightarrow \infty$, the term with the integral will go to minus infinity, using Assumption 2.2. We know that $p_{pat}(t)$ and $p_{lung}(t^*)$ are bounded using Assumption 2.3 and Lemma 2.4, respectively. Hence, the left-hand side of the equation will become negative for large values of T_0 and the right-hand side is always positive by Assumption 2.2. Since (2.32) does not hold for $T_0 \rightarrow \infty$, we know that (2.29) does not hold for any t^* for some very large T_0 . Therefore, we can conclude that $Q_{out}(p_{lung}(t), e_{LS}(t), p_{target}(t))$ is PE, according to Definition 2.1. \square

Finally, using Lemma 2.1, and Lemmas 2.4 and 2.5 in the Appendix, stability of the closed-loop system including the RLS estimator is proved. More precisely, Theorem 2.1 shows exponential convergence of the least squares error $e_{LS}(t)$ and the tracking error $e(t)$ to zero.

Theorem 2.1. *Consider the system dynamics (2.17), (2.18), (2.26), and (2.27) and suppose that Assumptions 2.1, 2.2, and 2.3 hold. Then, solutions of the dynamical system (2.17), (2.18), (2.26), and (2.27) have the following properties:*

- $P(t)$, $P^{-1}(t)$, $p_{lung}(t)$ and $Q_{out}(t)$ are bounded $\forall t \geq 0$,
- $e_{LS}(t) = R_{lin} - \hat{R}_{lin}(t)$ and $e(t) = p_{target}(t) - p_{aw}(t)$ exponentially converge to zero.

Proof. First of all, the boundedness of p_{lung} and Q_{out} are shown in Lemma 2.4 and 2.5, respectively, see the Appendix. Furthermore, using Lemma 2.2 we know that $P(t)$ and $P^{-1}(t)$ are bounded $\forall t \geq 0$.

From Lemma 2.1, we know that the PE property holds for $Q_{out}(t)$. Therefore, Corollary 4.3.2 in Ioannou and Sun (1996) can be used to show that $e_{LS}(t)$ is exponentially converging to zero.

Finally, we have to show that $e(t)$ exponentially converges to zero. By substituting the airway pressure p_{aw} , defined in (2.17) and (2.18), into the error definition $e(t)$, defined in (2.1), the tracking error can be written as:

$$\begin{aligned} e(t) &= \frac{-R_{leak}p_{lung}(t) + (R_{leak} + R_{lung})p_{target}(t)}{e_{LS}(t)(R_{leak} + R_{lung}) + R_{leak}R_{lung}} e_{LS}(t) \\ &=: v(t)e_{LS}(t). \end{aligned} \quad (2.33)$$

Since, firstly $p_{lung}(t)$ is bounded (Lemma 2.4), secondly $p_{target}(t)$ is bounded (Assumption 2.2) and, thirdly $e_{LS}(t)(R_{leak} + R_{lung}) + R_{leak}R_{lung}$ is bounded away from zero (as shown in Lemma 2.4), it is guaranteed that $v(t)$ in (2.33) is bounded. Since $v(t)$ is bounded $\forall t \geq 0$, i.e., there exists a bounded v_{max} , such that $|v(t)| \leq v_{max}, \forall t \geq 0$, we can write

$$|e(t)| \leq v_{max}|e_{LS}(t)|, \forall t > 0. \quad (2.34)$$

Since $e_{LS}(t)$ converges to zero exponentially, (2.34) shows that $e(t)$ also converges to zero exponentially. \square

Theorem 2.1 ensures exponential convergence of the tracking error $e(t)$ to zero for a time-varying target pressure, under mild conditions on the initial estimate for the hose resistance and the target pressure profile $p_{target}(t)$. Furthermore, this property is independent of the unknown disturbance induced by the patient's breathing effort, as long as it remains bounded. In control systems, perfect tracking is typically possible when inverse-plant feedforward is applied and no further disturbances are present. In this case, it is achieved by compensating for the disturbance through feedback. More precisely, the measured flow Q_{out} that is used in the feedback loop contains the disturbance, i.e., Q_{out} depends on \dot{p}_{pat} through p_{lung} . The estimate of the hose resistance is used to compensate for the pressure drop, such the target pressure is an invariant solution of the closed-loop dynamics. This can be seen in equation (2.24) with $e_{LS} = 0$, which gives $p_{aw} = p_{target}$ independent of the patient effort and dynamics. This is achieved independent of the system, i.e., patient and hose, parameters as mentioned in Remark 2.1. The system parameters only affect the flow and therewith the convergence speed of the hose-resistance estimate.

Remark 2.1. *The relation between the hose-induced pressure drop Δp and the measured flow through the hose Q_{out} is independent of the patient and leak parameters, and the patient effort. The patient and leak parameters only influence the measured blower output flow Q_{out} and therewith the convergence speed of the estimator is affected. However, exact tracking of the target pressure independent of patient and leak parameters, and the patient effort is achieved.*

2.5 Simulation case study

In this section, the improvement in tracking performance of the proposed adaptive control approach compared to state-of-practice control strategies is shown through simu-

Table 2.1. Estimation parameters of the adaptive controller and the patient and hose parameters, as used in the simulations.

Parameter	Value	Unit
β	0.7	1/s
$P(0)$	5×10^{-8}	s/mL ²
$\hat{R}_{lin}(0)$	0	mbar s/L
m	1	-
R_{leak}	24	mbar s/L
R_{lung}	5	mbar s/L
$R_{lin}(0)$	4.4	mbar s/L
C_{lung}	20	mL/mbar

lations. Performance of the different control strategies is compared by analyzing the pressure tracking, i.e., rise-time, overshoot, undershoot, and settling time. Furthermore, overshoot in patient flow is considered, since a decrease in overshoot prevents false triggering and improves patient comfort.

Two different scenarios are considered in this section. In Section 2.5.1, a sedated patient, i.e., $p_{pat}(t) = 0, \forall t$, under Pressure Controlled Ventilation (PCV) ventilation is considered. In Section 2.5.2, a spontaneously breathing patient, i.e., $\exists t \geq 0 : p_{pat}(t) \neq 0$, under Continuous Positive Airway Pressure (CPAP) ventilation is considered.

In the case with a sedated patient, a step in the hose resistance is introduced to show that the new control approach can handle changes in resistance, which may be induced by clogging of a filter. The following two state-of-practice control strategies are considered to benchmark against:

- feedforward control; and
- linear feedback control.

The feedforward controller is a unit feedforward; in other words, the desired airway pressure is applied as $p_{target} = p_{control} = p_{out}$ and no feedback based on measurements is used. For the linear feedback controller, an integral controller is used to compensate for the pressure drop Δp over the hose. This feedback controller is used in addition to the unit feedforward controller. The integral controller results in convergence of the tracking error to zero for constant target pressures. Because the plant variations are large, the linear feedback controller is tuned for robustness instead of performance resulting in an integral controller with transfer function $C(s) = \frac{10}{s}$, with $s \in \mathbb{C}$ the Laplace variable. The RLS estimator parameters and the patient-hose system parameters are presented in Table 2.1.

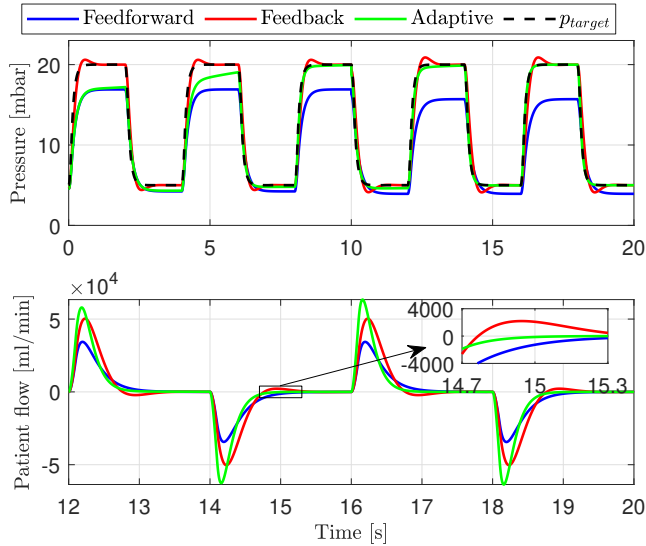


Fig. 2.6. Simulation results of the feedforward, feedback and adaptive control strategy. This figure shows the resulting airway pressure and patient flow.

2.5.1 Scenario with sedated patients

First of all, ventilation of sedated patients under PCV is considered. This section is divided in the test case description, the simulation results, and a summary of the main conclusions.

2.5.1.1 Test case

In these simulations, target pressures of 5 and 20 mbar are used for the Positive End-Expiratory Pressure (PEEP) and the Inspiratory Positive Airway Pressure (IPAP), respectively. Furthermore, we introduce a step in the hose resistance at $t = 10$ s, to show that the controller can handle a change in resistance. This step in resistance is depicted in the bottom figure of Fig. 2.7. Finally, simulations with different patient characteristics, such as compliance and resistance, are performed to show that the controller works for a wide range of patients.

2.5.1.2 Simulation results

The resulting airway pressure of the simulations is shown in Fig. 2.6. These results clearly show that the feedforward controlled system has a steady-state tracking error, which is caused by the pressure drop Δp over the hose. For the linear feedback controller it is observed that the pressure is converging to the desired pressure but there

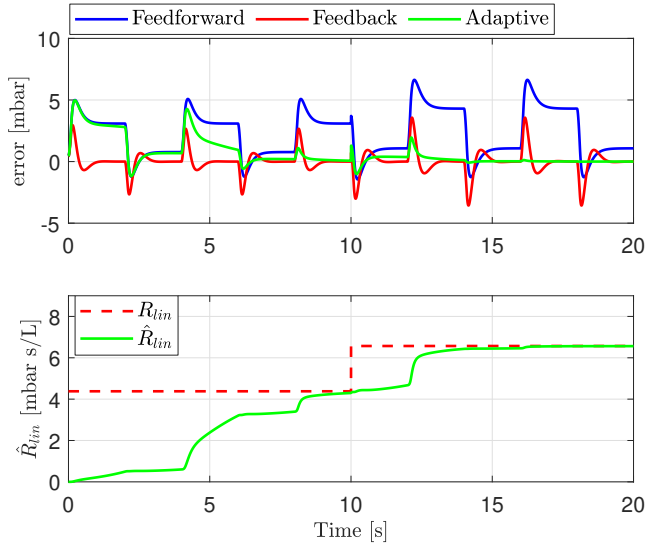


Fig. 2.7. Tracking errors of the different controllers and convergence of \hat{R}_{lin} of the adaptive controller.

is undesired overshoot and undershoot caused by the feedback controller. This results in non-optimal patient support. More specifically, the undershoot in pressure causes overshoot in the patient flow, see the zoomed inset in the bottom figure of Fig. 2.6. Overshoot in patient flow may result in false triggers during ventilation modes that allow for patient-triggered breaths, see Van de Wouw et al. (2018). The resulting airway pressure of the developed adaptive controller is also displayed in Fig. 2.6. It shows that during the first breathing cycle the proposed controller behaves almost the same as the feedforward controller. This is caused by the initial estimate of $\hat{R}_{lin}(0) = 0$, resulting in $\Delta\hat{p} \approx 0$ during the first breath, i.e., the adaptive controller is not compensating the pressure drop yet. In the third breathing cycle, almost perfect tracking with no overshoot and oscillations is achieved. Thereafter, at $t = 10$ s, the controller has to adapt to the step in R_{lin} , which introduces a deviation between the target pressure p_{target} and the airway pressure p_{aw} . This has almost completely vanished after the fifth breathing cycle.

In Fig. 2.7, the significant improvement in tracking performance is visualized. The tracking error of the adaptive controller indeed converges to zero. The tracking errors of the feedforward and feedback controllers remain the same over successive breaths, with a slight increase when the hose resistance is increased. Furthermore, this figure shows that the estimated resistance is converging to the actual value, as expected. Therefore, no manual calibration of the hose is required, such that no additional time of the hospital staff is required. It is also clearly observed that the controller can handle the step in

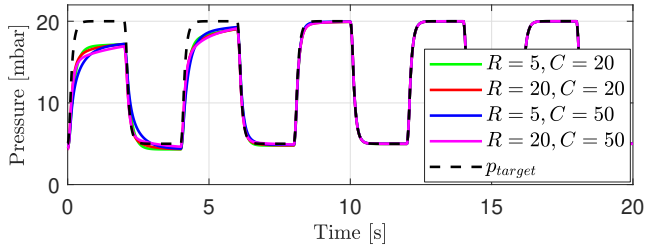


Fig. 2.8. Airway pressure p_{aw} for multiple types of lungs, with the adaptive controller. The lung characteristics are given in the legend where the units for R are mbar s/L and the units for C are mL/mbar.

hose resistance, since the tracking error is converging to zero again after the step in resistance.

Convergence of the estimator takes about 10 seconds, i.e., 2-3 breaths. In practice, this is sufficiently fast because a patient breathes over 20,000 times a day. Therefore, these three breaths are considered negligible in practice. Furthermore, a manual calibration typically takes longer, during which the patient is not ventilated at all. Therefore, the adaptive scheme is preferred over a manual calibration procedure.

Pressure profiles for different lung characteristics (resistance and compliance, see legend) are displayed in Fig. 2.8. This figure shows that the control approach works for a broad range of patients. The patient parameters do affect the flow and, therewith, the estimator performance is slightly affected. However, the estimator will converge and the compensation ultimately achieves perfect tracking independent of the patient parameters.

2.5.1.3 Main conclusions

The simulations show that the estimation error $e_{LS}(t)$ converges to zero and, therewith, the tracking error $e(t)$ converges to zero as well, as expected from Section 2.4.3. Furthermore, the simulations show that there is no overshoot in patient flow, preventing false triggering of breaths. It is also shown that the adaptive controller works for a broad range of patients and is able to handle changes in the hose resistance.

2.5.2 Scenario with spontaneously breathing patients

Since many patients are conscious, and therewith able to breathe them selves, another common ventilation mode is considered, namely, CPAP. CPAP aims to maintain a constant positive airway pressure to assist the patient's breathing and to keep the lungs open. Also this section is divided in the test case description, the simulation results, and a summary of the main conclusions.

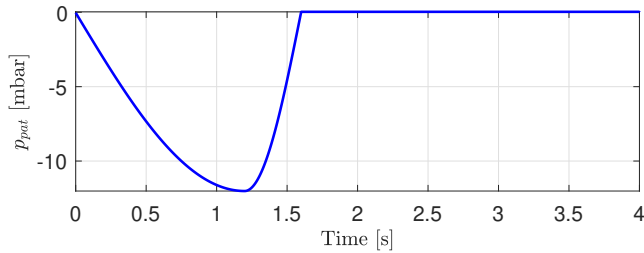


Fig. 2.9. Figure of the patient effort of the spontaneously breathing patient. This patient effort is used in the simulations and experiments.

2.5.2.1 Test case

The considered patient has a respiratory rate of 15 breaths per minute and generates a pressure of -12 mbar in the lungs. The patient effort profile is a semi-sinusoidal profile, similar to semi-sinusoidal profile of the ASL 5000 Breathing Simulator, which is used in the experiments in Section 2.6. The patient effort curve is depicted in Fig. 2.9. Note that there is no consensus on how to model realistic patient effort according to Olivieri et al. (2011). However, the default semi-sinusoidal of the ASL 5000 Breathing Simulator is most often used according to Fresnel et al. (2014). The target pressure used in this simulation is 5 mbar. Furthermore, we used the same control and patient-hose parameters as in the previous section, see Table 2.1.

2.5.2.2 Simulation results

The resulting airway pressure p_{aw} for the feedforward, feedback, and adaptive controller are depicted in Fig. 2.10. It is clearly shown that the airway pressure converges to the desired constant pressure with the adaptive controller. In the other two control approaches, we observe undesired pressure oscillations, caused by the patient's effort, around the pressure target. This case study shows that the developed adaptive controller improves tracking performance significantly during CPAP ventilation.

2.5.2.3 Main conclusions

These simulations show that the tracking performance is improved, see Fig 2.10. The adaptive controller achieves exact tracking of the desired airway pressure, whereas the feedforward and feedback controller show significant spikes in the airway pressure, caused by the patient's effort.

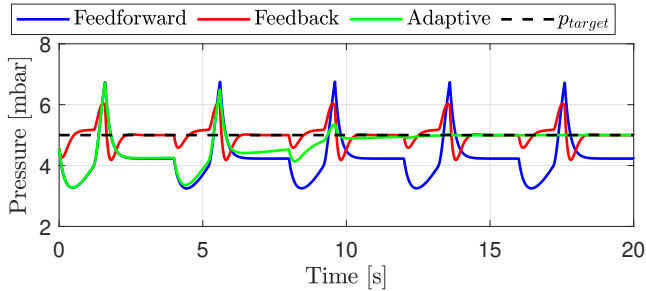


Fig. 2.10. Simulation results of the feedforward, feedback, and adaptive control strategy. This figure shows the resulting airway pressure of a spontaneously breathing patient with the CPAP ventilation mode.

2.6 Experimental case study

In order to show the practical applicability and performance of the adaptive controller, an experimental case study has been conducted. First of all, the results of two experiments for the scenario of a fully sedated patient on PCV are shown. Thereafter, the results for the scenario of a spontaneously breathing patient with CPAP ventilation are presented.

The main components of the experimental setup used in this case study are depicted in Fig. 2.11. In Fig. 2.11a, a blower-driven mechanical ventilation module of Macawi is depicted (DEMCON Macawi respiratory systems, Best, The Netherlands). Inside this module, the commercially available Macawi respiratory centrifugal blower with its custom motor and motor controller are used for actuation of the system. The blower flow Q_{out} is measured using a MEMS thermal flow sensor inside the respiratory module. The airway pressure p_{aw} and the blower outlet pressure p_{out} are both measured using a gauge pressure sensor inside the respiratory module. The ventilator is attached to a dSPACE system (dSPACE GmbH, Paderborn, Germany), where the controls are implemented using MATLAB Simulink (MathWorks, Natick, MA) running at a sampling frequency of 500 Hz.

Furthermore, the ASL 5000™ Breathing Simulator (IngMar Medical, Pittsburgh, PA), as depicted in Fig. 2.11b, is used to emulate the patient. This lung simulator can be used to emulate a wide variety of patients with a linear resistance and compliance. Furthermore, it is able to simulate a patient with breathing effort.

The patient and controller parameters in the experiments are the same as the corresponding parameters in the simulations of Section 2.5, see Table 2.1. However, the hose and leak resistance in the simulations are estimated using an offline least squares fit of the actual hose resistance, this results in a slight parametric difference between the simulation and experimental scenarios.

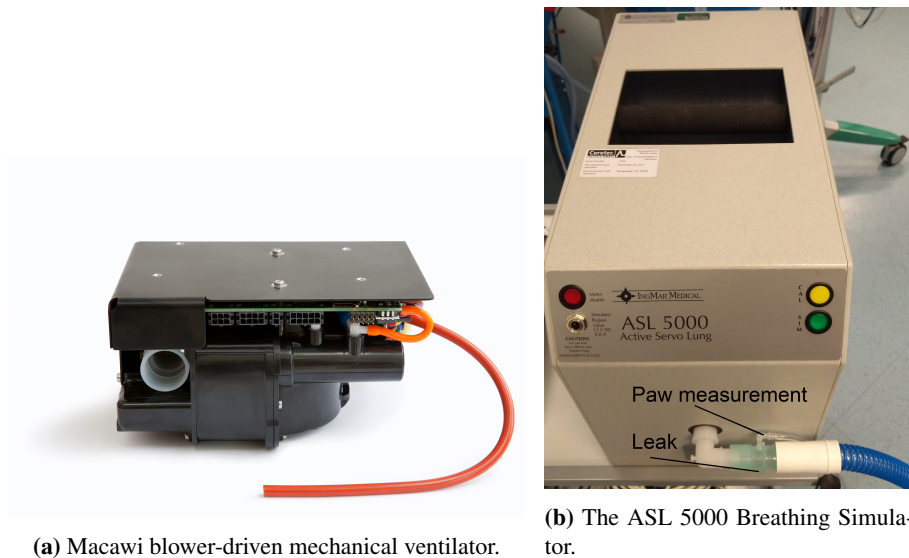


Fig. 2.11. The main components of the experimental setup.

2.6.1 Scenario with sedated patients

In this section, ventilation of a sedated patient under PCV is considered. This section is divided in the test case description, experimental results, and a summary of the main conclusions.

2.6.1.1 Test case

The same patient and controller parameters as in the simulation case study for sedated patients are used, see Table 2.1. Furthermore, two different target profiles are considered. First of all, a target profile is used with a PEEP and IPAP of 5 and 10 mbar, respectively. This first test case, with low pressures, is considered to validate the developed control strategy and its theory. These low pressures result in low flows, hence, the linear component of the hose resistance is dominant over the quadratic part. Thereafter, the same target profile as in the simulation case study is used with a PEEP and IPAP of 5 and 20 mbar, respectively. Another difference with the simulation-based case study is that the hose resistance in the experiments is constant. In other words, the experiments do not contain a step in the hose resistance.

2.6.1.2 Experimental results

First of all, the results of the experiments with the IPAP of 10 mbar are presented and discussed. Thereafter, the results of the experiments with the IPAP of 20 mbar are

shown and discussed.

The results of the experiments with the IPAP of 10 mbar are displayed in Fig. 2.12 and 2.13. The airway pressure and tracking error $e = p_{target} - p_{aw}$ are depicted in this figure. The figure clearly shows the constant offset in the airway pressure for the unit feedforward controller. Furthermore, it is clearly shown that the feedback controller has significant overshoot and undershoot. As expected, the adaptive controller converges after approximately 3 breaths, see Fig. 2.13. The resistance estimate is slightly oscillating upon convergence, this is caused by the quadratic nature of the hose-resistance. However, these oscillations are considered small because the outlet flow Q_{out} remains in a small interval. Fig. 2.12 shows that upon convergence the adaptive controller achieves significantly better tracking performance than the feedforward controller. Furthermore, the adaptive controller shows significantly less overshoot and undershoot than the linear feedback controller. These overshoots are undesired because the resulting peak pressures might damage the lungs. Furthermore, the undershoot is undesired since it causes oscillations in the patient flow possibly resulting in false triggering. Considering the tracking error in the bottom figure of Fig. 2.12, it is noticed that still sharp peaks are present during the increase and decrease of the pressure, for both feedback control strategies. These peaks are mainly caused by a delay in the blower transfer from $p_{control}$ to p_{out} and the measurement delay of the airway pressure p_{aw} . The blower delay causes a timing mismatch between the desired controller pressure $p_{control}$ and the blower outlet pressure p_{out} . Furthermore, the measurement delay of the airway pressure p_{aw} causes a timing mismatch between the performance variable p_{aw} and the target pressure p_{target} . This measurement delay is clearly visible in the tracking error during changes of p_{target} .

The results of the experiments with the IPAP of 20 mbar are displayed in Fig. 2.14 and 2.15. The obtained response is similar to the simulations for both the feedback as the feedforward controller. The feedforward controller does not compensate the pressure drop over the hose. The feedback controller shows overshoot and undershoot in airway pressure p_{aw} . This causes overshoot in the patient flow, which might cause false triggering in triggered ventilation modes. Hence, such overshoots are highly undesired.

The adaptive controller shows convergence of the airway pressure during the first few strokes. Thereafter, a clear decrease in overshoot and undershoot compared to the linear feedback controller is seen. The reduction in overshoot prevents ventilator-induced lung injury caused by peak pressures. Furthermore, the reduction in undershoot is beneficial in preventing oscillations in the patient flow. These oscillations are unpleasant for the patient and might result in false ventilator induced triggering. Therefore, the adaptive controller improves patient comfort and consistency of the treatment. Besides all these improvements, during the 5th breath the adaptive controller is slightly overcompensating the pressure drop, causing overshoot in the airway pressure, see Fig. 2.14. This is explained by the fact that a linear resistance model is used to estimate the quadratic hose resistance of the actual hose. This causes the estimator to overestimate the resistance during the start of inhalation. The high flows during in-

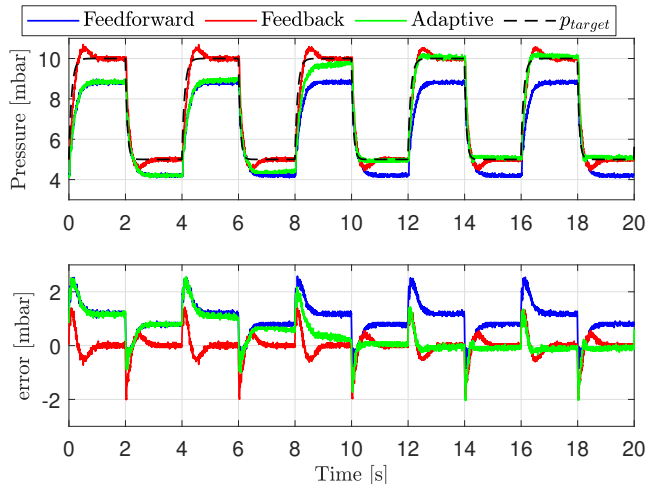


Fig. 2.12. Experimental results of the feedforward, feedback, and adaptive control strategy. This figure shows the resulting airway pressure and tracking error of the different controllers with a target pressure of PEEP and IPAP of 5 and 10 mbar, respectively.

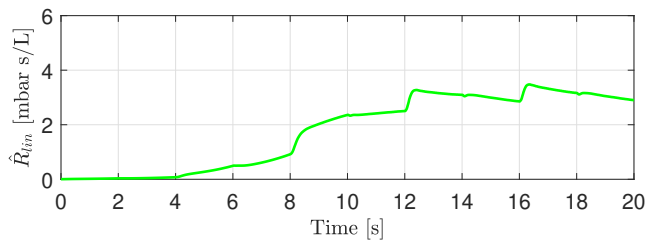


Fig. 2.13. Experimentally obtained estimate of the hose resistance for a target pressure of PEEP and IPAP of 5 and 10 mbar, respectively.

halation result in a large contribution of the quadratic term to the pressure drop. When the flow has converged to a steady value during the remainder of the inhalation, the controller will overcompensate the pressure drop, causing the pressure to exceed IPAP level. This oscillation of the estimated resistance is clearly shown in Fig. 2.15.

A visualization of the resistance estimate \hat{R}_{lin} compared to the actual resistance is depicted in Fig. 2.16. This figure shows the pressure drop Δp over the hose on the left vertical axis and the flow through the hose Q_{out} on the horizontal axis. The estimated resistance model, i.e., after 16 seconds in Fig. 2.15, is depicted by the blue area, the estimated resistance model is oscillating in this area. The blue dots show the actual measured resistance model of the hose. This shows that the estimate is still fairly

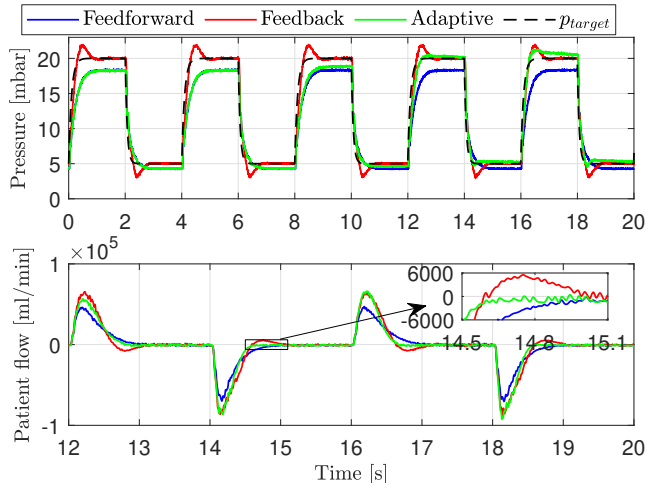


Fig. 2.14. Experimental results of the feedforward, feedback and adaptive control strategy. This figure shows the resulting airway pressure and patient flow with a target pressure of PEEP and IPAP of 5 and 20 mbar, respectively.

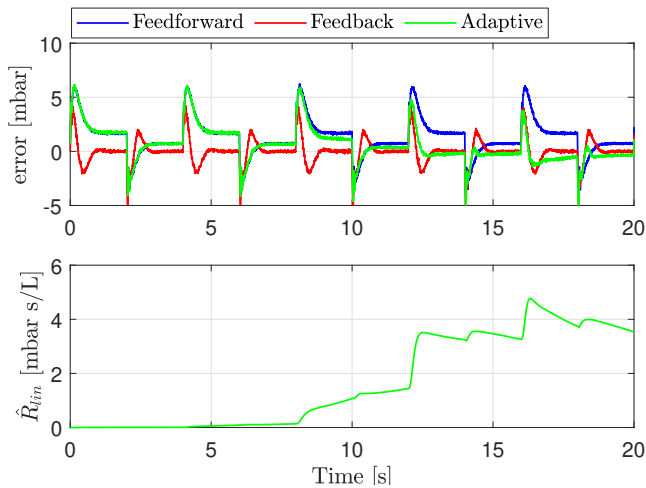


Fig. 2.15. Tracking errors of the different controllers and convergence of \hat{R}_{tin} of the adaptive controller with a target pressure of PEEP and IPAP of 5 and 20 mbar, respectively.

accurate in the low outlet flow area, up to 4×10^4 ml/min. The histogram in Fig. 2.16 displays how often a given flow is measured. Since the flow is mainly in the low flow

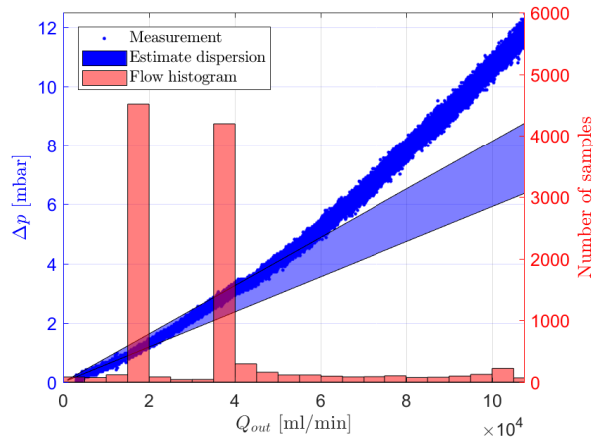


Fig. 2.16. Variation of the estimated hose model, linear resistance with estimated \hat{R}_{lin} , with the actual measured model with a target pressure of PEEP and IPAP of 5 and 20 mbar, respectively. Maximum flow in this figure is the same as the maximum flow Q_{out} through the hose in the experiment.

regime, the linear estimate is fairly accurate on average.

2.6.1.3 Main conclusions

This experimental study shows that the adaptive controller is practically applicable to sedated patients under PCV. The experimental study with low flows shows that the tracking error converges to zero and decreases overshoot and undershoot significantly compared to the linear feedback controller. The error is clearly converging to zero except for the region where the pressure is increasing and decreasing. In these areas the controller is responding slightly too late, which is mainly caused by the presence of delays in the system. In the experimental case study with higher pressures and flows, the tracking error decreased significantly compared to the state-of-practice controllers. In particular, the adaptive controller prevents overshoot in patient flow, which prevents false triggering. It should be noted that performance could be further improved by using a quadratic resistance model in the adaptive controller; this could prevent oscillations of the resistance estimate. Furthermore, it may improve the accuracy of the estimated pressure drop and therewith the tracking performance. To improve performance even further, the delays in the system should be analyzed and compensated in the control strategy. The latter two aspects are considered outside the scope of this work.

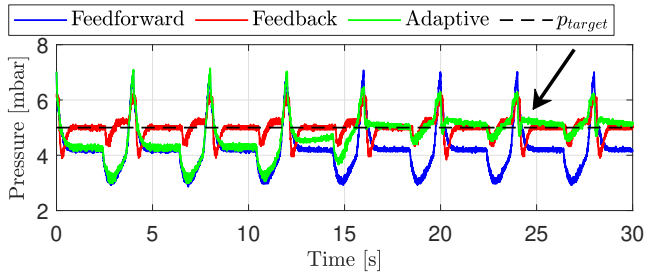


Fig. 2.17. Experimental results of the feedforward, feedback, and adaptive control strategy. This figure shows the resulting airway pressure of a spontaneously breathing patient with the CPAP ventilation mode.

2.6.2 Scenario with spontaneously breathing patients

In this section, the results of an experiment with a spontaneously breathing patient under CPAP ventilation are presented and discussed. Again, the section is divided in the same subsections, i.e., the test case description, experimental results, and a summary of the main conclusions.

2.6.2.1 Test case

The same setup, i.e., patient, hose, leak, and controllers are used as in the previous experiments. Furthermore, the patient effort is the same as in the simulations and is depicted in Fig. 2.9. This profile is generated by the ASL 5000 Breathing Simulator, which is used in the experiments. The target pressure used in this simulation is 5 mbar.

2.6.2.2 Experimental results

The resulting airway pressure for all three controllers is depicted in Fig. 2.17. The feedforward and feedback controller show results comparable to the simulations. The adaptive controller shows an improvement in tracking performance. The biggest improvement is the decrease in undershoot, see the arrow in Fig. 2.17. Furthermore, the same problem as for the fully sedated patient is seen; the controller is slightly overestimating the resistance during inhalation. This causes the pressure to be slightly higher than desired after inhalation and it is slowly converging to the desired value, see Fig. 2.17. Furthermore, the figure shows some peaks when the patient starts and ends inhalation, this indicates that the controller does not respond fast enough to the patient-induced disturbance.

2.6.2.3 Main conclusions

This experimental case study shows that the adaptive controller is practically applicable to spontaneously breathing patients as well. The overall performance is improved over the state-of-practice controllers. However, it shows oscillations in the patient airway pressure p_{aw} , whereas the simulations showed exact convergence.

Concluding, the adaptive controller shows an overall improvement in performance over the state-of-practice controllers. However, performance of the adaptive controller could be further improved by using a more realistic hose model, i.e., including a quadratic term. Another problem that affects the performance in experiments is the delay in the sensor line of the airway pressure. This delay causes a timing mismatch between the measured signals. Compensation for this delay in the estimator might improve performance as well.

2.7 Conclusions and recommendations

In this chapter, an adaptive control approach for mechanical ventilation is presented. This control approach aims to improve tracking performance for large variations of patient-hose parameters, unintended leakages, and unknown patient breathing efforts. It has been shown through stability analysis that this controller ensures exact tracking of the desired pressure set-point, independent of the patient-hose parameters, unintended leakages, and unknown breathing efforts. Using this control approach requires no additional calibration of the hose-filter system, which saves valuable time in the intensive care unit of a hospital.

Furthermore, using a simulation study, it is shown that the adaptive controller achieves exact tracking, and therewith improves tracking performance significantly over state-of-practice controllers. Through an experimental case study it is shown that the controller is practically applicable. In these experiments, the adaptive controller shows an improvement in pressure tracking performance, i.e., improved rise-time, less overshoot and undershoot, and faster settling times, compared to the state-of-practice linear feedback controller. Furthermore, it prevents overshoot in patient flow, which might prevent false triggers and improve patient comfort.

To improve the performance in practice, the adaptive controller could be extended to contain a quadratic hose resistance term. Furthermore, the delays in the system should be incorporated in the controller design. This might prevent the oscillations of the hose resistance estimate, resulting in improved tracking performance in practice.

In future work other control methods should be considered to improve control performance of mechanical ventilation further. A key example is a data-driven control method, namely, repetitive control. Repetitive control makes use of tracking errors during previously executed tasks to improve performance in the current task. Therefore, it is particularly suitable for a repetitive process such as ventilation.

2.A Appendix

The lemmas presented in this Appendix are used to prove Lemma 2.1 and Theorem 2.1, in Section 2.4.3. Lemmas 2.2 to 2.4 below serve as auxiliary results to Lemma 2.5, in which boundedness of $Q_{out}(t)$ is shown. First, Lemma 2.2 shows that $P(t)$ is always non-negative.

Lemma 2.2. *Consider the covariance dynamics in (2.26) and suppose that Assumption 2.1 holds. Then, $P(t) > 0$ for all $t \geq 0$.*

Proof. Using (2.26), it can be concluded that sufficiently small positive P results in $\dot{P} > 0$. Hence, $P(t) > 0$ for all $t \geq 0$ if Assumption 2.1 ($P(0) > 0$) holds. \square

In Lemma 2.3, it is proven that $|e_{LS}(t)|$ is non-increasing (and bounded), hence, the sign of $e_{LS}(t)$ will never change.

Lemma 2.3. *Consider the least squares error dynamics in (2.27) and suppose that Assumption 2.1 holds. Then, $|e_{LS}(t)|$ is non-increasing (and bounded) for all $t \geq 0$ and the sign of $e_{LS}(t)$ will never change.*

Proof. The differential equation governing the dynamics of e_{LS} is given in (2.27), this can be written as $\dot{e}_{LS} = -\alpha(t)e_{LS}$, with $\alpha(t) := P \frac{Q_{out}^2(t)}{m^2}$. From Lemma 2.2, the fact that $Q_{out}^2(t) \geq 0$, and $m^2 > 0$, it is ensured that $\alpha(t) \geq 0$ and thus that $|e_{LS}(t)|$ is non-increasing (and bounded) for all $t \geq 0$ and the sign of $e_{LS}(t)$ will never change. \square

In Lemma 2.4, boundedness of p_{lung} is shown.

Lemma 2.4. *Consider the lung dynamics in (2.16) and suppose that Assumption 2.1, 2.2, and 2.3 hold. Then, $p_{lung}(t)$ is bounded for all $t \geq 0$.*

Proof. First, it should be noted that p_{target} is bounded by design (Assumption 2.2) and \dot{p}_{pat} is bounded (Assumption 2.3). Therefore, p_{lung} (see (2.16)) is bounded if, firstly, $\frac{-R_{leak} - e_{LS}}{C_{lung}(e_{LS}(R_{leak} + R_{lung}) + R_{leak}R_{lung})}$ remains negative and bounded for all $t \geq 0$, note that e_{LS} is bounded, see Lemma 2.3 and, secondly, $e_{LS}(R_{leak} + R_{lung}) + R_{leak}R_{lung}$ is bounded away from zero, i.e., $|e_{LS}(R_{leak} + R_{lung}) + R_{leak}R_{lung}| > \epsilon$, for some $\epsilon > 0$, for all $t \geq 0$. If these conditions hold, \dot{p}_{lung} in (2.16) has the opposite sign of $p_{lung}(t)$ for large enough values of $|p_{lung}(t)|$ and therefore $p_{lung}(t)$ is bounded. The following inequalities ensure the required properties:

- (I) $e_{LS}(t) > -R_{leak}, \forall t \geq 0$
- (II) $e_{LS}(t) \geq -\frac{R_{leak}R_{lung}}{R_{leak} + R_{lung}} + \epsilon, \forall t \geq 0$ for some $\epsilon > 0$.

Using Lemma 2.3, it is obtained that both inequalities, (I) and (II), hold for all $t \geq 0$ if these hold at $t = 0$, since the sign of e_{LS} will not change and $|e_{LS}|$ is non-increasing. Using $e_{LS} := R_{lin} - \hat{R}_{lin}$, it is obtained that both inequalities, (I) and (II), are ensured by Assumption 2.1, hence p_{lung} is bounded for all $t \geq 0$. \square

Finally, in Lemma 2.5 boundedness of $Q_{out}(t)$ is ensured.

Lemma 2.5. *Consider the output flow $Q_{out}(t)$ induced by the dynamics (2.17) and (2.18) and suppose that Assumptions 2.1, 2.2, and 2.3 hold. Then, for all $t \geq 0$, $Q_{out}(t)$ is bounded, hence, $Q_{out}(t) \in \mathcal{L}_\infty$.*

Proof. $Q_{out}(t)$ is characterized by (2.17) and (2.18). Since p_{lung} is bounded (Lemma 2.4) and p_{target} is bounded by design (Assumption 2.2), $Q_{out}(t)$ is bounded if $e_{LS}(R_{leak} + R_{lung}) + R_{leak}R_{lung}$ is bounded away from zero for all $t \geq 0$, see the expression $Q_{out}(t)$ in (2.17) and (2.18). The latter is ensured as well, as shown in the proof of Lemma 2.4. Since $Q_{out}(t)$ is bounded, we also know that $Q_{out}(t) \in \mathcal{L}_\infty$. \square

Accurate pressure tracking to support mechanically ventilated patients using an estimated nonlinear hose model and delay compensation

Abstract – Tracking of a desired pressure profile is key in mechanical ventilation to sufficiently support a patient. The aim of this chapter is to improve pressure tracking performance of mechanical ventilation systems. This is achieved by explicitly taking into account the nonlinear hose characteristics and delays in the control strategy. Through an experimental case study it is shown that this can significantly improve tracking performance.

3.1 Introduction

Mechanical ventilation is used in Intensive Care Units (ICUs) to support breathing of patients. The main goals of mechanical ventilation are to ensure oxygenation and carbon dioxide elimination (Warner and Patel, 2013). In the past decades, demand for ventilation has increased rapidly and is prospected to increase further in the coming years (Needham et al., 2005). Especially during the flu season or a world-wide pandemic such as the COVID-19 pandemic that started in 2019, demand for mechanical ventilation is high. Improved ventilation is desired to reduce overall ventilation time.

Mechanical ventilators are a life-saving device. A schematic overview of a mechanical ventilator, with a single-hose setup and a patient is depicted in Fig. 3.1. In this chapter, a blower-driven single-hose setup as depicted in Fig. 3.1 and Pressure Con-

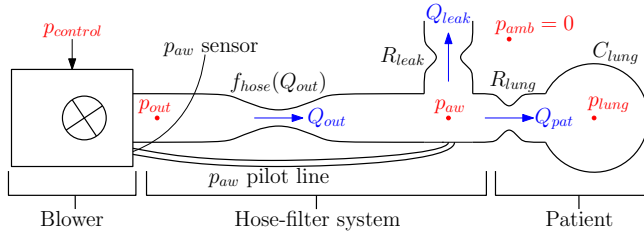


Fig. 3.1. Schematic representation of the blower-hose-patient system, with the corresponding resistances, lung compliance, pressures, and flows.

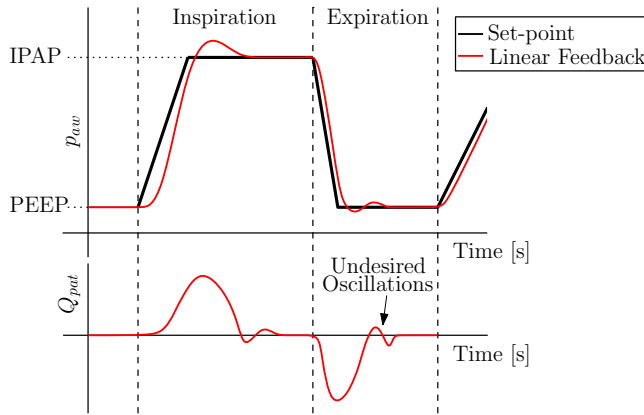


Fig. 3.2. Airway pressure p_{aw} and patient flow Q_{pat} during one breathing cycle of pressure controlled ventilation.

trolled Ventilation (PCV) of sedated patients are considered. In PCV, the mechanical ventilator aims to track a pressure profile near the patient's mouth as determined by the clinician, see Fig. 3.2. The Inspiratory Positive Airway Pressure (IPAP) and Positive End-Expiratory Pressure (PEEP) induce flow in and out of the lungs, respectively. This alternating flow of air allows the lungs to exchange CO_2 for O_2 in the blood. The objective of the control system is to achieve accurate tracking of the desired target pressure profile and therewith to achieve the desired ventilation of the patient.

Accurate tracking of the target pressure is important to achieve sufficient support for the patient, especially in cases of large flows as a result of large lungs and/or unintentional leaks during non-invasive ventilation. Furthermore, accurate pressure tracking results in better patient-ventilator synchrony (Hunneken et al., 2020). According to Blanch et al. (2015), asynchrony between patient and machine is associated with high mortality.

A large number of control strategies have been investigated to improve the performance of mechanical ventilators. In Borrello (2005), an overview of modeling and con-

control techniques for mechanical ventilation is presented. In Van de Wouw et al. (2018) and Hunnekens et al. (2020), variable-gain control is proposed to overcome the trade-off between fast pressure rise times and limited overshoot in patient flow. This variable-gain control strategy shows a reduction in patient flow overshoot. However, still some overshoot remains and the measured patient flow is used in this control strategy. The patient flow is typically not available for control in practice. In Borrello (2001), an adaptive control strategy is applied to mechanical ventilation. A patient model is estimated and the obtained parameters are used to adapt the controller parameters to achieve the desired closed-loop behavior. In practice, it is challenging to obtain accurate patient models, deteriorating performance of such strategies. Also funnel-based control is applied to mechanical ventilation (Pomprapa et al., 2015). However, the improvement in tracking performance is limited. In Scheel et al. (2017) and Li and Haddad (2012), model-based control and model predictive control are applied, respectively. Also these methods require accurate patient models, which are typically not available in practice. Furthermore, iterative learning control is applied in Scheel et al. (2015) and repetitive control is applied in Reinders et al. (2020). These methods achieve superior performance in case of a fully sedated patient, i.e., the reference is repetitive. However, in case a patient starts breathing spontaneously, performance of these methods degrades. Finally, in Reinders et al. (2019) and Reinders et al. (2021b), an adaptive control scheme is proposed. This control scheme estimates a *linear* hose-resistance model during ventilation and uses this model to compensate the pressure drop over the hose. In an experimental study, it is shown to improve performance significantly. However, overshoot and long settling times are observed in case of large flow variations. These performance limitations are mainly due to delays and nonlinearities in the system which are neglected.

Although the mentioned control approaches show a significant improvement in tracking performance, most of them are neglecting system delays and the nonlinear characteristics of the hose. The aim of this chapter is to develop a control method that automatically estimates the nonlinear characteristics of the hose while taking the relevant system delays into account. The estimated hose model is used to improve tracking performance. The control method in Reinders et al. (2021b) is recovered as a special case of the method proposed in this chapter in case of no system delays and nonlinearities of the hose.

The main contribution of this chapter is a control strategy that improves pressure tracking performance by explicitly taking into account delays and the nonlinear hose characteristics of ventilation systems. Specific contributions include the following. First, a control strategy with a linear hose-resistance estimator is presented that compensates the measurement delays in the system. Second, an input-to-state stability proof of the closed-loop dynamics with this control strategy is provided. Third, a control strategy that takes into account the nonlinear characteristics of the hose-resistance is developed. Fourth, an experimental case study evidences a significant improvement in tracking performance.

The outline of this chapter is as follows. In Section 3.2, the detailed problem def-

initiation is given. Then, in Section 3.3, a high-level description of the proposed control strategy is given. In Section 3.4, linear models of the open-loop and closed-loop plant with delays are presented. Thereafter, in Section 3.5, the linear resistance estimator with delay compensation is presented. Then, in Section 3.6, the nonlinear estimator with delay compensation and the nonlinear pressure drop compensation are presented to cope with the nonlinear hose characteristics. In Section 3.7, a simulation case study of the linear estimator is presented to show the effectiveness of delay compensation. Thereafter, in Section 3.8, the results of an experimental case study are presented. This experimental case study shows a clear performance improvement by taking measurement delays and the nonlinear hose characteristics into account. Finally, in Section 3.9, the main conclusions of this work are given.

3.2 Problem formulation

3.2.1 Control goal

The control goal in PCV is to achieve accurate pressure tracking of a time-varying pressure target $p_{target}(t)$ for a wide variety of patients. In Fig. 3.2 an example of such target pressure profile is shown. The controlled variable is the airway pressure p_{aw} , i.e., the pressure near the patient's mouth. The airway pressure is measured using the pilot line and a pressure sensor inside the module, see Fig. 3.1. The goal is to ensure that the tracking error

$$e(t) := p_{target}(t) - p_{aw}(t), \quad (3.1)$$

is small, i.e., $|e(t)|$ is small for all $t \geq 0$.

3.2.2 System description

The blower-patient-hose system is depicted in Fig. 3.1. The main components in the system are the blower, the hose-filter system, and the patient. The blower compresses ambient air to change the blower outlet pressure p_{out} , such that the airway pressure p_{aw} tracks the desired target pressure. The difference between the outlet pressure p_{out} and the airway pressure p_{aw} results in a flow through the hose Q_{out} , related by the hose resistance model $R_{hose}(Q_{out})$. $R_{hose}(Q_{out})$ can refer to different hose models, in this chapter $R_{hose}(Q_{out})$ refers to the considered linear and a quadratic hose model. The change in airway pressure p_{aw} results in two flows, namely, the leak flow Q_{leak} and the patient flow Q_{pat} . The leak flow is used to flush exhaled CO_2 -rich air from the hose and is modeled using a linear leak resistance R_{leak} . The patient flow is a result of the linear resistance R_{lung} and the difference between the airway pressure and the lung pressure p_{lung} , i.e., the pressure inside the lungs. The patient flow results in a change in the lung pressure. The relation between patient flow and lung pressure is given by the linear lung compliance C_{lung} . This patient model, defined by C_{lung} and R_{lung} , is

referred to as the linear one-compartmental lung model, analyzed in Bates (2009, pp. 37–60). Note that for notational convenience all pressures are defined relative to the ambient pressure, i.e., $p_{amb} = 0$. A mathematical description of the system dynamics is derived in Section 3.4.

3.2.3 Control relevant system properties

As mentioned in Section 3.1, previously developed control strategies for mechanical ventilation often neglect several essential system properties. The properties addressed in this chapter are 1) time delays and 2) nonlinear hose characteristics. Another challenge for mechanical ventilation is that it should achieve the desired performance for a wide range of patients.

Several components depicted in Fig. 3.1 introduce time delays. Two delays are caused by the propagation speed of a pressure wave through air as mentioned in Borrello (2005). The first pressure propagation delay is the hose delay τ_h from p_{out} to p_{aw} . This delay is defined as the time it takes for a pressure wave to propagate through the hose, i.e., from the blower outlet to the patient's airway. The second pressure propagation delay is the pilot-line delay τ_p from p_{aw} to the p_{aw} sensor, which represents the time it takes for a pressure wave to propagate through the pilot line. For simplicity τ_h and τ_p are lumped into one output delay from p_{aw} to the p_{aw} -sensor called the sensor delay $\tau_s = \tau_h + \tau_p$. The third delay is a delay in the blower dynamics. More specifically, it is a delay from the control input $p_{control}$ to the blower outlet pressure p_{out} . A method to partially compensate for these delays is presented in Section 3.5.

In Fig. 3.3, the measured hose resistance characteristics clearly shows a quadratic relation between the flow through the hose Q_{out} and the pressure drop over the hose $\Delta p := p_{out} - p_{aw}$. These nonlinear hose characteristics are often approximated by a linear hose-resistance model. In Fig. 3.3 it is shown that the linear models accurately describe the hose-characteristics for a small flow range, in particular in the low flow regime. However, for a large flow range a quadratic model is significantly more accurate. Therefore, in Section 3.6, a control strategy is presented that incorporates a nonlinear hose-resistance model.

Concluding, a control strategy for mechanical ventilation should achieve accurate pressure tracking performance for a wide range of patients. In previous work, the system delays and nonlinear hose characteristics are often neglected. Therefore, in this chapter a control strategy is presented that takes these system properties into account to improve pressure tracking performance for a variety of patients.

3.3 Proposed high-level control strategy

A controller for mechanical ventilation has to ensure that the airway pressure p_{aw} tracks the target pressure p_{target} . The main cause of a difference in these pressures is the pressure drop over the hose $\Delta p = p_{out} - p_{aw}$. By increasing p_{out} , such that $p_{out} =$

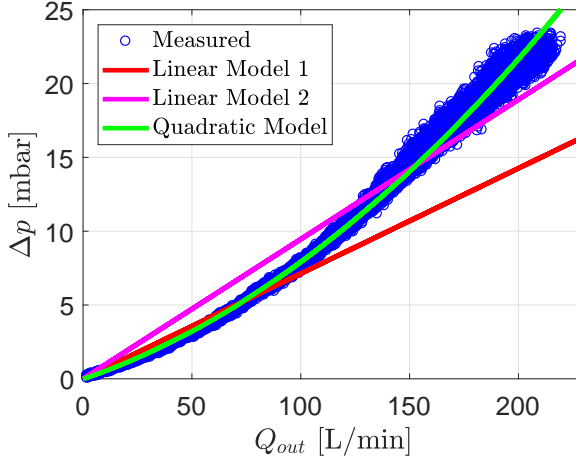


Fig. 3.3. Calibration curve of the hose with two linear resistance models and a quadratic resistance model. This figure clearly shows the nonlinear nature of the hose resistance.

$p_{target} + \Delta p$, p_{aw} will be equal to p_{target} . In the developed control strategy a hose-resistance model is used to estimate Δp as a function of the measured flow through the hose Q_{out} and hose-resistance parameters. The hose-resistance parameters can be obtained using an estimator. Because Q_{out} is measured and used in the control loop, this strategy is independent of the attached patient type as long as the hose-resistance parameters are obtained correctly.

A block diagram of the developed control strategy is depicted in Fig. 3.4. The blower, patient-hose, and delay block denote the ventilation system dynamics. The estimator, $\hat{R}_{hose}(Q_{out})$, and delay blocks with $\hat{\tau}_s$ denote the proposed control strategy. The estimated hose-resistance model $\hat{R}_{hose}(Q_{out})$ and the measured flow through the hose Q_{out} are used in a feedback loop to estimate the pressure drop over the hose. By adding this estimated pressure drop $\Delta\hat{p}$ to the target pressure p_{target} , the airway pressure converges to the desired target pressure if the estimated hose model is correct. Because the hose characteristics are typically unknown in practice an estimator is used to estimate the parameters of the hose-resistance model during ventilation.

The block diagram in Fig. 3.4 has two dashed arrows; these dashed arrows distinguish between two different phases. Estimation of the hose-resistance model and compensation for the pressure drop are separated in two phases. In the estimation phase, the ventilator is controlled in open loop while estimating the hose parameters. After convergence, estimation is stopped and the obtained parameters are used in the compensation strategy, i.e., the compensation phase. In other words, only one of the two dashed lines is active simultaneously.

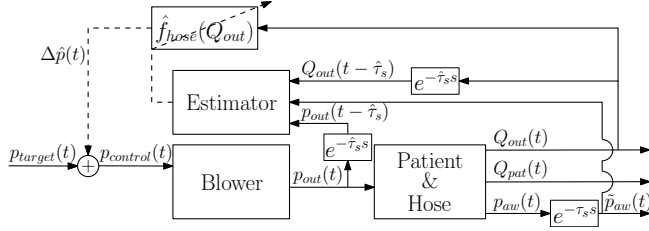


Fig. 3.4. Schematic representation of the proposed closed-loop system with an estimator for the hose resistance estimation. Furthermore, delay compensation for estimation is included. Only one of the dashed lines is active simultaneously. This means that either the hose model is estimated during open-loop control or the estimated hose model is used in the control loop.

The delays in the system and the nonlinear hose characteristics are explicitly taken into account in this control strategy. The output delay τ_s is compensated by delaying the estimator inputs that are unaffected by the delay τ_s . This is achieved by choosing $\hat{\tau}_s$ appropriately, this is described in detail in Section 3.5. To take the nonlinear hose characteristics in account a quadratic hose model is used for $\hat{R}_{hose}(Q_{out})$ of which the parameters are estimated by the estimator, this is described in detail in Section 3.6. The control method presented in Reinders et al. (2021b) is retrieved as a special case of the strategy presented in this chapter. In an experimental case study, it is shown that the method in this chapter outperforms the control strategy in Reinders et al. (2021b).

3.4 Linear closed-loop dynamics

In this section, the linear system dynamics with delays are presented. First of all, the open-loop system dynamics are presented in Section 3.4.1, i.e., the system dynamics in the estimation phase. Thereafter, in Section 3.4.2 the closed-loop system dynamics with a constant hose-resistance estimate are presented, i.e., the system in the compensation phase. The hose resistance is assumed to be linear throughout this section.

3.4.1 Open-loop system dynamics

To obtain the open-loop system dynamics, the patient is modeled using the linear one-compartmental lung model described in Bates (2009, pp. 37–60), i.e.,

$$\dot{p}_{lung}(t) = \frac{p_{aw}(t) - p_{lung}(t)}{C_{lung}R_{lung}}. \quad (3.2)$$

Furthermore, the hose, leak, and lung resistance are assumed linear, hence

$$Q_{out}(t) = \frac{\Delta p}{R_{lin}} = \frac{p_{out}(t) - p_{aw}(t)}{R_{lin}}, \quad (3.3)$$

$$Q_{leak}(t) = \frac{p_{aw}(t)}{R_{leak}}, \text{ and} \quad (3.4)$$

$$Q_{pat}(t) = \frac{p_{aw}(t) - p_{lung}(t)}{R_{lung}} \quad (3.5)$$

with R_{lin} the linear hose resistance, note that $R_{hose}(Q_{out})$ becomes $R_{lin}Q_{out}$ in case of the linear hose model.

Moreover, it is assumed that the internal blower controller achieves a blower transfer function from $p_{control}(t)$ to $p_{out}(t)$ of magnitude one. The presence of the blower delay τ_b results in the following relation between the blower outlet pressure p_{out} and the control pressure $p_{control}$:

$$p_{out}(t) := p_{control}(t - \tau_b). \quad (3.6)$$

Combining (3.2), (3.3), (3.4), (3.5), and (3.6), using conservation of flow, i.e., $Q_{out} = Q_{pat} + Q_{leak}$, results in the following open-loop system dynamics with blower delay:

$$\begin{aligned} \dot{p}_{lung}(t) &= A_h p_{lung}(t) + B_h p_{control}(t - \tau_b) \\ p_{aw}(t) &= C_h p_{lung}(t) + D_h p_{control}(t - \tau_b) \end{aligned} \quad (3.7)$$

with

$$\begin{aligned} A_h &= -\frac{R_{lin} + R_{leak}}{C_{lung}\bar{R}}, \quad B_h = \frac{R_{leak}}{C_{lung}\bar{R}}, \\ C_h &= \frac{R_{lin}R_{leak}}{\bar{R}}, \text{ and } D_h = \frac{R_{leak}R_{lung}}{\bar{R}} \end{aligned} \quad (3.8)$$

with $\bar{R} := R_{lin}R_{leak} + R_{lin}R_{lung} + R_{leak}R_{lung}$.

Furthermore, the lumped output delay τ_s , in the measurement of p_{aw} , results in

$$\tilde{p}_{aw}(t) := p_{aw}(t - \tau_s) \quad (3.9)$$

with \tilde{p}_{aw} the measured airway pressure.

3.4.2 Closed-loop error dynamics for a constant resistance estimate

In this section, the open-loop system dynamics defined in (3.7) and (3.8) are combined with the control strategy depicted in Fig. 3.4 for a constant linear hose model estimate \hat{R}_{lin} . Note that the hose-resistance estimate is considered constant; therefore, the measured airway pressure \tilde{p}_{aw} and the delay τ_s do not appear in these error dynamics.

From Fig. 3.4 it is obtained that

$$\begin{aligned} p_{control}(t) &= p_{target}(t) + \Delta\hat{p}(t) \\ &= p_{target}(t) + \hat{R}_{lin}Q_{out}(t), \end{aligned} \quad (3.10)$$

where the estimated pressure drop $\Delta\hat{p}$ is computed using (3.3). Next, $Q_{out}(t)$ is rewritten using conservation of flow, the patient model in (3.2), and the resistance models (3.4) and (3.5). This gives

$$Q_{out}(t) = Q_{pat} + Q_{leak} \quad (3.11)$$

$$= \frac{p_{aw}(t) - p_{lung}(t)}{R_{lung}} + \frac{p_{aw}(t)}{R_{leak}} \quad (3.12)$$

$$= C_{lung} \left(1 + \frac{R_{lung}}{R_{leak}} \right) \dot{p}_{lung}(t) + \frac{1}{R_{leak}} p_{lung}(t). \quad (3.13)$$

Substitution of (3.13) in (3.10) results in the control law

$$\begin{aligned} p_{control}(t) &= p_{target}(t) \\ &+ \hat{R}_{lin} \left(C_{lung} \left(1 + \frac{R_{lung}}{R_{leak}} \right) \dot{p}_{lung}(t) + \frac{1}{R_{leak}} p_{lung}(t) \right). \end{aligned} \quad (3.14)$$

Next, (3.14) is substituted in the open-loop dynamics of (3.7) and (3.8). This results in the closed-loop dynamics in terms of the state p_{lung} :

$$\begin{aligned} \frac{d}{dt} \left(p_{lung}(t) - \hat{R}_{lin}B_hC_{lung} \left(1 + \frac{R_{lung}}{R_{leak}} \right) p_{lung}(t - \tau_b) \right) \\ = A_h p_{lung}(t) + \frac{\hat{R}_{lin}B_h}{R_{leak}} p_{lung}(t - \tau_b) + B_h p_{target}(t - \tau_b). \end{aligned} \quad (3.15)$$

The patient model in (3.2) is rewritten to obtain:

$$p_{aw}(t) = \dot{p}_{lung}(t)C_{lung}R_{lung} + p_{lung}(t). \quad (3.16)$$

Substituting (3.16) in the error definition in (3.1) and differentiating with respect to time results in

$$\dot{e}(t) = \dot{p}_{target}(t) - \ddot{p}_{lung}(t)C_{lung}R_{lung} - \dot{p}_{lung}(t). \quad (3.17)$$

From (3.15),

$$\begin{aligned} \dot{p}_{lung}(t) &= \hat{R}_{lin}B_hC_{lung} \left(1 + \frac{R_{lung}}{R_{leak}} \right) \dot{p}_{lung}(t - \tau_b) \\ &+ A_h p_{lung}(t) + \frac{\hat{R}_{lin}B_h}{R_{leak}} p_{lung}(t - \tau_b) \\ &+ B_h p_{target}(t - \tau_b) \end{aligned} \quad (3.18)$$

and its time derivative are obtained and substituted in (3.17). Finally, rewriting gives the closed-loop error dynamics:

$$\begin{aligned} & \frac{d}{dt} \left(e(t) - \hat{R}_{lin} B_h C_{lung} \left(1 + \frac{R_{lung}}{R_{leak}} \right) e(t - \tau_b) \right) \\ &= A_h e(t) + \frac{\hat{R}_{lin} B_h}{R_{leak}} e(t - \tau_b) + w(t) \end{aligned} \quad (3.19)$$

with

$$\begin{aligned} w(t) &= \dot{p}_{target}(t) - C_{lung} R_{lung} B_h \dot{p}_{target}(t - \tau_b) \\ &\quad - B_h p_{target}(t - \tau_b) - A_h p_{target}(t) - \frac{\hat{R}_{lin} B_h}{R_{leak}} p_{target}(t - \tau_b) \\ &\quad - \hat{R}_{lin} B_h C_{lung} \left(1 + \frac{R_{lung}}{R_{leak}} \right) \dot{p}_{target}(t - \tau_b). \end{aligned} \quad (3.20)$$

These closed-loop error dynamics are described by a Neutral Delay Differential Equation (NDDE), i.e., the delay τ_b is present in both e and \dot{e} .

3.5 Output delay compensation and linear estimator design

In this section, a method to compensate the effect of the output delay τ_s on the estimator is presented. Thereafter, a linear resistance estimator is presented. Finally, stability of the controlled system is analyzed. In other words, the first and second contribution of this chapter are addressed in this section.

3.5.1 Output delay compensation

As mentioned in Section 3.2, the lumped output delay τ_s is considered. This delay represents the time it takes for the actual $p_{aw}(t)$ to propagate to the p_{aw} -sensor in the ventilation module. The actual measured airway pressure is $\tilde{p}_{aw}(t)$, see (3.9). In Fig. 3.4, a timing mismatch between the estimator inputs can be recognized when no delay compensation is included, i.e., $\hat{\tau}_s = 0$. Namely, $Q_{out}(t)$, $p_{out}(t)$, and $\tilde{p}_{aw}(t) = p_{aw}(t - \tau_s)$ are used by the estimator. This mismatch in timing results in oscillations of the estimated hose resistance parameters $\hat{R}_{hose}(Q_{out})$ when the ventilation dynamics are in a transient phase. If the ventilation system is in steady state $p_{aw}(t) = \tilde{p}_{aw}(t)$, hence, the delay does not affect the estimator inputs.

This mismatch in timing is solved by delaying $p_{out}(t)$ and $Q_{out}(t)$ before using them in the estimator, such that they match the timing of $\tilde{p}_{aw}(t) = p_{aw}(t - \tau_s)$. This is achieved by choosing the delay estimate $\hat{\tau}_s \approx \tau_s$ in Fig. 3.4. Choosing this estimate correctly, i.e., $\hat{\tau}_s = \tau_s$, results in matching timing of the estimator inputs. Several methods from literature can be used to identify the time delay $\hat{\tau}_s$ experimentally (Bjorklund

and Ljung, 2003). In the remainder of this chapter it is assumed that the parameter τ_s is known; hence, it can be compensated exactly in the estimator.

3.5.2 Linear estimator design

In this chapter, a Recursive Least Squares (RLS) estimator with exponential forgetting factor, see Ioannou and Sun (1996, p. 200), is used to estimate the linear hose resistance R_{lin} . Other estimators can be used with the same method to compensate for the output delay τ_s . The RLS estimator with delay compensation is designed as follows:

$$\begin{aligned} \dot{\hat{R}}_{lin}(t) = & P(t) \frac{p_{out}(t - \hat{\tau}_s) - p_{aw}(t - \tau_s)}{m^2} Q_{out}(t - \hat{\tau}_s) \\ & - P(t) \frac{\hat{R}_{lin}(t) Q_{out}(t - \hat{\tau}_s)}{m^2} Q_{out}(t - \hat{\tau}_s), \end{aligned} \quad (3.21)$$

$$\dot{P}(t) = \beta P(t) - P(t)^2 \frac{Q_{out}^2(t - \hat{\tau}_s)}{m^2}, \quad (3.22)$$

where the outlet flow Q_{out} is the exciting variable, $P(t)$ is called the covariance, m is a normalization parameter, and β is an exponential forgetting factor.

If the sensor delay estimate is exact, i.e., $\tau_s = \hat{\tau}_s$, the signals used by the estimator are matched in time. Such exact delay compensation leads to:

$$\begin{aligned} \dot{\hat{R}}_{lin}(t) = & P \frac{\Delta p(t - \tau_s) - \hat{R}_{lin} Q_{out}(t - \tau_s)}{m^2} Q_{out}(t - \tau_s) \\ = & P \frac{R_{lin} Q_{out}(t - \tau_s) - \hat{R}_{lin} Q_{out}(t - \tau_s)}{m^2} Q_{out}(t - \tau_s) \end{aligned} \quad (3.23)$$

$$\dot{P}(t) = \beta P(t) - P(t)^2 \frac{Q_{out}^2(t - \tau_s)}{m^2}. \quad (3.24)$$

Because all estimator inputs are delayed by τ_s , this delay remains present in the estimator dynamics. Because τ_s is very small compared to the convergence time, its effect on the convergence time is considered negligible. Finally, the estimator dynamics can be expressed in terms of the estimation error $e_{LS}(t) := R_{lin} - \hat{R}_{lin}(t)$, resulting in

$$\dot{e}_{LS}(t) = -P(t) \frac{Q_{out}^2(t - \tau_s)}{m^2} e_{LS}(t). \quad (3.25)$$

A proof of convergence of this estimator with delay compensation in open-loop ventilation, i.e., the calibration phase, is presented in the next section.

3.5.3 Stability analysis

In this section, stability of the mechanical ventilation system with the control strategy proposed in Section 3.4.2 and 3.5.2 is analyzed. The stability analysis in this section

consists of two parts. In Section 3.5.3.1, stability of the open-loop dynamics in (3.7) and (3.8), and convergence properties of the estimator in (3.23) and (3.24) are analyzed; these dynamics represent the estimation phase. Thereafter, input-to-state stability (ISS) of the closed-loop system with a constant hose-resistance estimate in (3.19) and (3.20), i.e., compensation phase, is proved in Section 3.5.3.2. In these dynamics $w(t)$ is considered the external input, which depends on $p_{target}(t)$.

Throughout this chapter, the follow definition of persistence of excitation is adopted.

Definition 3.1. *A piece-wise continuous scalar signal $\phi(t)$ is Persistently Exciting (PE) if there exist constants $\alpha_0, \alpha_1, T_0 \in \mathbb{R}_{>0}$ such that*

$$\alpha_1 \geq \frac{1}{T_0} \int_t^{t+T_0} \phi^2(\tau) d\tau \geq \alpha_0, \forall t \geq 0. \quad (3.26)$$

Furthermore, it is assumed that the RLS estimator in (3.23) and (3.24) satisfies Assumption 3.1.

Assumption 3.1. *The RLS estimator in (3.23) and (3.24) is designed and initialized such that the following properties hold:*

- $P(0)$ is initialized to be positive, i.e., $P(0) > 0$.
- \hat{R}_{lin} is initialized to ensure $0 \leq \hat{R}_{lin}(0) \leq R_{lin}$.
- β is designed to be positive, i.e., $\beta > 0$.

Assumption 3.2 states that the target pressure profile is always positive and bounded. Practically, this is a non-restrictive assumption because PCV requires a strictly positive and bounded pressure target.

Assumption 3.2. *$p_{target}(t)$ is bounded and positive by design; in particular, $\epsilon_1 < p_{target}(t) < \infty, \forall t \geq 0$, with $\epsilon_1 > 0$ a positive constant.*

Finally, Assumption 3.3 states that the estimated sensor delay, used for delay compensation, is exactly equal to the true sensor delay, i.e., the sensor delay is perfectly compensated.

Assumption 3.3. *The estimated sensor delay $\hat{\tau}_s$ is exactly equal to the true sensor delay τ_s , i.e., $\hat{\tau}_s = \tau_s$.*

Next, these assumptions are used to show that the hose-resistance estimate converges to the true parameter in Section 3.5.3.1 and that the closed-loop dynamics with hose compensation are ISS in Section 3.5.3.2.

3.5.3.1 Convergence of the linear estimator

During the calibration phase, the system is controlled in open loop, i.e., $p_{control}(t) = p_{target}(t)$. The open-loop system dynamics are described by (3.7) and (3.8) and the linear estimator dynamics with delay compensation are given by (3.24) and (3.25). In this section, the following properties of the system in the calibration phase are proved under Assumption 3.1-3.3:

- exponential stability of the open-loop dynamics in (3.7) and (3.8), see Lemma 3.1;
- exponential convergence of the estimation error $e_{LS}(t)$ in (3.25) to zero; and
- $\hat{R}_{lin}(t)$ remains in the set $[0, R_{lin}]$ for all $t \geq 0$.

Exponential stability of the open-loop dynamics, i.e., the system dynamics in the calibration phase, is proved in Lemma 3.1.

Lemma 3.1. *The open-loop dynamics in (3.7) and (3.8) are exponentially stable.*

Proof. The blower delay τ_b in (3.7) and (3.8) is a pure input delay, hence, it does not affect stability of these linear dynamics. Therefore, the open-loop dynamics are stable iff $A_h = -\frac{R_{lin} + R_{leak}}{C_{lung}R} < 0$. This holds because all physical parameters in A_h are strictly positive. \square

Next, the PE property of the exciting variable $Q_{out}(t)$ is proved in Lemma 3.2.

Lemma 3.2. *Consider the open-loop dynamics in (3.7) and (3.8), i.e., the system in estimation phase, and Assumption 3.2. Then, the output $Q_{out}(t)$ is PE according to Definition 3.1.*

Proof. The PE upper bound is ensured by showing that $Q_{out}(t)$ is bounded. According to (3.3), $Q_{out} = \frac{p_{out} - p_{aw}}{R_{lin}}$. Since R_{lin} is bounded, $Q_{out}(t)$ is bounded if p_{out} and p_{aw} are bounded. In open loop $p_{out}(t) := p_{control}(t - \tau_b) = p_{target}(t - \tau_b)$, invoking Assumption 3.2 it is ensured that $p_{out}(t)$ is bounded. The airway pressure is defined as $p_{aw}(t) = C_h p_{lung}(t) + D_h p_{control}(t - \tau_b)$, see (3.7). Because the dynamics in (3.7) are exponentially stable according to Lemma 3.1 and the target pressure is bounded, $p_{aw}(t)$ is bounded as well. Hence, $Q_{out}(t)$ is bounded and its PE upper bound is ensured.

The proof of the PE lower bound is a special case of the proof presented in Reinders et al. (2021b, Lemma 1). In Reinders et al. (2021b, Lemma 1), patient effort (\dot{p}_{pat}) is considered and \hat{R}_{lin} is not equal to zero, i.e., not in open-loop ventilation. By following the same strategy but considering $\dot{p}_{pat} = 0$ and $\hat{R}_{lin} = 0$, the PE lower bound α_0 is ensured. Therewith both PE bounds for $Q_{out}(t)$ are proved, hence $Q_{out}(t)$ is PE. \square

Theorem 3.1. *Consider the estimator dynamics with delay compensation in (3.24) and (3.25), and adopt Assumptions 3.1, 3.2, and 3.3. Then, $\hat{R}_{lin}(t)$ converges exponentially and monotonically to $R_{lin}(t)$ and $0 \leq \hat{R}_{lin}(t) \leq R_{lin}$ holds for $t \geq 0$.*

Proof. First, Corollary 4.3.2 in Ioannou and Sun (1996) is invoked. This corollary guarantees that if the exciting variable, i.e., $Q_{out}(t)$, is PE and $\beta > 0$, then the estimated parameter $\hat{R}_{lin}(t)$ converges exponentially to the true parameter R_{lin} . These conditions are met by invoking Lemma 3.2 and Assumption 3.1. Therewith, the least-squares estimation error $e_{LS}(t) = R_{lin} - \hat{R}_{lin}(t)$ converges to zero exponentially, i.e., $\hat{R}_{lin}(t)$ converges to R_{lin} exponentially.

Next, it is proved that $\hat{R}_{lin}(t)$ converges monotonically and therewith remains in the set $0 \leq \hat{R}_{lin}(t) \leq R_{lin}$ for $t \geq 0$. First, it is shown that $P(t)$ remains positive if the estimator design ensures Assumption 3.1. For an arbitrary small positive $P(t)$ in (3.24) it is seen that $\dot{P}(t) > 0$, because $\beta > 0$. Therefore, $P(t) > 0$ for all $t \geq 0$. Next, (3.25) is used to show monotonic convergence of $\hat{R}_{lin}(t)$. The estimation error dynamics are $\dot{e}_{LS}(t) = -P(t) \frac{Q_{out}^2(t-\tau_s)}{m^2} e_{LS}(t)$, with $P(t) > 0$, $Q_{out}^2(t-\tau_s) > 0$, and $m > 0$. Therefore, $e_{LS}(t)$ is converging monotonically to zero and never changing sign. Furthermore, $\hat{R}_{lin}(0)$ is chosen as defined in Assumption 3.1, hence, $0 \leq \hat{R}_{lin}(t) \leq R_{lin}$ for all $t \geq 0$. \square

Concluding, it is shown that the system is exponentially stable during the calibration phase. Furthermore, the hose-resistance estimate converges to the true parameter exponentially and monotonically, and $0 \leq \hat{R}_{lin}(t) \leq R_{lin}, \forall t \geq 0$.

3.5.3.2 ISS of the closed-loop system with linear compensation

In this section, ISS of the closed-loop tracking error dynamics as presented in (3.19) with respect to the input $w(t)$ is ensured. In other words, ISS of the controlled system in the compensation phase is guaranteed. This is achieved by using Theorem 3.2 below, the proof of this theorem is appended in Appendix 3.A.

Theorem 3.2. *Consider a scalar NDDE*

$$\frac{d}{dt} (e(t) - \gamma e(t - \tau)) = ae(t) + be(t - \tau) + w(t) \quad (3.27)$$

with an external input $w(t)$, a state $e(t)$, a positive real delay τ , and real scalar system parameters γ , a , and b . The given neutral delay differential equation is input-to-state stable if

- $0 \leq \gamma < 1$;
- $a < 0$;
- $b \geq 0$;
- $|a| > |b|$.

Theorem 3.2 states that the scalar NDDE (3.19), representing the error dynamics in the compensation phase, is ISS with respect to the input $w(t)$ if the parametric bounds

in Theorem 3.2 are satisfied. Substituting the system parameters of (3.19) in the inequalities in Theorem 3.2 results in the following inequality conditions on the system parameters:

$$0 \leq \hat{R}_{lin} B_h C_{lung} \left(1 + \frac{R_{lung}}{R_{leak}} \right) < 1, \quad (3.28)$$

$$A_h < 0, \quad (3.29)$$

$$\frac{\hat{R}_{lin} B_h}{R_{leak}} \geq 0, \quad (3.30)$$

$$|A_h| > \left| \frac{\hat{R}_{lin} B_h}{R_{leak}} \right|. \quad (3.31)$$

Assuming that all system parameters, i.e., resistances and compliance, are positive, bounds on \hat{R}_{lin} are obtained such that the inequalities are satisfied. From these bounds a single bound for the resistance estimate \hat{R}_{lin} is obtained that ensures all bounds (3.28)-(3.29):

$$0 \leq \hat{R}_{lin} < R_{lin} + \frac{R_{leak} R_{lung}}{R_{leak} + R_{lung}}. \quad (3.32)$$

If the bound in (3.32) is ensured, then the NDDE in (3.19) is ISS according to Theorem 3.2. In Theorem 3.1 it is ensured that $0 \leq \hat{R}_{lin}(t) \leq R_{lin}$ in the estimation phase. Therefore, \hat{R}_{lin} in the compensation phase always satisfies (3.32). Therewith, the system is ISS in the compensation phase. Therewith, the second contribution of this chapter is complete.

3.6 Quadratic hose resistance and estimator

In this section, the quadratic hose resistance is addressed and included in the proposed control strategy to improve performance. This is the third contribution of this chapter.

3.6.1 Quadratic hose resistance

In Section 3.2, the nonlinearity of the hose is recognized as a relevant system property for control which is often neglected in literature. In Fig. 3.3, it is clearly seen that the relation between the flow through the hose Q_{out} and the pressure drop over the hose Δp is nonlinear. This nonlinearity is accurately modeled by the following relation:

$$\Delta p = R_{lin} Q_{out} + R_{quad} Q_{out} |Q_{out}| \quad (3.33)$$

with R_{lin} and R_{quad} the linear and quadratic resistance coefficients, respectively. Note that $R_{hose}(Q_{out})$ in Fig. 3.4 is replaced by the quadratic hose model in (3.33). To compensate for the pressure drop Δp in the control strategy of Fig. 3.4, estimates of the parameters R_{lin} and R_{quad} are used to compute the estimated pressure drop $\Delta \hat{p} = \hat{R}_{lin} Q_{out} + \hat{R}_{quad} Q_{out} |Q_{out}|$.

3.6.2 Quadratic hose model estimation

To estimate the parameters of the quadratic hose model, R_{lin} and R_{quad} , the estimator with delay compensation in (3.21) and (3.22) is extended to

$$\begin{aligned} \dot{\hat{\theta}}(t) = & P(t) \frac{p_{out}(t - \hat{\tau}_s) - p_{aw}(t - \tau_s)}{m^2} \phi_0(t - \hat{\tau}_s) \\ & - P(t) \frac{\hat{\theta}(t) \phi_0(t - \hat{\tau}_s)}{m^2} \phi_0(t - \hat{\tau}_s) \end{aligned} \quad (3.34)$$

and

$$\dot{P}(t) = \beta P(t) - P(t) \frac{\phi_0(t - \hat{\tau}_s) \phi_0^T(t - \hat{\tau}_s)}{m^2} P(t), \quad (3.35)$$

where $\hat{\theta}(t) = \begin{bmatrix} \hat{R}_{lin}(t) \\ \hat{R}_{quad}(t) \end{bmatrix}$, $P(t) = \begin{bmatrix} P_{11}(t) & P_{12}(t) \\ P_{21}(t) & P_{22}(t) \end{bmatrix}$, $\phi_0(t) = \begin{bmatrix} Q_{out}(t) \\ Q_{out}(t) | Q_{out}(t) | \end{bmatrix}$, m is the scalar normalization parameters, and β is the scalar exponential forgetting factor. To handle the output delay τ_s in the estimator the same method as proposed in Section 3.5.1 is used, i.e., $p_{out}(t)$ and $Q_{out}(t)$ are delayed by $\hat{\tau}_s$ before entering the estimator. The performance gain with this quadratic hose model is experimentally shown in Section 3.8.

3.7 Simulation case study

In this section, the results of a simulation case study are presented. In this case study, the dynamics with a linear hose-resistance model from Section 3.4 and the linear estimator and compensator from Section 3.5 are considered. The goal of this simulation case study is threefold. First, it shows the effect of delay compensation, proposed in Section 3.5.1, on the estimator and resulting tracking performance. Second, it shows the potential of the proposed control strategy. Third, it validates the obtained analytical results of Section 3.5.3.2.

A test case description is given in Section 3.7.1 and the simulation results are presented and discussed in Section 3.7.2.

3.7.1 Test case description

In this simulation case study, a sedated patient under Pressure Controlled Ventilation (PCV) ventilation is considered. The patient and hose parameters are presented in Table 3.1. The considered target pressure consists of a filtered block signal where PEEP and IPAP are 5 and 20 mbar, respectively. The breathing frequency, i.e., respiratory rate, of the target pressure is 15 breaths per minute.

Three different controllers are compared in this simulation case study. An integral feedback controller with transfer function $C(s) = \frac{6.285}{s}$, with $s \in \mathbb{C}$ the Laplace

Table 3.1. Controller settings and the patient-hose configuration, as used in the simulations.

Parameter	Value	Unit
β	0.7	s^{-1}
$P(0)$	5×10^{-8}	s/mL^2
$\hat{R}_{lin}(0)$	0	mbar s/L
m	1	-
R_{leak}	24	mbar s/L
R_{lung}	5	mbar s/L
R_{lin}	4.4	mbar s/L
C_{lung}	20	mL/mbar

variable, is used as a benchmark control strategy. Furthermore, two hose-compensation (HC) controllers are considered. The first HC controller does not compensate the sensor delay, i.e., $\hat{\tau}_s = 0$. The second HC controller compensates the sensor delay exactly, i.e., $\hat{\tau}_s = \tau_s = 16$ ms. The HC controllers are in the estimation phase for approximately 5 breaths. Thereafter, estimation is turned off and compensation is turned on with a constant hose-resistance estimate \hat{R}_{lin} . The controller parameters for both controllers are also presented in Table 3.1.

3.7.2 Simulation results

The results of the simulations are shown in Fig. 3.5 and 3.6. Fig. 3.5 shows the resulting airway pressure and the patient flow for the considered control strategies, and the estimated resistance \hat{R}_{lin} is shown in Fig. 3.6. The calibration phase is indicated by the gray background in the figures and the compensation phase is indicated by the white background.

First the control strategies are compared during the calibration phase. The airway pressure for both HC controllers does not converge to the target pressure because hose compensation is not active yet, see Fig. 3.5. Fig. 3.6 shows convergence of both estimators during the calibration phase. It is clearly observed that the timing mismatch in the signals, i.e., $\hat{\tau}_s = 0$, causes oscillations in the estimate. The compensation for these delays, i.e., $\hat{\tau}_s = \tau_s$, solves this problem and results in exact convergence of the estimate, as supported by the analysis in Section 3.5.3.1. Note that the worst-case switching time is considered for the HC controller with $\hat{\tau}_s = 0$.

Next, performance of all three controllers is analyzed during the compensation phase. Fig. 3.5 shows that the benchmark controller has significant overshoot and undershoot in the airway pressure. Another important limitation of the benchmark controller is the overshoot in patient flow, as shown in Fig. 3.5. This overshoot in patient flow can induce false triggering of breaths.

Both HC controllers show a significant improvement in tracking performance. They have a small mismatch between the airway and target pressure during the transient

phases. This mismatch is caused by the blower delay τ_b , which causes the compensation to be slightly too late. These mismatches are significantly smaller than the mismatch of the benchmark controller. Fig. 3.5 shows that both HC controllers have zero overshoot in the patient flow. Finally, it is observed that the HC controller without delay compensation is slightly overcompensating, see the first zoom plot in Fig. 3.5. This is caused by the fact that the constant estimate \hat{R}_{lin} is slightly too high.

Concluding, it is shown that delay compensation ensures convergence of the resistance estimate to the true hose resistance and improved tracking performance. Also the analytical results of Section 3.5.3.2 are validated.

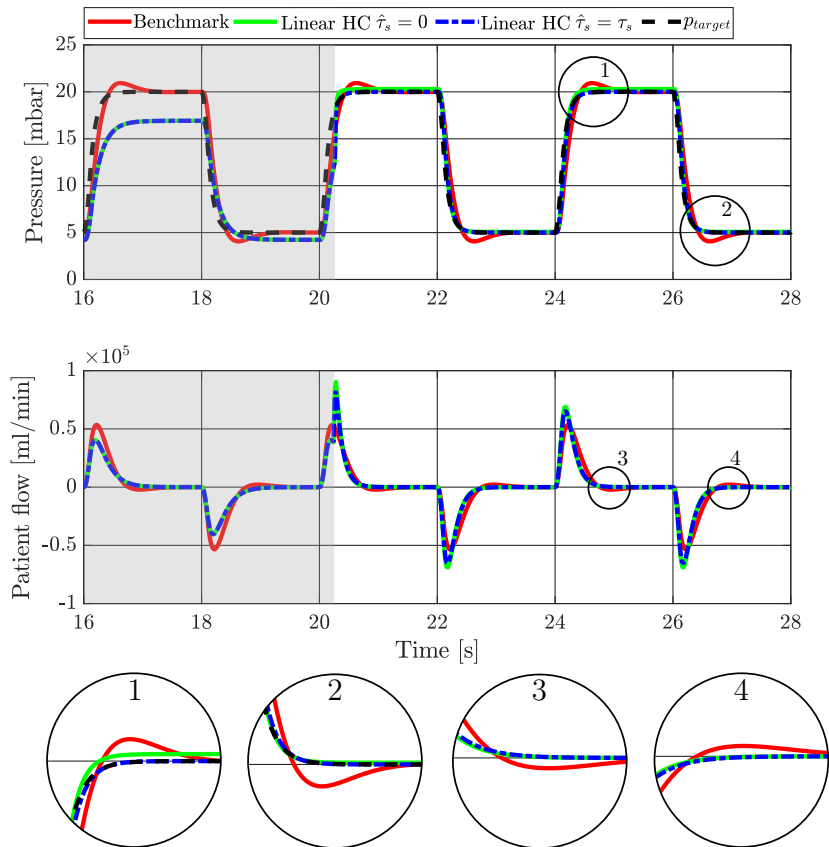


Fig. 3.5. Simulation results of the benchmark and both linear hose-compensation control strategies. This figure shows the resulting airway pressure and patient flow for all control strategies. It clearly shows that both hose-compensation strategies avoid overshoot in both pressure and flow. Furthermore, it shows that the delay compensation avoid a slight mismatch in pressure at the plateau values as shown in the first inset.

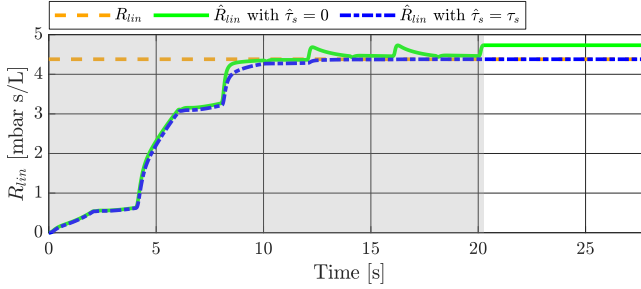


Fig. 3.6. Estimated hose resistance \hat{R}_{lin} of both hose-compensation controllers, showing that the delay compensation avoids oscillations and results in an exact estimation of the hose resistance.

3.8 Experimental case study

In this section, an experimental case study is conducted to show that explicitly accounting for the output delay and nonlinear nature of the hose-resistance model in the control strategy can significantly improve performance. In Section 3.8.1, the experimental setup and considered case are presented. The results with the control strategy using a linear hose-resistance model are analyzed in Section 3.8.2. Then, in Section 3.8.3, experimental results of the controller with the quadratic hose-resistance estimator with and without delay compensation are shown.

3.8.1 Experimental setup and case description

The main components of the experimental setup used in this case study are depicted in Fig. 3.7. This figure shows a Macawi blower-driven mechanical ventilation module (DEMCON Macawi respiratory systems, Best, The Netherlands). The ventilator is attached to a dSPACE system (dSPACE GmbH, Paderborn, Germany), where the controls are implemented using MATLAB Simulink (MathWorks, Natick, MA) running at a sampling frequency of 500 Hz. Furthermore, the ASL 5000™ Breathing Simulator (IngMar Medical, Pittsburgh, PA) is used to emulate the patient.

The patient and controller parameters used in Section 3.8.2 are presented in Table 3.1. The control parameters of the quadratic HC controller, used in Section 3.8.3, are given in Table 3.2.

3.8.2 Sequential estimation and compensation with a linear hose model

In this section, the control scheme as described in Sections 3.3, 3.4, and 3.5 is implemented in the experimental setup. The resulting airway pressure and patient flow are

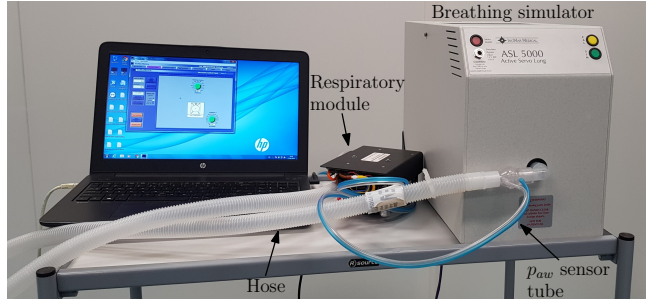


Fig. 3.7. Experimental setup with the most important parts, i.e., blower-driven ventilator, ASL 5000 breathing simulator, and the hose.

Table 3.2. Control parameters of the nonlinear hose-compensation controller.

Parameter	Value	Unit
β	0.5	s^{-1}
$P(0)$	$\begin{bmatrix} 5 \times 10^{-8} & 0 \\ 0 & 1 \times 10^{-14} \end{bmatrix}$	$\begin{bmatrix} s \text{ mL}^{-2} & s^2 \text{ mL}^{-3} \\ s^2 \text{ mL}^{-3} & s^3 \text{ mL}^{-4} \end{bmatrix}$
$\hat{R}_{lin}(0)$	0	mbar s/L
$\hat{R}_{quad}(0)$	0	mbar s^2/L^2

depicted in Fig. 3.8. Fig. 3.9 shows the linear resistance estimate for both HC controllers. The gray area in these figures represents the calibration phase of the HC controllers. The white area represents the compensation phase of the HC control strategies.

The tracking performance of the different controllers in the compensation phase is shown in Fig. 3.8. The benchmark controller shows clear overshoot and undershoot in the airway pressure and the patient flow. The HC control strategies show a strong reduction in pressure overshoot. A slight overcompensation is observed in the plateau phases, indicating an overestimation of the hose-resistance in these phases. Furthermore, the HC controllers show almost no overshoot and undershoot in patient flow. It is concluded that the HC control strategy improves performance significantly.

Fig. 3.9 shows a clear difference between the two HC control strategies. It is observed that both resistance estimates are oscillating in the calibration phase. This is caused by the nonlinear nature of the hose resistance. The linear resistance estimate is oscillating with the flow because it cannot capture the quadratic hose resistance. The dispersion of the estimate with delay compensation is significantly smaller than without delay compensation. Also, delay compensation results in a lower estimate value. This is also observed in the performance of the controller. Fig. 3.8 shows that the steady-state overcompensation is slightly smaller when compensating for the delay. Note that the switch times represent the worst-case scenario.

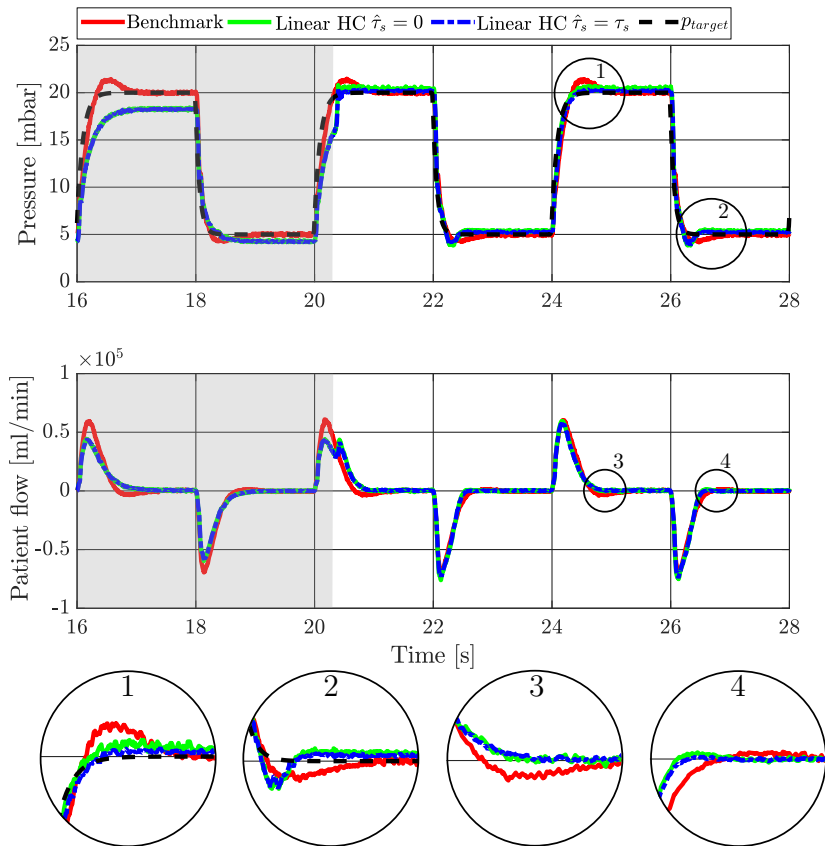


Fig. 3.8. Experimental results of the benchmark and linear hose-compensation control strategies with open-loop estimation. This figure shows the resulting airway pressure and patient flow. It clearly shows that both hose-compensation strategies reduce overshoot in both pressure and flow. Furthermore, it shows that the delay compensation reduces the mismatch in pressure at the plateau values as shown in the first zoom plot.

From these experiments, it is concluded that the HC control strategy significantly improves pressure tracking performance and delay compensation improves performance even further.

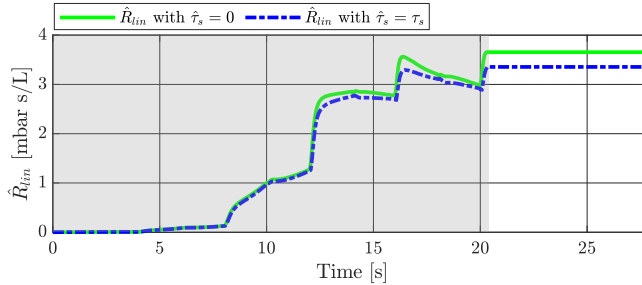


Fig. 3.9. Estimate \hat{R}_{lin} of the hose-compensation controllers. Showing that the delay compensation results in slightly lower values and smaller oscillations. The figure shows that the delay compensation reduces oscillations in the resistance estimate slightly.

3.8.3 Simultaneous estimation and compensation with a quadratic hose model

In this section, the control scheme as described in Sections 3.3 and 3.6 is analyzed in an experimental case study. Note that estimation and compensation are performed simultaneously in this section. A significant advantage of simultaneous estimation and compensation is that performance is improved immediately, and that the controller adapts to changes immediately.

The results of the experiments with the nonlinear HC controllers are shown in Fig. 3.10 and 3.11. The benchmark controller is exactly the same as in the previous section; therefore, it is not addressed separately here.

The HC controller without delay compensation shows significant pressure overshoot in Fig. 3.10. This is caused by the peak in the hose-resistance estimate, see Fig. 3.11. This peak in the estimates is a result of the timing mismatch between the signals. This controller shows overshoot comparable to the overshoot of the benchmark controller; however, settling time is significantly shorter. Overshoot and undershoot in patient flow is significantly reduced compared to the benchmark.

The HC controller with delay compensation, i.e., $\hat{\tau}_s = 16$ ms, shows almost no overshoot in pressure and zero overshoot in patient flow. Considering the hose-resistance estimate, see Fig. 3.11, it is observed that the estimate is significantly lower and has a smaller dispersion than the HC controller without delay compensation. Concluding, the nonlinear HC controller with delay compensation outperforms the other control strategies presented in this chapter in terms of steady state-tracking error, pressure overshoot, and patient flow overshoot. This case study shows that the pressure tracking performance depends on the accuracy of the estimated delay $\hat{\tau}_s$. However, for $\hat{\tau}_s = 0$, which is a very poor delay estimate, the proposed control strategy still outperforms the benchmark controller. This fact also underlines the robustness of the proposed approach for a mismatch in the delay estimate.

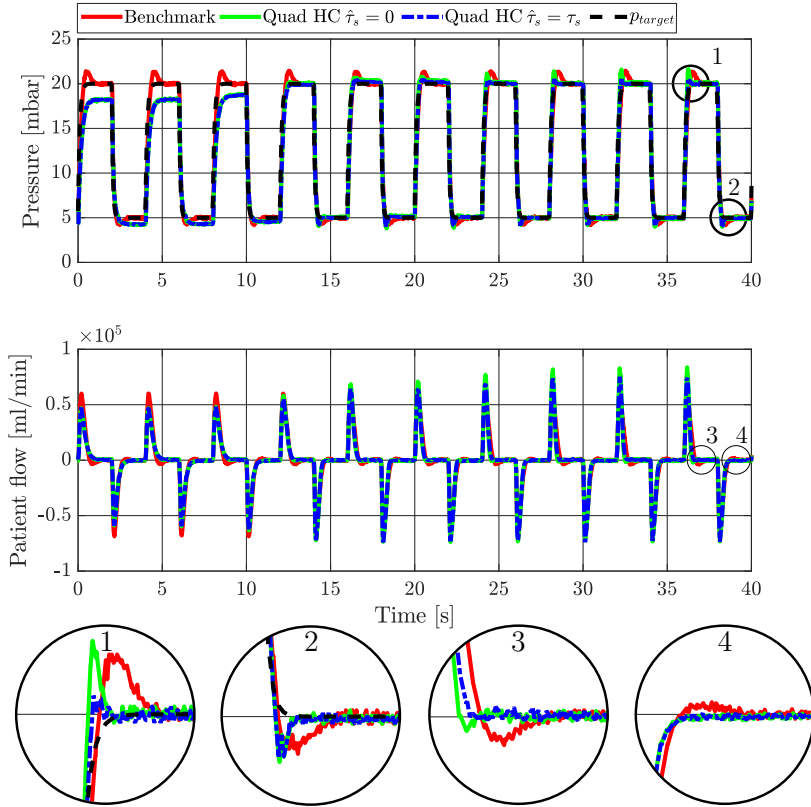


Fig. 3.10. Experimental results of the benchmark and the nonlinear hose compensation control strategies with online estimation. This figure shows the resulting airway pressure and patient flow. The figure clearly shows that the hose-compensation control strategies reduce overshoot in both flow and pressure significantly. Furthermore, it shows that overshoot in pressure is reduced significantly by including delay compensation in the controller.

The estimated hose models and the actual hose model are displayed in Fig. 3.12. It shows a hose-resistance curve obtained through a static calibration, the dispersion of the two estimated models upon convergence, and a hose-resistance curve measured during ventilation. Firstly, a clear difference between the static calibration and the online curve is observed. Because of the relatively low pressures during calibration, the calibration resistance is significantly lower than the resistance during ventilation. It is clearly observed that the estimated curve without delay compensation resembles the hose-resistance curve of the static calibration the best. The HC controller with delay compensation obtains an accurate estimate of the online hose-resistance curve. Also,

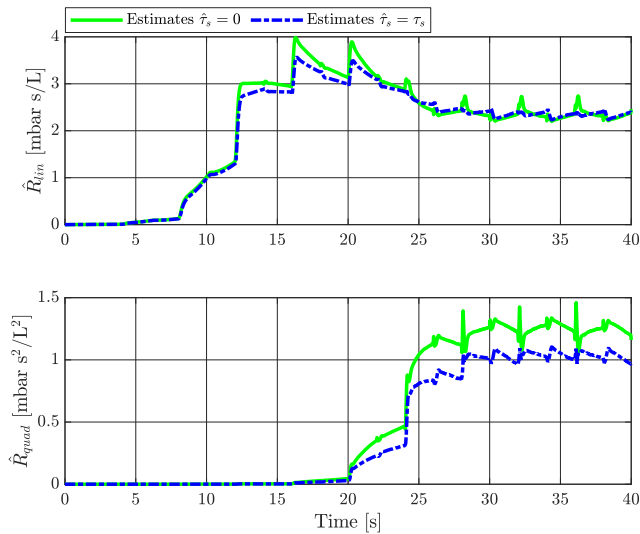


Fig. 3.11. Estimated \hat{R}_{lin} and \hat{R}_{quad} of the different hose-compensation controllers with a quadratic hose-resistance model. The figure shows that the delay compensation reduces oscillations in the resistance estimates significantly.

the dispersion of this estimate is much smaller than the dispersion of the curve without delay compensation. Hence, online estimation with delay compensation results in the best model of the hose resistance during ventilation.

Concluding, explicitly taking into account the nonlinearity of the hose and compensating for the measurements delays in the estimators can significantly improve estimation and pressure tracking performance in ventilation systems.

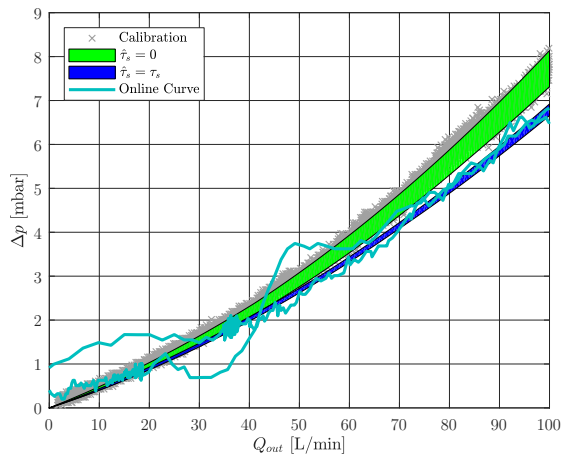


Fig. 3.12. Actual hose-resistance model and the dispersion of the estimated models. The figure shows that the dispersion of the estimated model is smaller when compensating for the sensor delay τ_s . Furthermore, the estimated hose-model when compensating for the sensor delay gives a better representation of the actual hose resistance during ventilation.

3.9 Conclusions and future work

In this chapter, pressure tracking performance for mechanical ventilation is significantly improved. This is achieved by addressing two system properties of mechanical ventilation system, namely, delays in the system dynamics and nonlinear characteristics of the hose resistance. It is shown that using explicit knowledge about these system properties in the controller improves pressure tracking performance significantly.

A control strategy that estimates a hose-resistance model and uses this estimated model to compensate the pressure drop over the hose is presented. Then, a compensation of the output delay is included in the estimator of this control strategy. Analytically it is proved that the estimated hose resistance with this delay compensation converges to the true hose resistance and that the closed-loop system is Input-to-State Stable (ISS). Furthermore, it is shown in simulations and experiments that this delay compensation improves performance.

Thereafter, the linear hose-resistance model used in this control strategy is extended to a quadratic resistance model. In an experimental case study a significant increase in tracking performance compared to the other control strategies is observed. Concluding, this chapter shows that explicitly taking into account output delays and the nonlinear hose characteristics in the control strategy can improve pressure tracking performance. Therewith, patient support and comfort is improved.

Experimental validation of the proposed control strategy on use-cases with spontaneously breathing patients is left for future work. The results in Reinders et al. (2021b) are promising regarding the robustness of the proposed method in case of spontaneously breathing patients. Also, analytical stability proofs of the controller with the quadratic hose-resistance model is left for future work.

3.A Appendix

This appendix contains the proof of Theorem 3.2. The proof of Theorem 3.2 consists of three main steps:

- Lemma 3.3 shows that the unforced scalar NDDE, i.e., (3.27) with $w(t) = 0 \forall t$, is exponentially stable, i.e., converging to zero exponentially fast.
- Lemma 3.4 shows that the system response of (3.27) for a bounded input $w(t)$ and zero initial condition, i.e., $e(t) = 0, \forall t \in [-\tau, 0]$, is bounded.
- Theorem 3.2 is proved using the obtained properties of the unforced and forced solution of (3.27), and the fact that the explicit solution of (3.27) is the sum of the unforced and forced solution.

In Definition 3.2 the fundamental function $k(t)$ for the NDDE in (3.27) without input is given.

Definition 3.2 (Scalar version of the fundamental matrix defined in Kharitonov (2013) and Bellman and Cooke (1963)). *Let $k(t)$ be a solution of the equation*

$$\frac{d}{dt}[k(t) - \gamma k(t - \tau)] = ak(t) + bk(t - \tau), \quad t \geq 0, \quad (3.36)$$

that satisfies the following conditions:

- *initial condition, $k(t) = 0$, for $t < 0$, and $k(0) = 1$;*
- *sewing condition, $k(t) - k(t - \tau)\gamma$ is continuous for $t \geq 0$.*

Then $k(t)$ is known as the fundamental function of system (3.27) with $w(t) = 0$ for all $t \geq 0$.

The definition of global exponential stability of a scalar NDDE is given in Definition 3.3.

Definition 3.3 (Based on Definition 1.21 in Michiels and Niculescu (2014)). *The null solution of the scalar NDDE in (3.27) with zero input, i.e., $w(t) = 0 \forall t$, is globally exponentially stable if and only if there exist constants $C > 0$ and $\gamma > 0$ such that*

$$\forall \varphi \in \mathcal{C}([- \tau, 0], \mathbb{R}), \|e_t(\varphi)\|_s \leq Ce^{-\gamma t} \|\varphi\|_s, \quad (3.37)$$

where the function segment φ is the initial condition of (3.27) and $\|\cdot\|_s$ denotes the supremum norm.

In Proposition 3.1 properties of the NDDE without input that ensure global exponential stability of its null solution are given.

Proposition 3.1 (Based on Proposition 1.22 in Michiels and Niculescu (2014)). *The null solution of the scalar NDDE in (3.27) with zero input, i.e., $w(t) = 0 \forall t$, is globally exponentially stable if and only if all characteristic roots are located in the open left half plane and bounded away from the imaginary axis.*

The characteristic roots of an NDDE are defined in (Michiels and Niculescu, 2014, p. 16). The characteristic roots are the values for λ for which the characteristic equation holds. The characteristic equation of the scalar NDDE (3.27) with zero input $w(t) = 0 \forall t$ is

$$\det(\Delta_N(\lambda)) = 0 \quad (3.38)$$

with

$$\Delta_N(\lambda) := \lambda(1 - \gamma e^{-\lambda\tau}) - a - be^{-\lambda\tau}. \quad (3.39)$$

Next, Lemma 3.3 proves that the unforced scalar NDDE, i.e., (3.27) with $w(t) = 0 \forall t$, is globally exponentially stable, i.e., its solutions are converging to zero exponentially. First it is shown that the real parts of the roots of its characteristic equations are

strictly negative. Thereafter it is shown that the spectral abscissa, i.e., the asymptote to which the infinite sequence of poles of the NDDE converge, is strictly negative. This ensures that the infinite sequence of poles is negative and does not converge towards the imaginary axis. Finally, Proposition 3.1 is invoked to ensure exponential stability.

Lemma 3.3. *The scalar NDDE (3.27) with zero input $w(t) = 0 \forall t$ is globally exponentially stable if $0 \leq \gamma < 1$, $a < 0$, $b \geq 0$, and $|a| > |b|$.*

Proof. From (3.38), the characteristic roots of (3.27) are given by

$$\lambda = \frac{a + be^{-\lambda\tau}}{1 - \gamma e^{-\lambda\tau}}. \quad (3.40)$$

Using the definition of products of exponentials, Euler's formula, $c := \cos(-\text{Im}(\lambda)\tau)$, and $s := \sin(-\text{Im}(\lambda)\tau)$ gives

$$\begin{aligned} e^{-\lambda\tau} &= e^{-\text{Re}(\lambda)\tau} e^{-j\text{Im}(\lambda)\tau} \\ &= e^{-\text{Re}(\lambda)\tau} (\cos(-\text{Im}(\lambda)\tau) + j \sin(-\text{Im}(\lambda)\tau)) \\ &= e^{-\text{Re}(\lambda)\tau} (c + js), \end{aligned} \quad (3.41)$$

where j is the imaginary unit. Substitution of (3.41) in (3.40) gives

$$\lambda = \frac{\overbrace{a + be^{-\text{Re}(\lambda)\tau}c}^{\lambda_A} + \overbrace{jbe^{-\text{Re}(\lambda)\tau}s}^{\lambda_B}}{\underbrace{1 - \gamma e^{-\text{Re}(\lambda)\tau}c}_{\lambda_C} + \underbrace{-j\gamma e^{-\text{Re}(\lambda)\tau}s}_{\lambda_D}} = \frac{\lambda_A + \lambda_B}{\lambda_C + \lambda_D}, \quad (3.42)$$

where λ_A and λ_C are real numbers and λ_B and λ_D are pure imaginary numbers. Next, this equation is rewritten by multiplying the numerator and denominator by the complex conjugate of the denominator:

$$\lambda = \frac{\lambda_A + \lambda_B}{\lambda_C + \lambda_D} \frac{\lambda_C - \lambda_D}{\lambda_C - \lambda_D} = \frac{\lambda_A\lambda_C - \lambda_A\lambda_D + \lambda_B\lambda_C - \lambda_B\lambda_D}{\lambda_C^2 - \lambda_D^2}. \quad (3.43)$$

Since $\lambda_A\lambda_C$, $\lambda_B\lambda_D$, λ_C^2 , and λ_D^2 are real numbers and $\lambda_A\lambda_D$ and $\lambda_B\lambda_C$ are pure imaginary numbers, the real part and imaginary parts of this equation are separated, resulting in an equation for the real parts of the characteristic roots:

$$\text{Re}(\lambda) = \frac{\lambda_A\lambda_C - \lambda_B\lambda_D}{\lambda_C^2 - \lambda_D^2}. \quad (3.44)$$

For λ to be an eigenvalue, it must satisfy this equation. Next, it is shown that for non-negative real parts of λ , i.e., $\text{Re}(\lambda) \geq 0$, this equation cannot be satisfied given the bounds on the parameters a , b , and γ . It is shown that for $\text{Re}(\lambda) \geq 0$ the denominator of (3.44) is strictly positive and its numerator is strictly negative, i.e., the right-hand side

is strictly negative. Therewith, it is shown that (3.44) cannot be satisfied for $Re(\lambda) \geq 0$, hence, there exist no non-negative eigenvalues.

It is shown that for $Re(\lambda) \geq 0$ the denominator of (3.44) is strictly positive, i.e.,

$$1 + \gamma^2 e^{-2Re(\lambda)\tau} - 2\gamma e^{-Re(\lambda)\tau} c > 0. \quad (3.45)$$

For $Re(\lambda) \geq 0$ it holds that $e^{-Re(\lambda)\tau} \in [0, 1]$, hence $2\gamma e^{-Re(\lambda)\tau} \geq 0$. Using this, the left-hand side of (3.45) is lower bounded for $c = 1$ using $c := \cos(-Im(\lambda)\tau) \in [-1, 1]$. This gives an inequality that is more strict than (3.45)

$$1 + \gamma^2 e^{-2Re(\lambda)\tau} - 2\gamma e^{-Re(\lambda)\tau} = (1 - \gamma e^{-Re(\lambda)\tau})^2 > 0. \quad (3.46)$$

This inequality holds because $0 \leq \gamma < 1$ and $e^{-Re(\lambda)\tau} \in [0, 1]$, hence, $0 \leq \gamma e^{-Re(\lambda)\tau} < 1$. Therefore, it is proved that the denominator of (3.44) is strictly positive for $Re(\lambda) \geq 0$.

Next, it is shown that the numerator of (3.44) is strictly negative for $Re(\lambda) \geq 0$, i.e.,

$$a + b e^{-Re(\lambda)\tau} c - a\gamma e^{-Re(\lambda)\tau} c - b\gamma e^{-2Re(\lambda)\tau} < 0. \quad (3.47)$$

Because $b \geq 0$, $-a\gamma \geq 0$, and $e^{-Re(\lambda)\tau} \in [0, 1]$, it is known that $c = 1$ gives an upper bound for (3.47). Therefore, showing that (3.47) with $c = 1$ is strictly negative is sufficient. This gives

$$\begin{aligned} & (a + b e^{-Re(\lambda)\tau}) - (a + b e^{-Re(\lambda)\tau})\gamma e^{-Re(\lambda)\tau} \\ & = (a + b e^{-Re(\lambda)\tau})(1 - \gamma e^{-Re(\lambda)\tau}) < 0. \end{aligned} \quad (3.48)$$

Using the parameter bounds and $Re(\lambda) \geq 0$, the first part between brackets is strictly negative, and the second part between brackets is strictly positive. Therefore, it is ensured that the numerator of (3.44) is strictly negative for $Re(\lambda) \geq 0$. Hence, the characteristic roots of (3.27) with the given parameter bounds are strictly negative.

It remains to proof that the spectral abscissa c_D are in the open left-half plane. The spectral abscissa c_D is, according to Michiels and Niculescu (2014, p. 19), defined as

$$c_D := \sup\{Re(\lambda) : \det \Delta_D(\lambda) = 0\} \quad (3.49)$$

with $\Delta_D(\lambda) = 1 - \gamma e^{-\lambda\tau}$. The spectral abscissa is the supremum of the real part of the solution of (using the definition of products of exponentials and Euler's formula):

$$1 - \gamma e^{-Re(\lambda)\tau} (c - js) = 0. \quad (3.50)$$

Considering the real part only gives

$$1 - \gamma e^{-Re(\lambda)\tau} c = 0. \quad (3.51)$$

This gives

$$Re(\lambda) = -\frac{1}{\tau} \ln \left(\frac{1}{\gamma c} \right). \quad (3.52)$$

For $c < 0$, the right-hand side is imaginary, hence, it has no solutions. The supremum for this equation is given by $c = 1$, which gives spectral abscissa $c_D = -\frac{1}{\tau} \ln \left(\frac{1}{\gamma} \right)$. Since $0 \leq \gamma < 1$, it is concluded that $c_D < 0$, i.e., the spectral abscissa is strictly smaller than zero.

Invoking Proposition 3.1 ensures exponential stability of the scalar NDDE in (3.27) with zero input, given the bounds on the parameters. Therewith, the proof of this lemma is completed. \square

In Lemma 3.4 it is proved that the states of the scalar NDDE in (3.27) with input $w(t)$ and zero initial condition, i.e., $e(t) = 0, \forall t \in [-\tau, 0]$, remain bounded if the parameters satisfy $0 \leq \gamma < 1, a < 0, b \geq 0$, and $|a| > |b|$. In the proof of Lemma 3.4 an explicit solution of (3.27) with zero initial condition is derived. Thereafter, it is shown that this expression is bounded, i.e., $e(t)$ is bounded, for bounded inputs $w(t)$.

Lemma 3.4. *The scalar NDDE in (3.27) with input $w(t)$ and zero initial condition, i.e., $e(t) = 0, \forall t \in [-\tau, 0]$, remains bounded if the parameters satisfy $0 \leq \gamma < 1, a < 0, b \geq 0$, and $|a| > |b|$ and the input $w(t)$ is bounded.*

Proof. To obtain the explicit solution of (3.27) for zero initial condition, the proof of Theorem 6.1 in Kharitonov (2013) is followed. Let $t > 0$ and $\xi \in (0, t)$. Using (3.36), the following partial derivative is computed

$$\begin{aligned} J &:= \frac{\partial}{\partial \xi} ([k(t - \xi) - \gamma k(t - \xi - \tau)] e(\xi, \varphi)) \\ &= -[ak(t - \xi) + bk(t - \xi - \tau)] e(\xi, \varphi) \\ &\quad + [k(t - \xi) - \gamma k(t - \xi - \tau)] \dot{e}(\xi, \varphi) \end{aligned} \quad (3.53)$$

The last line in the previous equation is rewritten using the fact that $e(\xi, \varphi)$ is a solution of (3.27). This results in

$$\begin{aligned} J_1 &:= [k(t - \xi) - \gamma k(t - \xi - \tau)] \dot{e}(\xi, \varphi) \\ &= k(t - \xi) [ae(\xi, \varphi) + be(\xi - \tau, \varphi) \\ &\quad + \gamma \dot{e}(\xi - \tau, \varphi) + w(t)] \\ &\quad - \gamma k(t - \xi - \tau) \dot{e}(\xi, \varphi). \end{aligned} \quad (3.54)$$

Now, (3.54) is substituted in (3.53) and terms are canceled out, resulting in the following

equality:

$$\begin{aligned}
J &:= \frac{\partial}{\partial \xi} ([k(t - \xi) - k(t - \xi - \tau)] e(\xi, \varphi)) \\
&= k(t - \xi) \gamma \dot{e}(\xi - \tau, \varphi) - k(t - \xi - \tau) \gamma \dot{e}(\xi, \varphi) \\
&\quad + k(t - \xi) b e(\xi - \tau, \varphi) - b k(t - \xi - \tau) e(\xi, \varphi) \\
&\quad + k(t - \xi) w(t).
\end{aligned} \tag{3.55}$$

Integrating this equality by ξ from 0 to t results in:

$$\begin{aligned}
&[k(0) - \gamma k(-\tau)] e(t, \varphi) - [k(t) - \gamma k(t - \tau)] e(0, \varphi) \\
&= \int_0^t \gamma k(t - \xi) \dot{e}(\xi - \tau, \varphi) d\xi - \int_0^t \gamma k(t - \xi - \tau) \dot{e}(\xi, \varphi) d\xi \\
&+ \int_0^t b k(t - \xi) e(\xi - \tau, \varphi) d\xi - \int_0^t b k(t - \xi - \tau) e(\xi, \varphi) d\xi \\
&+ \int_0^t k(t - \xi) w(t) d\xi.
\end{aligned} \tag{3.56}$$

Now, filling in the initial condition property for $k(t)$, i.e., $k(0) = 1$ and $k(-\tau) = 0$, and some rewriting (by shifting the integration interval) gives the explicit solution of (3.27):

$$\begin{aligned}
e(t, \varphi) &= [k(t) - \gamma k(t - \tau)] e(0, \varphi) \\
&\quad + \int_{-\tau}^0 b k(t - \xi - \tau) e(\xi) d\xi \\
&\quad + \int_{-\tau}^0 \gamma k(t - \xi - \tau) \dot{e}(\xi) d\xi \\
&\quad + \int_0^t k(t - \xi) w(t) d\xi.
\end{aligned} \tag{3.57}$$

Next, the zero-initial condition values are filled in, i.e., $e(0, \varphi) = 0$ and $e(\xi) = \dot{e}(\xi) = 0, \forall \xi \in [-\tau, 0]$. Filling in gives the explicit solution of (3.27) with zero initial condition:

$$e(t, \varphi) = \int_0^t k(t - \xi) w(\xi) d\xi, \quad t \geq 0. \tag{3.58}$$

From Definition 3.2, it is known that the fundamental function $k(t)$ satisfies the same NDDE as the considered system (3.27) with zero input, i.e., $w(t) = 0$. Therefore, invoking Lemma 3.3 shows that $k(t)$ is exponentially stable, i.e., $\|k(t)\| \leq C e^{-\gamma t}$ for some positive constants C and γ , see Definition 3.3. Using this property of $k(t)$ and

(3.58), the following result is obtained for the scalar NDDE with zero initial condition:

$$\begin{aligned}
|e(t, \varphi)| &\leq \int_0^t |C e^{-\gamma(t-\xi)}| d\xi \sup_{s \geq 0} |w(s)| \\
&= \frac{C}{\gamma} \sup_{s \geq 0} |w(s)| [e^{-\gamma(t-\xi)}]_0^t \\
&= \frac{C}{\gamma} \sup_{s \geq 0} |w(s)| (1 - e^{-\gamma t}) \leq \frac{C}{\gamma} \sup_{s \geq 0} |w(s)|.
\end{aligned} \tag{3.59}$$

This result ensures that the state of the NDDE in (3.27) is bounded if it has a bounded input and starts with zero initial condition, i.e., $e(t) = 0$ for $t \leq 0$. \square

Finally, in the proof of Theorem 3.2, the results of Lemma 3.3 and 3.4 are used to show that the NDDE in (3.27) is ISS.

Proof of Theorem 3.2. The explicit expression for $e(t, \varphi)$ in (3.57) shows that the explicit solution of (3.27) is the sum of the solution with non-zero initial condition and zero input, and the solution with zero initial condition and non-zero input. This ensures that the following bound on $e(t, \varphi)$ exists (using Lemma 3.3 and 3.4, and Proposition 3.1):

$$|e(t, \varphi)| \leq C_1 e^{-\gamma_1 t} + \frac{C_2}{\gamma_2} \sup_{s \geq 0} |w(s)| \tag{3.60}$$

with C_1 , C_2 , γ_1 , and γ_2 all positive scalar values. Therewith, the ISS proof of a scalar NDDE (3.27) with parameters that satisfy $0 \leq \gamma < 1$, $a < 0$, $b \geq 0$, and $|a| > |b|$ is complete. \square

Improving mechanical ventilation for patient care through repetitive control

Abstract – Mechanical ventilators sustain life of patients that are unable to breathe (sufficiently) on their own. The aim of this chapter is to improve pressure tracking performance of mechanical ventilators for a wide variety of sedated patients. This is achieved by utilizing the repetitive nature of sedated ventilation through repetitive control. A systematic design procedure of a repetitive controller for mechanical ventilation is presented. Thereafter, the controller is implemented in an experimental setup showing superior tracking performance for a variety of patients.

4.1 Introduction

Mechanical ventilators are essential equipment in Intensive Care Units (ICUs) to assist patients who cannot breathe on their own or need support to breathe sufficiently. The goal of mechanical ventilation is to ensure adequate oxygenation and carbon dioxide elimination (Warner and Patel, 2013), and thereby sustaining the patient's life. In 2005 over 790,000 patients required ventilation in the United States alone (Wunsch et al., 2010). Therefore, improving mechanical ventilation improves treatment for a large population worldwide.

In pressure controlled ventilation modes, the mechanical ventilator aims to track a clinician set pressure profile at the patient's airway. An example of such profile is depicted in Fig. 4.1. The Inspiratory Positive Airway Pressure (IPAP) and Positive End-Expiratory Pressure (PEEP) induce airflow in and out of the lungs, respectively. This alternating flow of air allows the lungs to exchange CO_2 for O_2 in the blood.

Accurate tracking of the preset pressure profile is essential to ensure sufficient patient support and has spurred substantial research to improve control performance. Ac-

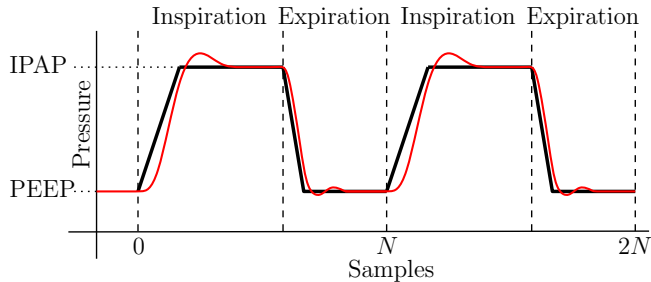


Fig. 4.1. Typical airway pressure for two breathing cycles of pressure controlled ventilation, showing the set-point (—) and the typical response (—).

According to Hunnekens et al. (2020), improved pressure tracking can prevent patient-ventilator asynchrony. In Blanch et al. (2015), patient-ventilator asynchrony is even associated with increased mortality rates. Furthermore, accurate tracking for a wide variety of patients improves consistency of treatment over these different patients.

The challenging problem of pressure tracking in presence of uncertain patients has spurred the development of a wide range of pressure control methodologies. In Hunnekens et al. (2020), variable-gain control is applied to overcome the trade-off between fast rise times and small overshoot. A significant improvement in tracking performance is shown in this work. However, the tracking error is still significant and the patient flow is used in the control strategy, which is typically not available. In Borrello (2001), adaptive feedback control is used. A patient model is estimated and the controller is adaptively tuned to obtain the desired transfer-function characteristics. It is shown to significantly improve performance in an experimental setting. However, in practice, i.e., on actual patients, it is complex to obtain an accurate patient model, therewith performance is expected to deteriorate. In Scheel et al. (2017), a model-based control approach is applied to mechanical ventilation. It is shown that this can improve performance. However, an accurate patient model is required which are typically not available in practical scenarios. In Li and Haddad (2012), model predictive control is used to improve tracking performance in ventilation. However, this method also requires an accurate patient which is typically not available. In Reinders et al. (2021b), adaptive hose-compensation control is used to significantly improve tracking performance in ventilation. However, using the repetitive nature of breathing, tracking performance can be improved even further.

Iterative Learning Control (ILC) and Repetitive Control (RC) can achieve superior tracking performance utilizing limited model information and the repetitive nature of a disturbance, e.g., the reference. ILC (Arimoto et al., 1984; Bristow et al., 2006; Moore, 1993) and RC (Hara et al., 1988; Inoue et al., 1981; Longman, 2010; Pipeleers et al., 2009) are well-known control strategies. In these methods, the controller learns an input signal using errors of previous tasks. In other application fields, ILC and RC are extensively analyzed and successfully implemented, e.g., industrial robotics (Arimoto

et al., 1984), wafer stages (De Roover and Bosgra, 2000), printer systems (Blanken et al., 2020; Van Zundert et al., 2016), and in medical applications for a device to help with stroke rehabilitation (Freeman et al., 2012).

Since an exact patient model is typically unavailable, such learning methods are particularly suitable for mechanical ventilation. In Scheel et al. (2015) and De Castro and Tôrres (2019), ILC has been applied to mechanical ventilation. In De Castro and Tôrres (2019), a significant improvement in pressure tracking performance is shown. However, only simulation results are presented. In Scheel et al. (2015), a strong improvement in tracking performance is shown in experiments. However, only causal filters are used in the ILC design. In sharp contrast, non-causal filters could potentially improve performance significantly because of the delays in ventilation systems (Borrello, 2005). Furthermore, in this chapter, it is argued that RC is a more suitable approach in a mechanical ventilation setting, because it is a continuous process, i.e., the system states are not reset between repetitions.

Although control has substantially improved tracking performance of ventilation, data of previous breaths and a learning control approach can be used to improve tracking performance by compensating all repeating disturbances. Therefore, the aim of this chapter is to improve pressure tracking performance for fully sedated patients utilizing the periodic nature of their breaths.

The main contribution of this chapter is the design of an RC in application to mechanical ventilation that achieves superior tracking performance for a wide variety of patients. A step-by-step design process of this RC is presented. Thereafter, this controller is implemented in an experimental setup and the performance is analyzed for a variety of plants, varying from a baby to an adult patient.

The outline of this chapter is as follows. In Section 4.2, the control problem and envisioned solution are presented. Thereafter, in Section 4.3, the control concept, stability results, and design procedure for RC are briefly explained. Then, in Section 4.4, the design process of the RC for mechanical ventilation is explained in detail and performance of the controller is analyzed in experiments. Finally, in Section 4.5, the main conclusions are presented.

4.2 Control problem

In this section, the control problem is described in detail. In Section 4.2.1, a high-level system description of the considered ventilation setup is given. Then, in Section 4.2.2, the control problem and main challenges are described. Finally, the envisioned control approach is briefly described in Section 4.2.3.

4.2.1 System description

A schematic of the considered blower-patient-hose system, with the relevant parameters, is shown in Fig. 4.2. The main components in the system are the blower, the hose-filter system, and the patient.

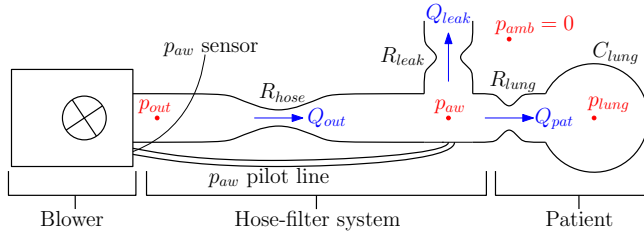


Fig. 4.2. Schematic representation of the blower-hose-patient system, with the corresponding resistances, lung compliance, pressures, and flows.

A centrifugal blower compresses ambient air to achieve the desired blower outlet pressure p_{out} . This change in p_{out} is controlled to achieve the desired airway pressure p_{aw} near the patient's mouth. The airway pressure is measured using a pilot line attached to the module and the end of the hose. All pressures are defined relative to the ambient pressure, i.e., $p_{amb} = 0$.

The hose-filter system connects the blower to the patient. The difference between the outlet pressure and the airway pressure results in a flow through the hose Q_{out} , related by a hose resistance R_{hose} . The change in airway pressure p_{aw} results in two flows, namely, the leak flow Q_{leak} and the patient flow Q_{pat} . The leak flow is used to flush exhaled CO_2 -rich air from the hose. The patient flow is required to ventilate the patient.

The patient is modeled as a resistance R_{lung} and a compliance C_{lung} . The patient flow is a result of the lung resistance and the difference between the airway pressure and the lung pressure p_{lung} , i.e., the pressure inside the lungs. The patient flow results in a change in the lung pressure, the relation between patient flow and lung pressure is given by the lung compliance. In this chapter, Frequency Response Function (FRF) models of the experimental setup are considered as presented in Section 4.4.2.

4.2.2 Control problem and challenges

This chapter considers Pressure Controlled Mandatory Ventilation (PCMV) of fully sedated patients. The goal in PCMV is to track a given airway pressure reference, i.e., preset by the clinician, repeatedly, see Fig. 4.1 for an example reference. This reference is exactly periodic with a period length of N samples. In case of a fully sedated patient N is preset by the clinician and exactly known. Besides this reference pressure, no other disturbances are considered to be present.

In mechanical ventilation, it is challenging to track such references accurately because of the large plant variations. One single controller should achieve accurate tracking for all possible plant variations. The following components of the plant are typically unknown and varying between patients:

- the patient can vary from a neonate to an adult;

- the hose and leak resistance can vary dependent on the available hoses in the hospital;
- the exact blower dynamics vary slightly from module to module.

Due to these unknown plant variations accurate inverse plant feedforward and high-gain feedback control are infeasible.

Besides the plant variations, another challenge is the presence of delays in the system. In the system a blower delay is present from the control output $p_{control}$ to the blower outlet pressure p_{out} . Furthermore, delays from p_{out} to p_{aw} and from the actual airway pressure p_{aw} to the measured airway pressure are present. Such delays typically deteriorate performance of classical feedback control strategies.

Because of the plant variations, the delays in the system, and the repetitive nature of the reference signal, ILC and RC are considered particularly suitable control approaches for this application. These control approaches in application to this control problem are briefly discussed in the following section.

4.2.3 Control approach

ILC and RC are control approaches that learn a control signal to suppress the tracking error caused by a reproducing disturbance (or reference). The key aspect in these approaches is that control actions are updated based on measured data from past disturbance realizations. Only limited model knowledge is utilized to guarantee fast and stable convergence. Using limited model knowledge and sufficient data, i.e., repetitions of the reproducing disturbance, the consequences of inevitable modelling errors can be suppressed and tracking performance can be improved. Therewith, these approaches can achieve accurate tracking for wide plant variations using a model of an 'average' system. Furthermore, these control approaches allow non-causal control actions, since the control action is a priori known. This can result in a significant performance gain in systems with delays, such as the considered ventilation system.

The key difference between ILC and RC is that in ILC the system is reset in between tasks, i.e., the initial conditions are exactly the same, whereas in RC the system operates in continuous time, without reset. Mechanical ventilation is a continuous process and there is no reset between breaths. Hence, the initial conditions of a breath depend on the previous breaths and inputs and are not always the same. Therefore, RC is considered a more suitable control approach for the application of mechanical ventilation. In the next section, the concept and theory of RC are treated.

4.3 Repetitive control

A closed-loop control system with a feedback controller and an add-on RC is depicted in Fig. 4.3. In this figure, P denotes the plant, C is a linear stabilizing feedback controller, R is the add-on RC, the robustness filter is denoted by Q , the learning filter is denoted

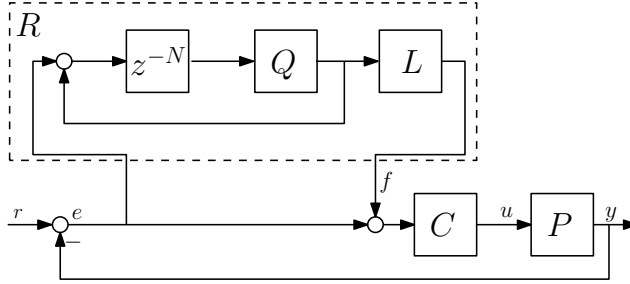


Fig. 4.3. Block diagram of a classic feedback control system including an add-on repetitive controller.

by L , and N denotes the length of the reproducing disturbance, i.e., the reference r , in samples. The repetitive controller is designed in the z -domain, based on a discrete-time plant model P in Fig. 4.3.

RC is based on the Internal Model Principle (IMP) (Francis and Wonham, 1975). The IMP states that asymptotic disturbance rejection of an exogenous disturbance is achieved if a model of the disturbance generating system is included in a stable feedback loop. For general N -periodic disturbances, a model of the disturbance generating system can be obtained using a memory loop. Including this memory loop in the control loop, see Fig. 4.3 with $Q = L = 1$, results in a transfer function from the reference to the error with infinite rejection at the harmonics of N . Hence, a reference signal that is exactly periodic with period length N is perfectly rejected.

In the remainder of this section, stability and filter design for RC are explained in Section 4.3.1 and 4.3.2, respectively.

4.3.1 Stability analysis of repetitive control

In this section, stability properties of the controlled system with an RC are presented. The presented stability conditions are a special case of the conditions in Longman (2010, Theorem 4). First, the full closed-loop transfer function is obtained from Fig. 4.3

$$\begin{aligned}
 e &= (I + PC(I + R))^{-1}r \\
 &= (I + PC + (I + PC)(I + PC)^{-1}PCR)^{-1}r \\
 &= (I + PC + (I + PC)TR)^{-1}r \\
 &= ((I + PC)(I + TR))^{-1}r = \underbrace{(I + TR)^{-1}}_{S_R} \underbrace{(I + PC)^{-1}}_S r,
 \end{aligned} \tag{4.1}$$

where S is the sensitivity of the closed-loop system with $R = 0$, T is the complementary sensitivity with $R = 0$, i.e., $T = 1 - S$, and S_R is referred to as the modifying sensitivity. It is assumed that the sensitivity S is asymptotically stable due to design

of C . Using this assumption and (4.1), it follows that the closed-loop is asymptotically stable if and only if S_R is asymptotically stable.

By substituting the transfer function of $R := Lz^{-N}Q(I - z^{-N}Q)^{-1}$ in S_R , it is obtained that

$$S_R = (I - z^{-N}Q)(I - (I - TL)z^{-N}Q)^{-1}. \quad (4.2)$$

This equation depends on the period length N , however, stability properties independent of N are desired. Stability conditions independent of N are desired because the breath length is often changed by a clinician. Hence, conditions independent of N allow for filter design independent of N . Therefore, the Single-Input Single-Output (SISO) stability condition in Theorem 4.1 below is commonly used, which is a special case of the multi-variable case in Longman (2010, Theorem 4) and is independent of N . Since this theorem is independent of N , controller design can be done independent of the period length N .

Theorem 4.1. *Assume that S and T are asymptotically stable. Then, S_R is asymptotically stable for all N if*

$$|Q(z)(1 - T(z)L(z))| < 1, \forall z = e^{i\omega}, \omega \in [0, 2\pi). \quad (4.3)$$

Essentially, this theorem ensures that $-(1 - TL)z^{-N}Q$ in (4.2) stays inside the unit-circle and, therewith, encirclements of the -1 point never occur, i.e., S_r is asymptotically stable. This implies that the entire loop in Fig. 4.3 is asymptotically stable.

4.3.2 Filter design for repetitive controller

Using the stability condition in Theorem 4.1, the following two-step design procedure is followed for SISO RC systems, see Hara et al. (1988), Steinbuch (2002), Tomizuka et al. (1989), and Blanken et al. (2020):

Procedure 4.1. (*Frequency-domain SISO RC design, from Blanken et al. (2020)*).

1. *Given a parameteric model of the 'nominal' complementary sensitivity $T(z)$, construct $L(z)$ as an approximate stable inverse of $T(z)$, i.e., $L(z) \approx T^{-1}(z)$.*
2. *Using non-parametric FRF models, $T_i(e^{i\omega})$, $i \in \{1, \dots, N_p\}$ with N_p the number of patient models, of different patients, design one $Q(z)$ such that Theorem 4.1 is satisfied for $T_i(e^{i\omega}) \forall i \in \{1, \dots, N_p\}$.*

This procedure describes a systematic robust design method for RC. In step 1, the L filter is based on a coarse parametric model of a 'nominal' patient. In case T is non-minimum phase or strictly proper, algorithms such as Zero Phase Error Tracking Control (ZPETC), see Tomizuka (1987), can be used to obtain a stable L filter. Then,

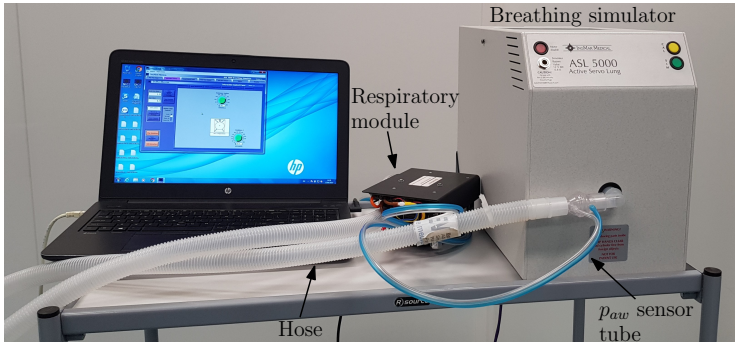


Fig. 4.4. Experimental setup consisting of the blower driven ventilator, ASL 5000 breathing simulation, and a hose.

in step 2, robustness to modeling errors and plant variations can be handled effectively. This is done by using non-parametric FRF models of the complementary sensitivity, which are easily obtained from experimental data (Pintelon and Schoukens, 2012). Using FRF models of different plants, stability for these different plants can be ensured using step 2 of the procedure. In the following section, the described design procedure is applied to the considered mechanical ventilation system.

4.4 Repetitive control applied to mechanical ventilation scenarios

Next, RC is applied to a mechanical ventilation setup. First, the experimental ventilation setup is described in Section 4.4.1. The learning filter and robustness filter are designed in Section 4.4.2 and 4.4.3, respectively. Finally, the RC is implemented on the experimental setup and performance is compared to PID control in Section 4.4.4.

4.4.1 Setup and use-case description

The main components of the experimental setup used in this case study are depicted in Fig. 4.4. The figure shows a Macawi blower-driven mechanical ventilation module (DEMCON macawi respiratory systems, Best, The Netherlands). Furthermore, the ASL 5000™ Breathing Simulator (IngMar Medical, Pittsburgh, PA) is shown in the figure. This breathing simulator is used to emulate a linear one-compartmental patient model as described in Bates (2009). Furthermore, a typical hose-filter system for ventilation of a patient in a hospital setting is shown. The developed control algorithms are implemented in a dSPACE system (dSPACE GmbH, Paderborn, Germany), which is not shown in the figure.

Table 4.1. Patient parameters and ventilation settings used for filter design and in the experiments.

Parameter	Adult	Pediatric	Baby	Unit
R_{lung}	5	50	50	mbar s / L
C_{lung}	50	10	3	L/mbar $\cdot 10^{-3}$
Respiratory rate	15	20	30	breaths / min
PEEP	5	5	10	mbar
IPAP	15	35	25	mbar
Inspiratory time	1.5	1	0.6	s
Expiratory time	2.5	2	1.4	s

To design and evaluate an RC for mechanical ventilation, three different patients and ventilation scenarios are considered. The considered patient scenarios are a baby, pediatric, and adult scenario from the ISO standard for PCMV obtained from Table 201.104 in NEN-EN-ISO 80601-2-12:2011 (NEN, Delft, The Netherlands). For these standardized scenarios, the patient parameters and the ventilator settings are given in Table 4.1. Note that all scenarios use the same hose-filter-leak configuration. The PID controller that is used in all scenarios, and in the benchmark PID control strategy is a pure integral controller. The benchmark controller is implemented as shown in Fig. 4.3 with $R = 0$. This controller is robustly designed to satisfy performance specifications and ensure stability for a large variation of plants. The transfer function of this controller is $C(z) = \frac{0.01257}{z-1}$, with sampling time 2×10^{-3} s.

To design the RC filters, a Frequency Response Function (FRF) of the complementary sensitivity is identified for every patient scenario at the PEEP pressure level and the IPAP pressure level. These FRFs and the mean of these FRFs are shown in Fig. 4.5. The mean FRF is used to design the learning filter as described in Section 4.4.2. To ensure stability, all separate FRFs are used in the design process of the Q filter in Section 4.4.3.

4.4.2 L -filter design

According to step one in Procedure 4.1, the learning filter L should be designed as an approximate stable inverse of the complementary sensitivity T . If $L = T^{-1}$ stability is always ensured, independent of the choice for Q , see Theorem 4.1.

Next, L filter design specifically for this application is considered. FRFs of different patients are displayed in Fig. 4.5. However, it is desired to design one controller for all patients. Therefore, for the design of L , the average FRF in Fig. 4.5 is used for L filter design. There is a significant time delay in the transfer function from the reference to the airway pressure, which is also observable in the FRFs. This time delay τ_d is identified to be approximately 24 ms or 12 samples. The main cause of this delay is the finite propagation speed of pressure waves through the hose and sensor line.

Therefore, a parametric estimate of the mean complementary sensitivity with 24 ms

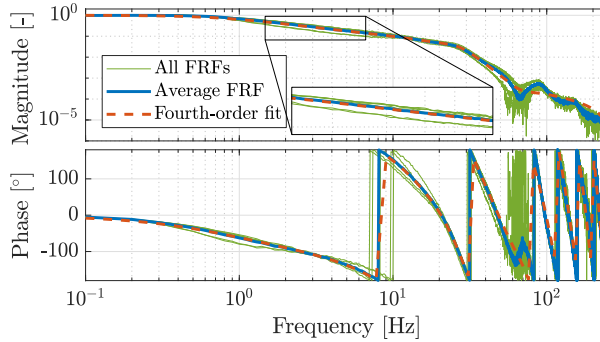


Fig. 4.5. Complementary sensitivity of the different measured FRFs, an average of these FRFs, and a fourth-order fit of the average FRF.

of delay is obtained. For the estimate of the average plant a fourth-order fit is used, which is shown in Fig. 4.5; this fit is denoted by T_{fit} . T_{fit} is obtained by using the *ssest* function in MATLAB (MathWorks, Natick, MA). This function uses a prediction error minimization (Ljung, 1999) to estimate a state-space model of the mean plant. It is shown that this fit is accurate up to approximately 30 Hz. This is considered sufficient for this application, since, the target profile contains mainly low frequency information, typically up to 15 Hz. Furthermore, a higher-order fit might improve the fit for these specific patients, but might be less accurate for other patients.

Next, T_{fit} is used to design the L filter. According to step one in Procedure 4.1, L should be designed as T_{fit}^{-1} . A strictly proper system has an improper inverse. Therefore, T_{fit} is inverted using ZPETC. This gives a causal L filter, L_c , which is used to obtain a non-causal learning filter

$$L = z^{p+d}L_c, \quad (4.4)$$

where p and d are the relative degree of T_{fit} and the number of samples delay in T_{fit} , respectively. Because of the memory loop, with N samples delay, this non-causal filter can easily be implemented as long as $p + d \leq N$. Next, the design procedure of Q is described to ensure stability of the closed-loop system.

4.4.3 Q -filter design

Next, step 2 in Procedure 4.1 is followed to ensure stability, i.e., to ensure satisfaction of the conditions in Theorem 4.1. In particular, a robustness filter Q is included to guarantee closed-loop stability and to improve robustness against plant variations. First, the stability condition in Theorem 4.1 is checked for the system without Q filter, i.e., $Q = 1$. This result is shown in the left plot of Fig. 4.6, Pat. 1, Pat. 2, and Pat. 3 correspond with the adult, pediatric, and baby patient of Table 4.1. Clearly, (4.3) does

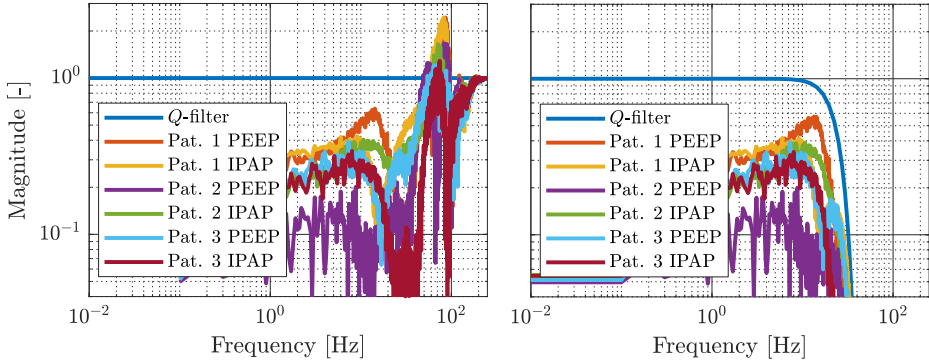


Fig. 4.6. Left: stability condition for all FRFs with $Q = 1$. Right: stability conditions for all FRFs with Q a low-pass filter with cut-off frequency at 23 Hz. The stability criterion in Theorem 4.1 is not ensured for $Q = 1$ and stability is guaranteed for all patient with Q a low-pass filter.

not hold for any patient. That reveals that stability cannot be guaranteed for any patient, see Theorem 4.1.

Because implementing just an L filter does not guarantee stability, a Q filter is included. This Q filter is designed such that the stability condition in Theorem 4.1 is ensured for all FRFs in Fig. 4.5. To ensure the stability condition, a low-pass filter with cut-off frequency of 23 Hz is used. This filter is implemented as a 50th order non-causal zero-phase Finite Impulse Response (FIR) filter. This FIR filter is implemented by computing a causal symmetric FIR-filter Q_c and applying a forward shift of z^{p_q} with p_q half the order of the FIR-filter. This makes it a zero-phase FIR filter that is symmetric around zero lag, such that no phase lag is introduced by the filter. The forward shift is possible because of the memory loop, as long as $p + d + p_q \leq N$.

Implementing the designed Q filter ensures the stability condition of Theorem 4.1, see the right plot in Fig. 4.6. Note that the cut-off frequency could be slightly higher, while still ensuring closed-loop stability. However, some margin between $|Q(1 - T_{FRFL})|$ and 1 is desired to improve robustness against plant variations. This margin allows additional plant variations, e.g., patient variations, without violating the stability conditions. Next, the performance of the system with and without RC is compared for all three patient scenarios.

4.4.4 Performance analysis

In this section, the performance of the benchmark controller is compared to the performance of the developed RC. This comparison is executed for the different patient scenarios which are given in Table 4.1. First, the results of the adult scenario are thoroughly analyzed. Thereafter, the main results of the other two scenarios are briefly presented.

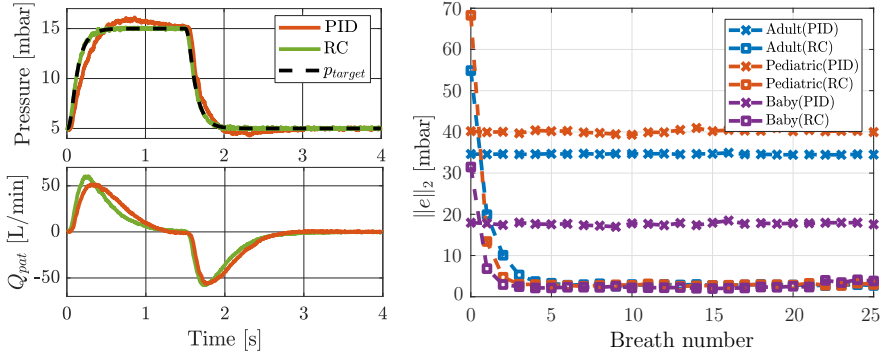


Fig. 4.7. Left: airway pressure p_{aw} and patient flow Q_{pat} of adult scenario (breath 20). Right: error 2-norm of all cases comparing PID with RC.

The results of the experiments are given in Fig. 4.7. The left-hand figure shows the airway pressure and the patient flow of the 20th breath of the adult scenario. The right-hand figure shows the error 2-norm of every breath for both control strategies, where the tracking error is defined as $e(t) = p_{target}(t) - p_{aw}(t)$ and its error 2-norm per breath is defined as $\|e\|_{2,j} = \sqrt{\sum_{k=j}^{j+N} e^2(k)}$ with j the breath number and N the breath length.

Fig. 4.7 shows that the benchmark controller has significant overshoot and undershoot, and a much longer settling time. Furthermore, it shows that the RC makes the airway pressure almost exactly the same as the target pressure upon convergence. Hence, pressure tracking performance is significantly improved. Furthermore, the patient flow shows that the RC fills the lungs significantly faster due to the improved pressure tracking. In Fig. 4.7, it is visible that the controller converges to a significantly smaller error 2-norm for all three scenarios. The improvement in error 2-norm is up to a factor 10 for the pediatric case. Furthermore, the controllers converge in approximately 5 breaths, which is considered sufficiently fast.

Since the stabilizing controller used in addition to the RC is the same as benchmark controller, the same initial error 2-norm, i.e., during the first breath, is expected. However, another internal control loop is omitted from the RC, such that the RC takes care of this part as well. Therefore, a difference in initial error 2-norm is observed between the two control strategies. Furthermore, a significant difference is seen in error 2-norm from patient to patient. This is caused by the difference in breathing profile. A short breath, such as the baby breath, naturally results in a smaller error 2-norm, since the error 2-norm is not normalized to the breath length.

4.5 Conclusions

The presented repetitive control framework in this chapter allows for superior pressure tracking performance for a wide variety of mechanically ventilated patients. This is achieved by using the periodicity of breaths in case a patient is fully sedated. To achieve this, a non-causal learning filter, based on an 'average patient', is designed. Thereafter, a robustness filter is designed to ensure stability. This robustness filter is designed such that the controller is robust with respect to plant variations. Finally, through experiments, it is shown that superior pressure tracking performance is achieved for a wide variety of patients.

Linear repetitive control for a nonlinear mechanical ventilation system using feedback linearization

Abstract – Mechanical ventilators sustain life of patients that are unable to breathe on their own. The aim of this chapter is to improve pressure tracking performance of a nonlinear mechanical ventilation system using linear repetitive control, while guaranteeing stability. This is achieved by using feedback linearization and subsequently applying linear repetitive control to the linearized plant. The design procedure of this control strategy is developed in this chapter. Thereafter, the controller is implemented in simulations and experiments showing superior pressure tracking performance of this control strategy compared to feedback control.

5.1 Introduction

Mechanical ventilators are essential equipment in Intensive Care Units (ICUs) to assist patients who cannot breathe on their own or need support to breathe sufficiently. The goal of mechanical ventilation is to ensure adequate oxygenation and carbon dioxide elimination (Warner and Patel, 2013), and thereby sustaining the patient's life. In 2005 over 790,000 patients required ventilation in the United States alone (Wunsch et al., 2010). Therefore, improving mechanical ventilation improves treatment for a large population worldwide, especially during the flu-season or a world wide pandemic, such as the COVID-19 pandemic.

In pressure-controlled ventilation modes, the mechanical ventilator aims to track a pressure profile at the patient's airway set by a clinician (Tobin, 2013). An example of such profile is depicted in Fig. 5.1. The Inspiratory Positive Airway Pressure (IPAP)

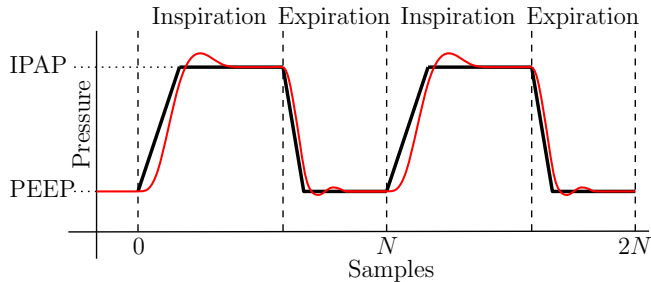


Fig. 5.1. Typical airway pressure for two breathing cycles of pressure controlled ventilation, showing the set-point (—) and the typical response (—).

and Positive End-Expiratory Pressure (PEEP) induce airflow in and out of the lungs, respectively. This alternating flow of air allows the lungs to exchange CO_2 for O_2 in the blood.

Accurate tracking of the preset pressure profile ensures sufficient patient support and enhances patient comfort. According to Hunnekens et al. (2020), improved pressure tracking can prevent patient-ventilator asynchrony. In Blanch et al. (2015), patient-ventilator asynchrony is even associated with increased mortality rates. Furthermore, accurate tracking for a wide variety of patients improves consistency of treatment over these different patients.

The challenging problem of pressure tracking in presence of widely varying and uncertain patients parameters has spurred the development of a wide range of pressure control methodologies. Some examples of such control strategies applied to mechanical ventilation are variable-gain control in Hunnekens et al. (2020), adaptive feedback control in Borrello (2001), model predictive control in Li and Haddad (2012), and adaptive hose compensation control in Reinders et al. (2021b) and Reinders et al. (2021a). All those methods improve pressure tracking performance in mechanical ventilation.

Pressure tracking performance has been improved further using learning control strategies by exploiting the repetitive nature of breathing. Learning control strategies, such as Iterative Learning Control (ILC) (Arimoto et al., 1984; Bristow et al., 2006; Moore, 1993) and Repetitive Control (RC) (Hara et al., 1988; Inoue et al., 1981; Longman, 2010; Pipeleers et al., 2009), can achieve superior tracking performance utilizing the repetitive nature of breathing, i.e., the target pressure. In these learning control strategies, the controller learns an input signal using errors of previous tasks. In other application fields, with repetitive tasks, ILC and RC are successfully implemented, e.g., industrial robotics (Arimoto et al., 1984), wafer stages (De Roover and Bosgra, 2000), printer systems (Blanken et al., 2020; Van Zundert et al., 2016), and in medical applications for a device to help with stroke rehabilitation (Freeman et al., 2012).

Since an exact plant model is typically unavailable and breathing is a repeating process, such learning control strategies are particularly suitable for mechanical ventilation. In Scheel et al. (2015) and de Castro and Tôrres (2019), ILC has been applied to mechanical ventilation. They show a significant performance improvement in ex-

periments and simulations. However, only causal filters are used in the ILC design. In sharp contrast, non-causal filters can potentially improve performance significantly because of the delays that are present in ventilation systems, as mentioned in Borrello (2005) and Reinders et al. (2021a). Furthermore, RC may be more suitable than ILC for ventilation systems because there is no system reset in between tasks, i.e., breaths. Therefore, in Reinders et al. (2020), RC with non-causal filters is applied to mechanical ventilation. Through an experimental case-study in Reinders et al. (2020), it is shown that RC improves performance significantly, up to a factor 10 in terms of the pressure error 2-norm, for a wide variety of patients.

Although learning control has substantially improved pressure tracking performance of mechanical ventilation, stability is typically ensured for a set of linearized plants and not for the full nonlinear dynamics of the ventilation system caused by the nonlinearity of the hose. Therefore, the aim of this chapter is to use repetitive control to improve tracking performance of the non-linear mechanical ventilation system while providing stability guarantees. This is achieved by applying feedback linearization to obtain a linearized plant. Thereafter, linear RC is applied to this linearized plant, rendering the standard RC stability proofs valid.

The main contribution of this chapter is the design of a control strategy for a non-linear mechanical ventilation system that combines feedback linearization and linear repetitive control. The first sub-contribution is that this combination of feedback linearization and linear repetitive control renders the stability and convergence analysis for linear repetitive control valid when it is applied to a non-linear system. The second sub-contribution is a performance analysis of this control strategy in simulations and in experiments.

The outline of this chapter is as follows. In Section 5.2, the considered system, the control goal, and the envisioned solution are presented. Then, in Section 5.3, the dynamic model of the nonlinear ventilation system is presented. Thereafter, in Section 5.4, the control concept and design procedure are explained. Then, in Section 5.5, the feedback linearized RC strategy is applied in a simulation case study. Next, in Section 5.6, the feedback linearized RC strategy is applied in an experimental case study. Finally, in Section 5.7, the main conclusions and extensions for future work are presented.

5.2 Control problem

The considered nonlinear ventilation system is described in Section 5.2.1. Thereafter, the control problem and challenges are presented in Section 5.2.2. Then, in Section 5.2.3, a high-level description of the control framework is given.

5.2.1 High-level system description

A schematic of the considered blower-patient-hose system, with the relevant parameters, is shown in Fig. 5.2. The main components of this system are the blower, the

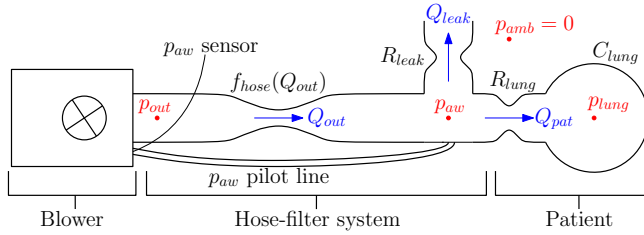


Fig. 5.2. Schematic representation of the blower-hose-patient system, with the corresponding resistances, lung compliance, pressures, and flows.

hose-filter system, and the patient.

The blower compresses ambient air to achieve the desired blower outlet pressure p_{out} . The change in p_{out} is controlled to achieve the desired airway pressure p_{aw} near the patient's mouth. The airway pressure is measured using a pilot line attached to the module and the end of the hose. All pressures are defined relative to the ambient pressure, i.e., $p_{amb} = 0$.

The hose-filter system connects the blower to the patient. The difference between the outlet pressure and the airway pressure results in a flow through the hose Q_{out} , related by a nonlinear hose resistance model f_{hose} . A visualization of the nonlinear hose characteristics is shown in Fig. 5.3. This figure shows a non-linear model fitting the calibration data accurately. The change in airway pressure p_{aw} results in two flows, namely, the leak flow Q_{leak} and the patient flow Q_{pat} . The leak flow is used to flush exhaled CO_2 -rich air from the hose. The patient flow is required to ventilate the patient.

The patient is modeled as a resistance R_{lung} and a compliance C_{lung} . The patient flow Q_{pat} is a result of the lung resistance and the difference between the airway pressure p_{aw} and the lung pressure p_{lung} , i.e., the pressure inside the lungs. The patient flow results in a change in the lung pressure, the relation between patient volume and lung pressure is given by the lung compliance.

5.2.2 Control goal and open challenge

This chapter considers Pressure Controlled Mandatory Ventilation (PCMV) of fully sedated patients. The goal in PCMV is to track a given airway pressure reference, i.e., preset by the clinician, repeatedly, see Fig. 5.1 for an example reference. This reference is exactly periodic with a period length of N samples. Besides this reference pressure, no other disturbances are considered to be present.

Because of the plant variations, the delays in the system, and the repetitive nature of the reference signal, repetitive control (RC) has been successfully applied to achieve superior tracking performance in PCMV for a variety of patient in Reinders et al. (2020). However, in Reinders et al. (2020) the stability properties of the closed-loop system are guaranteed for Frequency Response Functions (FRFs) characterizing the linearized dynamics at different steady-state pressure levels, i.e., linearizations of

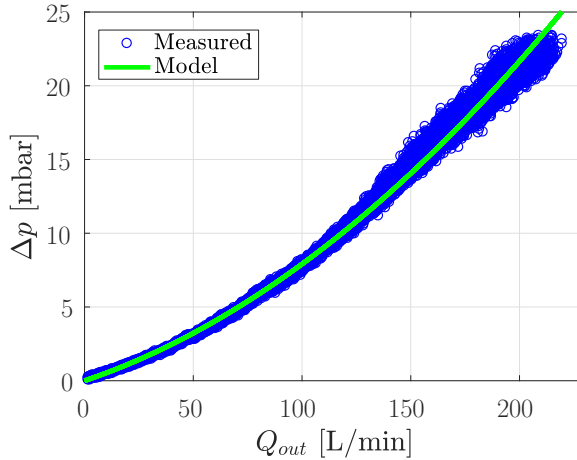


Fig. 5.3. Pressure drop over the hose Δp versus the outlet flow Q_{out} . Showing a measured data points of a calibration and a fit of the considered nonlinear hose model.

the actual non-linear mechanical ventilation system around certain steady-state working points. Therefore, the stability analysis does not hold for time-varying pressure levels during operation. The challenge of ensuring stability is tackled in this chapter.

5.2.3 Control approach

Here, a high-level explanation of the control approach in this chapter is presented. The goal of this control approach is to achieve the superior performance of RC, while guaranteeing stability for time-varying target pressure levels. This is achieved by first using feedback linearization to retrieve a linearized plant. Thereafter, linear RC is used to achieve the desired tracking performance.

As seen in (5.2), the hose resistance contains a nonlinear component. In order to linearize the nonlinear plant, this nonlinearity has to be compensated for. To achieve this, an estimate of the quadratic hose resistance \hat{R}_{quad} is used in a positive feedback loop similar to the hose-resistance compensation strategy in Reinders et al. (2021a). If the estimate is correct, i.e., $\hat{R}_{quad} = R_{quad}$, this results in a linearized plant. Details and the results of this feedback linearization method are presented in Section 5.4.1.

Thereafter, a linear repetitive controller is designed for this linearized plant. This is done similar to the method presented in Reinders et al. (2020). However, in this chapter we consider only one adult patient instead of designing the repetitive controller for a variety of patients. This is done without loss of generality and merely for the sake of simplicity and clarity. The design procedure of this repetitive controller is described in

Section 5.4.2.

5.3 Nonlinear ventilation system dynamics

In this section, the most important equations of the nonlinear ventilation system are presented. These equations are used to model the separate components: the blower, the hose, and the patient. Finally, it is described how these separate components are connected.

For the blower model, it is assumed that an internal control loop of the blower results in a transfer function from the control input $p_{control}$ to p_{out} that is equal to one, i.e.,

$$p_{out}(t) = p_{control}(t). \quad (5.1)$$

According to Reinders et al. (2021a), the pressure drop over the hose-filter system can be modeled accurately with a nonlinear algebraic equation defined as

$$\Delta p = f_{hose}(Q_{out}) := R_{lin}Q_{out} + R_{quad}Q_{out}|Q_{out}| \quad (5.2)$$

with $\Delta p := p_{aw} - p_{out}$ the pressure drop over the hose, R_{lin} the linear resistance component, and R_{quad} the quadratic resistance component. The inverse of this nonlinear hose model gives an expression for the outlet flow

$$\begin{aligned} Q_{out} &= f_{hose}^{-1}(\Delta p) \\ &= \text{sign}(\Delta p) \frac{-R_{lin} + \sqrt{R_{lin}^2 + 4R_{quad}|\Delta p|}}{2R_{quad}}. \end{aligned} \quad (5.3)$$

The leak is modeled as a linear resistance, which gives the leak flow

$$Q_{leak} = \frac{p_{aw} - p_{amb}}{R_{leak}} = \frac{p_{aw}}{R_{leak}}. \quad (5.4)$$

The patient is modeled with a linear one-compartmental lung model, as described in Bates (2009), as follows:

$$\dot{p}_{lung} = \frac{p_{aw} - p_{lung}}{C_{lung}R_{lung}} = \frac{1}{C_{lung}}Q_{pat}. \quad (5.5)$$

These different components are connected using conservation of flow, i.e., $Q_{out} = Q_{leak} + Q_{pat}$. Combining conservation of flow with (5.3), (5.4), and (5.5) results in the full nonlinear dynamics. The full nonlinear state-space model is omitted for brevity. This nonlinear dynamics can be represented by a block diagram as shown by the black part of Fig. 5.4, where the red part should be neglected for now.

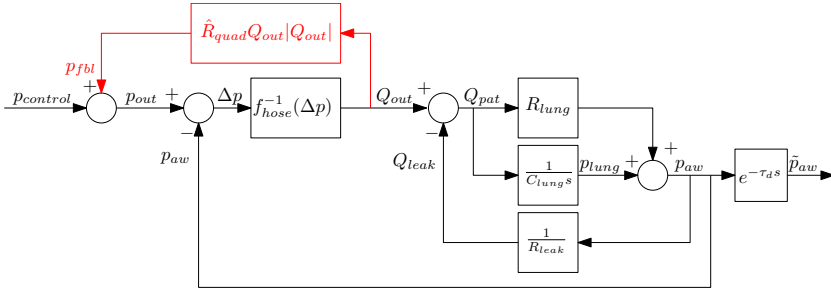


Fig. 5.4. Block diagram showing how the different components of the continuous-time plant are interconnected. The feedback linearization method is visualized in red. With feedback linearization this gives the linearized plant P_{lin} .

5.4 Feedback linearization for repetitive control with guaranteed closed-loop stability

In this section, the proposed control structure and design methodology are presented. Before going into details about the design methodology, the challenge and the high-level solution are described.

The main challenge is a result of the nonlinear system dynamics in combination with the repetitive target pressure for breathing. Because of the repetitive target pressure the Internal Model Principle (IMP), as described in Francis and Wonham (1975), can be exploited. The IMP states that asymptotic disturbance rejection of an exogenous disturbance is achieved if a model of the disturbance generating system is included in a stable feedback loop. Therefore, we would like to include a disturbance generating system of our target pressure in our feedback loop to achieve asymptotic tracking of this target pressure for our nonlinear system.

RC is exploiting the IMP and can be used to achieve asymptotic rejection of a repetitive disturbance. However, stability analysis and design methods for RC are typically developed for linear systems. Therefore, in Section 5.4.1, we are using feedback linearization to reduce our plant to a linear plant. Thereafter, in Section 5.4.2, a repetitive controller design methodology for this linear plant is presented, such that high performance is achieved and stability is guaranteed.

5.4.1 Feedback linearization of the ventilation system

A linearized plant is retrieved by applying feedback linearization to the nonlinear ventilation system in Section 5.3. The feedback linearization method uses an estimated value of the quadratic hose resistance \hat{R}_{quad} to compensate the nonlinear resistance term R_{quad} of the actual hose in (5.2). This is achieved by adding the estimated con-

tribution of the nonlinear component of the hose, i.e., $p_{fbl} := \hat{R}_{quad}Q_{out}|Q_{out}|$, to the plant input, see the red part of Fig. 5.4. Intuitively, the pressure drop caused by the quadratic part of the hose resistance in (5.2) is added to the outlet pressure to compensate the nonlinear term in the hose model.

Mathematically, it is shown that this linearizes the system if $\hat{R}_{quad} = R_{quad}$. The proposed feedback linearization strategy results in the following pressure drop over the hose:

$$\Delta p = p_{control} + p_{fbl} - p_{aw}. \quad (5.6)$$

Assuming that the estimate \hat{R}_{quad} is indeed the same as the true quadratic resistance parameter, i.e., $\hat{R}_{quad} = R_{quad}$, and substitution of (5.6) in $f_{hose}^{-1}(\Delta p)$ results in:

$$Q_{out} = \frac{p_{control} - p_{aw}}{R_{lin}}. \quad (5.7)$$

Therewith, the nonlinear resistance term R_{quad} is eliminated, if $\hat{R}_{quad} = R_{quad}$ holds. Hence, a linear system is retrieved. Concluding, feedback linearization results in the following linearized system:

$$\begin{aligned} \dot{p}_{lung} &= \mathbf{A}_l p_{lung} + \mathbf{B}_l p_{control} \\ \begin{bmatrix} p_{aw} \\ Q_{pat} \end{bmatrix} &= \mathbf{C}_l p_{lung} + \mathbf{D}_l p_{control} \end{aligned} \quad (5.8)$$

with

$$\begin{aligned} \mathbf{A}_h &= -\frac{R_{lin} + R_{leak}}{C_{lung}\bar{R}}, \quad \mathbf{B}_h = \frac{R_{leak}}{C_{lung}\bar{R}}, \\ \mathbf{C}_h &= \left[\frac{R_{lin}R_{leak}}{\bar{R}} \quad -\frac{R_{lin}+R_{leak}}{\bar{R}} \right]^T, \\ \mathbf{D}_h &= \left[\frac{R_{leak}R_{lung}}{\bar{R}} \quad \frac{R_{leak}}{\bar{R}} \right]^T, \end{aligned} \quad (5.9)$$

and $\bar{R} := R_{lin}R_{leak} + R_{lin}R_{lung} + R_{leak}R_{lung}$. Note that due to the output delay of τ_d on p_{aw} , the measured airway pressure is defined as $\tilde{p}_{aw}(t) := p_{aw}(t - \tau_d)$. This gives the linearized plant transfer function with output delay:

$$\begin{aligned} P_{lin}(s) &= \frac{\tilde{p}_{aw}(s)}{p_{control}(s)} \\ &= \frac{(R_{leak} + C_{lung}R_{leak}R_{lung}s)e^{-\tau_d s}}{R_{leak} + C_{lung}R_{leak}R_{lung}s + R_{lin}(1 + C_{lung}(R_{leak} + R_{lung})s)} \end{aligned} \quad (5.10)$$

with $s \in \mathbb{C}$ the Laplace variable. The linear plant P_{lin} is used for repetitive controller design in the next section.

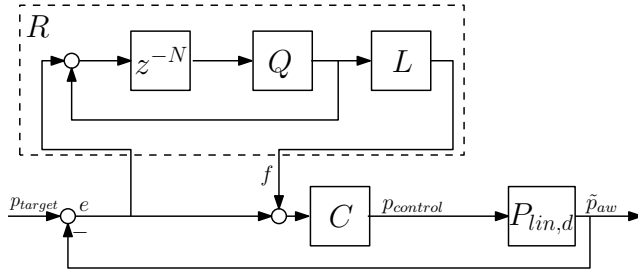


Fig. 5.5. Block diagram of a classic feedback control system including an add-on repetitive controller.

5.4.2 Repetitive controller design

In this section, a linear repetitive controller is designed for the linearized plant P_{lin} in (5.10). To achieve this, a brief background, stability properties, and the design methodology of an add-on repetitive controller are explained.

A closed-loop control system with a feedback controller and an add-on RC is depicted in Fig. 5.5. For the design and implementation of the repetitive controller discrete-time filters are developed. Therefore, the transfer function of the linearized plant P_{lin} , in (5.10), is discretized, this discrete transfer function is denoted by $P_{lin,d}$. Furthermore, in Fig. 5.5, C is a linear stabilizing feedback controller, R is the add-on RC, the robustness filter is denoted by Q , the learning filter is denoted by L , and N denotes the length of a single breath in samples, the breath length is visualized in Fig. 5.1. The repetitive controller is designed in the z -domain, based on the discrete-time plant model $P_{lin,d}$.

For N -periodic disturbances, a model of the disturbance generating system can be obtained using a memory loop. Including this memory loop in the control loop, see Fig. 5.5 with $Q = L = 1$, results in a transfer function from the reference to the error with infinite disturbance rejection at the harmonics of N . Hence, a reference signal that is exactly periodic with period length N is perfectly tracked. In the remainder of this section, stability and filter design for RC are briefly addressed.

The stability conditions considered in this chapter are a special case of the conditions in (Longman, 2010, Theorem 4). Stability conditions independent of N are desired because the breath length can be changed by a clinician. Hence, conditions independent of N allow for filter design independent of the target signals length N . Therefore, the Single-Input Single-Output (SISO) stability condition in Theorem 5.1 is commonly used, which is a special case of the multi-variable case in (Longman, 2010, Theorem 4) and is independent of N .

Theorem 5.1. (Longman, 2010, Theorem 4) Assume that $S = (1 + P_{lin,d}C)^{-1}$ and $T = 1 - S$ are asymptotically stable. Then, the closed-loop system with repetitive

control of Fig. 5.5 is asymptotically stable for all N if

$$|Q(z)(1 - T(z)L(z))| < 1, \forall z = e^{i\omega}, \omega \in [0, 2\pi). \quad (5.11)$$

□

Using the stability condition in Theorem 5.1, the following two-step design procedure is followed for SISO RC systems, see Blanken et al. (2020); Hara et al. (1988); Steinbuch (2002); Tomizuka et al. (1989).

Procedure 5.1. (*Frequency-domain SISO RC design, from Blanken et al. (2020)*).

1. Given a parametric model of the complementary sensitivity $T(z)$, construct a learning filter $L(z)$ as an approximate stable inverse of $T(z)$, i.e., $L(z) \approx T^{-1}(z)$.
2. Using a model $T(e^{i\omega})$, design a robustness filter $Q(z)$ such that Theorem 5.1 is satisfied.

This procedure describes a systematic robust design method for RC. In step 1, the L filter is based on a parametric model of the system. This first step can be motivated by considering $L = T^{-1}$, which results in $|Q(z)(1 - T(z)L(z))| = 0 < 1, \forall z = e^{i\omega}, \omega \in [0, 2\pi)$. Therefore, stability is guaranteed if $L = T^{-1}$. In case T is non-minimum phase or strictly proper, algorithms such as Zero Phase Error Tracking Control (ZPETC), see Tomizuka (1987), can be used to obtain a stable L filter. Then, in step 2, a robustness filter is added to ensure stability and improve robustness to modeling errors. This is done by using a model of the complementary sensitivity T and checking the stability condition in Theorem 5.1.

Moreover, the memory loop allows for implementation of non-causal filters. This is possible because the signals can be shifted by N samples in time. This property is used to compensate for the error introduced by the output delays using pre-actuation, i.e., the plant is actuated before the reference is changing. Furthermore, the robustness filter Q is implemented as a non-causal filtering to avoid phase delay, this is achieved by shifting a symmetric FIR-filter.

Concluding, this control strategy allows design methods for linear repetitive control, with its stability guarantees, to be applied to the nonlinear ventilation system. This is achieved by first linearizing the nonlinear system by feedback linearization. Thereafter, a linear repetitive controller is designed for this linearized plant.

5.5 Simulation results

In this section, the proposed control strategy of Section 5.4 is applied in a simulation case study. First, the considered use-case is described in Section 5.5.1. Thereafter, the designed controller is presented in Section 5.5.2. Finally, the simulation results are presented in Section 5.5.3.

Table 5.1. Patient parameters and ventilation settings used for filter design and in the simulations and experiments.

Parameter	Adult	Unit
R_{lung}	5	mbar s / L
C_{lung}	50	L/mbar $\cdot 10^{-3}$
Respiratory rate	15	breaths / min
PEEP	5	mbar
IPAP	15	mbar
Inspiratory time	1.5	s
Expiratory time	2.5	s
R_{lin}	1.7	mbar s/L
R_{quad}	1.6	mbar s ² /L ²
R_{leak}	43.1	mbar s/L

5.5.1 Simulation case description

In the simulation and experimental case study an adult patient scenario from the ISO standard for PCMV obtained from Table 201.104 in NEN-EN-ISO 80601-2-12:2011 (NEN, Delft, The Netherlands) is considered. For this standardized scenario, the patient parameters, the ventilator settings, and the considered hose parameters are given in Table 7.1. In the simulations and experimental case study, three different control strategies are compared. More specifically, a pure PID control strategy, the proposed linear repetitive control strategy with feedback linearization, and linear repetitive control without feedback linearization are compared.

5.5.2 Controller design

In this section, the final controller designs for the simulation case study are presented. First, the benchmark PID controller is presented. Then, the feedback linearization method is explained. Finally, the filter design for the RC strategies is presented.

The benchmark PID controller, which is also used in the RC strategies, is a pure integral controller that is implemented as shown in Fig. 5.5. This controller is robustly designed to ensure stability for a large variation of plants. The transfer function of this controller is $C(z) = \frac{0.01257}{z-1}$, with sampling time 2×10^{-3} s.

The feedback linearization method is implemented as described in Section 5.4.1, where \hat{R}_{quad} is assumed to be retrieved using a calibration such that $\hat{R}_{quad} = R_{quad}$. This feedback linearization results in the linearized plant P_{lin} given by (5.8).

Before designing the RC filters, it is argued that for both RC strategies the same filters should be used. Linearizing the nonlinear plant at a blower outlet flow zero, i.e., $Q_{out} = 0$, gives the same linear plant as P_{lin} . Furthermore, it is known in practice that the outlet flow through the hose will be both positive and negative. Therefore, designing the filters with the plant that is linearized around zero outlet flow, i.e., P_{lin} , makes sense

for the system without feedback linearization as well.

Using the discretization of the linearized plant P_{lin} , denoted by $P_{lin,d}$, and the proposed PID controller C , interconnected as shown in Fig. 5.5, the complementary sensitivity T is computed and Procedure 5.1 is followed to compute the RC filters. First, a stable inverse of T is computed using ZPETC which gives the learning filter L . In simulations, we exactly know what T is and can implement non-causal filters in the memory loop. Therefore, an exact inverse of T can be implemented as a learning filter L . Hence, the stability criterion in Theorem 5.1 is always satisfied for a robustness filter $Q = 1$. To resemble the experiments more closely, the same Q filter as in the experiments is used in the simulations. As a Q filter, a 20th-order symmetric FIR filter with a cutoff frequency of 23 Hz is used. Using this Q filter, stability of the system with feedback linearization is ensured using Theorem 5.1. Note that we cannot check stability for the non-linear system without feedback linearization.

Finally, a learning gain α is added to the learning filter. This means that the learning filter is multiplied by a gain $\alpha \in (0, 1]$. Low values for this learning gain reduce the convergence rate but do avoid that non-periodic disturbances, such as noise, are fed back into the loop. Therewith, the pressure tracking performance upon convergence can be improved. For the controllers in this study, it is found that $\alpha = 0.5$ gives the desired trade-off between convergence speed and reduction of the effect of noise.

5.5.3 Results

The control strategies designed in the previous section are implemented in simulations with the use case as presented in Section 5.5.1. The results of these simulations are presented in Fig. 5.6 and 5.7.

The time-domain results for the three control strategies are shown in Fig. 5.6. This figure shows the airway pressure of all control strategies upon convergence. The figure shows that the PID controller achieves a sub-optimal rise-time and has significant overshoot, which can damage the patient's lungs. Furthermore, the figure shows that both RC strategies achieve near perfect tracking upon convergence, the airway pressure is almost exactly the same as the target pressure. This improves the patient's comfort and avoids harmful peak pressures.

The error 2-norm per breath for every control strategy is shown in Fig. 5.7. It shows that the error two norm of the PID controller is approximately 35 mbar. Furthermore, it shows that both RC strategies converge to a significantly smaller error 2-norm just above 10^{-1} mbar. The error 2-norm also shows that the feedback linearization results in a smaller initial error and faster convergence of the RC controller. The reduced initial error is a result of the feedback linearization. The faster convergence is a result of the fact that L resembles the linearized T^{-1} better over the entire flow region. More precisely, in the feedback linearized case $L = T^{-1}$ holds exactly for every pressure level. In the case without feedback linearization a linear T^{-1} that holds for every pressure level does not exist.

Concluding, RC with feedback linearization results in faster convergence and a

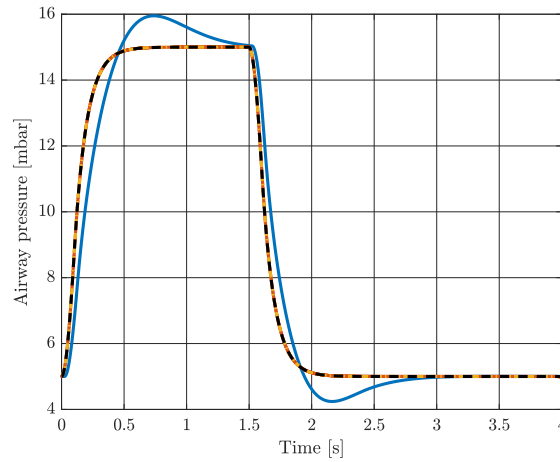


Fig. 5.6. Simulation results of the 20th breath in time domain upon convergence of the repetitive controllers. Showing the target pressure (---), the PID control strategy (—), repetitive control without feedback linearization (—), and repetitive control with feedback linearization (---).

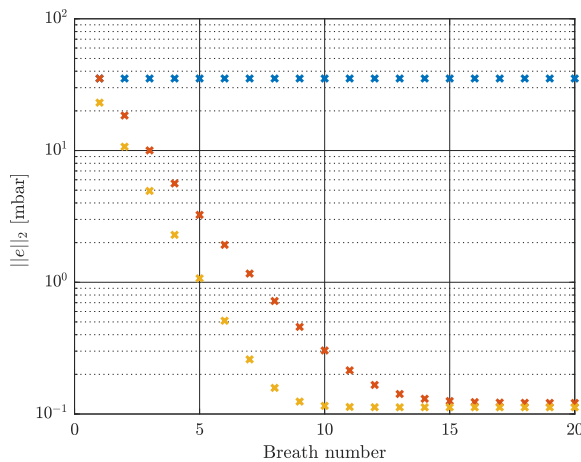


Fig. 5.7. Error 2-norm per breath for every control strategy in simulations. This figure contains the PID control strategy (×), the RC without feedback linearization (×), and the RC with feedback linearization (×).

slightly lower error upon convergence. Furthermore, stability is guaranteed. Next, these control strategies are compared in experiments.

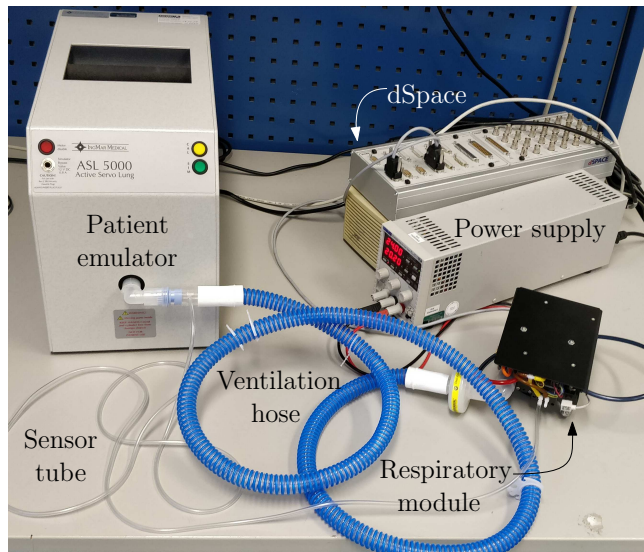


Fig. 5.8. Experimental setup with the most important parts, i.e., blower driven ventilator, ASL 5000 breathing simulation, dSpace module, and the hose.

5.6 Experimental results

In this section, the proposed control strategy of Section 5.4 is applied in an experimental case study, the particular case study, i.e., patient type and pressure levels, is the same as in Section 5.5. First, the experimental setup is presented in Section 5.6.1. Thereafter, the final designed controller is presented in Section 5.6.2. Finally, the experimental results are presented in Section 5.6.3.

5.6.1 Experimental setup

The main components of the experimental setup used in this case study are depicted in Fig. 5.8. The figure shows a Macawi blower-driven mechanical ventilation module (DEMCON macawi respiratory systems, Best, The Netherlands). Furthermore, the ASL 5000™ Breathing Simulator (IngMar Medical, Pittsburgh, PA) is shown in the figure. This breathing simulator is used to emulate a linear one-compartmental patient model. Furthermore, a typical hose-filter system for ventilation of a patient in a hospital setting is shown. The developed control algorithms are implemented in a dSPACE system (dSPACE GmbH, Paderborn, Germany).

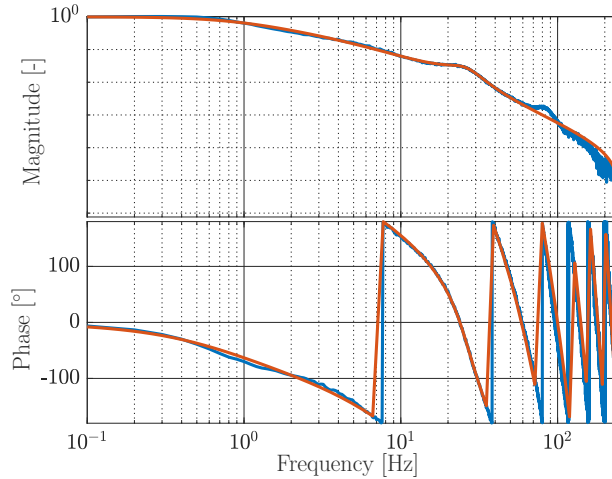


Fig. 5.9. Showing an FRF measurement of the complementary sensitivity T (—) and a fourth order fit of the complementary sensitivity (—).

5.6.2 Controller design

Again, three different controllers are considered, the benchmark PID controller, the linear RC without feedback linearization, and the linear RC with feedback linearization. In this section, the final designs for these controllers for the experimental case study are presented.

The benchmark PID controller, which is also used in the RC strategies, is the same controller as in the simulations. Also the feedback linearization strategy is the same as in the simulation case study. The estimate \hat{R}_{quad} is retrieved through a calibration procedure prior to ventilation, as shown in Fig. 5.3. Furthermore, the same argumentation as in the simulations is used to design the same Q and L filter for both RC strategies.

The filters for the repetitive controller are retrieved by first taking an FRF measurements of the open-loop plant. This open-loop FRF measurement and the considered feedback controller are combined to retrieve a non-parametric model of the complementary sensitivity T_{FRF} as depicted in Fig. 5.9. Next, a fourth-order fit of this process sensitivity is used to retrieve a parametric model of the complementary sensitivity T_{fit} , also shown in Fig. 5.9. A stable inverse of this parametric model T_{fit} is computed with ZPETC to retrieve the learning filter L . Next, stability is checked with Theorem 5.1 and this result is visualized in Fig. 5.10. This figure shows that stability is guaranteed with $Q = 1$. However, to improve robustness against plant variations a Q filter is added as depicted in Fig. 5.10. This Q filter is a 20th-order symmetric FIR filter with a cutoff frequency of 23 Hz. This results in more robustness against plant variations. Finally, to reduce the effect of non-periodic disturbances a learning gain α of 0.5 is added to both repetitive control strategies.

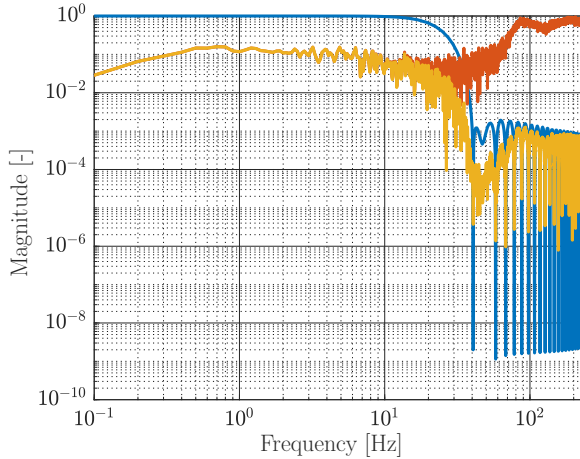


Fig. 5.10. Stability condition for the experimental setup. Showing Q as a low-pass filter with cut-off frequency at 23 Hz (—), the stability condition (5.11) with $Q = 1$ (—), and the stability condition (5.11) with Q the low-pass filter (—).

5.6.3 Results

The control strategies designed in the previous section are implemented in the experimental setup of Section 5.6.1 with the use case as presented in Section 5.5.1. The results of these experiments are presented in Fig. 5.11 and 5.12.

The time-domain results of the 20th breath for the three control strategies are shown in Fig. 5.11. This figure shows the airway pressure of all control strategies upon convergence. The results are similar to the simulation results. The figure shows that the PID controller achieves a sub-optimal rise-time and has significant overshoot, which is non-optimal for the patient's lungs. Furthermore, the figure shows that the RC strategies achieve near perfect tracking upon convergence, the airway pressure is almost exactly the same as the target pressure. This improves the patient's comfort and avoids harmful peak pressures.

The error 2-norm per breath for every control strategy is shown in Fig. 5.12. It shows that the error two norm with the PID controller remains around 35 mbar. Furthermore, it shows that both RC strategies converge to a significantly smaller error 2-norm of approximately 3 mbar. Also it shows that the feedback linearization results in a smaller initial error.

Besides the different initial error norm these experiments do not show a large difference between the RC strategies. Therefore, it would be interesting in future work to test this control strategy on a system with a more dominant nonlinearity. This might increase the effect of feedback linearization, resulting in faster convergence. However,

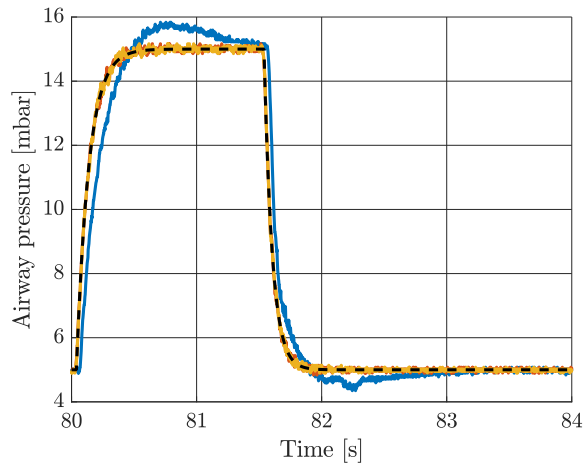


Fig. 5.11. Experimental results of the 20th breath in time domain upon convergence of the repetitive controllers. Showing the target pressure (---), the PID control strategy (—), repetitive control without feedback linearization (—), and repetitive control with feedback linearization (—).

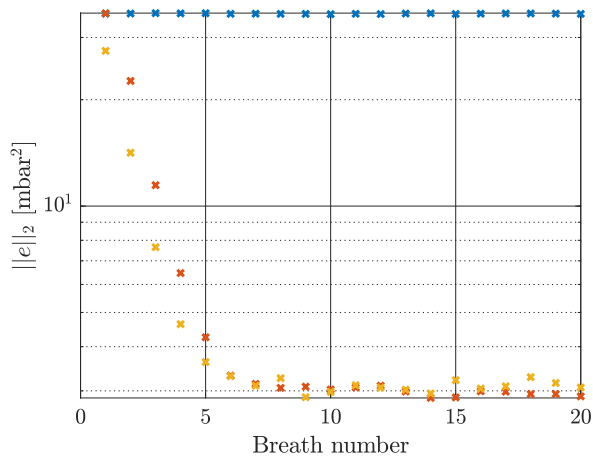


Fig. 5.12. Error 2-norm per breath for every control strategy in experiments. This figure contains the PID control strategy (×), the RC without feedback linearization (×), and the RC with feedback linearization (×). This figure shows that both RC strategies achieve very accurate tracking performance.

stability is guaranteed for the closed-loop system with feedback linearization and repetitive control. In contrast to the other control strategies, for which no stability guarantees are provided.

5.7 Conclusions

In this chapter, linear repetitive control in combination with feedback linearization is applied to a nonlinear mechanical ventilation such that the closed-loop stability properties of linear repetitive control are valid for this nonlinear plant.

The main contribution of this chapter is the combination of feedback linearization and linear repetitive control, such that the closed-loop nonlinear ventilation system is stable. In addition, the performance of the control strategy is analyzed by means of simulations and experiments. In simulations, it is shown that convergence speed of the repetitive controller is improved by applying feedback linearization. The performance in terms of error 2-norm upon convergence are similar for the method with and without feedback linearization. Thereafter, in experiments it is shown that the repetitive controller achieves accurate pressure tracking. The experiments show no significant effect on the performance by adding feedback linearization. However, the closed-loop system with feedback linearization and repetitive control is guaranteed to be stable. Whereas, no stability guarantees for the other presented control strategies are provided.

Repetitive control for Lur'e-type systems: application to mechanical ventilation

Abstract – Repetitive control has shown to achieve superior rejection of periodic disturbances. Many nonlinear systems are subject to repeating disturbances. The aim of this chapter is to develop a continuous-time RC design with stability guarantees for nonlinear Lur'e-type systems. Approximate output tracking is achieved by combining an internal model, consisting of a finite number of linear oscillators with frequencies at the reference frequency and at its multiples, with a stabilizer to guarantee convergence of the closed-loop system. The developed RC approach is applied to a nonlinear mechanical ventilation system for Intensive Care Units (ICUs), which are modeled as a Lur'e-type system. The experimental study confirms that the repetitive control scheme is able to successfully follow the desired target pressure profile to properly support the ventilation needs of an adult patient.

6.1 Introduction

Repetitive Control (RC) schemes are particularly suitable to achieve robust tracking of a periodic reference signal, see Astolfi et al. (2021a); Ghosh and Paden (2000); Longman (2010); Mattavelli and Marafao (2004). Tracking of periodic signals is a common control problem in many relevant application fields, for example in healthcare. In this chapter, the application of mechanical ventilation of patients on an Intensive Care Units (ICUs) is considered. Mechanical ventilation is used to support the breathing of patients by providing the correct oxygen support and elimination of carbon dioxide (Warner and Patel, 2013). Here, tracking of a periodic signal, i.e., pressure target, is desired. The

considered ventilation system is a nonlinear dynamical system, which can be modeled as a Lur'e-type system. Lur'e-type systems consist of the interconnection of linear time-invariant dynamics with a static nonlinearity in the feedback loop. These systems form a practically relevant sub-class of nonlinear systems, also for other application domains. To achieve robust tracking of the periodic pressure target of the ventilation system, a generically applicable RC scheme for Lur'e-type systems is developed.

The structural idea of RC is based on the *internal model principle*, namely on the fact that when a periodic signal with known period T must be tracked, a copy of the disturbance model generating such a signal must be included in the regulator (Bin et al., 2020). This is generally done through a universal generator of a T -periodic signal. Such a generator is implemented using a memory loop with a delay of length T . This memory loop places an infinite number of poles on the imaginary axes at the fundamental frequency $2\pi/T$ and its multiples, see, e.g., Ghosh and Paden (2000); Hara et al. (1988). Then, the extended system composed by the plant and such memory loop is stabilized with feedback control.

Because a delay is easily implemented in discrete-time, significant research efforts have been devoted to the development of discrete-time implementations of RC. In this approach, mostly linear systems are addressed from the theoretical point of view and good tracking performance is achieved in these systems, see, e.g., Blanken et al. (2020); Costa-Castelló and Grinó (2006); Onuki and Ishioka (2001); Reinders et al. (2020); Tomizuka et al. (1988, 1989). Unfortunately, the developed frequency analysis tools cannot be directly employed in the presence of nonlinearities. Therefore, typically no formal stability proofs are provided for repetitive control applied to nonlinear systems. In Reinders et al. (2020), discrete-time frequency domain RC has been applied to a ventilation system. However, no formal stability guarantees are given for the Lur'e-type closed-loop ventilation system.

In existing literature, several studies have considered output tracking problems for continuous-time nonlinear systems. For instance, in Astolfi et al. (2021a,b); Byrnes and Isidori (2004); Marconi et al. (2007) the problem of output tracking for nonlinear systems that can be written in the canonical normal form is considered. In Pavlov and Marconi (2008), incremental passivity concepts are used for the design of global regulators and in Pavlov et al. (2007b) output regulation of Lur'e-type systems using convergent system properties is considered. However, a constructive design of the stabilizer and guaranteed harmonic regulation properties are not presented. The design in Astolfi et al. (2015, 2021b); Ghosh and Paden (2000) relies on state-feedback approaches, and the domain of attraction of the periodic solution is only local in the size of the reference (Astolfi et al., 2015, 2021b) or not discussed (Ghosh and Paden, 2000). Finally, in Giaccagli et al. (2020, 2022) contractive feedback laws in tracking problems are developed for constant references, but not for periodic references.

Although significant progress on output regulation for nonlinear systems has been made, an RC-scheme for nonlinear Lur'e-type systems with a formal stability guarantee is not yet available. To achieve this, a finite-dimensional realization of the exact RC-scheme in Astolfi et al. (2021a); Califano et al. (2018) is used. The reason to con-

sider a finite-dimensional realization is the difficulty to analyze the interconnection of an infinite-dimensional system, i.e., the internal model, with nonlinear plant dynamics with nonlinear outputs. In this chapter, we follow an approach that relies on the harmonic representation of the delay, see, e.g., Astolfi et al. (2015, 2021b); Ghosh and Paden (2000); Mattavelli and Marafao (2004). The RC-scheme is implemented by including a finite number n_o of linear oscillators in the control loop. This results in n_o poles on the imaginary axes at the frequency of the periodic reference and its multiples. Therewith, if the resulting closed-loop trajectories converge to a periodic solution, *harmonic regulation* of the tracking error is guaranteed. More precisely, the Fourier coefficients of the error signal corresponding to the frequencies embedded in the linear oscillators are zero, and the L^2 -norm of the error signal is sufficiently small if n_o is large enough (Astolfi et al., 2015, 2021b; Ghosh and Paden, 2000). To guarantee the existence of globally asymptotically stable periodic solutions, the theory of convergent systems is exploited, see, e.g., Pavlov and van de Wouw (2017); Pavlov et al. (2007a, 2005, 2006). To this end, we suppose that the static nonlinearity in the Lur'e-type system satisfies an incremental sector bound condition. Then, using the strictly positive real lemma, sufficient conditions for a stabilizing output-feedback law are established. From a practical point of view, such an approach is interesting because the conditions can be checked by visual inspection of the Nyquist plot and linear analysis tools (potentially using measured data only). Eventually, the repetitive controller design is applied to the practical problem of mechanical ventilation.

Summarizing, the main contributions of this chapter are:

- an RC strategy for nonlinear Lur'e-type systems including a formal stability analysis, and
- the implementation and analysis of this RC scheme on the practical use-case of a nonlinear mechanical ventilator, including experimental validation.

This chapter is organized as follows. In Section 6.2, the problem statement is formalized. In Section 6.3, the main results concerning the RC controller design are presented. Then, in Section 6.4, the RC paradigm is applied to the mechanical ventilation use-case. Finally, the main conclusions and recommendations for future work are presented in Section 6.5.

Notations. Throughout this chapter, s represents the Laplace variable. Given an $n \times n$ symmetric matrix P , we write $P \succ 0$ ($\prec 0$) if P is strictly positive (negative) definite. Given a $n \times n$ matrix P , the operator $\text{blkdiag}(P \dots P)$ represents a block-diagonal matrix with P as block-diagonal elements, the dimensions are specified case-wise. Furthermore, \dot{x} represents the continuous-time derivative of x . Finally, we define $\mathcal{P}_T(\tilde{r})$ as the set of C^1 T -periodic functions with bounded infinity norm and bounded infinity norm of its derivative. In particular, we say that $r(t) \in \mathcal{P}_T(\tilde{r})$ if r is C^1 , T -periodic, and satisfies $\sup_{t \in [0, T]} |r(t)| \leq \tilde{r}$ and $\sup_{t \in [0, T]} |\dot{r}(t)| \leq \tilde{r}$ for some non-negative real number

\tilde{r} .

6.2 Problem statement

Consider a Single-Input Single-Output (SISO) Lur'e-type system of the form

$$\begin{aligned} \dot{x} &= Ax + Bu + Ew \\ y &= Mx + Nw \\ w &= -\varphi(y) \\ v &= Cx + Dw, \end{aligned} \tag{6.1}$$

where $x \in \mathbb{R}^n$ is the state, $u \in \mathbb{R}$ is the control input, w, y are in \mathbb{R} , $v \in \mathbb{R}$ is the measured output, and A, B, E, M, N, C , and D are real matrices of appropriate dimensions. The static nonlinearity $\varphi : \mathbb{R} \mapsto \mathbb{R}$ satisfies $\varphi(0) = 0$, and the following incremental sector bound condition:

$$\underline{\varphi} \leq \frac{\varphi(y_1) - \varphi(y_2)}{y_1 - y_2} \leq \bar{\varphi} \quad \forall y_1 \neq y_2, \tag{6.2}$$

for some known non-negative constants $0 \leq \underline{\varphi} \leq \bar{\varphi}$. The control objective is to regulate the output v of the system (6.1) to a T -periodic bounded reference $r \in \mathcal{P}_T(\bar{r})$. Hence, the output regulation error is defined as

$$e(t) := r(t) - v(t). \tag{6.3}$$

With the mechanical ventilation application in mind, where the full-state x is not available for feedback, we aim to design a dynamic output feedback controller for system (6.1), processing only the regulated output error e , such that *harmonic regulation* is achieved in the following sense.

Problem 6.1 (Harmonic regulation of order n_o). *Consider system (6.1) with regulation error (6.3) and assume that the nonlinearity φ satisfies the incremental sector bound condition (6.2). Given any $\tilde{r} > 0$, $n_o > 0$, determine a dynamic output feedback controller of the form*

$$\begin{aligned} \dot{z} &= \xi(z, e) \\ u &= \zeta(z, e), \end{aligned} \tag{6.4}$$

such that for any reference $r \in \mathcal{P}_T(\tilde{r})$ and any initial condition $x_{cl}(0)$ defined as $[x^T(0), z^T(0)]^T \in \mathbb{R}^{n_x}$, the corresponding steady-state trajectory $\bar{x}_{cl} := [\bar{x}^T, \bar{z}^T]^T$ of the closed-loop (6.1), (6.3), (6.4) is bounded, T -periodic, exponentially stable¹, and the steady-state output error \bar{e} has no harmonic content at frequencies $\omega = k\frac{2\pi}{T}$, $k = 0, 1, \dots, n_o$.

¹a time-varying solution $\bar{x}(t)$ is called exponentially stable if $\|x(x(0), t) - \bar{x}(\bar{x}(0), t)\| \leq \alpha \|x(0) - \bar{x}(0)\| e^{-\lambda t}$ for some $\alpha, \lambda > 0$.

The repetitive control approach in Astolfi et al. (2015, 2021b); Ghosh and Paden (2000) is followed to achieve the harmonic regulation objective stated in Problem 6.1. The main idea is to include linear oscillators at the periodic reference frequency and its multiples in the regulator dynamics (6.4). This approach achieves, if the closed-loop steady-state trajectories are bounded and periodic, structural zeros at the frequencies $k\omega$ with the blocking property of zeroing the Fourier coefficients of the output e corresponding to these frequencies. As a consequence, the strategy that we propose in this work is to:

- 1) design of the function ξ in (6.4) to include the linear oscillators;
- 2) design the feedback ζ in (6.4) to ensure the desired stability properties for the resulting closed-loop system; and
- 3) analyze the resulting trajectories and show that the harmonic content is zero at the desired frequencies. As a byproduct, we verify that if the number of oscillators included in the regulator are large enough, the asymptotic ℓ^2 -norm of the output e can be regulated to an arbitrarily small value.

6.3 Repetitive control of Lur'e-type systems

In this section, the repetitive controller design for Lur'e-type systems is presented. First, in Section 6.3.1, the repetitive controller design is presented, the closed-loop dynamics are obtained, and a loop transformation is applied that allows the use of known results on exponentially convergent Lur'e-type systems. In Section 6.3.2, known results on convergent Lur'e-type systems are presented as a stepping stone to the stability analysis. Finally, in Section 6.3.3, it is shown that the proposed controller design solves Problem 6.1.

6.3.1 Controller design

To provide a solution to Problem 6.1, the repetitive control approach in Ghosh and Paden (2000) is adopted by including n_o linear oscillators in the control loop, at the reference frequency and its multiples, that process the output e to be regulated, as in standard output regulation problems, see, e.g., Astolfi et al. (2015, 2021b); Pavlov et al. (2006). To this end, the control structure in (6.4) is defined as:

$$\dot{z} = \xi(z, e) := \Phi z + \Gamma e \quad (6.5)$$

$$u = \zeta(z, e) := Kz \quad (6.6)$$

where $z = [z_0 \ z_1^T \ \dots \ z_{n_o}^T]^T \in \mathbb{R}^{(2n_o+1) \times 1}$ with $z_0 \in \mathbb{R}$ and $z_k \in \mathbb{R}^{2 \times 1}$ for $k = 1, \dots, n_o$, and where the matrices $\Phi \in \mathbb{R}^{(2n_o+1) \times (2n_o+1)}$, $\Gamma \in \mathbb{R}^{(2n_o+1) \times 1}$, and $K \in$

$\mathbb{R}^{1 \times (2n_o+1)}$ are defined as

$$\begin{aligned}\Phi &:= \text{blkdiag}(0 \ \phi_1 \ \dots \ \phi_{n_o}), \\ \Gamma &:= [\gamma_0 \ \gamma_1^T \ \dots \ \gamma_{n_o}^T]^T, \\ K &:= [\kappa_0 \ \kappa_1 \ \dots \ \kappa_{n_o}],\end{aligned}\tag{6.7}$$

where

$$\phi_k := k \begin{bmatrix} 0 & \frac{2\pi}{T} \\ -\frac{2\pi}{T} & 0 \end{bmatrix}, \quad k = 1, \dots, n_o,\tag{6.8}$$

with $\gamma_0 \neq 0$ the integrator gain such that z_0 embeds an integrator, and the matrix $\gamma_k \in \mathbb{R}^{2 \times 1}$ is chosen such that the pair (ϕ_k, γ_k) is controllable for any $k = 1, \dots, n_o$. By construction, the pair (Φ, Γ) is therefore controllable. In this control structure, the z -dynamics represent the state-space representation of n_o linear oscillators at the periodic reference frequency and its multiples. The number of oscillators n_o represents a degree of freedom of the controller design as it defines the dimension of the chosen internal model and allows to suppress the first n_o -harmonics of the steady-state trajectory which is formalized later.

Next, the closed-loop system consisting of the plant (6.1), (6.3) and the repetitive controller (6.5), (6.6) is written as a Lur'e-type system

$$\begin{aligned}\dot{x}_{cl} &= A_{cl}x_{cl} + E_{cl}w_{cl} + d(t) \\ y_{cl} &= M_{cl}x_{cl} + N_{cl}w_{cl} \\ w_{cl} &= -\varphi(y_{cl})\end{aligned}\tag{6.9}$$

where

$$\begin{aligned}A_{cl} &:= \begin{bmatrix} A & BK \\ -\Gamma C & \Phi \end{bmatrix}, \quad E_{cl} := \begin{bmatrix} E \\ -\Gamma D \end{bmatrix}, \quad Q_{cl} := \begin{bmatrix} 0 \\ \Gamma \end{bmatrix}, \\ M_{cl} &:= [M \ 0], \quad N_{cl} := N,\end{aligned}\tag{6.10}$$

where $x_{cl} := [x^T, z^T]^T \in \mathbb{R}^{n_x}$, $w_{cl} := w$, $y_{cl} := y$, and $d(t) := Q_{cl}r(t)$, is a periodic, with period time T , time-varying piece-wise continuous disturbance (induced by the periodic reference).

Next, a loop-transformation as described in (Khalil, 2002, Chapter 7) is applied to the closed-loop dynamics. This loop-transformation gives an equivalent Lur'e-type system where the transformed nonlinearity $\tilde{\varphi}(y_{lt})$ satisfies the incremental sector bound in (6.2) with $\tilde{\varphi} = 0$ and $\tilde{\varphi} = \infty$. This enables direct application of the known results on exponentially convergent Lur'e-type systems in Section 6.3.2. This loop-transformation gives the following loop-transformed Lur'e-type system:

$$\begin{aligned}\dot{x}_{lt} &= A_{lt}x_{lt} + E_{lt}w_{lt} + d(t) \\ y_{lt} &= M_{lt}x_{lt} + N_{lt}w_{lt} \\ w_{lt} &= -\tilde{\varphi}(y_{lt})\end{aligned}\tag{6.11}$$

where

$$\begin{aligned}
 A_{lt} &:= A_{cl} - (E_{cl}\varphi(M_{cl} + N_{cl}(1 + \varphi N_{cl})^{-1}\varphi M_{cl})), \\
 E_{lt} &:= E_{cl}(1 - \varphi D_{cl}(1 + \varphi N_{cl})^{-1}), \\
 M_{lt} &:= \phi M_{cl} - \phi N_{cl}(1 + \varphi N_{cl})^{-1}\varphi M_{cl}, \\
 N_{lt} &:= 1 + \phi N_{cl}(1 + \varphi N_{cl})^{-1}
 \end{aligned} \tag{6.12}$$

where $x_{lt} \in \mathbb{R}^{n_x}$, $y_{lt} \in \mathbb{R}$, $w_{lt} \in \mathbb{R}$, $\phi = \bar{\varphi} - \varphi$, and $\tilde{\varphi}(y_{lt})$ satisfies the incremental sector bound in (6.2) with $\tilde{\varphi} = 0$ and $\bar{\varphi} = \infty$. Furthermore, it is assumed that the controller is designed such that Assumption 6.1 holds.

Assumption 6.1. *The pair (A_{lt}, E_{lt}) is controllable and the pair (A_{lt}, M_{lt}) in (6.11) is observable.*

Next, to solve Problem 6.1 it must be shown that the closed-loop system exhibits a globally exponentially stable steady-state trajectory that is well-defined, bounded, T -periodic, and that the associated output error \bar{e} has no harmonic content at the frequencies included in the internal model. To show this, known results on exponentially convergent Lur'e-type systems are used. These results are provided next.

6.3.2 Exponentially convergent Lur'e-type systems

First, we provide the following definition of convergent systems, see, e.g., Pavlov and van de Wouw (2017); Pavlov et al. (2007a); Ruffer et al. (2013), applicable to the Lur'e-type systems of the form (6.11), with \mathcal{D} a set of piece-wise continuous, bounded disturbances.

Definition 6.1. *Given $d(t) \in \mathcal{D}$, the system (6.11) is said to be globally exponentially convergent if*

- *there exists a solution $\bar{x}_{lt,d}(t)$ defined and bounded for all $t \in \mathbb{R}$;*
- *the solution $\bar{x}_{lt,d}(t)$ is globally exponentially stable.*

System (6.11) is called convergent for $d \in \mathcal{D}$ if it is convergent for any $d(t) \in \mathcal{D}$ see (Pavlov et al., 2006, Definition 2.16). Note that for an exponentially convergent system, the steady-state solution is unique, see (Pavlov et al., 2006, Property 2.15). Moreover, if the input $d(t)$ is T -periodic, then, for exponentially convergent systems, $\bar{x}_{lt,d}(t)$ is also T -periodic, as recalled in the next property, see, e.g., Pavlov and van de Wouw (2017); Pavlov et al. (2007a, 2006).

Property 6.1. *Consider system (6.11) and suppose it is exponentially convergent. If d is a periodic signal with period $T > 0$, i.e., $d(t) = d(t + T)$ for all t , then the corresponding steady-state solution $\bar{x}_{lt,d}(t)$ is also periodic with period T .*

To show that the closed-loop Lur'e-type system of the form (6.11) is a globally exponentially convergent system, let

$$\mathcal{H}(s) = M_{lt}(sI - A_{lt})^{-1}E_{lt} + N_{lt}. \quad (6.13)$$

Then, results from Yakubovich (1964) and (Pavlov et al., 2006, Chapter 5) can be used. By combining the definition of a Strictly Positive Real (SPR) transfer function and the incremental sector bound condition (6.2), Lemma 6.1 is obtained that expresses sufficient conditions that guarantee that the system (6.11) is globally exponentially convergent, which is proved in (Khalil, 2002, Chapter 7).

Lemma 6.1. *Let Assumption 6.1 hold. If (6.2) holds and the transfer function $\mathcal{H}(s)$ is Strictly Positive Real (SPR), then the system (6.11) is globally exponentially convergent.*

Using Lemma 6.1, global exponential convergence of the closed-loop Lur'e-type system in (6.11) can be guaranteed by showing that $\mathcal{H}(s)$ is SPR. The transfer function $\mathcal{H}(s)$ is SPR if and only if the following conditions hold, see Pavlov and van de Wouw (2017); Yakubovich (1964):

1. $\mathcal{H}(s)$ is Hurwitz;
2. $\operatorname{Re}\{\mathcal{H}(j\omega)\} > 0 \forall \omega \in \mathbb{R}$; and
3. $\mathcal{H}(\infty) > 0$ or $\mathcal{H}(\infty) = 0$ and $\lim_{\omega \rightarrow \infty} \omega^2 \mathcal{H}(j\omega) > 0$.

Note that the SPR conditions on $\mathcal{H}(s)$ can be visually verified with the Nyquist plot, see (Khalil, 2002, Chapter 7). This makes these conditions particularly useful to verify in practical applications, see Section 6.4. Next, these results are used to design the feedback gain K in the feedback law (6.6), such that Problem 6.1 is solved.

6.3.3 Harmonic regulation of Lur'e-type systems

The results of Lemma 6.1 enable the main theoretical result of this chapter, which solves Problem 6.1. More specifically, it is shown that the presented repetitive controller achieves the desired harmonic regulation properties and convergence properties of the closed-loop system if the feedback gain K is designed properly.

If we can design the feedback law (6.6) such that the closed-loop (6.1), (6.3), (6.5), (6.6) is globally exponentially convergent for any $d(t)$, then by virtue of Definition 6.1 and Property 6.1, for every initial condition the solutions of (6.9) exponentially converge to a unique, bounded, and well-defined steady-state solution, which is T -periodic if the reference $r(t)$ is T -periodic. Then, using Lemma 6.2 below (Astolfi et al., 2015; Ghosh and Paden, 2000), it is shown that the Fourier coefficients, of the associated steady-state solution \bar{e} of the error e , corresponding to the n_o frequencies embedded in the internal model (6.5), must be zero. Hence, harmonic regulation is achieved.

Lemma 6.2. *Let the steady-state solution (\bar{x}, \bar{z}) be a bounded trajectory of the cascade (6.1), (6.3), and (6.5), with corresponding steady-state output error $\bar{e}(t)$. Suppose that $\bar{e}(t+T) = \bar{e}(t)$ for all $t \geq 0$. Then, necessarily*

$$\int_0^T \cos(k\frac{2\pi}{T}t)\bar{e}(t)dt = \int_0^T \sin(k\frac{2\pi}{T}t)\bar{e}(t)dt = 0, \quad (6.14)$$

for all $k \in [0, 1, \dots, n_o]$. Moreover, for any compact set $C_x \subset \mathbb{R}^n$, for any $\tilde{r} > 0$, $\bar{u} > 0$, and $\varepsilon > 0$ such that $\bar{x}(t) \in C_x$, $r \in \mathcal{P}_T(\tilde{r})$, and $|\bar{u}(t)| \leq \bar{u}$ for all $t \geq 0$, there exists $n_o^* \geq 1$ such that the following holds:

$$\|\bar{e}(t)\|_{L^2} := \left(\int_0^T |\bar{e}(t)|^2 dt \right)^{\frac{1}{2}} \leq \varepsilon, \quad \forall n_o \geq n_o^*. \quad (6.15)$$

Then, combining these harmonic regulation properties and the convergent system properties of the loop-transformed closed-loop system solves Problem 6.1, which brings us to the result in Theorem 6.1.

Theorem 6.1. *Consider the Lur'e-type system (6.1), (6.3), with the nonlinearity $\varphi(\cdot)$ satisfying the incremental sector condition in (6.2), in closed loop with a dynamical controller (6.5), (6.6). Given an arbitrary integer $n_o > 0$ and suppose that the matrix K is chosen such that the transfer function $\mathcal{H}(s)$ in Lemma 6.1, with the matrices $A_{lt}, E_{lt}, M_{lt}, N_{lt}$ defined in (6.10), satisfies Assumption 6.1 and the SPR conditions in Lemma 6.1. Then, Problem 6.1 is solved, namely harmonic regulation of order n_o , as defined by (6.14), is achieved.*

Proof. Consider system (6.1), (6.3) in closed-loop with (6.5), (6.6), which can be written in the form of (6.9) and (6.10). Then, the loop-transformation can be applied to obtain (6.11) and (6.12). Since the conditions of Lemma 6.1 are satisfied and the loop-transformed system is equivalent to the original closed-loop system, the closed-loop system is globally exponentially convergent. Hence by Property 6.1, if $r(t)$ is periodic with period $T > 0$, there exists a bounded, globally exponentially stable solution $\bar{x}(t), \bar{z}(t)$ which is T -periodic. As a consequence, the resulting output steady-state trajectory \bar{e} is also bounded and T -periodic. By direct application of Lemma 6.2 it satisfies (6.14). This concludes the proof. \square

The statement of Theorem 6.1 establishes a set of sufficient conditions for the design of the regulator in (6.5) and (6.6). In particular, the matrices K and Γ should be designed such that the desired SPR conditions on $\mathcal{H}(s)$ are satisfied to ensure the satisfaction of the conditions in Lemma 6.1. The SPR conditions at the end of Section 6.3.2 can be supported by graphical checks in a Nyquist plot, similar to frequency-domain design techniques for linear controller design.

In case the system in (6.9) is a minimum-phase system with unitary relative degree²,

²In this case, we refer to a system in normal form with stable zero-dynamics. See for instance, (5) and Assumption 2 in Astolfi et al. (2021a). Necessary and sufficient conditions under which a system of the form (6.9) can be written in canonical normal form are well known in the literature, see, e.g., Isidori (1995).

a systematic design of the gain K can be done by following Astolfi et al. (2021b). The system in (6.9) can be put in this form, for instance when $CB \neq 0$ and $D = 0$. In such case, it can be put in the canonical normal form following (Isidori, 1995, Chapter 4). Then, additional properties can be established. In particular, by selecting K such that the bound

$$K\Gamma\Gamma^TK^T \leq a \quad (6.16)$$

holds with a a positive and bounded scalar which is independent of n_o , it can be proved that the asymptotic L^2 -norm of \bar{e} can be made arbitrarily small by increasing the number of oscillators. More specifically, in such case ϵ in (6.15) can be made arbitrarily small by increasing the number of oscillators n_o . For instance, one can match the condition (6.16) by selecting the gains γ_k in (6.7) as $\gamma_k = k^{-(1+\epsilon)}\bar{\gamma}_k$ with $\bar{\gamma}_k$ so that $|\bar{\gamma}_k| \leq \bar{\gamma}$ for any $k = 1, \dots, n_o$, for some $\bar{\gamma} > 0$, and by selecting κ_k in (6.7) such that $|\kappa_k| \leq \bar{\kappa}$ for any $k = 1, \dots, n_o$, for some $\bar{\kappa} > 0$. Note that the condition (6.16) essentially establishes that the regulator (6.5), (6.6) has an L^2 -gain between the input e and the output u which does not depend on the number of oscillators n_o . This design philosophy will be pursued in the mechanical ventilation application to experimentally show the desired approximate L^2 output regulation objective (6.15).

6.4 Application to mechanical ventilation

In this section, the RC strategy is applied to a nonlinear mechanical ventilation system, i.e., this section describes the second contribution of this chapter. First, in Section 6.4.1, an overview of the considered ventilation system and the control goal for ventilation are described. Thereafter, the mathematical ventilation model and the actual mechanical ventilation setup are presented in Section 6.4.2. Then, repetitive controllers for mechanical ventilation are designed and stability of the closed-loop system is analyzed in Section 6.4.3. Then, in Section 6.4.4, the experimental results are presented and analyzed. Thereafter, another ventilation use-case is briefly considered to analyze the conservatism of Theorem 6.1 in Section 6.4.5. Finally, a remark on RC design is made based on observations from the experimental case study.

6.4.1 Ventilation system overview and control goal

Mechanical ventilators are essential equipment in Intensive Care Units (ICUs) to assist patients who cannot breathe on their own or need support to breathe sufficiently. The goal of mechanical ventilation is to ensure adequate oxygenation and carbon dioxide elimination (Warner and Patel, 2013), and thereby sustaining the patient's life. Next, the considered ventilation system and corresponding control goal are described.

6.4.1.1 Ventilation system overview

A schematic overview of the considered ventilation system is depicted in Fig. 6.1. The main components of this system are the blower, the hose-filter system, and the patient.

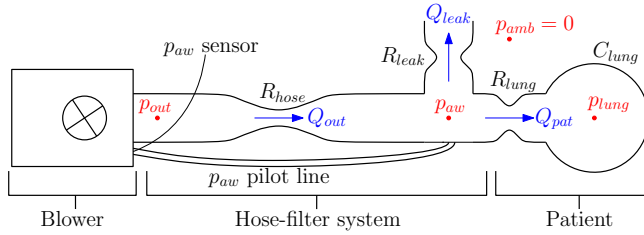


Fig. 6.1. Schematic representation of the blower-hose-patient system, with the corresponding resistances, lung compliance, pressures, and flows.

A centrifugal blower compresses ambient air to achieve the desired blower outlet pressure p_{out} . The difference between p_{out} and the airway pressure p_{aw} results in the outlet flow Q_{out} through the hose. This hose is modeled using a nonlinear hose model. The flow through the hose, i.e., the outlet flow Q_{out} , is divided into a patient flow Q_{pat} and a leak flow Q_{leak} . The intended leak near the patient is used to flush CO_2 -rich air from the system. Finally, the patient's lungs are inflated and deflated by the patient flow.

6.4.1.2 Control goal

In this experimental use-case, Pressure Controlled Ventilation (PCV) is considered. A schematic example of PCV is depicted in Fig. 6.2. In PCV, the pressure near the patient's mouth, the airway pressure p_{aw} , should track a desired pressure target p_{target} , i.e., $r := p_{target}$. On a preset periodic interval, of length T , the pressure level is increased to the Inspiratory Positive Airway Pressure (IPAP), and consequently lowered to the Positive End-Expiratory Pressure (PEEP). These varying pressure levels ensure the desired airflow in and out of the patient's lungs. The total breath length T consists of the inspiration time T_i and expiration time T_e , i.e., $T = T_i + T_e$.

The control goal for PCV is to achieve a small tracking error $e := r - p_{aw} = r - v$, where the reference $r(t)$ is a time-varying signal that is perfectly periodic with an interval length T , i.e., $r(t) = r(t+T)$ for a known $T > 0$ and all $t \geq 0$. Because of this periodicity property and the nonlinear nature of the hose model, the Repetitive Control (RC) strategy developed in this chapter is particularly suitable for this application.

6.4.2 Mathematical model and experimental ventilation system

For controller design and the stability analysis, a mathematical Lur'e-type system model is derived. The ventilation model is based on Reinders et al. (2021a). Thereafter, the actual experimental ventilation setup is presented.

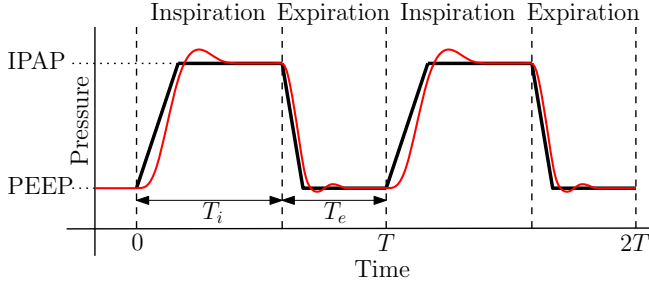


Fig. 6.2. Typical airway pressure for two breathing cycles of pressure controlled ventilation, showing the set-point (—) and the typical response (—).

6.4.2.1 Mathematical model of the ventilation system

In this section, first the separate models for the plant components are derived, i.e., blower model G_b , hose model R_{hose} , and patient-leak model G_p . Thereafter, these models are combined to obtain the open-loop Lur'e-type ventilation system model for the controller design and associated stability analysis. The complete plant and the considered control strategy are visualized in the blockdiagram in Fig. 6.4.

The blower model G_b is obtained by means of a sixth-order fit of a Frequency Response Measurement (FRF) of the actual blower dynamics (Pintelon and Schoukens, 2012). This state-space model accurately describes the input-output relation of the blower, i.e., from the control signal p_c to the blower output p_{out} . The measured FRF and the blower model G_b are depicted in Fig. 6.3, showing that G_b is an accurate representation of the FRF measurement of the actual blower. The blower G_b is modeled as the following state-space system:

$$\begin{aligned} \dot{x}_b &= A_b x_b + B_b p_c \\ p_{out} &= C_b x_b, \end{aligned} \quad (6.17)$$

with $x_b \in \mathbb{R}^6$, $p_c \in \mathbb{R}$, $p_{out} \in \mathbb{R}$, and system matrices of appropriate dimensions.

The hose is modeled by the nonlinear hose resistance R_{hose} , which describes the relation between the flow through the hose Q_{out} and the pressure drop over the hose $\Delta p := p_{out} - p_{aw}$. From experiments it is concluded that the hose can be modeled as follows:

$$\begin{aligned} Q_{out} &:= R_{hose}(\Delta p) \\ &= \text{sign}(\Delta p) \frac{-R_1 + \sqrt{R_1^2 + 4R_2|\Delta p|}}{2R_2}, \end{aligned} \quad (6.18)$$

where R_1 and R_2 are the hose-resistance parameters.

Next, the combined patient-leak model G_p describes the relation between the outlet flow Q_{out} and the system output $y = p_{aw}$. This patient model is described by the

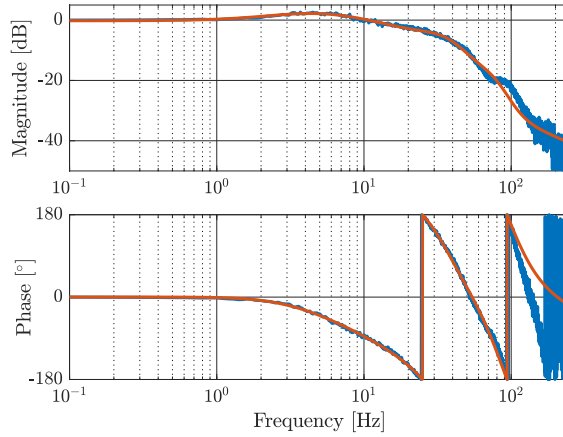


Fig. 6.3. Frequency response measurement (—) and 6th order identified parametric model (—) of the blower, i.e., from p_c to p_{out} .

following first-order state-space model, based on the linear one-compartmental lung model in Bates (2009):

$$\begin{aligned} \dot{p}_{lung} &= a_p p_{lung} + b_p Q_{out} \\ p_{aw} &= c_p p_{lung} + d_p Q_{out} \end{aligned} \quad (6.19)$$

with

$$\begin{aligned} a_p &= -\frac{1}{C_{lung}(R_{leak} + R_{lung})}, \\ b_p &= \frac{R_{leak}}{C_{lung}(R_{leak} + R_{lung})}, \\ c_p &= \frac{R_{leak}}{R_{leak} + R_{lung}}, \quad d_p = \frac{R_{leak}R_{lung}}{R_{leak} + R_{lung}}. \end{aligned} \quad (6.20)$$

Finally, these separate models are combined to obtain the open-loop plant model, as depicted inside the dashed box in Fig. 6.4. Note that an additional term $\eta\Delta p$ is added to the nonlinear hose-resistance, i.e., $\varphi(\Delta p) := R_{hose}(\Delta p) + \eta\Delta p$, and subtracted in the parallel path; this is included to ensure that the linear dynamics of the open-loop plant in Lur'e-type form are controllable and observable. The total system's dynamics, i.e., the full Lur'e-type ventilation system, are independent of the choice of $\eta \in \mathbb{R}$.

To obtain the open-loop plant model, the blower, hose, and patient model are combined. This gives the open-loop model from p_c to p_{aw} in the form of (6.1). The open-

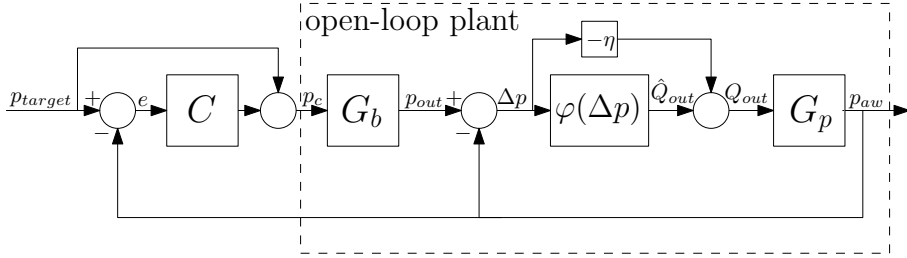


Fig. 6.4. Block diagram of the full ventilation system, with G_b the blower dynamics, C an arbitrary feedback controller, G_p the patient-leak dynamics, and $\varphi(\Delta p) = R_{hose}(\Delta p) + \eta\Delta p$ the nonlinear hose model.

loop ventilation system is defined by (6.1) with the system matrices

$$\begin{aligned}
 A &= \begin{bmatrix} A_b & 0 \\ -(1 - \eta d_p)^{-1} \eta C_b b_p & a_p + \eta c_p (1 - \eta d_p)^{-1} b_p \end{bmatrix}, \\
 B &= \begin{bmatrix} B_b \\ 0 \end{bmatrix}, \quad E = \begin{bmatrix} 0 \\ -b_p (1 - \eta d_p)^{-1} \end{bmatrix}, \\
 M &= \begin{bmatrix} C_b + d_p (1 - \eta d_p)^{-1} \eta C_b \\ -c_p - d_p (1 - \eta d_p)^{-1} \eta c_p \end{bmatrix}^T, \\
 N &= d_p (1 - \eta d_p)^{-1}, \quad D_o = -d_p (1 - \eta d_p)^{-1}, \\
 C &= \begin{bmatrix} -d_p (1 - \eta d_p)^{-1} \eta C_b & c_p + d_p (1 - \eta d_p)^{-1} \eta c_p \end{bmatrix},
 \end{aligned} \tag{6.21}$$

and the nonlinearity

$$\varphi(y) := R_{hose}(y) + \eta y. \tag{6.22}$$

These open-loop system matrices and the nonlinearity in combination with the RC that is designed in Section 6.4.3 are used to retrieve the closed-loop ventilation system and to guarantee that it solves Problem 6.1 using Theorem 6.1.

6.4.2.2 Experimental ventilation setup

The main components of the experimental setup used in this case study are depicted in Fig. 6.5. The figure shows the Macawi blower-driven mechanical ventilation module (DEMCON macawi respiratory systems, 2021). The dSPACE system (dSPACE GmbH, Paderborn, Germany) is used to implement the controls in MATLAB Simulink (MathWorks, Natick, MA). Furthermore, the ASL 5000™ Breathing Simulator (Ing-Mar Medical, Pittsburgh, PA) represents the patient. This lung simulator can be used to emulate a wide variety of patients with a linear resistance and compliance. Furthermore, a typical ventilation hose with leak is used to attach the ventilation module to the lung simulator. The system parameters that are used for the stability analysis are shown

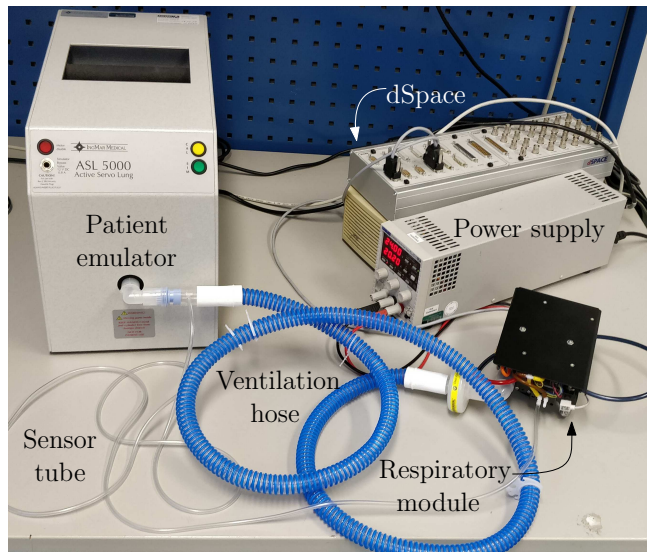


Fig. 6.5. The experimental setup with the mechanic patient simulator, the respiratory module, ventilation hose, and dSPACE module.

in Table 6.1. The leak and hose parameters are obtained by a calibration and the patient parameters are the settings used on the mechanic lung simulator, i.e., patient emulator in Fig. 6.5.

The analysis in the following section is done using a continuous-time representation of the controller and plant model. However, the controller is implemented in dSPACE using a discrete-time representation of the continuous-time control strategy. The discrete-time controllers are obtained using zero-order hold discretization at a sampling frequency of 500 Hz. This sampling frequency is significantly higher than the relevant system dynamics, e.g., the blower shows strong roll-off at frequencies above 10 Hz. Furthermore, 500 Hz is significantly higher than the frequency content of the reference signal. Therefore, the continuous-time controller design and stability analysis is deemed relevant for this application.

6.4.3 Controller design for mechanical ventilation

Next, the RC controller design for mechanical ventilation is described and it is shown that it solves Problem 6.1 for this ventilation use-case.

6.4.3.1 Controller design

For the design of the feedback controller C in Fig. 6.4, the control strategy in (6.5), (6.7), and (6.8) with feedback law (6.6) is followed. This means that the feedback con-

Table 6.1. The relevant system and experiment parameter for the stability analysis.

Parameter	Value	Unit
R_{leak}	24	mbar s/L
R_1	2.8	mbar s/L
R_2	1.6	mbar s ² /L ²
R_{lung}	5	mbar s/L
C_{lung}	50	mL/mbar
η	-0.1	mL/s/mbar

troller C consists of an integrator and n_o oscillators from the first up until the n_o^{th} harmonic of the breathing frequency $\omega_b = 2\pi/T$ rad/s. Besides this feedback controller, a unity feedforward controller as depicted in Fig. 6.4 is used. The unity feedforward term is included to improve the overall regulation accuracy. Note that it does not affect stability since it is included in the closed-loop ventilation system through the disturbance term d in (6.9). The stability analysis is independent of this disturbance in view of the convergence properties of the closed-loop dynamics.

For the final RC design, different controllers are designed to analyze the effect of the number of oscillators, i.e., $n_o \in \{0, 1, 5, 15, 20\}$. We select the integrator gain as $\gamma_0 = 2\pi$, and oscillator gains as $\gamma_k = [1 \ 1] \frac{2}{k^{1+\epsilon}}$ with $\epsilon = 0.4$, for $k = 1, 2, \dots, n_o$. The feedback law is chosen as $K \in \mathbb{R}^{1 \times (2n_o+1)}$ with all entries 1. Note that the design of the gains Γ, K satisfies the condition (6.16). Next, the stability properties of the closed-loop ventilation system with the RC controller are analyzed.

6.4.3.2 Stability analysis

To guarantee exponential convergence of the closed-loop ventilation system, and thereby showing that Problem 6.1 is solved, Theorem 6.1 is verified. First of all, the controlled system is written in the closed-loop form of (6.9), and the upper $\bar{\varphi}$ and lower $\underline{\varphi}$ sector bounds of the nonlinearity $\varphi(y)$ in (6.22) are computed. Using these bounds, the loop-transformation is applied to obtain the system in (6.11). Thereafter, Lemma 6.1 is verified, which ensures that Theorem 6.1 holds.

The upper sector bound $\bar{\varphi}$ is defined by taking the derivative of $\varphi(\Delta p)$ at the origin, where the slope of φ is the largest, see Fig. 6.6, which gives $\bar{\varphi} = \frac{1}{R_1} + \eta$. The lower sector bound $\underline{\varphi}$ is obtained from visual inspection, such that it holds on a finite domain of $\Delta p \in [-20, 20]$ mbar; this domain is sufficient for the practical application of ventilation. This leads to the sector $\varphi \in [\underline{\varphi}, \bar{\varphi}] = [80, \frac{1}{R_1} + \eta]$ for the nonlinearity in (6.22). The nonlinearity and these sector bounds are visualized in Fig. 6.6.

Using these sector bounds, the loop-transformation is performed to obtain the system in (6.11), and it is verified that the pair (A_{lt}, E_{lt}) is controllable and the pair (A_{lt}, M_{lt}) is observable for every n_o , i.e., Assumption 6.1 holds. Thereafter, $\mathcal{H}(s)$ is constructed using the matrices of the loop-transformed system.

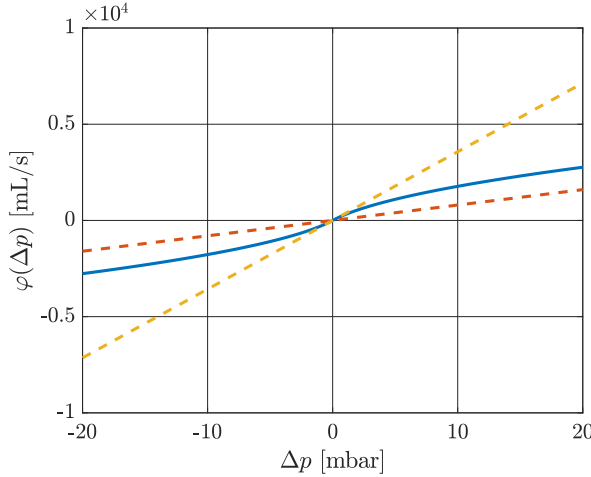


Fig. 6.6. Visualization of the nonlinearity $\varphi(\Delta p)$ (—), and its sector bounds $\underline{\varphi}\Delta p$ (- - -) and $\bar{\varphi}\Delta p$ (- · - ·), showing that the incremental sector condition holds for $[\underline{\varphi}, \bar{\varphi}] = [80, \frac{1}{R_1} + \eta]$.

Then, it is guaranteed that $\mathcal{H}(s)$ is SPR, it is first verified that for all $n_o \in \{0, 1, 5, 15, 20\}$ the transfer function $\mathcal{H}(s)$ is Hurwitz, which is verified by computing the poles and checking that they reside in the open left-half plane. Thereafter, it is graphically validated that $\text{Re}(\mathcal{H}(j\omega)) > 0 \forall \omega \in [-\infty, \infty]$. This is validated in Fig. 6.7; it is clearly shown that for all considered values of n_o the real part of $\mathcal{H}(j\omega)$ is strictly positive. Finally, it is verified that $\mathcal{H}(\infty) > 0$. This is also the case for all $n_o \in \{0, 1, 5, 15, 20\}$.

From these results, Lemma 6.1, and Theorem 6.1, it is concluded that the nonlinear closed-loop ventilation system is exponentially convergent on a compact domain³ in state space for which $\Delta p \in [-20, 20]$ mbar and that this controller solves the repetitive control problem. Next, the performance of the different controllers is analyzed by means of experiments.

³Such domain can be explicitly formulated using a quadratic Lyapunov function following from the Kalman-Yakubovich-Lemma for the SPR transfer function $\mathcal{H}(s)$.

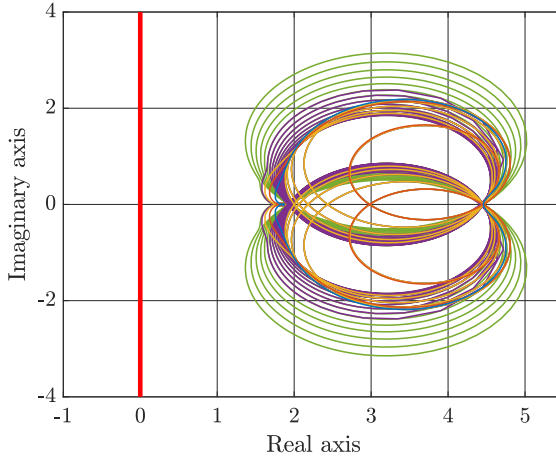


Fig. 6.7. Nyquist plot of $\mathcal{H}(s)$ for $n_o = 0$ (—), $n_o = 1$ (—), $n_o = 5$ (—), $n_o = 15$ (—), and $n_o = 20$ (—). The figure shows that $\text{Re}(\mathcal{H}(j\omega)) > 0 \forall \omega \in [-\infty, \infty]$.

6.4.4 Experimental results for mechanical ventilation

The main experimental results are shown in Fig. 6.8 and 6.9. The time-domain results of the 20th breath with the integrator only, i.e., $n_o = 0$, and the repetitive controller with 20 oscillators, i.e., $n_o = 20$, are visualized in Fig. 6.8. The top plot shows the reference and the measured outputs and the bottom plot shows the tracking error for both controllers. The figure clearly shows that the tracking error is significantly reduced by the repetitive controller. The overshoot is eliminated and the rise-time is significantly shorter. Note that the residual error with repetitive control contains oscillatory behavior, especially during the expiration at PEEP level, i.e., between 82 and 84 seconds. These oscillations contain mostly frequency content higher than 20 times the breathing frequency, i.e., above 5 Hz. It is observed that the tracking error's frequency content at frequency above the n_o th harmonic is increased. In Section 6.4.6, a remark and analysis of this phenomenon is included, since this phenomenon could potentially deteriorate the system's tracking performance.

The ℓ^2 -norm of the error per breath for every controller is shown in Fig. 6.9. The ℓ^2 -norm of the error of a particular breath j is defined as $\|e\|_2 = \left(\sum_{k=1+(j-1)\rho}^{j\rho} |e(k)|^2 \right)^{\frac{1}{2}}$ with $\rho = \frac{T}{\Delta T}$ and ΔT the sampling time. The figure clearly shows that increasing the number of oscillators reduces the ℓ^2 -norm of the error upon convergence. Including 20 oscillators in the loop reduces the ℓ^2 -norm of the error by more than a factor 3 compared to integral action only. Furthermore, it is observed that the convergence time is longer for an increasing number of oscillators and the controller with 20 oscillators converges in approximately 15 breaths.

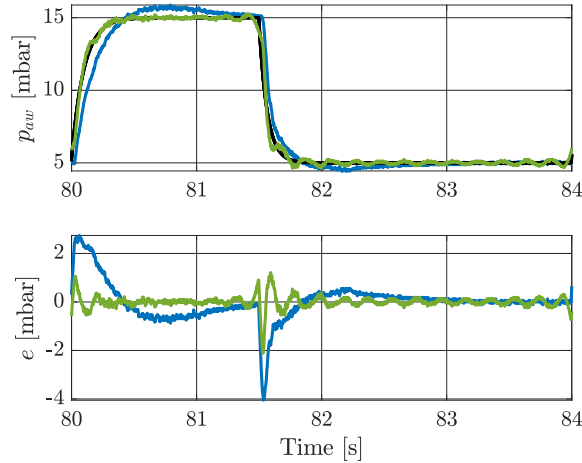


Fig. 6.8. The time domain results upon convergence for $n_o = 0$ (—) and $n_o = 20$ (—), and the target pressure (—). The figure shows that the error is significantly reduced by the repetitive controllers.

Concluding, all controllers show convergent behavior in the experiments, as expected by the analysis. Furthermore, the tracking error is reduced significantly, by more than a factor 3, by including repetitive control. The Fourier coefficients of the steady-state output error $\bar{e}(t)$ are suppressed at the frequencies $\omega = k\frac{2\pi}{T}$, $k = 0, 1, \dots, n_o$.

6.4.5 Analysis of conservatism

To analyze how conservative the convergence properties of Theorem 6.1 are, an experimental use-case is presented where the SPR properties are violated. This is achieved by considering a ventilation use-case with lung parameters that represent a baby patient, i.e., $C_{lung} = 3$ mL/mbar and $R_{lung} = 50$ mbar s/L. The same hose and blower system as for the adult use-case are used, hence, the same sector conditions for the linearity can be used. Furthermore, the same RC design as for the adult use-case is followed for $n_o = 20$. The transfer function $\mathcal{H}(s)$ is computed for this system and visualized in Fig. 6.10. This figure clearly shows that the second condition for SPR transfer functions is violated for $n_o = 20$. Therefore, the desired convergence properties of the system cannot be guaranteed for this controller design with $n_o = 20$ oscillators.

The resulting ℓ^2 -norm of the error per breath is shown in Fig. 6.11. This figure clearly shows that the system behaves unstable for $n_o = 20$. Concluding, this use-case shows that the sufficient conditions in Theorem 6.1 have limited conservatism, which is a desirable property for practical controller design because it allows more design freedom.

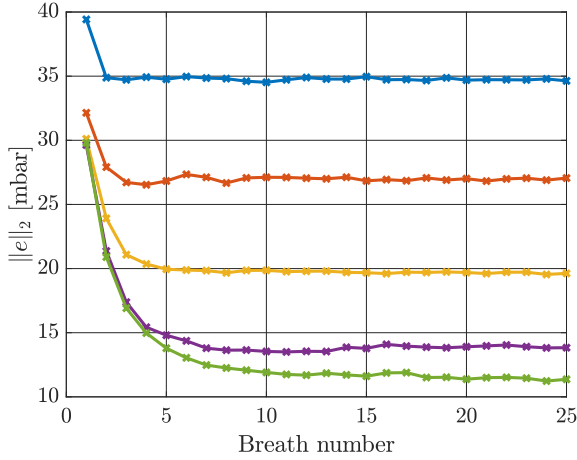


Fig. 6.9. The ℓ^2 -norm of the error for every breath for $n_o = 0$ (—), $n_o = 1$ (—), $n_o = 5$ (—), $n_o = 15$ (—), and $n_o = 20$ (—). The figure shows that more oscillators results in a smaller error and the controllers converge in approximately 10 breaths.

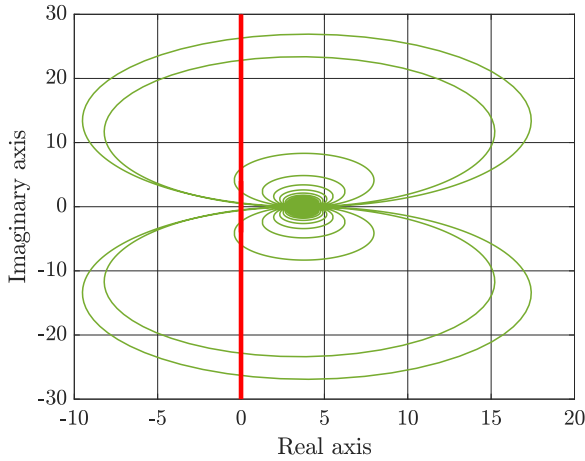


Fig. 6.10. Nyquist plot of $\mathcal{H}(s)$ for $n_o = 20$ (—) for the baby use-case. The figure shows that $\text{Re}(\mathcal{H}(j\omega)) > 0 \forall \omega \in [-\infty, \infty]$ does not hold, hence, convergence is not guaranteed.

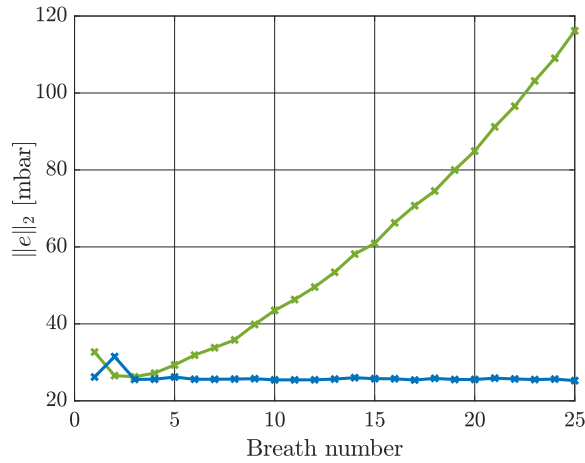


Fig. 6.11. The ℓ^2 -norm of the error for every breath for $n_o = 0$ (—), and $n_o = 20$ (—) for the baby use-case. The figure shows unstable behavior for that the closed-loop system with $n_o = 20$.

6.4.6 Remark on repetitive controller design

In the experimental analysis, especially in the baby use-case, it is observed that the remaining error consists of oscillations at frequencies above the harmonics of the n_o^{th} oscillator. These oscillations in the error are increasing for an increasing number of oscillators, limiting the overall tracking performance. Especially in other use-cases it is observed that increasing the number of oscillators can significantly deteriorate the system performance. This effect can be explained by analyzing the sensitivity S_{re} , i.e., transfer function from the reference r to the tracking error e , of a linearization of the closed-loop ventilation system. This linearized closed-loop system is obtained by replacing the nonlinearity in Fig. 6.4 by a linear resistance, i.e., $R_{hose}(\Delta p)$ is replaced by $\frac{\Delta p}{R_{lin}}$ with $R_{lin} = \frac{2}{\varphi + \bar{\varphi}}$, and $\eta = 0$. The resulting Bode magnitude plot of S_{re} is shown in Fig. 6.12. This Bode magnitude plot clearly shows that the tracking error is zero at the harmonics of the breathing frequencies. However, it also shows an increase in magnitude at frequency above the oscillator frequencies. The magnitude at these frequencies is increasing for an increasing number of oscillators. This increase in magnitude causes the oscillations at these frequencies as shown in the experiments. Therefore, in future work, it should be analyzed how this increase in magnitude at these specific frequencies can be eliminated.

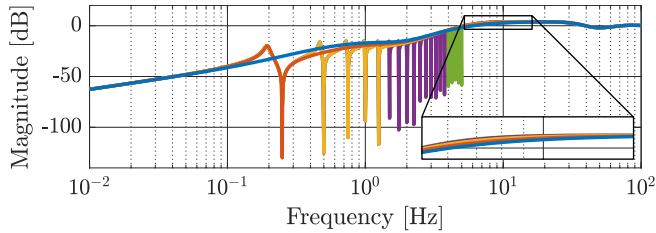


Fig. 6.12. Bode magnitude plot of the sensitivity S_{re} for the linearization of the closed-loop system with $n_o = 0$ (—), $n_o = 1$ (—), $n_o = 5$ (—), $n_o = 15$ (—), and $n_o = 20$ (—). The figure shows a magnitude increase at frequencies around 8 Hz, causing oscillations at these frequencies.

6.5 Conclusion and future work

In this chapter, a Repetitive Control (RC) scheme that achieves robust tracking for non-linear Lur'e-type systems with stability guarantees is presented. The RC scheme is composed of a dynamical system consisting of n_o linear oscillators at the reference's period and its multiples, which represents the internal model, processing the tracking error, and a pure integral controller guaranteeing the closed-loop system to be convergent. This convergence property ensures that the steady-state trajectory is periodic and therefore harmonic regulation is achieved at the frequencies included in the internal model.

This RC scheme is successfully implemented in a mechanical ventilation system for Intensive Care Units, a medical application to support the breathing of patients. Through a stability analysis based on the Nyquist plot it is shown that this closed-loop ventilation system is convergent and hence the designed controller solves the repetitive control problem at hand. Additionally, it is also shown experimentally that by increasing the number of oscillators the asymptotic L^2 -norm of the regulated output is reduced. Furthermore, experiments show that the presented controller design is able to significantly improve pressure tracking when compared to pure integral action.

Triggered repetitive control: application to mechanically ventilated patients

Abstract – Asymptotic rejection of a periodic disturbance can be achieved using repetitive control. The aim of this chapter is to develop a triggered repetitive control framework that can handle repeating tasks that are initiated by an external disturbance induced trigger on varying intervals, which clearly violates the periodicity assumption in repetitive control. A design method for this triggered repetitive control framework is presented with a stability guarantee. Finally, through an experimental use case, it is shown that pressure tracking performance for mechanically ventilated patients is improved significantly.

7.1 Introduction

Mechanical ventilators are essential equipment in Intensive Care Units (ICUs) to assist patients who need support to breathe sufficiently. The main goals of mechanical ventilation are to ensure oxygenation and carbon dioxide elimination (Warner and Patel, 2013). Especially during the flu season or a world-wide pandemic such as the COVID-19 pandemic (Wells et al., 2020), mechanical ventilation is a life saver for many patients around the world.

An important ventilation mode, that allows patient's more control over their breathing, is Pressure Controlled - Assist Control Ventilation (PC-ACV). In PC-ACV the ventilator synchronizes with the patient. When the patient starts an inspiration the ventilator increases the pressure near the patient's airway to ensure sufficient flow into the patient. Then, after a preset time, the ventilator decreases its pressure to allow an expi-

ration flow of carbon dioxide rich air. After this expiration, the ventilator waits for the next patient induced breath again.

Accurate tracking of the pressure profile is essential to ensure sufficient patient support and enhance patient comfort. According to Hunnekens et al. (2020), improved pressure tracking prevents patient-ventilator asynchrony. In Blanch et al. (2015), patient-ventilator asynchrony is even associated with increased mortality rates. Furthermore, accurate tracking avoids undesired pressure peaks caused by overshoot. These peaks can possibly harm the patient's lungs and therewith prolong the ICU stay.

The challenging problem of pressure tracking in presence of widely varying and uncertain patient parameters has spurred the development of a wide range of pressure control methodologies. In Borrello (2005), an overview of modeling and control techniques for mechanical ventilation is presented. In Hunnekens et al. (2020), variable-gain control is employed to overcome the trade-off between fast pressure rise times and limited overshoot in patient flow. This variable-gain control strategy shows a reduction in patient flow overshoot. However, the method uses the patient flow in control, which is typically unavailable for control. In Borrello (2001), an adaptive control strategy, using an estimated patient model, is applied to mechanical ventilation. In practice, it is challenging to obtain accurate patient models, deteriorating performance of such strategies. In Pomprapa et al. (2015), funnel-based control is applied to mechanical ventilation. However, the improvement in tracking performance is limited. In Scheel et al. (2017) and Li and Haddad (2012), model-based control and model predictive control are applied, respectively. Also these methods require accurate patient models, which are typically not available in practice. Furthermore, in Reinders et al. (2021b) and Reinders et al. (2021a), an adaptive control scheme is shown to improve performance significantly compared to other control strategies. However, overshoot and relatively long settling times are observed in case of large flow variations.

Recently, learning control strategies have been applied to mechanical ventilation. For example, Iterative Learning Control (ILC) is applied in De Castro and Tôrres (2019); Hazarika and Swarup (2020); Scheel et al. (2015) and Repetitive Control (RC) is applied in Reinders et al. (2020). These methods achieve superior performance in case of a fully sedated patient, i.e., when the pressure reference is fully repetitive. However, in case a patient starts breathing spontaneously (as in PC-ACV), performance of these methods degrades significantly.

Although significant tracking performance improvements in mechanical ventilation have been obtained, the superior tracking performance achieved by learning control strategies is not achieved for triggered ventilation modes such as PC-ACV, where the duration in between breaths is varying and apriori unknown. The aim of this chapter is to develop a triggered learning control framework that learns from data of previous breaths to improve tracking performance in case of PC-ACV. The developed framework could also be applied in other application fields with similar challenges, e.g., pick-and-place machines and dual-stage positioning systems.

Two interesting learning control strategies to consider are Iterative Learning Control (ILC) (Arimoto et al., 1984; Bristow et al., 2006; Freeman et al., 2012; Moore, 1993)

and Repetitive Control (RC) (Hara et al., 1988; Inoue et al., 1981; Longman, 2010; Pipeleers et al., 2009). The main assumption in ILC is that the states are reset between subsequent tasks. Breathing is a continuous process, hence, this assumption is not satisfied. Therefore, RC is the learning control strategy that is favorable in mechanical ventilation and considered in this chapter.

The main contribution of this chapter is

- a triggered RC framework that can improve tracking performance for systems with perfectly repetitive tasks, where the start of a task is triggered at a priori unknown varying timing intervals.

Besides the main contribution, the chapter contains several sub-contributions:

- a method to guarantee exponential stability of the closed-loop system with the proposed triggered RC framework;
- a design methodology of the triggered RC framework for a mechanical ventilation system in PC-ACV;
- an experimental case-study showing the performance increase, compared to a state-of-the-art control strategy, in mechanical ventilation.

The outline of this chapter is as follows. In Section 7.2, PC-ACV is explained and a general, not ventilation-specific, control problem is formulated. Then, in Section 7.3, the triggered repetitive control framework is presented. In Section 7.4, the relevant system models for mechanical ventilation are described. Thereafter, in Section 7.5, a triggered repetitive controller for mechanical ventilation is designed and its performance is experimentally tested. Finally, in Section 7.6, the main conclusions and future work are presented.

7.2 Control problem formulation

In this section, the control problem of Pressure Controlled - Assist Control Ventilation (PC-ACV) is reformulated to a general control problem. First of all, a description of PC-ACV of spontaneously breathing patients is given in Section 7.2.1. Thereafter, in Section 7.2.2, the control problem for mechanical ventilation in PC-ACV is stated and it is translated to a general triggered repetitive control problem that is solved in this chapter. Next, in Section 7.2.3, the main challenges when applying triggered repetitive control are explained and demonstrated through a simulation example.

7.2.1 PC-ACV of spontaneously breathing patients

The goal in the PC-ACV mode is to assist the patient's breathing when the spontaneous breathing effort is insufficient. The ventilator assists the patient to achieve the desired tidal volume. In such assisted ventilation modes it is important to synchronize the

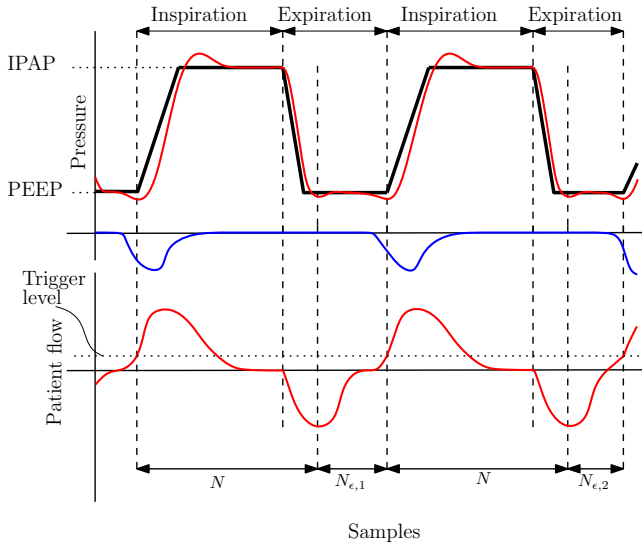


Fig. 7.1. A schematic example of PC-ACV controlled ventilation with two breaths, where the inspiration is triggered by a flow trigger and the expiration is timed. The figure shows the target pressure (—), the airway pressure and patient flow (—), and the patient's breathing effort (—).

ventilator strokes with the patient's spontaneous breathing effort for the comfort of the patient.

A schematic example of PC-ACV pressure and flow curves is depicted in Fig. 7.1. The figure shows that the patient is generating a negative pressure in the lung, resulting in a small positive patient flow. However, this effort is not enough to achieve the desired volumes. Therefore, when the patient flow exceeds a predefined trigger level, the ventilator increases the airway pressure, i.e., the pressure near the patient's airway, to the Inspiratory Positive Airway Pressure (IPAP) level, to increase the patient flow and volume. Then, after a predefined time, the ventilator pressure decreases again, to the Positive End-Expiratory Pressure (PEEP) level, to allow for an expiration. After the ventilator breath, of N samples long, is finished, the ventilator waits until a new patient-induced trigger is detected. Then, it starts a new ventilator-assisted breath. The time inbetween breaths is unknown and varying since it is determined by the patient. During the idle phase, this controller aims at keeping the pressure at PEEP level.

7.2.2 Control problem

As mentioned in the introduction, Repetitive Control (RC) is a suitable control strategy to handle the variety of patients in ventilation. Therefore, a general control problem is formulated using Fig. 7.1 and the block diagram of a plant with a parallel structured

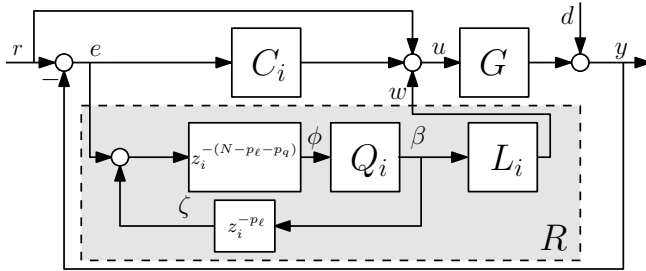


Fig. 7.2. Block diagram of the plant G , feedback controller C_i , and a parallel repetitive controller R_i . The index i indicates that in the triggered RC setting the controller blocks are potentially different in the active and idle phase. Switching between these states can have different causes, in mechanical ventilation this is the detection of the disturbance d . The dashed arrow is included in the ventilation examples without loss of generality of the framework.

RC in Fig. 7.2. Now, we aim to describe a generic control problem here, but in the scope of PC-ACV, G represents the patient-hose-ventilator dynamics, y is the airway pressure, and r is the target pressure, see black line in Fig. 7.1.

A plant G has to be controlled using a stabilizing feedback controller C and repetitive control controller R such that the output y tracks the reference r , i.e., the error e goes to zero. As seen in Fig. 7.1, the reference r is exactly the same in shape and duration in the gray area, i.e., during the active phase from $k = k_{s,j}$ until $k = k_{s,j} + N \forall j \in \mathbb{N}^+$ (with j a breath counter). In between active phases, the system is in the idle phase for $N_{\epsilon,j}$ samples, see Fig. 7.1. In the idle phase, the output should track a constant reference r , which is a constant that corresponds with the last value of the active phase. Then, after the a priori unknown $N_{\epsilon,j}$ samples, the system switches to the active phase again and should track the predefined reference profile again for fixed N samples. Switching of the system to the active phase is caused by the detection of an external disturbance d , which causes a tracking error at the start of a task¹.

Switching between these phases at varying intervals obstructs usage of conventional RC. Simply switching standard RC on and off results in an undesired actuation spike at the end of a task. The performance issue using switching of standard RC is investigated in the next section by means of a simulation use-case.

7.2.3 Example: Towards triggering repetitive control

In this section, the challenge of triggering a standard repetitive controller is visualized through simulations. First, the simulation use-case is described. Then, the time-domain simulation results and the resulting problem are presented. Finally, the challenges that

¹In the case of PC-ACV, d reflects the patient-induced disturbance on the airway pressure due to a breathing action.

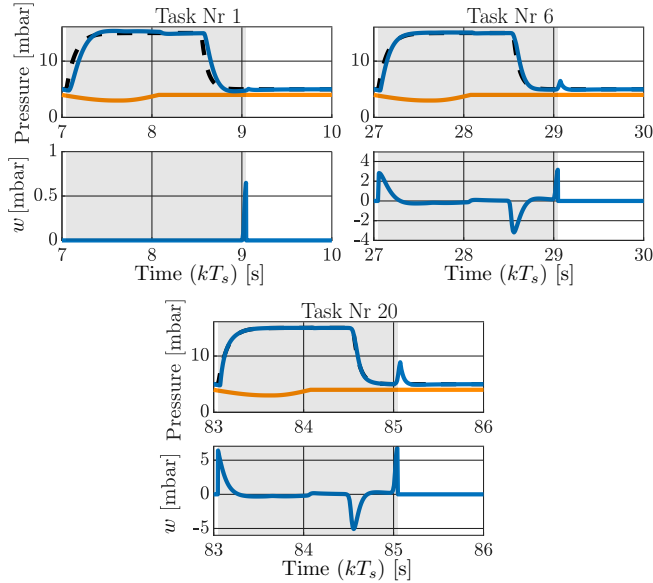


Fig. 7.3. Simulation result of PC-ACV that shows standard repetitive control that is turned on and off upon the trigger of the active phases, which is indicated by the gray area. The figures shows the reference r or p_{target} (---), the output y or \tilde{p}_{aw} and RC output w (—), and a scaled disturbance d or p_{mus} (—). Showing that standard RC in a triggered setting results in an undesired actuation spike at the end of the task.

should be solved are described.

7.2.3.1 Simulation use-case

In this simulation, PC-ACV in the mechanical ventilation application is adopted as a use-case and a standard parallel RC structure is adopted as presented in Fig. 7.2. The RC filters in this example are designed following the design methodology in Reinders et al. (2020). However, in the current chapter a parallel structured RC is adopted, for which the design approach in Reinders et al. (2020) is appropriately modified. To handle the varying times in between tasks, i.e., breaths, the repetitive controller is turned on at the start of the active phase and turned off at the end of the active phase. During the idle phase the internal states of the RC are kept constant and its output is set to zero. This represents an intuitive RC design for such scenario.

7.2.3.2 Time-domain results

The time-domain results of the simulation are depicted in Fig. 7.3. The figures show three separate tasks in the simulations, i.e., the first, the sixth, and the twentieth task. During these tasks it shows the reference (or target pressure), the output (or measured airway pressure), the RC output w , and a scaled version of the disturbance (or patient effort). The figure shows that the tracking performance during the tasks significantly improves over subsequent tasks. However, at the transition from the active to the idle phase a problem is observed. The RC output in the bottom plot of all three figures increases at the end of the active breath. This results in an increasing undesired peak in the measured output at the start of the idle phase, see the blue line in the top figure of the sixth and twentieth task. This spike in the output deteriorates control performance at the start of the idle phase, and is therefore undesired.

7.2.3.3 Challenges

The spike in the RC output is a result of the non-causal filters and errors at the beginning of the task. These non-causal filters allow a standard RC implementation to start actuation $p_l + p_q$ samples before the end of task j . More specifically, if an error is entering the memory block, $z_i^{-(N-p_\ell-p_q)}$ in Fig. 7.2, at the beginning of the task, it propagates through the causal filters Q_i and L_i before the N^{th} time step, i.e., before the end of the task. This allows the control output w to increase before the end of the task to compensate the error at the start of the subsequent task. This actuation can eliminate the tracking error at the start of task $j + 1$ in standard RC. However, the task $j + 1$ does not start immediately after the end of the active phase of task j due to the varying and uncertain length $N_{\epsilon,j}$ of the idle phase. Therefore, this actuation results in an undesired peak at the start of the idle phase, which is increasing over subsequent breaths.

Two distinct causes for the error at the beginning of a task, and therewith causes of the actuation spike, are identified. The first cause of the error at the start of the active phase is the immediate ramp-up of the reference r , i.e., the target pressure. Because the system output does not respond to this instantaneously, this results in an error at the start of the active phase. The second cause of the error at the start of the active phase is the disturbance d , which causes a slight dip in the output y . This disturbance and its timing are unknown and the resulting error can not be compensated perfectly. To overcome these challenges, a Triggered RC (TRC) framework is developed, which is presented in Section 7.3.

7.3 Triggered repetitive control framework

In this section, the TRC framework is presented and its theoretical support is established. The main contribution of this chapter, i.e., the TRC framework is presented in Section 7.3.1. Thereafter, a stability proof of the controlled system is presented in Section 7.3.2.

7.3.1 Triggered repetitive control framework

In this section, the exact implementation of the TRC framework is explained. This means that for both the idle and active phase the content of the building blocks in R_i of Fig. 7.2 is explained. Note that this section does not contain the design of the feedback controller C_i and the exact TRC filter design method. For the mechanical ventilation use-case this is explained in Section 7.5.3. Next, the RC building blocks during the active phase, $i = 1$, and thereafter the building blocks in the idle phase, $i = 2$, are explained.

7.3.1.1 Active phase

In the active phase, the learning filter L_1 and the robustness filter Q_1 are designed similar to standard parallel RC.

To avoid that the error at the start of active phase j causes an actuation spike at the end of the active phase j , this initial error should not be propagated through the robustness and learning filter. To avoid that the immediate increase of the reference causes an error, the reference is delayed. Such that it does not change immediately when the task is started. This allows the repetitive controller to respond to the change in reference at the start of the task, eliminating this error.

Furthermore, it should be avoided that the error caused by the disturbance d causes an actuation spike. This is achieved by altering the delay blocks, i.e., memory block ($z_i^{-(N-p_\ell-p_q)}$) and preview buffer ($z_i^{-p_\ell}$), in Fig. 7.2. The memory block is changed such that it behaves as a pure delay in the first $N - p_\ell - p_q$ samples in a task. Thereafter, it holds its last output but keeps updating its internal states, preventing that the error at the beginning of the task is propagated to the learning and robustness filter. To achieve this, the main memory block $z_1^{-(N-p_\ell-p_q)}$ is replaced by the following switching state-space system during task j :

$$\begin{aligned} x_Z(k+1) &= A_Z x_Z(k) + B_Z \theta(k), \\ \phi(k) &= \begin{cases} C_Z x_Z(k) + D_Z \theta(k), & \text{for } k - k_{s,j} < N - p_\ell - p_q, \\ \phi(k-1), & \text{for } N - p_\ell - p_q \leq k - k_{s,j} \leq N, \end{cases} \end{aligned} \quad (7.1)$$

where

$$\begin{aligned} A_Z &= \begin{bmatrix} 0 & 0 & \cdots & 0 \\ & I_{N-p_\ell-p_q-1} & & \\ & & \ddots & \\ & & & 0 \end{bmatrix}, \quad B_Z = \begin{bmatrix} 1 \\ 0 \\ \vdots \\ 0 \end{bmatrix}, \\ C_Z &= [0 \ \dots \ 0 \ 1], \quad D_Z = 0, \end{aligned} \quad (7.2)$$

where $k_{s,j}$ is defined as the sample number k at the start of task j , i.e., $k_{s,j} = (j-1)N + \sum_{m=1}^{j-1} N_{\epsilon,m} + 1$.

Also the preview buffer $z_1^{-p_\ell}$ in Fig. 7.2 has a contribution to the actuation spike. Therefore, the preview buffer is altered such that it is a direct feedthrough at times $k - k_{s,j} \in [N - p_\ell, N]$, during every active phase. This means that at the end of the task both the learning and robustness filter are causal filters and no actuation spike will occur. This is implemented using the following switching state-space system for the preview buffer in the active phase during task j :

$$\begin{aligned} x_P(k+1) &= A_P x_P(k) + B_P \beta(k), \\ \zeta(k) &= \begin{cases} C_P x_P(k) + D_P \beta(k), & \text{for } k - k_{s,j} < N - p_\ell, \\ \beta(k), & \text{for } N - p_\ell \leq k - k_{s,j} \leq N, \end{cases} \end{aligned} \quad (7.3)$$

where

$$\begin{aligned} A_P &= \begin{bmatrix} 0 & 0 & \cdots & 0 \\ & I_{N-p_\ell-1} & & \vdots \\ & & & 0 \end{bmatrix}, \quad B_P = \begin{bmatrix} 1 \\ 0 \\ \vdots \\ 0 \end{bmatrix}, \\ C_P &= [0 \ \dots \ 0 \ 1], \quad D_P = 0. \end{aligned} \quad (7.4)$$

This preview buffer behaves as a pure delay during the first $N - p_\ell$ samples of a task. Thereafter, it behaves as a direct feedthrough and its internal states are updated.

7.3.1.2 Idle phase

During the idle phase, i.e., $k - k_{s,j} \in [N + 1, N + N_{\epsilon,j}]$, the design of the different building blocks of R_2 is straightforward. During this phase it is desired to hold the internal states of all blocks, such that the controller remembers what it learned during previous active phases. Therefore, the state-space models in the different blocks of R_2 all have an A matrix equal to an identity matrix of the proper size. All other system matrices contain only zeros. Using these state-space models, the states of the different blocks are held and no new information is going in or out of R_2 .

7.3.2 Stability of the closed-loop system

In this section, a stability proof for the closed-loop controlled system with TRC is presented. First, the closed-loop system with TRC within a single breath is written as a switching system. Thereafter, this switching system is rewritten to a switching system over successive breaths. This switching system describes the dynamics from the start of task j to the start of task $j + 1$. Finally, this switching system representation is used to prove stability using a Common Quadratic Lyapunov Function (CQLF).

The closed-loop system within a single task is described by the block diagram in Fig. 7.2. For generality the disturbance and the dashed arrow are omitted. This closed-loop system is written as a switching state-space model as follows:

$$\left. \begin{aligned} x(k+1) &= A_l x(k) + B_l r(k) \\ y(k) &= C_l x(k) + D_l r(k) \end{aligned} \right\} \text{ for } l \in 1, 2, 3, 4, \quad (7.5)$$

where x represents the states of all different blocks in Fig. 7.2, i.e.,

$$x = [x_G \ x_L \ x_Q \ x_C \ x_Z \ x_P]^T, \quad (7.6)$$

where the subscripts in the state vector represent the different building blocks, i.e., G represents the plant, L the learning filter, Q the robustness filter, C the linear feedback controller, Z the main buffer, and P the preview buffer. The corresponding state-space system matrices are retrieved by combining the state-space models of all subsystems and are given in Appendix 7.A. In the state-space system (7.5), $l = 1, 2, 3$ represent the system in the active phase and $l = 4$ represents the system in the idle phase. More specifically, during breath j , $l = 1 \forall k - k_{s,j} \in [1, N - p_\ell - p_q - 1]$, $l = 2 \forall k - k_{s,j} \in [N - p_\ell - p_q, N - p_\ell - 1]$, $l = 3 \forall k - k_{s,j} \in [N - p_\ell, N]$, and $l = 4 \forall k - k_{s,j} \in [N + 1, N + N_{\epsilon,j}]$.

Next, the closed-loop dynamics are written as a state-space model over multiple breaths. This state-space model represents the relation between the system state at the start of active phase j , at $k = k_{s,j}$, and the systems state at the start of active phase $j + 1$, at $k = k_{s,j+1}$. The state at the start of task j is defined as $\gamma(j) = x(k_{s,j})$. The switching system is obtained by using the knowledge that the system always switches in a fixed order and that the system matrices in these distinct states are known. This results in the following state-space model:

$$\gamma(j+1) = A(N, N_{\epsilon,j})\gamma(j) + B(N, N_{\epsilon,j})\underline{r}(j) \quad (7.7)$$

with

$$\begin{aligned} A(N, N_{\epsilon,j}) &= A_4^{N_{\epsilon,j}} A_3^{p_\ell} A_2^{p_q} A_1^{N-p_\ell-p_q} \\ B(N, N_{\epsilon,j}) &= \begin{bmatrix} A_4^{N_{\epsilon,j}} A_3^{p_\ell} A_2^{p_q} A_1^{N-p_\ell-p_q-1} B_1 & A_4^{N_{\epsilon,j}} A_3^{p_\ell} A_2^{p_q} A_1^{N-p_\ell-p_q-2} B_1 & \dots \\ A_4^{N_{\epsilon,j}} A_3^{p_\ell} A_2^{p_q} B_1 & A_4^{N_{\epsilon,j}} A_3^{p_\ell} A_2^{p_q-1} B_2 & \dots \\ A_4^{N_{\epsilon,j}} A_3^{p_\ell} B_2 & A_4^{N_{\epsilon,j}} A_3^{p_\ell-1} B_3 & \dots & A_4^{N_{\epsilon,j}} B_3 & A_4^{N_{\epsilon,j}-1} B_4 & \dots & B_4 \end{bmatrix}, \end{aligned} \quad (7.8)$$

where $\underline{r}(j) = [r(n(j)) \ \dots \ r(n(j) + N + N_{\epsilon,j})]^T$ is the input vector. Note that the system matrices in (7.7) depend on the length of the idle phase, which in turn varies over j . Hence, a new switching system is retrieved where the system matrices depend on the length of the idle phase, i.e., $N_{\epsilon,j}$.

The switching state-space system on task level in (7.7) is used to prove stability of the closed-loop system. For this stability proof, it is assumed that the idle phase has a known maximum duration in samples N_{max} , i.e., $N_{\epsilon,j} \in \{0, 1, \dots, N_{max}\}$. Furthermore, it is assumed that the value $N_{\epsilon,j}$ can change arbitrarily within this set from task to task. Finally, if a CQLF is found for the dynamics in (7.7) for all possible values of $N_{\epsilon,j} \in \{0, 1, \dots, N_{max}\}$, then the system in (7.7) is exponentially stable for arbitrary switching between values of $N_{\epsilon,j} \in \{0, 1, \dots, N_{max}\}$. To find a CQLF, a matrix P should be obtained that satisfies the discrete-time Lyapunov equation from Hespanha (2009), which is defined as:

$$\underbrace{A(N, N_{\epsilon,j})^T P A(N, N_{\epsilon,j}) - P}_{:=D_\ell(N, N_{\epsilon,j})} \prec 0, \quad \forall N_{\epsilon,j} \in \{0, 1, \dots, N_{max}\}, \quad (7.9)$$

where the P matrix must be symmetric and positive definite, i.e.,

$$P = P^T \succ 0. \quad (7.10)$$

If a P matrix exists such that it satisfies (7.9) and (7.10), then the system in (7.7) can switch arbitrarily between $N_{\epsilon,j} \in \{0, 1, \dots, N_{max}\}$ values and it is (robustly) exponentially stable.

7.4 Ventilation system and patient effort modeling

In this section, models of the ventilation system and patient effort are presented. In Section 7.4.1, a high-level description of the ventilation system is presented. Then, in Section 7.4.2, models of the considered ventilation system are presented. First, a first principles model is derived that is used in the closed-loop stability analysis in Section 7.5.4. Then, an experimental FRF model is presented that is used for the TRC filter design in Section 7.5.3. Thereafter, in Section 7.4.3, the considered patient effort model is given.

7.4.1 High-level system description

A schematic of the considered blower-patient-hose system, with the relevant parameters, is shown in Fig. 7.4. The main components are the blower, the hose-filter system, and the patient.

7.4.1.1 Blower

A centrifugal blower compresses ambient air to achieve the desired blower outlet pressure p_{out} . The blower system is modeled as a second-order low-pass filter with an output delay τ_b . This describes the relation between the control output $p_{control}$ and the outlet pressure p_{out} .

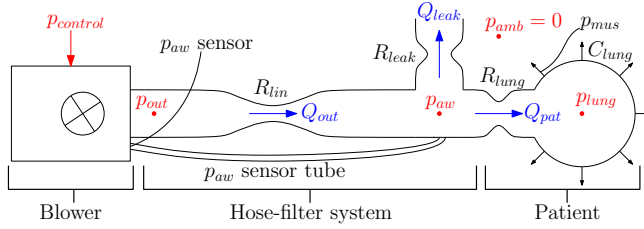


Fig. 7.4. Schematic representation of the blower-hose-patient system of the considered positive pressure ventilation system. Showing the resistances, lung compliance, flows, and pressures.

7.4.1.2 Hose-filter system

The hose-filter system connects the blower to the patient. The difference between p_{out} and p_{aw} results in a flow through the hose Q_{out} . This pressure difference and flow relation are modeled by a linear hose resistance R_{lin} . The change in airway pressure p_{aw} results in two flows, namely, the leak flow Q_{leak} and the patient flow Q_{pat} . The leak flow is used to flush exhaled CO_2 -rich air from the hose. The patient flow is required to ventilate the patient. The airway pressure is measured using a pilot line attached to the module and the end of the hose. The pressure transfer through the hose and the pilot line results in delays in the system, caused by the finite propagation speed of the pressure waves. This delay is assumed to be a measurement delay of p_{aw} referred to as the hose delay τ_h . For simplicity, all system delays are lumped as one output delay $\tau_d = \tau_b + \tau_h$ on the measurement of the airway pressure. The measured, i.e., delayed, airway pressure is denoted by \hat{p}_{aw} .

7.4.1.3 Patient

The patient is modeled by a linear one-compartmental lung model as described in Bates (2009, pp. 37–60). This model consists of a linear resistance R_{lung} and a linear compliance C_{lung} . The patient flow is a result of the lung resistance and the difference between the airway pressure and the lung pressure p_{lung} , i.e., the pressure inside the lungs. The patient flow results in a change in the lung pressure, the relation between patient flow and lung pressure is given by the lung compliance. Finally, in this chapter a patient with spontaneous, muscle-induced, breathing effort $p_{mus}(t)$ is considered. The patient effort is an unknown disturbance introduced by the patient's spontaneous breathing effort that affects the lung pressure. This patient effort allows a patient to (partially) inhale and exhale by themselves.

7.4.2 Ventilation system model with hose compensation

In this section, a linear state-space model of the ventilation system is presented. First, a model of the uncontrolled ventilation system is presented. Thereafter, a state-of-the-art control strategy, i.e., hose-compensation control (Reinders et al., 2021b), is included in the model to obtain the full mechanical ventilation model. This model can be used as the plant G in the stability analysis of Section 7.5.4. Thereafter, experimental Frequency Response Functions (FRFs) of this controlled plant are presented. These FRF models are used for design of the repetitive controller filters in Section 7.5.3.

The uncontrolled ventilation system contains three components as shown in Fig. 7.4. These components are the blower, the hose-filter system, and the patient. First, the blower is modeled as a second-order low-pass filter with cutoff frequency $\omega_n = 30$ Hz. This gives the following state-space model of the blower:

$$\begin{aligned}\dot{x}_b &= \mathbf{A}_b x_b + \mathbf{B}_b p_{control} \\ p_{out} &= \mathbf{C}_b x_b\end{aligned}\quad (7.11)$$

with

$$\mathbf{A}_b = \begin{bmatrix} -\omega_n & 0 \\ \omega_n & -\omega_n \end{bmatrix}, \quad \mathbf{B}_b = \begin{bmatrix} \omega_n \\ 0 \end{bmatrix}, \quad \mathbf{C}_b = [0 \ 1]. \quad (7.12)$$

Second, the hose-filter patient system is obtained by assuming that all resistances are linear and that the patient is modeled by a linear one-compartment lung model. Detailed derivation of this model can be found in Reinders et al. (2021b). The different components, i.e., hose, leak, and patient, are connected by conservation of flow, i.e., $Q_{out} = Q_{pat} + Q_{leak}$. This results in the following linear state-space patient-hose model:

$$\begin{aligned}\dot{p}_{lung} &= \mathbf{A}_p p_{lung} + \mathbf{B}_p p_{out} + \mathbf{E}_p \dot{p}_{mus} \\ p_{aw} &= \mathbf{C}_p p_{lung} + \mathbf{D}_p p_{out}\end{aligned}\quad (7.13)$$

with

$$\begin{aligned}\mathbf{A}_p &= -\frac{R_{lin} + R_{leak}}{C_{lung} \bar{R}}, \quad \mathbf{B}_p = \frac{R_{leak}}{C_{lung} \bar{R}}, \quad \mathbf{C}_p = \frac{R_{lin} R_{leak}}{\bar{R}}, \\ \mathbf{D}_p &= \frac{R_{leak} R_{lung}}{\bar{R}}, \quad \mathbf{E}_p = 1, \\ \text{and } \bar{R} &= R_{lin} R_{leak} + R_{lin} R_{lung} + R_{leak} R_{lung}.\end{aligned}\quad (7.14)$$

Discrete-time models are used for Repetitive Controller (RC) design and the stability analysis. Therefore, the blower and the hose-filter patient system models are discretized using exact zero-order hold discretization with a sampling time $T_s = 2 \times 10^{-3}$ s. The associated discrete-time system matrices are denoted with an additional subscript d .

Third, a discrete-time model for the output delay τ_d is obtained. This model represents the delay between the actual airway pressure $p_{aw}(n)$ and the measured airway

pressure $\tilde{p}_{aw}(n)$. For this model, the delay length is computed in terms of sampling time T_s . This gives the delay length in samples $d_s = \frac{\tau_d}{T_s}$. The following discrete-time state-space model represents the output delay z^{-d_s} :

$$\begin{aligned} x_{\tau_d,d}(n+1) &= \mathbf{A}_{\tau_d,d}x_{\tau_d,d}(n) + \mathbf{B}_{\tau_d,d}p_{aw}(n) \\ \tilde{p}_{aw}(n) &= \mathbf{C}_{\tau_d,d}x_{\tau_d,d}(n) \end{aligned} \quad (7.15)$$

with

$$\mathbf{A}_{\tau_d,d} = \begin{bmatrix} 0 & \dots & 0 \\ & \ddots & \vdots \\ I_{d_s-1} & & 0 \end{bmatrix}, \quad \mathbf{B}_{\tau_d,d} = \begin{bmatrix} 1 \\ 0 \\ \vdots \\ 0 \end{bmatrix}, \quad \mathbf{C}_{\tau_d,d} = [0 \dots 0 \ 1]. \quad (7.16)$$

In this state-space model, the actual airway pressure $p_{aw}(n)$ first propagates for d_s samples through the state $x_{\tau_d,d}$ before it is seen in the output \tilde{p}_{aw} .

Next, the discretized models in (7.11)-(7.16) are combined. Using the combined state $x_{m,d} = [x_{b,d}^T \ p_{lung,d} \ x_{\tau_d,d}^T]^T$, gives the following discrete-time state-space model of the uncontrolled ventilation system:

$$\begin{aligned} x_{m,d}(n+1) &= \mathbf{A}_{m,d}x_{m,d}(n) + \mathbf{B}_{m,d}p_{control}(n) + \mathbf{E}_{m,d}\dot{p}_{mus}(n) \\ \tilde{p}_{aw}(n) &= \mathbf{C}_{m,d}x_{m,d}(n) \end{aligned} \quad (7.17)$$

with

$$\begin{aligned} \mathbf{A}_{m,d} &= \begin{bmatrix} \mathbf{A}_{b,d} & 0 & 0 \\ \mathbf{B}_{p,d}\mathbf{C}_{b,d} & \mathbf{A}_{p,d} & 0 \\ \mathbf{B}_{\tau_d,d}\mathbf{D}_{p,d}\mathbf{C}_{b,d} & \mathbf{B}_{\tau_d,d}\mathbf{C}_{p,d} & \mathbf{A}_{\tau_d,d} \end{bmatrix}, \\ \mathbf{B}_{m,d} &= \begin{bmatrix} \mathbf{B}_{b,d} \\ 0 \\ 0 \end{bmatrix}, \quad \mathbf{C}_{m,d} = [0 \ 0 \ \mathbf{C}_{\tau_d,d}], \quad \mathbf{E}_{m,d} = \begin{bmatrix} 0 \\ 1 \\ 0 \end{bmatrix}. \end{aligned} \quad (7.18)$$

Finally, linear hose compensation is added to the uncontrolled ventilation system to retrieve the desired plant model. The hose-compensation strategy in this chapter is a special case of the strategy in Reinders et al. (2021b). A schematic overview of the system with hose compensation is depicted in Fig. 7.5. The figure shows how hose compensation is added to the uncontrolled plant P represented by (7.17) and (7.18). This results in the controlled plant G represented by (7.20) below. Hose compensation aims to compensate the pressure drop $\Delta p := p_{out} - p_{aw}$ over the hose. This is achieved by increasing the target pressure p_{target} with the estimated pressure drop $\Delta \hat{p} = \hat{R}_{lin}Q_{out}$, where \hat{R}_{lin} is an estimated hose resistance. This compensation is implemented by adding the estimated pressure drop to the target pressure as

$$p_{control} = p_{target} + \Delta \hat{p} = p_{target} + \hat{R}_{lin}Q_{out}. \quad (7.19)$$

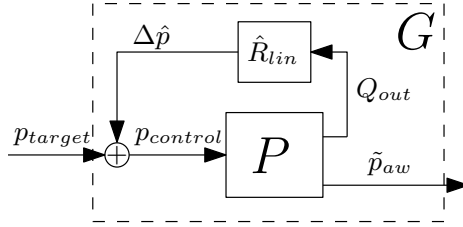


Fig. 7.5. Schematic overview of the uncontrolled plant P and the hose-compensation control strategy, combined this results in the plant G .

To obtain the final dynamics, Q_{out} is rewritten as $Q_{out} := \frac{p_{out} - p_{aw}}{R_{lin}}$, where $p_{out} = \mathbf{C}_{b,d}x_{b,d}$ and $p_{aw} = \mathbf{C}_{p,d}p_{lung,d} + \mathbf{D}_{p,d}\mathbf{C}_{b,d}x_{b,d}$, and (7.19) is substituted in (7.17) and (7.18). This results in

$$\begin{aligned} x_{f,d}(n+1) &= \mathbf{A}_{f,d}x_{f,d}(n) + \mathbf{B}_{f,d}p_{target}(n) + \mathbf{E}_{f,d}\dot{p}_{mus}(n), \\ \tilde{p}_{aw}(n) &= \mathbf{C}_{f,d}x_{f,d}(n), \end{aligned} \quad (7.20)$$

where $x_{f,d} = x_{m,d}$,

$$\begin{aligned} \mathbf{A}_{f,d} &= \mathbf{A}_{m,d} + \mathbf{B}_{m,d} \frac{\hat{R}_{lin}}{R_{lin}} [\mathbf{C}_{b,d} - \mathbf{D}_{p,d}\mathbf{C}_{b,d} - \mathbf{C}_{p,d} \ 0], \\ \mathbf{B}_{f,d} &= \mathbf{B}_{m,d}, \quad \mathbf{C}_{f,d} = \mathbf{C}_{m,d}, \quad \text{and} \quad \mathbf{E}_{f,d} = \mathbf{E}_{m,d}. \end{aligned} \quad (7.21)$$

For the RC filter design, experimental FRF models of the ventilation system with hose-compensation control are obtained. More specifically, FRFs from p_{target} to \tilde{p}_{aw} for different patients are depicted in Fig. 7.6. In these experiments, the estimated hose-resistance \hat{R}_{lin} is retrieved by a calibration procedure. The figure shows FRFs of different patients from babies to adults. Furthermore, these FRFs are obtained at different pressure levels, to capture the effect of the absolute pressure on the FRF. The significant phase lag that is seen in the FRFs is caused by the output delay τ_d . These FRFs are used to design the RC filters in Section 7.5.3.

7.4.3 Patient effort modeling

The patient's spontaneous effort p_{mus} enables a person, i.e., healthy or patient, to inhale and exhale air by themselves. Physically, the patient effort can be seen as a change in lung pressure caused by contractions and relaxation of the respiratory muscles, e.g., the diaphragm.

According to Fresnel et al. (2014), a sinusoidal half-wave is a common and accurate model of the patient effort. An example of the sinusoidal half-wave is depicted in Fig. 7.7. The decrease in p_{mus} results in a decrease in the lung pressure, which results in flow into the patient lungs. In other words, a decrease in p_{mus} represents an inspiration.

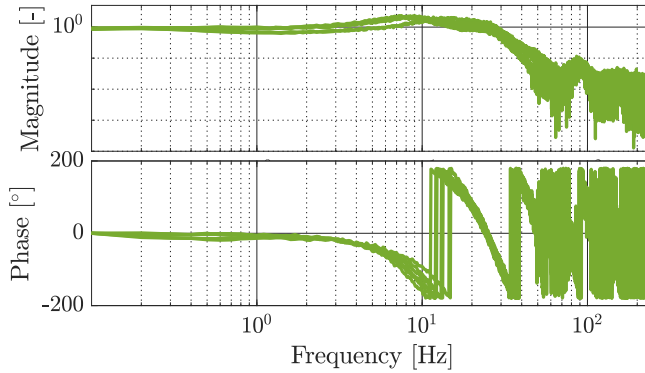


Fig. 7.6. Identified FRF models of the ventilation system with hose-compensation control from p_{target} to \tilde{p}_{aw} , i.e., the plant G . The different FRFs represent different patients from babies to adults at different pressure levels.

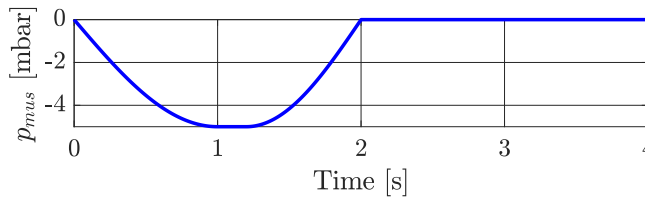


Fig. 7.7. Model of the muscle induced patient effort $p_{mus}(t)$, defined by the sinusoidal half-wave.

Thereafter, the increase in pressure results in an increase of the lung pressure and flow out of the lungs. In other words, an increase in p_{mus} represents an expiration.

In this chapter, it is assumed that the patient effort is an exogenous disturbance to the system. In practice, it is a result of the breathing behavior of the patient. Modeling of this behavior is out of scope for this chapter.

7.5 Triggered repetitive control applied to mechanical ventilation

In this section, the proposed TRC framework of Section 7.3 is used to improve pressure tracking performance of an experimental mechanical ventilation setup. First, in Section 7.5.1, the experimental setup and use cases are described. Thereafter, in Section 7.5.2, the overall controller design is presented. Next, the RC filter designs are explained in Section 7.5.3. Then, a stability analysis of the closed-loop system is presented in Section 7.5.4. Finally, in Section 7.5.5, the experimental results are presented

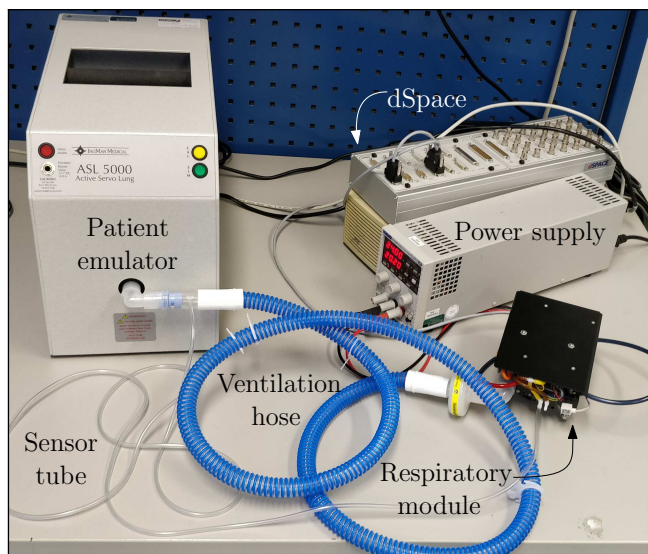


Fig. 7.8. Experimental setup consisting of the blower driven ventilator, ASL 5000 breathing simulation, dSpace, and a hose.

and compared to a benchmark control strategy.

7.5.1 Experimental setup and use cases

The main components of the experimental setup used in this case study are depicted in Fig. 7.8. The figure shows a Macawi blower-driven mechanical ventilation module (DEMCON macawi respiratory systems, Best, The Netherlands). Furthermore, the ASL 5000™ Breathing Simulator (IngMar Medical, Pittsburgh, PA) is shown in the figure. This breathing simulator is used to emulate a linear one-compartmental patient model as described in Bates (2009). Furthermore, a typical hose-filter system for ventilation of a patient in a hospital setting is shown. The control and ventilation algorithms are implemented in a dSPACE system (dSPACE GmbH, Paderborn, Germany).

To design and evaluate TRC for mechanical ventilation, three different patients and ventilation scenarios are considered. The considered patient scenarios are a baby, pediatric, and adult scenario from the ISO standard for pressure controlled mandatory ventilation obtained from Table 201.104 in NEN-EN-ISO 80601-2-12:2011 (NEN, Delft, The Netherlands). For these standardized scenarios, the patient parameters and the ventilator settings are given in Table 7.1. Furthermore, the patient effort p_{mus} for all three scenarios is depicted in Fig. 7.9. The variations in this patient effort are exaggerated to show the control strategy in a worst-case scenario. Note that all scenarios use the same hose-filter-leak configuration. As a benchmark controller the hose-resistance compen-

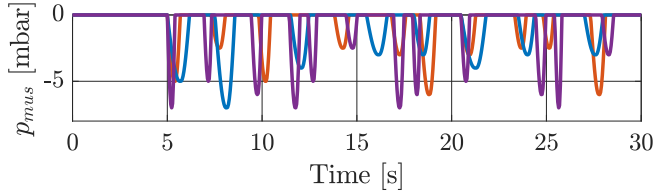


Fig. 7.9. The considered patient effort for all cases during the first 30 seconds. Showing the breathing effort of the adult (—), the pediatric (—), and the baby (—) use cases.

Table 7.1. Patient parameters and ventilation settings used for filter design and in the experiments.

Parameter	Adult	Pediatric	Baby	Unit
R_{lung}	5	50	50	mbar s / L
C_{lung}	50	10	3	mL/mbar
PEEP	5	5	10	mbar
IPAP	15	35	25	mbar
Inspiratory time	1.5	1	0.6	s
N	1000	650	450	samples

sation strategy, as discussed in Section 7.4 is considered. This corresponds to the first breath in every use-case, when the TRC has not yet learned from previous breaths.

7.5.2 Overall controller design

The overall controller design can be divided in four separate controllers, i.e., feedforward control, hose-compensation control, linear feedback control, and the TRC controller R . As a basis the control scheme in Fig. 7.2 is considered. First, as a feedforward controller unity feedforward is considered, i.e., the dashed arrow in Fig. 7.2. Next, the hose-resistance compensation controller is implemented to achieve adequate performance from the start, i.e., before the TRC has learned from previous breaths. Implementation of the hose-resistance controller results in the plant G described by (7.20). This control strategy ensures that the initial performance of the system is sufficient. The estimated hose resistance \hat{R}_{lin} is obtained by an offline calibration of the hose prior to ventilation.

The linear feedback controller C_i in Fig. 7.2 is set to be 0 in both the active and idle phase, i.e., $C_1 = C_2 = 0$. This choice for C_i is made because the hose-resistance compensation controller in G combined with unity feedforward already achieves sufficient performance during the first breath and during the idle phase.

Finally, the TRC controller R_i is designed using the framework presented in Section 7.3. The exact learning and robustness filter design is discussed next.

7.5.3 Repetitive control filter design

The filters for the TRC during the active phase are designed following the methodology of Reinders et al. (2020). More specifically, this means that the learning filter L_1 in Fig. 7.2 is based on an average FRF measurement of the plant G for several patients. Furthermore, the robustness filter Q_1 in Fig. 7.2 is designed such that it ensures stability of the standard RC, i.e., *without switching*, using the separate FRFs of all considered patients.

Before designing the RC filters for the mechanical ventilation system, a stability result and a design procedure are given. First, the sensitivity of the controlled system in Fig. 7.2, without the dashed arrow, during the active phase is defined as follows:

$$e = \underbrace{(1 + C_1G)^{-1}}_{S_1} \underbrace{(1 + P_{S,1}R_1)^{-1}}_{S_{R,1}}(r - d), \quad (7.22)$$

where $P_{S,1} = (1 + C_1G)^{-1}G$. Using this sensitivity, the following sufficient stability theorem is obtained for the system in the active phase.

Theorem 7.1. *(Based on the MIMO plug-in RC stability results in Longman (2010).) Assume that S_1 and $P_{S,1}$ are asymptotically stable. Then, $S_{R,1}$ is asymptotically stable for all N if*

$$|Q_1(z)(1 - P_{S,1}(z)L_1(z))| < 1, \forall z = e^{i\omega}, \omega \in [0, 2\pi). \quad (7.23)$$

This stability theorem ensures that the entire loop in Fig. 7.2 is asymptotically stable if no switching to the idle state occurs.

Using the stability condition in Theorem 7.1, the following two-step design procedure is followed for SISO RC systems, see Blanken et al. (2020); Hara et al. (1988); Steinbuch (2002); Tomizuka et al. (1989).

Procedure 7.1. *(Based on frequency-domain SISO RC design, from Blanken et al. (2020) and Reinders et al. (2020).)*

1. *Given a parametric model of the 'nominal' process sensitivity $P_{S,1}(z)$, construct $L_1(z)$ as an approximate, possibly non-causal, stable inverse of $P_{S,1}(z)$, i.e., $L_1(z) \approx P_{S,1}^{-1}(z)$.*
2. *Using non-parametric FRF models, $P_{S,1}^p(e^{i\omega})$, $p \in \{1, \dots, N_p\}$ with N_p the number of patient models, of different patients, design one $Q_1(z)$ such that Theorem 7.1 is satisfied for $P_{S,1}^p(e^{i\omega}) \forall p \in \{1, \dots, N_p\}$.*

To design the RC filters for the active phase, Procedure 7.1 is followed. First FRF measurements of the process sensitivity $P_{S,1}^p(z)$ for every patient are obtained, see Fig. 7.10. The average of these FRF measurements and a fourth-order fit with 12 samples delay are used to obtain a parametric model $P_{S,1}^n(z)$ of the 'nominal' process

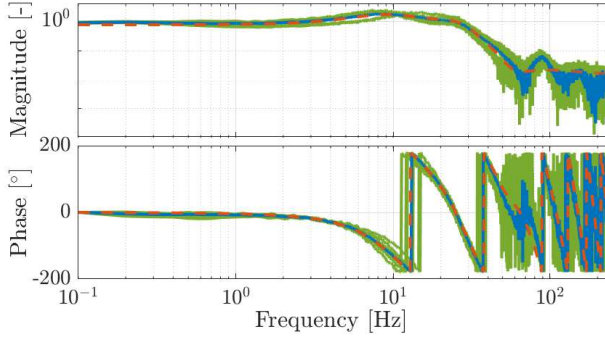


Fig. 7.10. The FRF measurements of the process sensitivity for the individual patients (—), the 'nominal' (average) process sensitivity (—), and the fourth-order fit of the 'nominal' process sensitivity (- - -).

sensitivity, see Fig. 7.10. This fit of the 'nominal' process sensitivity is used to construct a non-causal learning filter $L_1(z) = z^{p_l} L_c(z)$ as an approximate stable inverse of $F_{S,1}^n(z)$. This inverse is obtained using Zero Phase Error Tracking Control (ZPETC) (Tomizuka, 1987).

For the robustness filter design, the second step in Procedure 7.1 is followed. First, the stability condition of standard RC is checked for $Q_1 = 1$. In the left-hand side of Fig. 7.11, it is clearly seen that the stability conditions for standard RC are not guaranteed for all patients. Therefore, a 20th-order non-causal zero-phase Finite Impulse Response (FIR) filter with a cut-off frequency of 20 Hz is implemented as the robustness filter Q_1 . This FIR filter is implemented by computing a causal symmetric FIR-filter $Q_{1,c}$ and applying a forward shift of z^{p_q} with p_q half the order of the FIR-filter. This makes it a zero-phase FIR filter that is symmetric around zero lag, such that no phase lag is introduced by the filter. The forward shift is possible because of the memory loop, as long as $p_l + p_q \leq N$. With the implementation of this robustness filter the standard RC stability condition in Theorem 7.1 is ensured, as is shown in the right-hand side plot of Fig. 7.11.

Eventually, to reduce the effect of the varying disturbances, e.g., breathing effort, in subsequent breaths a learning gain $\alpha \in [0, 1]$ is included by multiplying L_1 with α . The choice of the learning gain is a trade-off between convergence speed and varying disturbance suppression. Therefore, a learning gain of 0.2 is implemented, this value is a result of extensive testing.

7.5.4 Stability analysis

In the previous section, stability of the closed-loop system is guaranteed in case the system does not switch to the idle phase. However, in the mechanical ventilation use-cases,

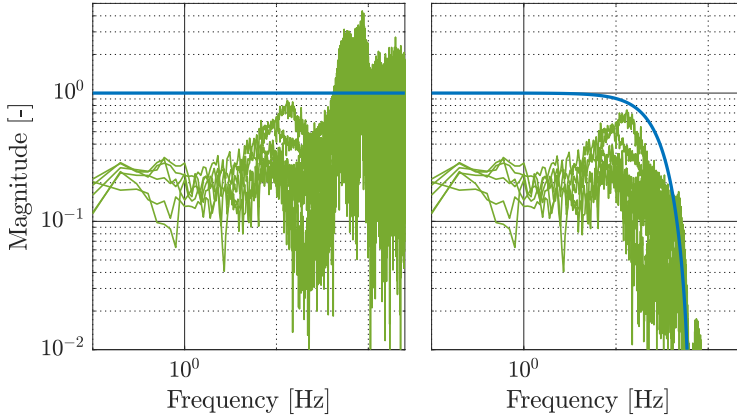


Fig. 7.11. Left: stability condition for all patients with $Q_1 = 1$. Right: stability condition for all patients with Q_1 a 20th order FIR filter with cut-off frequency at 20 Hz. The figures show $(|Q_1(1 - P_{S,1}L_1)|)$ for every patient (—) and the corresponding Q -filters (—).

the system switches to the idle phase after every ventilator assisted breath. Therefore, the results in Section 7.3.2 should be used to ensure stability of this system, controlled by TRC. To guarantee stability of the system, a CQLF, parameterized by P , should be computed that ensures (7.9) and (7.10). To do this for the considered use-cases, a challenge occurs. Namely, the P matrices are very large, up to 1042×1042 for the adult case. This is caused by the size of the system matrix $A(N, N_{\epsilon,j})$, which is large because of the states that are introduced by the memory loop in the TRC. Therefore, when attempting to solve a system of linear matrix inequalities in MATLAB to compute a suitable P matrix our system, an Intel Core i7-7700HQ, 2.8GHz processor with 16 GB RAM, runs out of memory and is unable to find a P matrix that satisfies the linear matrix inequalities and guarantees stability.

However, for smaller values of N we are able to find P matrices for all three use-cases that guarantee stability of the system. These P matrices guarantee stability when arbitrarily switching between different idle times $N_{\epsilon,j} \in \{0, 1, \dots, N_{max}\}$, with $N_{max} = 5000$ samples, which corresponds to a maximum of 10 seconds between breaths. Although a formal proof is missing for larger values of N , we conjecture that the system is stable for larger values of N . Finding CQLFs for larger values of N is left for future work.

7.5.5 Experimental results

In this section, the results of the experiments are presented. First, the time-domain results of the adult use-case are shown and analyzed. Thereafter, all use-cases are analyzed in terms of the pressure error 2-norm on breath level.

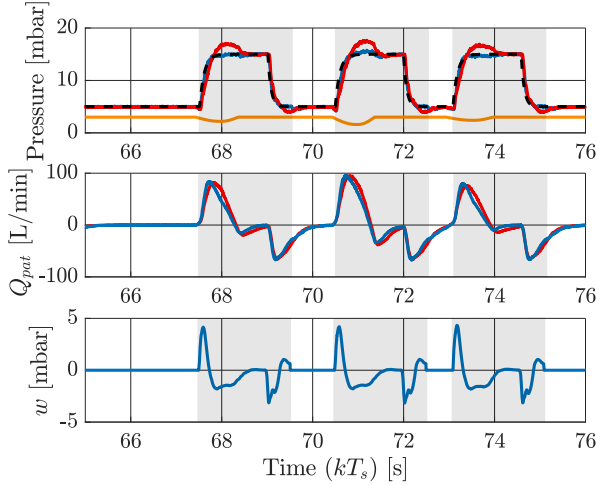


Fig. 7.12. The airway pressure, patient flow, and TRC output of the 19th-21th breath for the converged TRC controller (—) and hose-resistance compensation controller (—) for the adult case, and the target pressure (---) and the scaled patient effort p_{mus} (—). The TRC is in the active phase in the gray areas and in the idle phase in the white areas. The figure shows that the airway pressure tracking performance is improved.

The results of the 19th-21th breath of the adult use case are shown in Fig. 7.12. The figure shows the airway pressure and patient flow for the system with TRC and for the system with just hose-resistance compensation. It is clearly shown that the airway pressure tracking performance is improved significantly by TRC. Both the rise-times and overshoot are significantly reduced. Some slight oscillations in the airway pressure with TRC are seen at the IPAP level, these oscillations are caused by the varying patient effort. Because these are varying over breaths the TRC cannot compensate this perfectly. Furthermore, it is seen that the TRC output w is zero in the idle phase and has no actuation spike at the end of the active phase. However, w is not zero at the end of the active phase, this is because the system is not yet in steady state, i.e., the flow is not zero at the end of the active phase.

The error 2-norms per breath for all use-cases are shown in Fig. 7.13. The error 2-norm per breath is defined as the 2-norm of the tracking error, $e := p_{target} - \tilde{p}_{aw}$, during the active and the subsequent idle phase. The first data point in Fig. 7.13 represents the error 2-norm of the system with hose-resistance compensation only, i.e., the output of the RC is zero. It is seen in the figure that for all three use-cases the error converges in about 10 breaths, this is due to the particular choice of α . The figure shows that the tracking performance is improved with a factor 3.9 to 4.6. Upon convergence some oscillations are seen, these are caused by the varying length of the idle phase and the

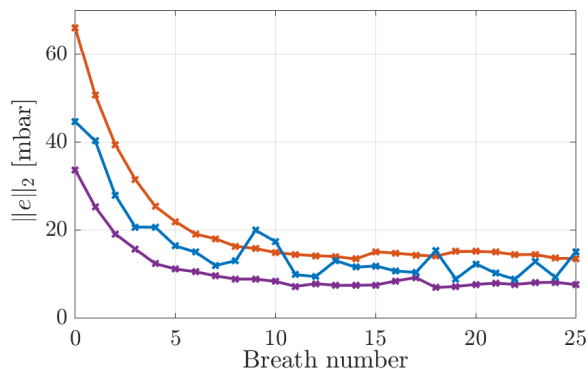


Fig. 7.13. Error 2-norm per breath for every use case, a single breath consists of the active phase and the subsequent idle phase. The first breath represents the system with hose-compensation control, since the RC output is zero. The figure shows the adult (—), the pediatric (—), and the baby (—) use cases.

varying patient effort. The adult use-case is especially sensitive to varying patient effort because of the high compliance and low resistance.

Concluding, pressure tracking performance is improved significantly for a wide-variety of spontaneously breathing patients by including TRC in the mechanical ventilation setup. Furthermore, the undesired actuation spike, as seen in Section 7.2.3, is resolved.

7.6 Conclusions and future work

The Triggered Repetitive Control (TRC) framework enables improved tracking performance improvement for systems with repeating tasks where the start of a task is triggered at varying inter-task times, and this provides a breakthrough for applying RC techniques to mechanical ventilation with possibly spontaneously breathing patients. The main challenge that is solved in this chapter is the fact that the period in between a task is not exactly the same for subsequent tasks, it depends on the timing of an external disturbance, deteriorating performance of traditional repetitive control (RC). This challenge is solved by activating and de-activating the repetitive controller when the repetitive task starts and ends, respectively. Furthermore, adjustments to the traditional RC filters are made to prevent undesired actuation peaks at the end of the repetitive task.

Furthermore, the TRC framework is theoretically supported by a stability analysis. Thereafter, a design procedure of TRC for mechanically ventilated patients is presented. Using this design procedure, TRC is implemented and tested in an experimental setup

for ventilation. A performance analysis of these experiments show a significant performance increase compared to other control strategies for ventilation. In the experimental case-study a reduction of the error 2-norm up to a factor 4.6 has been achieved compared to a state-of-the-art control strategy.

The experiments have shown that the proposed control strategy significantly improves pressure tracking performance compared to a state-of-the-art control strategy for mechanical ventilation. Several recommendations are considered relevant for future extensions and improvements. First, a variable learning gain could be considered to decrease the effects of varying patient effort on the tracking performance upon convergence while ensuring fast convergence. Second, an additional TRC for the expiration should be added to enable triggered off-cycling of the mechanical ventilator. This enhances the expiration synchrony between the patient and ventilator. Third, a simple method to guarantee stability of the closed-loop system with TRC should be developed, to avoid the computational burden of solving the linear matrix inequalities.

7.A Appendix

The full switching closed-loop system with TRC are described by the state-space system in (7.5). The corresponding state-space matrices are retrieved by working out the interconnections in Fig. 7.2 and considering the state vector in (7.6). This results in the following state-space system matrices:

$$\begin{aligned}
 A_l &= \begin{bmatrix} a_{l,11} & a_{l,12} & a_{l,13} & a_{l,14} & a_{l,15} & 0 \\ 0 & A_{L,l} & B_{L,l}C_{Q,l} & 0 & B_{L,l}D_{Q,l}C_{Z,l} & 0 \\ 0 & 0 & A_{Q,l} & 0 & B_{Q,l}C_{Z,l} & 0 \\ -B_{C,l}C_G & 0 & 0 & A_{C,l} & 0 & 0 \\ a_{l,51} & a_{l,52} & a_{l,53} & a_{l,54} & a_{l,55} & B_{Z,l}C_{P,l} \\ 0 & 0 & B_{P,l}C_{Q,l} & 0 & B_{P,l}D_{Q,l}C_{Z,l} & A_{P,l} \end{bmatrix}, \\
 B_l &= [B_G(1 + D_{C,l}) \ 0 \ 0 \ B_{C,l} \ B_{Z,l} \ 0]^T, \\
 C_l &= [C_G \ 0 \ 0 \ 0 \ 0 \ 0], \\
 D_l &= 0,
 \end{aligned} \tag{7.24}$$

where

$$\begin{aligned}
 a_{l,11} &= A_G - B_G D_{C,l} C_G & a_{l,51} &= -B_{Z,l} C_G \\
 a_{l,12} &= B_G C_{L,l} & a_{l,52} &= 0 \\
 a_{l,13} &= B_G D_{L,l} C_{Q,l} & a_{l,53} &= B_{Z,l} D_{P,l} C_{Q,l} \\
 a_{l,14} &= B_G C_{C,l} & a_{l,54} &= 0 \\
 a_{l,15} &= B_G D_{L,l} D_{Q,l} C_{Z,l} & a_{l,55} &= A_{Z,l} + B_{Z,l} D_{P,l} D_{Q,l} C_{Z,l}.
 \end{aligned} \tag{7.25}$$

Part II

Improved monitoring algorithms for ventilation

Noninvasive breathing effort estimation of mechanically ventilated patients using sparse optimization

Abstract – Mechanical ventilators facilitate breathing for patients who are unable to do so on their own. The aim of this chapter is to estimate relevant lung parameters and the spontaneous breathing effort of a ventilated patient that help keeping track of the patient’s clinical condition. A key challenge is that estimation using the available sensors for typical model structures results in a non-identifiable parametrization. A sparse optimization algorithm to estimate the lung parameters and the patient effort, without interfering with the patient’s treatment, using an ℓ_1 -regularization approach is presented. It is confirmed that accurate estimates of the lung parameters and the patient effort can be retrieved through a simulation case study and an experimental case study.

8.1 Introduction

Mechanical ventilation is a life-saving therapy used in Intensive Care Units (ICUs) to assist patients who need support to breathe sufficiently. The main goals of mechanical ventilation are to ensure oxygenation and carbon dioxide elimination (Warner and Patel, 2013). Especially during the flu season or a world-wide pandemic such as the COVID-19 pandemic (Wells et al., 2020), mechanical ventilation is a life saver for many patients around the world.

Accurately tracking the patient’s clinical condition is essential to optimize the patient’s treatment. A lung model, e.g., a linear one-compartmental lung model (Bates, 2009, pp. 37–60), can be estimated to retrieve valuable information about the patient’s

The contents of this chapter also appear in Reinders et al. (2022c). A patent application under application nr. 2028456 at the Netherlands Patent Office is filed for the algorithm presented in this chapter.

clinical condition. These estimates give an indication of the lung compliance, i.e., the inverse of the lung stiffness, and the resistance of the patient's airway. In Borrello (2001) and Avanzolini et al. (1997), such parameters have been estimated during ventilation of *fully sedated patients* using recursive least squares algorithms. However, during the weaning process the assistance delivered by the ventilator is reduced gradually and the patient is *breathing spontaneously* as well. This breathing effort causes the estimated patient models to be inaccurate and practically useless if this effort is not taken into account. Furthermore, if the breathing effort is not considered in the treatment it might cause the patient to overextend its own lungs, resulting in complications. Also, an accurate estimate of the patient effort can be used to detect, and eventually prevent, patient-ventilator asynchrony. According to Blanch et al. (2015), this patient-ventilator asynchrony is associated to increased mortality. Therefore, accurate estimates of this effort and the patient parameters are relevant to determine the patient's clinical condition and improve the patient's treatment.

Two distinct types of methods can be distinguished to obtain the desired patient information in case of *spontaneously breathing patients*. First, methods that are employing additional sensing equipment are available. The required additional sensors makes these methods unsuitable for use in the ICU, because placing additional sensors is error-prone and it demands more time for the ICU personnel. This is undesired because the ICUs are already understaffed (Angus et al., 2000; Needham et al., 2005). Second, algorithms that use the already available data in ventilation are available. Typically, these methods impose an extra maneuver, i.e., an additional change in pressure, or some assumption on the patient effort. Next, both such approaches are investigated in detail.

The first class of methods, requiring additional sensing, are error-prone and costly in terms of personnel time. Next, methods requiring additional sensing are presented. In Neurally Adjusted Ventilatory Assist (NAVA), in Navalesi and Costa (2003); Sinderby and Beck (2008); Sinderby et al. (1999), an invasive esophagus catheter is used to measure diaphragm activity. Using an esophagus catheter is both invasive and error-prone (Doorduyn et al., 2013). Therefore, it is not suitable for many patients. In Petersen et al. (2020), non-invasive surface electromyography (EMG) measurements are used to estimate the patient's breathing effort. The presented methods all require additional, possibly invasive, sensing. This is undesired because it costs valuable time of the ICU personnel and is error-prone.

The second class of methods do not require additional sensing, yet are highly challenging from an estimation perspective, typically imposing unrealistic restrictions on the patients breathing effort. In Navajas et al. (2000) and Dietz et al. (2003), a method is presented to estimate the patient parameters and effort during ventilation. These methods assume that the change in patient effort over significant breaths is insignificant and require an extra maneuver, interfering with the treatment. Therefore, they are not preferred in practice. In Maes et al. (2014, 2017), a device is developed that estimates the lung impedance of a spontaneously breathing patient by superimposing a multi-sine to the ventilation target. To extract the patient effort from the actual signal,

the patient is requested to breath with a specific frequency. In critically ill patients, it is typically not possible to demand this from a patient. Furthermore, this method interferes with the treatment as well. In Vicario et al. (2015), it is assumed that the patient effort first monotonically increases and thereafter monotonically decreases to zero. This limitation on the patient effort is considered too stringent in practice. In conclusion, the presented methods are able to retrieve valuable information about the patient's parameters and the patient effort. However, they restrict the estimated patient effort and interfere with the treatment.

Although several estimation algorithms have been developed that improve the estimation of patient effort and a patient model, these all require either more data, an extra maneuver, or use rather stringent assumptions on the patient effort. Indeed, in Olivieri et al. (2011) and Fresnel et al. (2014), it is concluded that there is no consensus on how patient effort should be modeled. However, from a practical point of view it is valid to assume that the effort is not changing arbitrarily within a particular breath. More specifically, the patient effort has some smoothness properties and does not arbitrarily change slope or jump up and down. Note that the patient effort can change significantly over successive breaths. The smoothness property of the patient effort can be ensured by assuming the second time derivative of the effort is sparse, i.e., it contains only a few non-zero elements. Therefore, in this chapter estimation methods of sparse signals are considered as a possible solution to the estimation problem at hand. In particular, ℓ_0 -regularization and its convex relaxation ℓ_1 -regularization are considered in this chapter. Such ℓ_1 -regularization is used in for example the Least Absolute Shrinkage and Selection Operator (lasso) (Tibshirani, 1996) and fused lasso (Tibshirani et al., 2005). These methods are used to compute sparse feedforward control signals (Oomen and Rojas, 2017) and to enhance sparsity in system identification (Ohlsson et al., 2010; Rojas and Hjalmarsson, 2011).

The main contribution of this chapter is an estimation framework, using sparse optimization, that enables estimation of the patient effort and the patient's lung model of a mechanically ventilated patient with spontaneous breathing effort. The presented approach meets the following requirements: 1) it only uses commonly available data; 2) it does not use an extra ventilation maneuver; and 3) it leaves freedom regarding the shape of the patient effort. As subcontributions, the performance of this algorithm is investigated through a simulation case study and through an experimental setup with an actual ventilator and a mechanical lung.

The outline of this chapter is as follows. In Section 8.2, the considered patient model is presented. In Section 8.3, the estimation goal and challenge are described in detail. Then, In Section 8.4, the proposed sparse estimation method is explained in detail. Thereafter, in Section 8.5, a simulation case study is presented to analyze the performance of the algorithm. Then, in Section 8.6, an experimental case study is used to show the performance of the proposed algorithm in practice. Finally, in Section 8.7, the main conclusions and recommendations for future work are presented.

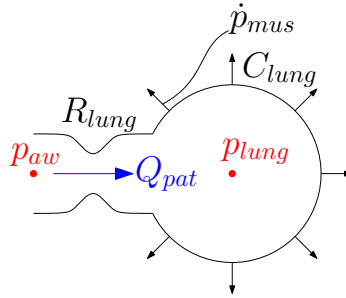


Fig. 8.1. Schematic representation of the patient's respiratory system, with the relevant patient parameters and signals. The signals p_{aw} and Q_{pat} are typically measured during mechanical ventilation.

8.2 Patient and breathing effort modeling

In this section, a description of the considered patient model is presented. In Section 8.2.1, the considered patient model and its relevant parameters are presented. Thereafter, in Section 8.2.2, the considered patient breathing effort model is presented.

8.2.1 Patient model

The model considered in this chapter is a linear one-compartmental lung model, which is extensively described in Bates (2009, pp. 37–60). An advantage of this model description is an ease of interpretation for clinicians. Including parameters such as the airway resistance and lung compliance.

Fig. 8.1 shows a schematic representation of the patient's respiratory system with the parameters and signals relevant for estimation. The patient model without patient effort consists of two components that are modeled; namely, the airway and the lungs. The airway model describes the relation between the pressure drop over the airway and the flow in and out of the patient's lungs. The lung model gives the relation between the flow in and out of the lungs and the pressure inside the lungs.

The airway is modeled by means of a linear resistance R_{lung} . This linear resistance gives the relation between the airway pressure, the lung pressure, and the patient flow:

$$Q_{pat}(t) = \frac{p_{aw}(t) - p_{lung}(t)}{R_{lung}}, \quad (8.1)$$

where p_{aw} is the airway pressure, the pressure near the patients mouth, and p_{lung} is the lung pressure, the pressure inside the lungs.

The lung model describes the relation between the patient volume V_{pat} , i.e., the volume inside the lungs, and the lung pressure p_{lung} . This relation is described by a

linear lung compliance C_{lung} . The pressure inside the lungs is expressed as

$$p_{lung}(t) = \frac{1}{C_{lung}} \underbrace{\int_{t_0}^t Q_{pat}(\tau) d\tau}_{V_{pat}(t)} + p_{lung}(t_0), \quad (8.2)$$

where integration of the flow over time gives the patient volume V_{pat} and $p_{lung}(t_0)$ is the initial lung pressure at time t_0 .

Contraction and relaxation of the respiratory muscles induce the patient effort p_{mus} . This patient effort is modeled as an additive disturbance to the lung pressure in (8.2). More details on the patient effort are presented in Section 8.2.2. This gives the following equation for the lung pressure p_{lung} with patient effort:

$$p_{lung}(t) = \frac{1}{C_{lung}} \underbrace{\int_{t_0}^t Q_{pat}(\tau) d\tau}_{V_{pat}(t)} + p_{lung}(t_0) + p_{mus}(t). \quad (8.3)$$

Combining (8.1) and (8.3) gives the following expression for the airway pressure p_{aw} :

$$p_{aw}(t) = \frac{1}{C_{lung}} V_{pat}(t) + R_{lung} Q_{pat}(t) + p_{lung}(t_0) + p_{mus}(t). \quad (8.4)$$

The discrete time expression of (8.4) is given by:

$$p_{aw}(k) = \frac{1}{C_{lung}} V_{pat}(k) + R_{lung} Q_{pat}(k) + p_{lung}(1) + p_{mus}(k), \quad (8.5)$$

where k denotes the discrete sample number and $p_{lung}(1)$ denotes the initial lung pressure. Equation (8.5) is used in the cost function of the estimation algorithm in Section 8.4. The considered patient effort model is investigated in the next section.

8.2.2 Patient effort model

Patient effort enables a person, i.e., healthy or patient, to inhale and exhale air by themselves. In this section, the most important properties of the patient effort are presented. Further, it is explained how these properties are translated to the effort model $p_{mus}(t)$. Physically, the patient effort can be seen as a change in lung pressure caused by contractions and relaxation of the respiration muscles, e.g., the diaphragm. For example, contraction of the diaphragm results in a downward motion of the diaphragm. This motion results in a pressure drop in the lungs. Various approaches are being used currently to model the patient effort. Based on physical properties of respiration, in this section two assumptions are made on the shape of patient effort. Furthermore, a commonly used patient effort model is briefly presented.

Firstly, the assumption is made that the modeled patient effort $p_{mus}(t)$ is non-positive. Typically inspiration is an active process, where the diaphragm is contracted. This results in a decrease in lung pressure. This decrease in lung pressure is modeled by a negative patient effort $p_{mus}(t)$. Expiration is typically a passive process, where the respiration muscles are relaxing and the elasticity of the lungs result in a negative airflow. Expiration is modeled by increasing the negative patient effort until it is zero again. Because expiration is typically passive, Assumption 8.1 is adopted throughout this chapter.

Assumption 8.1. *The patient effort $p_{mus}(t)$ is a non-positive signal, i.e.,*

$$p_{mus}(t) \leq 0, \forall t \geq 0. \quad (8.6)$$

Secondly, it is assumed that the shape of the modeled patient effort $p_{mus}(t)$ cannot change arbitrarily within one breath. However, the patient effort is allowed to change arbitrarily over successive breaths. According to Fresnel et al. (2014), it is common to use a sinusoidal half-wave for the patient effort. An example of the sinusoidal half-wave and a piecewise linear version of the effort, and their first and second time derivatives are depicted in Fig. 8.2. It is shown that a piecewise linear effort gives a fairly accurate representation of the sinusoidal half-wave. Furthermore, it is observed that the second time-derivative of the piecewise linear $p_{mus}(t)$ is sparse, i.e., it only contains a few non-zero elements. This sparsity property of $\ddot{p}_{mus}(t)$ is used as prior knowledge in the estimation algorithm, without fixing the exact timing and height of the signal. Using the presented patient models, the estimation goal and the main challenge are presented in the next section.

8.3 Estimation goal

In this section, the estimation goal is presented. Then, the practical estimation setting with its limitations and constraints is presented. Finally, the main challenge is presented.

The estimation goal is to retrieve accurate estimates of the patient's breathing effort, $p_{mus}(t)$, the lung compliance C_{lung} , and the patient's resistance R_{lung} . Accurate estimates of these parameters can be used to follow the patient's clinical condition and adjust the treatment accordingly. From discussions with experts in the field it is concluded that an accuracy of about 15 % of the compliance and resistance estimates is practically useful and therefore desired. Therefore, the requirement for estimation accuracy of the lung parameters is 15 %. The estimation goal must be achieved by using the typically measured signals, i.e., airway pressure $p_{aw}(t)$, the patient flow $Q_{pat}(t)$, and the patient volume $V_{pat}(t) = \int_{t_0}^t Q_{pat}(\tau) d\tau$.

The considered estimation setting is a particular ventilation mode, namely, Pressure Controlled - Assist Control Ventilation (PC-ACV), schematically depicted in Fig. 8.3.

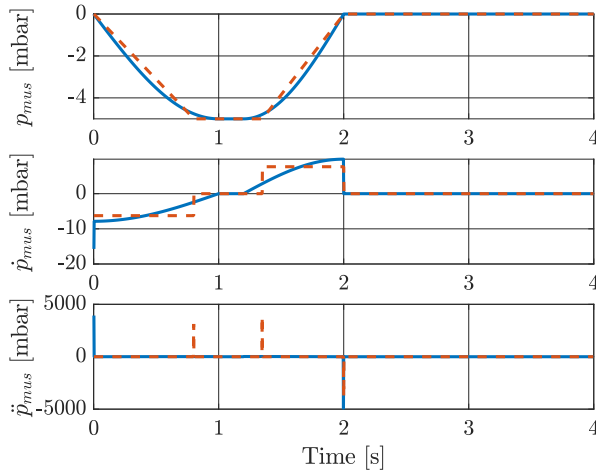


Fig. 8.2. Example of a model for the patient effort $p_{mus}(t)$ and its first and second time derivatives. A sinusoidal half-wave (—) and a piecewise linear (---) are shown.

The figure shows the airway pressure p_{aw} , patient flow Q_{pat} , and patient effort p_{mus} during one stroke of triggered ventilation. The ventilator is detecting the start of the patient effort to synchronize the machine with the patient. Typically the start of inspiration is detected by detecting an increase in the patient flow. This patient flow is caused by the patient's inspiration effort. When the start of the patient's effort is detected, a ventilation stroke of the mechanical ventilator is started to assist the patient. This ventilation stroke is induced by increasing the patient's airway pressure p_{aw} to the Inspiratory Positive Airway Pressure (IPAP) level. The pressure level generated by the mechanical ventilator is lowered after a preset time to the Positive End-Expiratory Pressure (PEEP) level to allow the air to leave the patient's lungs in the expiration phase.

Next, an assumption on the breathing effort and a restriction on the target pressure are presented. First, it is assumed that the patient effort can significantly change from breath to breath. It might change in breath depth, i.e., amplitude, as well as in shape such as timing, rise times, and length. This means that the estimation algorithm should be able to deal with such changes. Second, it is desired to not interfere with the treatment. Therefore, it is undesired to change the target pressure to obtain estimates of the patient parameters, i.e., it is not allowed to add an extra maneuver to the ventilator.

The main challenge in estimating physically interpretable parameters is the non-identifiability of the estimation problem. More specifically, the relation between the airway pressure, patient flow, and patient volume, given by (8.5) has infinitely many solutions, i.e., infinitely many combinations of the estimates, \hat{C}_{lung} , \hat{R}_{lung} , $\hat{p}_{lung}(1)$, and $\hat{p}_{mus}(k)$ with $k \in [1, N]$, describe the relation between the measured signals. This

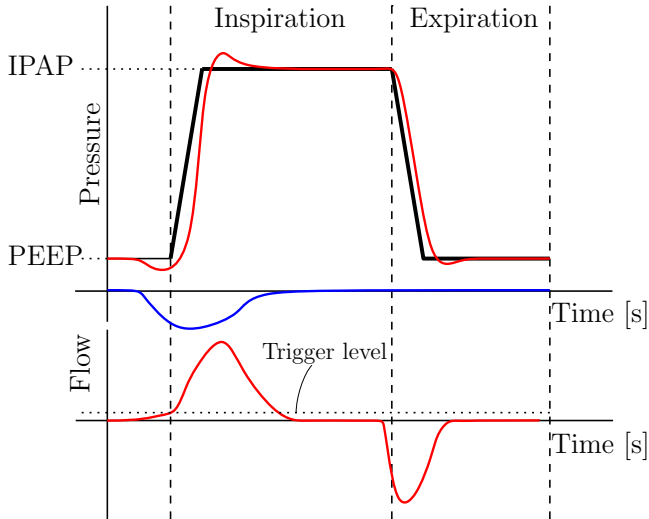


Fig. 8.3. Schematic example of PC-ASV. The figure shows the target pressure (—), the measured airway pressure p_{aw} and patient flow Q_{pat} (—), and the patient effort p_{mus} (—).

can be seen by writing (8.5) as follows:

$$Y = X\beta, \tag{8.7}$$

where

$$Y = \begin{bmatrix} p_{aw}(1) \\ p_{aw}(2) \\ \vdots \\ p_{aw}(N) \end{bmatrix}, \beta = \begin{bmatrix} \frac{1}{C_{lung}} \\ R_{lung} \\ p_{lung}(1) \\ p_{mus}(1) \\ p_{mus}(2) \\ \dots \\ p_{mus}(N) \end{bmatrix}, \text{ and}$$

$$X = \begin{bmatrix} V_{pat}(1) & Q_{pat}(1) & 1 & 1 & 0 & \dots & 0 \\ V_{pat}(2) & Q_{pat}(2) & 1 & 0 & 1 & \dots & 0 \\ \vdots & \vdots & \vdots & \vdots & \vdots & \ddots & \vdots \\ V_{pat}(N) & Q_{pat}(N) & 1 & 0 & 0 & \dots & 1 \end{bmatrix}.$$

Thus, in (8.7), Y reflects the measured airway pressure sampled at discrete time instants, X reflects, a.o., the measured patient volume and flow, and β represents the quantities to be estimated. Using this representation it can be shown that $X^T X$ is not invertible, hence, there exists an infinite number of solutions for β , β is not identifiable.

This can also be understood intuitively; by considering the following simulation-error based least-squares cost function:

$$J = \sum_{k=0}^{k=N} (p_{aw}(k) - \hat{p}_{aw}(k))^2 \quad (8.8)$$

with k the sample index of the discrete signals, N the length of the signals in samples, and $\hat{p}_{aw}(k)$ defined as:

$$\hat{p}_{aw}(k) = \frac{1}{\hat{C}_{lung}} V_{pat}(k) + \hat{R}_{lung} Q_{pat}(k) + \hat{p}_{lung}(1) + \hat{p}_{mus}(k). \quad (8.9)$$

It is observed that independent of the choice of \hat{C}_{lung} , \hat{R}_{lung} , and $\hat{p}_{lung}(k)$ choosing $\hat{p}_{mus}(k) = p_{aw}(k) - \left(\frac{1}{\hat{C}_{lung}} V_{pat}(k) + \hat{R}_{lung} Q_{pat}(k) + \hat{p}_{lung}(1) \right)$ results in $\hat{p}_{aw}(k) = p_{aw}(k)$, $\forall t \geq 0$. Therewith, the cost function (8.8) is zero.

Because the relation between the measured signals is non-unique, prior knowledge enables obtaining sensible estimates of the desired parameters and the patient effort. In literature, extra sensing (Navalesi and Costa, 2003; Petersen et al., 2020; Sinderby and Beck, 2008; Sinderby et al., 1999), maneuvers (Dietz et al., 2003; Maes et al., 2014, 2017; Navajas et al., 2000), or stringent assumptions on the shape of the effort (Dietz et al., 2003; Navajas et al., 2000; Vicario et al., 2015) are used to solve this challenge. However, from the earlier defined estimation setting, it is clear that this is practically undesired. Therefore, in the following section an estimation method is presented that does not require additional sensing or maneuvers and does not use unrealistically stringent constraints on the patient effort. Note that we are not considering the effect noise in this estimation problem, so in fact it is a realization problem.

8.4 Sparse estimation

In the previous section, the main estimation challenge is presented, namely, the relation between the measured signals and the estimated parameters and signal is underdetermined. In this section, a simulation-error based estimation algorithm is presented that uses the properties of the patient effort in Section 8.2.2 to overcome the identifiability challenge of Section 8.3.

In Section 8.2.2, it is argued that the patient effort $p_{mus}(k)$ does not change arbitrarily, more specifically, its second time-derivative $\ddot{p}_{mus}(k)$ can be accurately modeled as a sparse signal. Furthermore, the patient effort is non-positive by Assumption 8.1. These two properties of p_{mus} lead to a constrained optimization problem as follows:

$$\begin{aligned}
& \min_{\hat{C}_{lung}, \hat{R}_{lung}, \hat{p}_{lung}(1), \hat{p}_{mus}} \sum_{k=0}^{k=N} (p_{aw}(k) - \hat{p}_{aw}(k))^2 \\
& \text{subject to} \quad \|\hat{p}_{mus}\|_0 \leq v \\
& \quad \quad \quad \hat{p}_{mus}(k) \leq 0 \quad \forall k,
\end{aligned} \tag{8.10}$$

where $\|\hat{p}_{mus}\|_0$ denotes the number of non-zero elements in \hat{p}_{mus} and v gives the upper limit on the number of non-zero elements in \hat{p}_{mus} , i.e., the first inequality constraint in (8.10) enforces the sparsity property.

However, inclusion of such sparsity constraint in the optimization problem leads to a non-convex optimization problem, which is NP-hard (Natarajan, 1995). The ℓ_1 norm is a convex relaxation of the cardinality function $\|\cdot\|_0$. The ℓ_1 norm of \hat{p}_{mus} , denoted by $\|\hat{p}_{mus}\|_1$, is defined as the sum of absolute values of \hat{p}_{mus} . From Oomen and Rojas (2017) and Candès et al. (2008), it is well known that this relaxation also enhances sparsity. Applying this relaxation and writing it in the Lagrangian form results in the following regularized optimization problem:

$$\begin{aligned}
& \min_{\hat{C}_{lung}, \hat{R}_{lung}, \hat{p}_{lung}(1), \hat{p}_{mus}} \sum_{k=0}^{k=N} (p_{aw}(k) - \hat{p}_{aw}(k))^2 + \lambda \|\hat{p}_{mus}\|_1 \\
& \text{subject to} \quad \hat{p}_{mus}(k) \leq 0 \quad \forall k,
\end{aligned} \tag{8.11}$$

where λ is a weighting parameter.

The regularized optimization problem in (8.11) results in biased estimates. To eliminate this bias, the retrieved values for \hat{p}_{mus} can be used to select the set of non-zero elements in \hat{p}_{mus} . This subset can be used in a re-estimation procedure to retrieve an unbiased estimate. This re-estimation method is also used in Oomen and Rojas (2017) to eliminate the bias in the estimates. Although this can improve the quality of the estimates in view of (8.8), it is not shown in this chapter to facilitate the presentation. The main motivation for using the ℓ_1 norm is that it provides a convex relaxation of the ℓ_0 norm. The question whether the right sparse vector is retrieved using (8.11) remains. In Candès and Tao (2005), a sufficient condition that relies on the restricted isometry property is provided. However, these conditions are violated in many practical cases. Nonetheless, the ℓ_1 norm provides an effective way to ensure sparsity.

To solve the optimization problem in (8.11), CVX is used to solve problem (8.11). CVX is a package for specifying and solving convex programs (Grant and Boyd, 2008, 2014).

8.5 Simulation case study

In this section, the presented approach is validated using simulations and it is compared to a traditional estimation method. In Section 8.5.1, the considered use-cases are briefly

explained. Thereafter, the estimation results are presented and analyzed in Section 8.5.2.

8.5.1 Simulation case description

In the simulations, a single-hose ventilation setup is considered, as in Reinders et al. (2021b). The respiratory rate in every simulation is 15 breaths per minute and the values for PEEP and IPAP are 5 and 20 mbar, respectively. The ventilation stroke of the mechanical ventilator is triggered by the patient effort. In this simulation case study, it is assumed that the inspiration start of the ventilator and the patient are exactly synchronized. The data used for the optimization is sampled at 50 Hz.

In this simulation case study, four different patients and three different depths of patient effort are considered. The considered resistances R_{lung} are 5 and 10 mbar/l/s, and the considered compliances C_{lung} are 20 and 50 ml/mbar, where all four possible combinations are considered. Furthermore, every patient is simulated without effort, i.e., $p_{mus}(k) = 0, \forall k$, with a maximum effort of 5 mbar, i.e., $\min(p_{mus}) = -5$ mbar, and with a maximum effort of 10 mbar, i.e., $\min(p_{mus}) = -10$ mbar. The patient effort for all cases is shown in Fig. 8.4.

For these use cases, the presented approach of Section 8.4, described by the optimization problem in (8.11) is compared to a traditional least squares optimization which is currently implemented in many ventilation systems. For the optimization problem in (8.11), $\lambda = 2.5 \times 10^{-3}$ is used. This value for λ is retrieved by tuning such that sufficient performance is achieved for a variety of use-cases. In the traditional least squares optimization approach, it is assumed that the patient effort is zero, i.e., $p_{mus} = 0 \forall k$, in the optimization problem given in (8.11).

8.5.2 Simulation results

The two main results are the improved estimation of the patient parameters and the estimation of patient effort compared to the traditional algorithm. These main results are visualized in Fig. 8.4 and 8.5. In the remainder of this section, the results for the estimated parameters and the estimated patient effort are investigated separately.

The first results is the improved estimation of the patient parameters as shown in Fig. 8.5. The solid blue line in this figure represents the normalized true parameter and the dashed lines represent a 15 % accuracy interval. The red markers in Fig. 8.5 show the estimated parameters for every patient using the traditional estimation method, the green markers show the estimated parameters for every patient using the proposed algorithm. Furthermore, on the horizontal axis the depth of the patient effort is given, corresponding to the plots in Fig. 8.4. Note that for the case of no patient effort the red markers are exactly underneath the green markers. It is clearly seen that when there is no effort, i.e., breath depth is 0 mbar, all estimates are close to the true parameter. For an increasing breath depth the estimates of the traditional algorithm deviate from the true parameters and are clearly outside the desired 15 % accuracy interval. The effect of

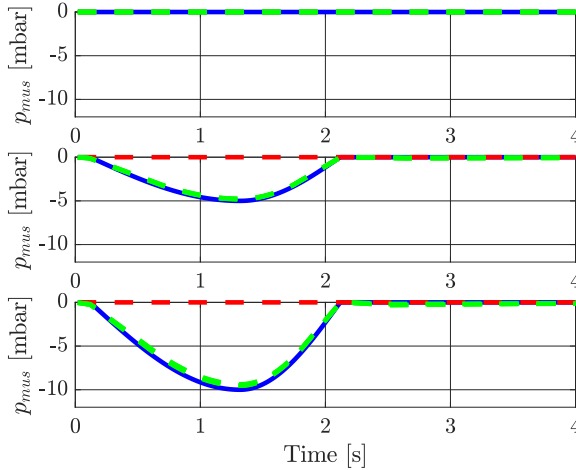


Fig. 8.4. The true and estimated effort for every patient in simulations. From top to bottom the figures show the patients with a breath depth of 0, 5, and 10 mbar, respectively. The figures show the patient effort (—), the patient effort considered by the algorithm assuming $p_{mus} = 0$ (- - -), and the estimated effort using the presented approach (- · -).

the breath depth on the estimated parameters is much smaller when using the proposed algorithm in (8.11). The parameters are slightly diverging, caused by the bias due to the regularization term, but remain very close to the true parameters. In conclusion, the proposed algorithm significantly outperforms the traditional estimation method in estimation the patient parameters.

The second result is the estimation of the patient effort as shown in Fig. 8.4. This figure shows the true effort for every experiment in blue, the assumed effort for the traditional in red, and the estimated effort for the proposed algorithm in green. It is clearly seen in case of no effort, i.e., the top plot, the proposed method retrieves the true effort and the assumption by the benchmark algorithm is correct as well. When increasing the effort, the proposed algorithm retrieves an accurate estimate of the true effort and the assumption in the traditional algorithm is clearly wrong. A small bias is introduced by the regularization term in (8.11). The estimated patient effort is almost perfectly matching the true effort in these simulations.

The bias in the parameter and the patient effort estimates can be completely eliminated by applying re-estimation, as explained in Section 8.4. It is omitted for brevity and clarity.

In conclusion, these simulation results show that the proposed algorithm retrieves useful estimates of the patient parameters and the patient effort. In contrast, the parameter estimates of the traditional method diverge significantly when patient effort is

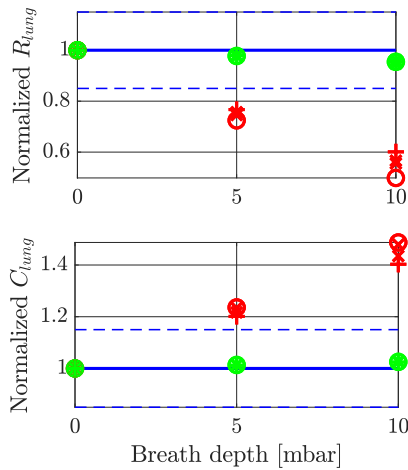


Fig. 8.5. The normalized values of the estimated parameters \hat{R}_{lung} and \hat{C}_{lung} for the different patients against the breath depths in simulations. The figures show the true normalized parameters (—), the 15 % accuracy interval (---), the estimated parameters neglecting the patient effort in red, and the estimated parameters using the presented approach in green. Four different patient types are considered namely: R5C20 (○), R10C20 (×), R5C50 (*), and R10C50 (+).

present, rendering these estimates inaccurate.

8.6 Experimental case study

In this section, the proposed algorithm is validated through an experimental study. First of all, in Section 8.6.1, the used experimental setup and use-cases are described. Thereafter, the estimation results are presented and analyzed in Section 8.6.2.

8.6.1 Experimental setup description

The main components of the experimental setup used in this case study are depicted in Fig. 8.6. The figure shows the blower-driven mechanical ventilation module of Demcon macawi respiratory systems (DEMCON macawi respiratory systems, 2021). The airway pressure p_{aw} is measured using the sensor tube and a gauge pressure sensor inside the respiratory module. The patient flow Q_{pat} is estimated based on the measured airway pressure and a leak model obtained through a calibration routine. The ventilator is attached to a dSPACE system (dSPACE GmbH, Paderborn, Germany), where the controls are implemented using MATLAB Simulink (MathWorks, Natick, MA) running at a sampling frequency of 500 Hz. Note that data sampling for estimation is done at 50

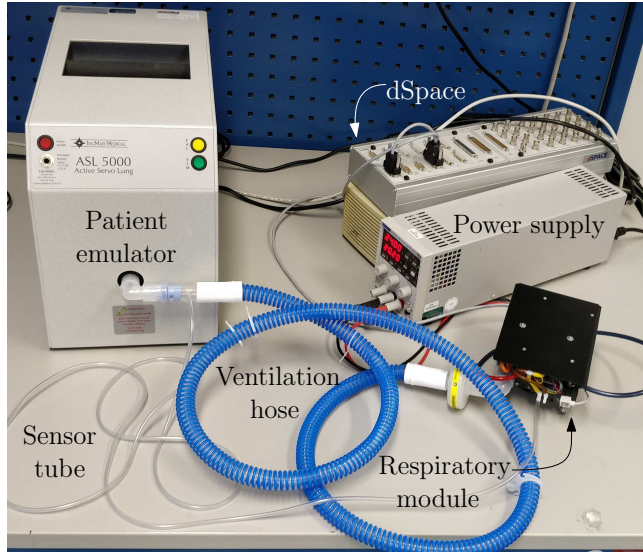


Fig. 8.6. The experimental setup showing the main components: the patient emulator, respiratory module, ventilation hose, dSpace module, and power supply.

Hz, similar to the simulations. This is done to reduce the required memory, which is limited on a typical ventilation system.

Furthermore, the ASL 5000™ Breathing Simulator (IngMar Medical, Pittsburgh, PA) represents the patient. This lung simulator can be used to emulate a wide variety of patients with a linear resistance and compliance. Furthermore, it is able to simulate predefined breathing effort.

Exactly the same settings as in the simulation case study in Section 8.5 are used. More specifically, the breathing simulator is set to emulate the same patients and patient effort that are considered in the simulations case-study. Furthermore, the ventilator generates a PEEP and IPAP of 5 and 20 mbar, respectively. The ventilator's inspiration is triggered by a flow trigger induced by the patient effort. Then, after two seconds the ventilator cycles off to PEEP.

8.6.2 Experimental results

The main results of the experiments are shown in Fig. 8.7 and 8.8. Next, the results for the estimated parameters and the estimated patient effort are analyzed separately.

First, the results of the estimated parameters are investigated. Fig. 8.7 shows the normalized estimated parameter. In general it shows similar results to the simulation results in Fig. 8.5. The traditionally obtained least squares parameters are diverging when increasing the patient effort and the estimates with the proposed method remain

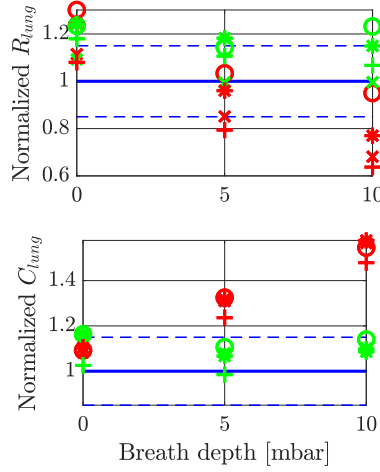


Fig. 8.7. The normalized values of the estimated parameters \hat{R}_{lung} and \hat{C}_{lung} for the different patients against the breath depths in experiments. The figures show the true normalized parameters (—), the 15 % accuracy interval (- - -), the estimated parameters neglecting the patient effort in red, and the estimated parameters using the presented approach in green. Four different patient types are considered namely: R5C20 (O), R10C20 (x), R5C50 (*), and R10C50 (+).

significantly more accurate.

The main difference with the simulations is that the resistance estimate without effort shows a significant offset from the “true” value, also in case of a least squares estimation where $\hat{p}_{mus} = 0$, i.e., the true effort. This is caused by tubing between the sensors of the module, which are used for estimation, and the sensors of the ASL 5000, which are used internally by the ASL 5000 to emulate the desired behavior. This additional tubing results in a slightly increased resistance.

Second, results of the estimated patient effort are analyzed. Fig. 8.8 shows the true effort for every experiment in blue, the assumed effort for the traditional algorithm in red, and the estimated effort for the proposed algorithm in green. It is clearly seen in case of no effort, i.e., the top plot, the estimates using the algorithm in (8.11) retrieves effort close to zero. However, there is some slight deviation. When increasing the effort, the proposed algorithm retrieves an accurate estimate of the true effort, which is highly useful in practice. It seems that the regularization term in (8.11) introduces bias in the estimates. Furthermore, at about 2 seconds, a slight spike in effort is seen. This happens at the start of the expiration of the ventilator. It seems that this spike is caused by the ASL 5000. It is seen that it takes some time for the ASL 5000 to respond to the pressure change that is introduced by the expiration.

Finally the sparsity of the estimated effort is analyzed in Fig. 8.9. This figure shows the second time derivative of the estimated patient effort \ddot{p}_{mus} in one particular use-

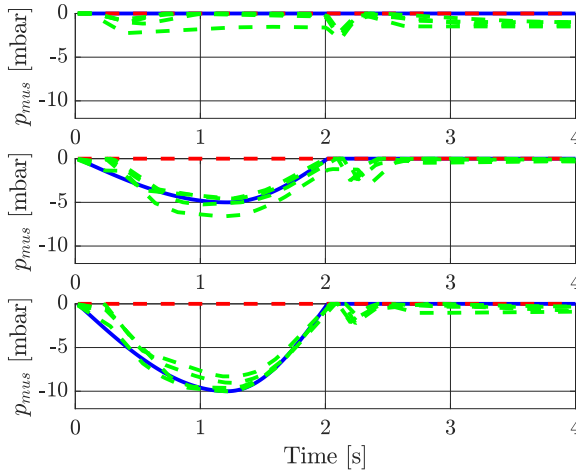


Fig. 8.8. The true and estimated effort for every patient in experiments. From top to bottom the figures show the patients with a breath depth of 0, 5, and 10 mbar, respectively. The figures show the patient effort (—), the patient effort considered by the algorithm assuming $p_{mus} = 0$ (- - -), and the estimated effort using the presented approach (- · -).

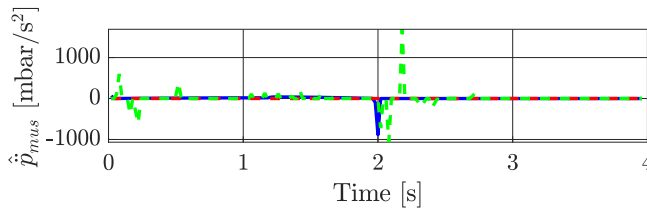


Fig. 8.9. The second time derivative of the patient effort \ddot{p}_{mus} for the R5C20 patient with a breath depth of 20 mbar. Showing the true value (—), the value considered by the algorithm assuming $p_{mus} = 0$ (- - -), and the estimated value using the presented approach (- · -).

case. It is clearly shown that a sparse estimate is retrieved, since many values are zero. Furthermore, it shows that the spike caused by the ASL 5000 causes significant spikes in $\hat{\ddot{p}}_{mus}$. This spike is quickly compensated by another spike. Therefore, the effect on the estimate patient effort $\hat{\ddot{p}}_{mus}$ is not as significant.

Concluding, this experimental case study shows that the proposed algorithm retrieves estimates of the patient parameters and the patient effort that are significantly more accurate than the parameters obtained by the traditional algorithm. Therefore, the retrieved parameters and patient effort can be used by a clinician to improve the patient's treatment.

8.7 Conclusions and recommendations

In this chapter, an estimation framework is presented that can help to identify a ventilated patient's clinical condition. This is achieved by a sparse parameter estimation method to retrieve estimates of relevant patient parameters and the patient effort of a spontaneously breathing mechanically ventilated patient.

The estimation problem, with the available sensors, is non-identifiable. This had to be overcome without interfering with the patient's regular treatment. This is achieved by embedding prior knowledge of the patient effort in the estimation problem. More specifically, that the patient effort cannot change arbitrarily, i.e., its second time derivative is sparse. Embedding this sparsity property in the optimization problem by means of an ℓ_1 -regularization term results in a convex optimization problem that retrieves realistic estimates.

The proposed method is validated by means of simulation and an experimental case studies. Through these case studies, it is shown that the presented algorithm retrieves realistic and useful estimates of the patient parameters and patient effort in a specific mode of triggered ventilation. The retrieved estimates can be used by clinicians to determine the patient's clinical condition and choose the best ventilator settings or treatment.

Several recommendations are considered relevant for future extensions. First, to validate that the algorithm gives clinically useful and realistic estimates in a practical setting, the algorithm should be tested on actual patient data. Second, the algorithm outcome should be compared to existing methods that give an indication about the patient effort, such as, the P0.1 test. Third, the current algorithm does not work in all modes of ventilation, e.g., Continuous Positive Airway Pressure (CPAP) ventilation. Therefore, more research is required to develop an algorithm that works in other modes of ventilation. Fourth, methods such as re-estimation (Oomen and Rojas, 2017) or reweighting (Candès et al., 2008) could be considered to improve estimation quality further in future work.

Automatic patient-ventilator asynchrony detection and classification framework using objective asynchrony definitions

Abstract – Patient-ventilator asynchrony is one of the largest challenges in mechanical ventilation and is associated with prolonged ICU stay and increased mortality. The aim of this chapter is to automatically detect and classify the different types of patient-ventilator asynchronies in real-time using the typically available data on commercially available ventilators. This is achieved by a detection and classification framework using an objective definition of asynchrony and a supervised learning approach. The achieved detection and classification accuracy of the framework is 92.9 % and 75.3 % on simulation data and experimentally generated data, respectively. These accuracy levels are a significant improvement over current clinical practice, therewith, they have the potential to significantly improve the treatment outcomes.

9.1 Introduction

Mechanical ventilation is a life-saving therapy used in Intensive Care Units (ICUs) to assist patients who need support to breathe sufficiently. The main goals of mechanical ventilation are to ensure oxygenation and carbon dioxide elimination (Warner and Patel, 2013). Especially during the flu season or a world-wide pandemic such as the COVID-19 pandemic (Wells et al., 2020), mechanical ventilation is a life saver for many patients around the world.

A common mode of ventilation is Pressure Support Ventilation (PSV). In PSV, the

The contents of this chapter also appear in Reinders et al. (2022d).

ventilator supports a spontaneously breathing patient who is unable to breathe sufficiently by itself. When the ventilator detects an inspiration by the patient, the ventilator increases the pressure levels to increase the air flow and assist the patient's breath. Then, when the patient starts its expiration the ventilator should lower the pressure to allow the patient's expiration. To maximize the patient's comfort, recovery, and safety, it is important that the ventilator support is synchronized with the patient's breathing. In other words, the ventilator's inspirations and expiration start times should be synchronized with the patient's inspiration and expiration start times.

Synchronization of the ventilator's and patient's timing is one of largest challenges in PSV. A mismatch between these timings is called Patient-Ventilator Asynchrony (PVA). Severe levels of PVA are observed in many ventilated patients, ranging from 24 % in Thille et al. (2006) to 43 % in Vignaux et al. (2009). According to Blanch et al. (2015); Epstein (2011); Pham et al. (2018); Thille et al. (2006), PVA is associated with prolonged ICU stay and even increased mortality.

Further improvement of ventilation outcomes therefore hinges on preventing these asynchronies. A first step towards preventing asynchronies is detecting them. However, detecting asynchronies, using the available flow and pressure waveforms, is highly time-consuming and challenging for clinicians (Colombo et al., 2011). Additionally, the workload for medical staff is very high and expected to further increase in the future (Angus et al., 2000). Therefore, it is necessary to detect and classify PVA automatically and reliably.

In recent years, substantial research has been done to develop algorithms that can detect and classify different types of asynchronies. In Adams et al. (2017) and Blanch et al. (2012), a rule-based algorithm based on bedside clinical rules is proposed that is able to detect one asynchrony type. In Mulqueeny et al. (2009), a naive Bayes algorithm based on 21 features from the pressure and flow is proposed. This algorithm is able to distinguish ineffective efforts from normal breaths. In Gholami et al. (2018), a random forest network is used that is able to automatically detect premature cycling and delayed cycling asynchronies from extracted features of the pressure and flow curves. In Zhang et al. (2020), a long-short term memory network is used that is able to classify double trigger and ineffective efforts also based on the pressure and flow curves. In Bakkes et al. (2020), a convolutional neural network is used that is able to identify the inspiration and expiration start times of the patient and the ventilator. Subsequently, these timings are translated to a specific asynchrony type. In Van Diepen et al. (2021), the performance of the algorithm of Bakkes et al. (2020) is evaluated on simulated PVA data. In Pan et al. (2021), a convolutional neural network is proposed that classifies a breath based on the corresponding PVA type and it gives an indication which part of the breath is important for the classification process.

Although existing literature shows that rule-based algorithms and machine learning algorithms are promising solutions to detect and classify PVA, the presented approaches have several limitations. First, an objective characterization of many relevant patient-ventilator asynchrony types is missing, this makes the labeling process inconsistent. Second, the labeling process using expert knowledge is challenging, see Colombo et al.

(2011), resulting in a poor data quality. Third, the proposed algorithms are unable to detect all different types of PVA; they focus on a small subset of asynchrony types. Fourth, the presented algorithms require pre-processing, for example, all algorithms in literature require that the data is divided into subsets with only one breath or asynchrony type. In practice, this is undesired because it requires knowledge about the asynchrony before the data can be divided, which is typically not available.

The aim of this chapter is to develop a detection and classification framework that can detect all types of asynchrony using the real-time measured data that is typically available in commercial ventilators. This is achieved by first presenting an objective characterization of PVA. Then, this definition and a simulation environment are used to generate labeled ventilation data. Thereafter, using the simulation data, a function approximator is designed and trained to recognize these asynchronies in real-time. Finally, performance of this algorithm is analyzed using simulation data and experimentally obtained data in a controlled lab-environment.

The main contribution of this chapter is formulated as follows:

- the design of a framework to automatically detect and classify different types of patient-ventilator asynchrony for real-time bedside monitoring.

Besides the main contribution, this chapter contains several subcontributions:

- a new objective characterization of many relevant patient-ventilator asynchrony types;
- a simulation environment to generate synthetic labeled patient-ventilator asynchrony data;
- a performance analysis of the developed algorithm, using simulation and experimental data.

Note that in this chapter simulation and experimental laboratory data is used. This has several advantages over clinical data and is therefore considered an important step towards a robust system for use in a clinical setting. First, using simulation data gives a better understanding of the different asynchrony types. Second, manual labeling of clinical data is error-prone, resulting in data of poor quality, while in simulation data the labels can be assigned in an unambiguous way. Third, it allows for faster development in cases where clinical data is not available yet. Therefore, in this chapter simulation data is used for training and an initial performance analysis of the algorithm. Thereafter, the trained algorithm's performance is experimentally analyzed using experimental data from a non-clinical setting. A natural next step in the development process is to use clinical data for the further improvement of the algorithms.

The outline of this chapter and the connections between the different sections is visualized in Fig. 9.1. In Section 9.2, the main components of the PVA detection and classification framework are described. Then, in Section 9.3, the relevant types of PVA are characterized. In Section 9.4, the simulation environment to generate synthetic training data is described. In Section 9.5, the design of a specific algorithm is described

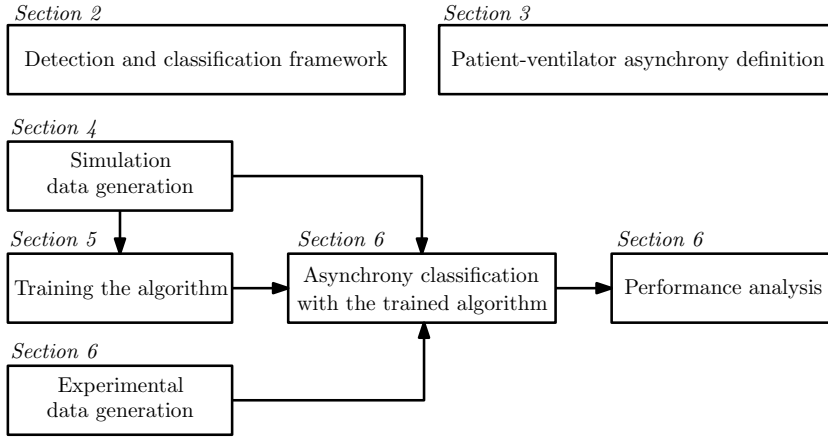


Fig. 9.1. The outline of this chapter, visualizing the connections between the different sections.

and the simulation data is used to train this algorithm. Then, in Section 9.6, the performance of this algorithm is evaluated using simulation and experimental ventilation data. Finally, in Section 9.7, the main conclusions and recommendations for future work are formulated.

9.2 PVA detection and classification framework

To develop the Patient-Ventilator Asynchrony (PVA) detection and classification algorithm, a framework is developed that can utilize different supervised learning algorithms. In supervised learning, a mapping from the available input (measured data) to the output (PVA type) is learned using a known set of input-output pairs (Murphy, 2012). To achieve this, a dataset, a model structure, and a fit criterion are required. The dataset is used to train and eventually validate the algorithm. The model structure is a function that can describe the relation between the input and the output data. The fit criterion is used to obtain the optimal parameters, i.e., weights and biases, of the model structure.

A supervised learning approach is used, because it is relatively easy to obtain a large set of asynchrony data for training an algorithm. Furthermore, supervised learning approaches have been successfully used in literature to classify PVA, as shown in the introduction. Next, the three different components of the framework, i.e., the *data*, the *model structure*, and the *fit criterion*, are described.

The *data* used in this PVA detection and classification problem is labeled ventilation data. The inputs of the detection and classification model are the measured airway pressure p_{aw} , the patient flow Q_{pat} , and the patient's lung volume V_{pat} . These signals

are available in commercial ventilation systems. The desired output of the algorithm is the type of PVA that is occurring in every breath. The data, i.e., input-output pairs, could be either measured data that is labeled by an expert or synthetic data from a simulation environment. Measuring and labeling real patient data is a labor intensive and error-prone task. Therefore, in this chapter, data is generated using a simulation environment. Accurate labels can be assigned to this simulation data because the inspiration and expiration start times of the ventilator and patient are known in these simulations. Once the simulation environment is developed, it is fast and inexpensive to generate a large data set with accurate labels, covering a wide range of PVA types, patient types, and ventilator settings.

The *model structure* is used to obtain a function, or mapping, from the input data (measured data) to the output data (PVA type). Different model structures can be used in the proposed framework for PVA detection and classification. In this chapter, a Recurrent Neural Network (RNN) structure (Goodfellow et al., 2016) is considered, because RNNs can use their internal state to process input sequences of variable length. This makes them particularly suitable for time-series classification problems. Furthermore, the RNN model structure has proven to successfully classify PVA, see Zhang et al. (2020), and has proven useful in many other medical time-series classification problems, such as Drumond et al. (2018) and Andersen et al. (2019).

The *fit criterion* is used to obtain the optimal model structure and parameters, i.e., weights and biases, such that the model optimally describes the relation between the input and output data. A suitable choice for the fit criterion is the cross-entropy loss function, as defined in Bishop (1995). According to Simard et al. (2003), this loss function results in faster training and improved generalization compared to the other fit criteria in classification problems. Of course, alternative criteria directly fit in the framework, which can easily be adapted to this end. Minimizing the loss function of choice with respect to the model structure parameters is referred to as the training process.

9.3 Patient-ventilator asynchrony definition

In this section, a new objective characterization of many relevant patient-ventilator asynchrony types is defined, which is the first sub-contribution of this chapter. First, in Section 9.3.1, Pressure Controlled Ventilation (PSV) is explained in more detail. Thereafter, in Section 9.3.2, patient-ventilator asynchrony is explained and defined. Note that the proposed PVA definition is not for PSV specifically, it can be applied to all modes of mechanical ventilation.

9.3.1 Pressure support ventilation

A schematic example of PSV pressure and flow curves is depicted in Fig. 9.2. The figure shows that the patient starts an inspiration at the black asterisk. During its inspiration, the patient is generating a negative pressure in its lungs, resulting in a small positive

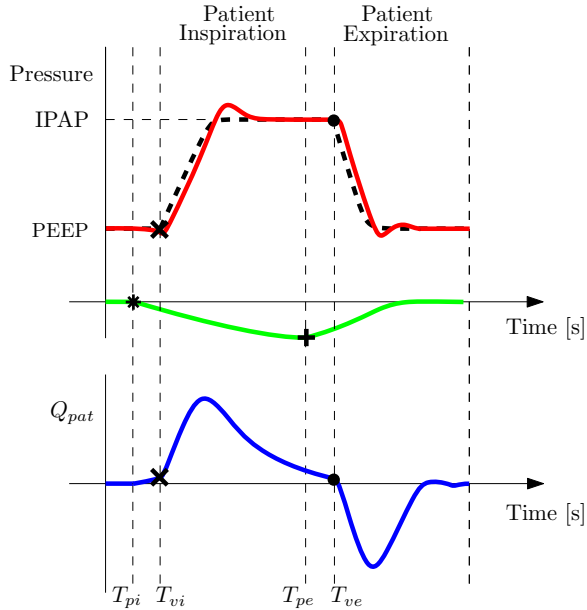


Fig. 9.2. A schematic PSV breathing cycle with a spontaneously breathing patient, showing the patient's spontaneous breathing effort p_{pat} (—), the target pressure p_{target} (---), the patient flow Q_{pat} (—), and airway pressure p_{aw} (—). Furthermore, the ventilator inspiration trigger (×), the ventilator expiration trigger (•), the patient's inspiration start (*), and the patient's expiration start (+), and their respective timings (T_{vi} , T_{ve} , T_{pi} , and T_{pe}) are depicted.

patient flow. When this patient flow exceeds a predefined trigger level indicated by the black cross, the ventilator increases the airway pressure, i.e., the pressure near the patient's airway, to the Inspiratory Positive Airway Pressure (IPAP) level. Then, after some time the patient starts its expiration, indicated by the black plus sign. During its expiration, the patient is increasing the lung pressure again. Then, when the patient flow is under a certain preset percentage of its peak flow, indicated by the black dot, the ventilator expiration starts. The airway pressure is lowered to the Positive End-Expiratory Pressure (PEEP) level to allow the expiration. After such breathing sequence is completed the ventilator waits until it detects the next patient inspiration. A mismatch in these timings results in PVA which is explained and defined in the next section.

9.3.2 Patient-ventilator asynchrony

PVA can be divided into two main categories, namely *timing asynchronies* and *severe asynchronies*. The timing asynchronies are related to a pair of a patient and ventilator breath that have a mismatch in timing. The severe asynchronies are related to patient

breaths that are not clearly linked to a single ventilator stroke or vice versa. In the remainder of this section, the different asynchrony types are described physically and defined mathematically. For the mathematical PVA definitions, the patient's inspiration $T_{pi}(j)$ and expiration $T_{pe}(j)$ timing and the ventilators inspiration $T_{vi}(k)$ and expiration timing $T_{ve}(k)$ are used, which are visualized in Fig. 9.2. The variable for the patient breath counter is denoted by $j \in [1, 2, \dots, n]$, with n the number of patient breaths, and the ventilator stroke counter is denoted by $k \in [1, 2, \dots, m]$, with m the number of ventilator strokes.

It should be noted that these timings cannot be defined random; they obey two important physical assumptions. The first assumption is that both the patient and the ventilator are always switching between an inspiration and expiration. For example, it is not allowed to have two patient inspirations without a patient expiration in between. The second assumption is that the timings are ordered in chronological order. This means that the patient and ventilator timings obey the following inequalities:

$$T_{pi}(j) < T_{pe}(j) < T_{pi}(j + 1), \forall j \in [1, 2, \dots, n] \quad (9.1)$$

and

$$T_{vi}(k) < T_{ve}(k) < T_{vi}(k + 1), \forall k \in [1, 2, \dots, m]. \quad (9.2)$$

In the remainder of this section the timing asynchronies and the severe asynchronies are described separately.

9.3.2.1 Timing asynchronies

Timing asynchronies are defined for breaths consisting of a single spontaneous breath by the patient and a single ventilator stroke that are related to each other, as depicted in Fig. 9.2. To validate that a patient breath j and a ventilator stroke k are related and should be analyzed for a timing asynchrony, the following inequalities should be satisfied for a pair (j, k) :

$$T_{pe}(j - 1) < T_{vi}(k) < T_{pe}(j) \quad (9.3)$$

and

$$T_{ve}(k - 1) < T_{pi}(j) < T_{ve}(k).$$

If these inequalities hold for a pair (j, k) , then the pair (j, k) is associated to either a synchronized breath or a timing asynchrony. The first inequality in (9.3) ensures that the start of a ventilator stroke k happens between the start of the patient's expiration $j - 1$ and j . The second inequality in (9.3) ensures that the patient inspiration j has to start after ventilator expiration $k - 1$ and before ventilator expiration k .

A pair of (j, k) that satisfies (9.3) can either be a synchronized breath or it can contain a so-called inspiration asynchrony, a cycling asynchrony, or both asynchronies. The different inspiration and cycling asynchronies are visualized in Fig. 9.3. The inspiration and cycling asynchronies are defined using the inspiration delay $\Delta t_{insp} := T_{vi}(k) - T_{pi}(j)$ and expiration delay $\Delta t_{exp} := T_{ve}(k) - T_{pe}(j)$, respectively. Using

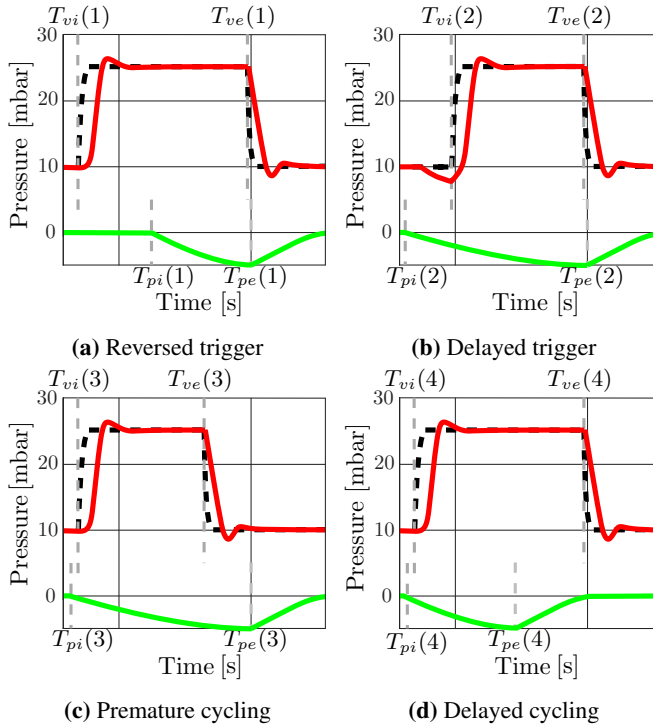


Fig. 9.3. Visualizations of the different timing asynchronies during PSV. The figure shows the spontaneous breathing effort p_{pat} (—), the target pressure p_{target} (---), and the airway pressure p_{aw} (—).

the inspiration and expiration delay, the following (a)synchronies are defined for a pair (j, k) that satisfy (9.3) (the timing asynchrony definitions, including the specific values, are based on Bakkes et al. (2020)):

- Synchronized Inspiration (SI): $0 \leq \Delta t_{insp} \leq 0.3$ s, the ventilator's inspiration (\times) starts not before and within 0.3 seconds after the patient's inspiration (\star), i.e., the ventilator's inspiration is synchronized with the patient's inspiration;
- Reversed Trigger (RT): $\Delta t_{insp} < 0.0$ s, the ventilator's inspiration (\times) starts before the patient's inspiration (\star), i.e., the ventilator is triggered before the start of the patient's inspiration;
- Delayed Trigger (DT): $\Delta t_{insp} > 0.3$ s, the ventilator's inspiration (\times) starts more than 0.3 seconds after the patient's inspiration (\star) start, i.e., the ventilator is triggered too late;

- Synchronized Cycling (SC): $-0.2 \leq \Delta t_{exp} \leq 0.2$ s, the ventilator's expiration (●) starts within 0.2 seconds before or after the patient's expiration (✕), i.e., the ventilator's expiration is synchronized with the patient's expiration;
- Premature Cycling (PC): $\Delta t_{exp} < -0.2$ s, the ventilator's expiration (●) starts more than 0.2 seconds before the patient's expiration (✕), i.e., the ventilator cycles off prematurely;
- Delayed Cycling (DC): $\Delta t_{exp} > 0.2$ s, the ventilator's expiration (●) starts more than 0.2 seconds after the patient's expiration (✕), i.e., the ventilator cycles off too late.

If a pair (j, k) satisfies the inequalities in (9.3), its PVA type is defined by a single Δt_{insp} and Δt_{exp} . Hence, every pair (j, k) that satisfies (9.3) can be classified as one of these timing (a)synchronies.

9.3.2.2 Severe asynchronies

In case a single patient breath is not clearly related to a single ventilator stroke or vice versa, a severe asynchrony is occurring. Three different types of severe asynchrony are considered: auto triggers, double triggers, and ineffective efforts. These asynchronies are visualized in Fig. 9.4. The auto trigger shows a ventilator stroke in absence of a patient breath. The double trigger consists of two ventilator strokes in the presence of only one patient breath. An ineffective effort is defined as a patient breath without a ventilator stroke.

Based on inspiration and expiration start times of the patient and ventilator, these severe asynchronies can be defined mathematically as well

- Auto Trigger (AT): If there exists a combination of k and j such that

$$\begin{aligned} T_{pe}(j-1) < T_{vi}(k) < T_{pe}(j) \\ \text{and} \\ T_{ve}(k) \leq T_{pi}(j) \end{aligned} \tag{9.4}$$

hold, then the ventilator stroke k is an auto trigger. The combination of these conditions ensures that there are no patient breaths during ventilator stroke k . In Fig. 9.4 with $j = 1$ and $k = 1$ the inequalities are satisfied and $k = 1$ is identified as an auto trigger.

- Double Trigger (DbT): If there exists a combination of k and j such that

$$\begin{aligned} T_{pe}(j-1) < T_{vi}(k) < T_{pe}(j) \\ \text{and} \\ T_{ve}(k-1) \geq T_{pi}(j) \end{aligned} \tag{9.5}$$

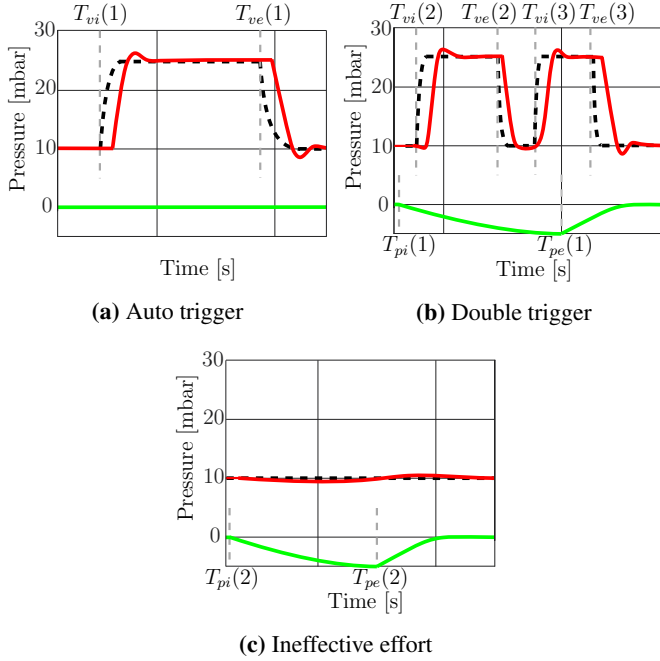


Fig. 9.4. Simulation results to visualize the different types of severe asynchronies during PSV. The figure shows the spontaneous breathing effort p_{pat} (—), the target pressure p_{target} (- - -), and the airway pressure p_{aw} (—).

hold, then the ventilator stroke k is a double trigger during the j -th patient breath. The combination of these conditions ensures that the start of ventilator stroke k is the second ventilator stroke during patient breath j . In Fig. 9.4 with $j = 1$ and $k = 3$ the inequalities are satisfied and $k = 3$ is identified as a double trigger during patient breath $j = 1$.

- Ineffective Effort (IE): If there exists a combination of k and j such that

$$\begin{aligned}
 T_{vi}(k) &\geq T_{pe}(j) \\
 &\text{and} \\
 T_{ve}(k-1) &< T_{pi}(j) < T_{ve}(k)
 \end{aligned}
 \tag{9.6}$$

hold, then the patient breath j is an ineffective effort. The combination of these conditions ensures that no ventilator stroke occurs during patient breath j . In Fig. 9.4 with $j = 2$ and $k = 4$ the inequalities are satisfied and $j = 2$ is identified to be an ineffective effort.

The defined combinations of the timing asynchronies and the severe asynchronies, describe the clinically relevant asynchrony types mathematically.

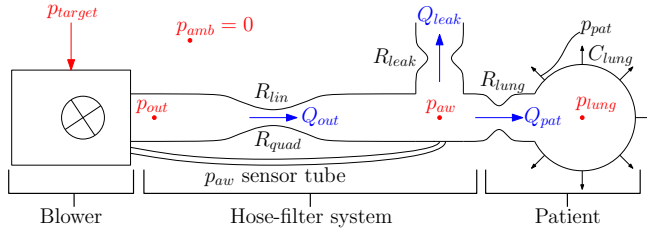


Fig. 9.5. Schematic overview of the considered single-hose ventilation system. Consisting of the blower, the hose-filter system, and the patient.

9.4 Synthetic PVA data generation

In this section, the simulation environment to generate a synthetic labeled dataset is described, which is the second sub-contribution of this chapter. Such a synthetically generated dataset allows to embed crucial domain-knowledge (on the dynamics of the ventilator, a wide range of patient characteristics, etc.) in the otherwise data-based asynchrony detection method proposed in Section 9.2. First, an overview of the full ventilation system is presented in Section 9.4.1. Thereafter, the mathematical model of the simulation environment is explained in Section 9.4.2. Then, the ground-truth labeling process is presented in Section 9.4.3. Finally, in Section 9.4.4, the generated datasets for training, validation, and testing of the algorithm are elaborated.

9.4.1 Ventilation system overview

A schematic overview of the ventilation system, consisting of the patient, hose, and the blower, with the relevant system parameters and signals is depicted in Fig. 9.5. The blower compresses ambient air to generate the desired pressure and flow profiles to ventilate the patient. The hose connects the blower to the patient; this hose is modeled by a quadratic hose-resistance with parameters R_{lin} and R_{quad} . The hose has an intended leak, modeled with leak resistance R_{leak} , to flush exhaled CO_2 rich air from the system. Finally, the patient model is modeled with a single-compartment lung model (Bates, 2009), consisting of a lung compliance C_{lung} and airway resistance R_{lung} . The full system has two inputs. The first is the time-varying profile for the target pressure p_{target} , which is the desired airway pressure. This target pressure depends on the ventilator settings and the ventilator strokes which are triggered by the patient's spontaneous breathing effort. This patient effort p_{pat} is the second input of the system. Next, a dynamic model of the full ventilation system is presented.

9.4.2 Dynamical ventilation model

The simulation environment is built upon a controlled dynamical model of the ventilation system in Reinders et al. (2021a). The dynamics of the ventilation system are

modeled by combining a blower model, a hose model, a leak model, and a patient model as depicted in Fig. 9.5. Furthermore, a simplification of the hose-compensation control strategy from Reinders et al. (2021a) is implemented to obtain the desired closed-loop behavior.

The blower model describes the relation between the controller output $p_{control}$ and the blower outlet pressure p_{out} . Then, the patient model, hose model, and leak model are combined to a single patient-hose-leak model. This patient-hose-leak model describes the relation between two inputs, i.e., the blower outlet pressure p_{out} and the patient effort p_{pat} , and a state of the system, i.e., the lung pressure p_{lung} . The hose-compensation control strategy uses the outlet flow Q_{out} and the target pressure p_{target} to compute the desired controller output $p_{control}$. These models are combined by using the output of one model as the input of the next model. More specifically, the output of the blower model is the input for the patient-hose-leak model, the output of the patient-hose-leak model is the input for the control strategy, and the output of the control strategy is the input of the blower model.

The full dynamic ventilation model has two distinct inputs, namely, the patient's breathing effort p_{pat} and the target pressure p_{target} . The patient effort is modeled using the flipped halfwave from Reinders et al. (2021d). This effort model gives a realistic representation of human breathing and it is easily varied in inspiration time, expiration time, breath depth, and breathing frequency. The target pressure is generated by the triggering algorithm which is explained in Section 9.3.1. Next, the distinct components, i.e., the blower model, the patient-hose-leak model, and the control strategy, of the full model are presented.

The blower model is a fourth-order state-space model which is obtained by fitting the measured frequency response function of an actual blower. This blower model describes the relation between the control output $p_{control}$ and the blower outlet pressure p_{out} . The blower model, with blower state x_b , is described by the following state-space model:

$$\begin{aligned} \dot{x}_b &= A_b x_b + B_b p_{control} \\ p_{out} &= C_b x_b, \end{aligned} \quad (9.7)$$

with

$$\begin{aligned} A_b &= - \begin{bmatrix} 3.2 \cdot 10^2 & 3.7 \cdot 10^4 & 2.5 \cdot 10^5 & 2.3 \cdot 10^5 \\ -1 & 0 & 0 & 0 \\ 0 & -1 & 0 & 0 \\ 0 & 0 & -1 & 0 \end{bmatrix}, \\ B_b &= [1 \ 0 \ 0 \ 0]^T, \text{ and} \\ C_b &= [0 \ 2.1 \cdot 10^4 \ 2.1 \cdot 10^5 \ 1.9 \cdot 10^5]. \end{aligned} \quad (9.8)$$

The patient-hose-leak model is described by the differential equation in (9.9). This differential equations describes the relation between the inputs: the blower outlet pressure p_{out} and the patient effort p_{pat} , and the state: the lung pressure p_{lung} . These are used to compute the outputs: the patient airway pressure p_{aw} , the patient flow Q_{pat} , the patient volume V_{pat} , and the outlet flow Q_{out} .

$$\dot{p}_{lung} = -\frac{1}{C_{lung}(R_{lung} + R_{leak})}p_{lung} + \dot{p}_{pat} + \frac{1}{C_{lung}(R_{lung} + R_{leak})} \times \frac{2R_{leak} \left(p_{out} - \frac{R_{leak}}{(R_{leak} + R_{lung})}p_{lung} \right)}{\left(R_{lin} + \frac{R_{leak}R_{lung}}{R_{leak} + R_{lung}} + \sqrt{\left(\frac{R_{leak}R_{lung}}{R_{leak} + R_{lung}} + R_{lin} \right)^2 + 4R_{quad} \left| \frac{R_{leak}}{R_{lung}R_{leak}}p_{lung} - p_{out} \right|} \right)} \quad (9.9)$$

The patient airway pressure is computed with

$$p_{aw} = Cp_{lung} + D \text{sign}(\zeta) \frac{-\xi + \sqrt{\xi^2 + 4R_{quad}|\zeta|}}{2R_{quad}} \quad (9.10)$$

with $\xi = D + R_{lin}$, $\zeta = p_{out} - Cp_{lung}$, $C = \frac{R_{leak}}{R_{leak} + R_{lung}}$, and $D = \frac{R_{leak}R_{lung}}{R_{leak} + R_{lung}}$. Using this, the patient flow, patient volume, and outlet flow are computed as:

$$\begin{aligned} Q_{pat}(t) &= \frac{p_{aw} - p_{lung}}{R_{lung}}, \\ V_{pat}(t) &= \int_0^t Q_{pat}(\tau) d\tau, \\ Q_{out}(t) &= \text{sign}(\Delta p) \frac{-R_{lin} + \sqrt{R_{lin}^2 + 4R_{quad}|\Delta p|}}{2R_{quad}} \end{aligned} \quad (9.11)$$

with $\Delta p = p_{out} - p_{aw}$.

The nonlinear hose-compensation control strategy from Reinders et al. (2021a) contains a unity feedforward of p_{target} in combination with a pressure drop compensation using the measured outlet flow Q_{out} , a nonlinear hose model, and estimated parameters of the hose model, i.e., \hat{R}_{lin} and \hat{R}_{quad} . This gives the following control strategy:

$$p_{control} := p_{target} + \hat{R}_{lin}Q_{out} + \hat{R}_{quad}Q_{out}|Q_{out}|. \quad (9.12)$$

Combining the presented models and the control strategy gives the full closed-loop ventilation model. This model can be used to generate the desired inputs to the algorithm, i.e., p_{aw} , Q_{pat} , and V_{pat} .

9.4.3 Ground-truth labeling

To generate time-series labels of the different asynchrony types, three subsequent steps are defined. First, the inspiration and expiration start times of both the patient and ventilator are extracted from the simulation data. Second, the logics-based rules as

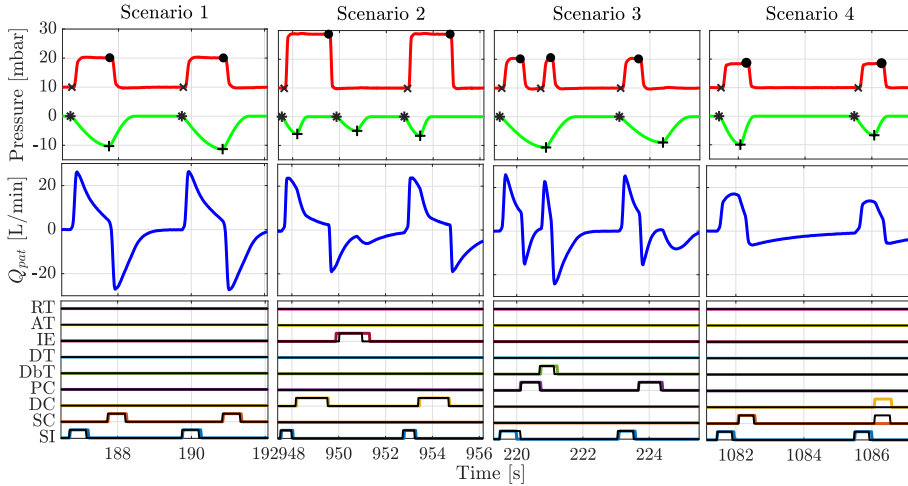


Fig. 9.6. An example of four different scenarios of a ventilation use case, where the airway pressure (—), patient effort (—), patient flow (—), the ground-truth labels $y(t)$ (the colored lines in the bottom plots), and the output of the developed algorithm $\hat{y}(t)$ (—) are shown. The different scenarios show different (a)synchronous breaths, as indicated by the ground-truth labels. The figure shows that the algorithm detects and classifies every breath phase correctly, except for the last expiration in the fourth scenario.

defined in Section 9.3 are applied to determine the PVA type. Third, the asynchrony labels per breath are converted to time-series with these same labels.

Some examples of labeled asynchrony data are shown in Fig. 9.6. This figure shows the airway pressure p_{aw} , patient effort p_{pat} , patient flow Q_{pat} , the corresponding ground-truth PVA labels $y(t)$, and the predicted labels $\hat{y}(t)$, which are predicted by the algorithm developed in the Section 9.5. If a certain PVA type is present in the data, the corresponding time-series is 1, otherwise it is 0. Note that the ‘zero label’ is not displayed in this figure; if all the displayed labels are zero, the zero label is 1.

The first scenario in Fig. 9.6 shows normal inspirations and expirations. In the second scenario, it shows normal inspirations, delayed cycling, and an ineffective effort. In the third scenario it shows normal inspirations, premature cycling, and double triggering. Finally, in the fourth scenario, a synchronous breath and delayed cycle are shown.

9.4.4 Dataset generation

To train and evaluate the performance of the trained algorithm, a dataset is generated. This is done with the presented simulation environment and labeling process. The

dataset is generated by running simulations with a varying and clinically relevant set of parameters. The parameters and their value or set from which they are generated are summarized as:

- ventilator settings;
 - PEEP $\in [5, 10]$ mbar;
 - IPAP $\in [7.5, 25]$ mbar;
 - Inspiration trigger $\in [0.1, 16]$ L/min;
 - Expiration trigger $\in [0.5, 70]$ % of the peak flow;
- hose and hose-compensation controller parameters;
 - $R_{lin} = 4.97 \times 10^{-3}$ mbar s/mL;
 - $R_{quad} = 9.71 \times 10^{-7}$ mbar s²/mL²;
 - $R_{leak} = 48 \times 10^{-3}$ mbar s/mL;
 - $\hat{R}_{lin} \sim \mathcal{N}(R_{lin}, 0.02R_{lin})$ mbar s/mL, with $\mathcal{N}(\mu, \sigma)$ a normal distribution with mean μ and standard deviation σ ;
 - $\hat{R}_{quad} \sim \mathcal{N}(R_{quad}, 0.02R_{quad})$ mbar s²/mL²;
- patient parameters.
 - $R_{lung} \in [5, 50]$ mbar s/L;
 - $C_{lung} \in [10, 60]$ mL/mbar;
 - p_{pat} , with breath depth $\alpha \in [2.5, 22.5]$ mbar and duration $t \in [1.2, 6]$ s.

Using these different settings, a total of 966 different ventilation use-cases is generated, where each use case contains a breathing sequence of 30 seconds with data generated at a sampling frequency of 50 Hz. Note that the parameters that are not in a normal distribution are not completely randomly sampled from the different sets. Particular combinations of the settings are used to retrieve realistic ventilation scenario's, e.g., IPAP is always larger than PEEP. Furthermore, the use-cases are defined such that all the PVA types are present in the dataset. Eventually, the entire dataset is divided into a training set of 594 use cases, a validation set of 148 use cases, and a test set of 224 use cases. The training set is used to train the model. The validation set is used to provide an unbiased evaluation of the model fit during the training process. Finally, the test set is used to provide an unbiased evaluation of the performance of the final model.

9.5 Detection and classification model

In this section, the presented framework is used to develop an algorithm to detect and classify PVA from ventilation data. First, the overall model structure is defined in Section 9.5.1. Then, the loss function is explained in Section 9.5.2. Thereafter, the final structure and parameters of the detection and classification model are defined and optimized in Section 9.5.3.

9.5.1 Overall model structure

The overall model structure is defined by the inputs, outputs, and the model structure itself, which is schematically visualized in Fig. 9.7.

9.5.1.1 Inputs

The input $x(t)$ of the classification network is a multivariate time-series sampled at 50 Hz, which includes the airway pressure, patient flow, and the volume in the patient's lungs, i.e., $x(t) = [p_{aw}(t), Q_{pat}(t), V_{pat}(t)]^T$. The choice for using the airway pressure, patient flow, and the volume is based on practical implications, as these signals are readily available on almost all mechanical ventilators.

9.5.1.2 Outputs

The output of the network $\hat{y}(t)$ should represent the ground-truth labels $y(t)$, as presented in Section 9.4.3, as close as possible. The output is also a multivariate time-series that contains ten separate time-series, one for each PVA type and one for the zero-label, i.e., $\hat{y}(t) = [\hat{y}^1(t), \dots, \hat{y}^{n_c}(t)]^T$ with n_c the number of classes in the vector. If a particular PVA type occurs, the value of that class in the ground-truth time-series is one, otherwise the value of the time-series equals zero, as shown in Fig. 9.6.

9.5.1.3 Model structure

To obtain a mapping from the inputs to the desired outputs, a Recurrent Neural Network (RNN) is considered. For the specific example in this chapter an RNN with Long Short-Term Memory (LSTM) cells is used. Note that other network structures can be used as well in the proposed framework. However, RNN structures with LSTM cells are effective sequence models used in practical applications (Goodfellow et al., 2016). This model structure allows a mapping that can handle varying sequence lengths and updates every sample. Therefore, asynchronies can be detected and classified in near real-time by feeding new data to the network as it is measured. Standard RNNs have problems with exploding/vanishing gradients when classifying long time-series (Pascanu et al., 2013). The problem of exploding/vanishing gradients is tackled by using LSTM cells in the RNN. These cells contain multiplicative gates that are capable of extracting and storing information over longer periods of time (Graves et al., 2009).

The overall model structure is schematically depicted in Fig. 9.7. The model consists of an LSTM layer with l cells, a linear layer, and a softmax layer. The LSTM layer maps the inputs into l different LSTM outputs q . Those LSTM outputs q are combined by a fully connected linear layer into n_c different outputs, where n_c denotes the number of output classes of the algorithm. These outputs are re-scaled between zero and one with the softmax function. The output of the softmax layer $\hat{y}_{p,l}(t, \theta)$ is a vector with n_c values between 0 and 1, which gives an indication of the probability that a particular

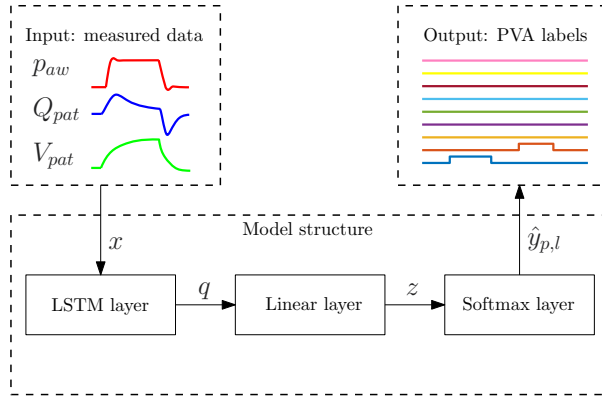


Fig. 9.7. Definition of the model structure that is used for patient-ventilator asynchrony detection. Showing the inputs, the overall model structure, and the desired output.

class is occurring at time step t . θ represents the model parameters, e.g., weights and biases. To determine which PVA type is predicted by the model, $\hat{y}_{p,l}(t, \theta)$ is transformed to a one-hot output vector as follows:

$$\hat{y}^c(t) := \begin{cases} 1 & \text{if } \hat{y}_{p,l}^c(t) \geq \hat{y}_{p,l}^m(t) \forall m \in \{1, \dots, n_c\} \\ 0 & \text{otherwise} \end{cases}, \quad (9.13)$$

where c denotes the class number in the vector. In words, $\hat{y}(t)$ is a vector with a one at the index where $\hat{y}_{p,l}$ is the highest, i.e., the PVA type that the algorithm expects to be present and zero everywhere else.

9.5.2 Loss function and optimization algorithm

The optimal values of the weights and biases θ are determined to obtain the optimal mapping from the inputs x to the ground-truth labels with the proposed model structure. This is achieved by minimizing a loss function. The loss function, or fit criterion, considered in this chapter is the cross-entropy loss function. Other loss functions can be used as well in the proposed framework. However, the cross-entropy loss function leads to faster training and improved generalization compared to the sum-of-squares in classification problems (Simard et al., 2003). The cross-entropy loss function is defined as

$$L_{CE}(\theta) = - \sum_{i=1}^N \sum_{t=1}^n y^i(t)^\top \cdot \log(\hat{y}_{p,l}^i(t, \theta)), \quad (9.14)$$

where N is the number of ventilation use cases, n the sequence length of the ventilation use case i in samples, $y^i(t) \in \mathbb{R}^{n_c \times 1}$ the ground truth one-hot label vector of case i at time t , and $\hat{y}_{p,l}^i(t, \theta) \in \mathbb{R}^{n_c \times 1}$ the predicted label vector of case i at time sample t .

To obtain the weights and biases θ that minimize this loss function, different optimization algorithms can be used. In this example, particularly good results have been obtained with the Adam solver (Kingma and Ba, 2015). Adam is a gradient descent optimization algorithm that is widely used in the field of deep learning (Soydaner, 2020).

9.5.3 Optimization of the model structure

Next, the detection and classification algorithm is optimized using the generated dataset, the model structure, the loss function, and the proposed optimization algorithm. First, a generic procedure is proposed on how to obtain the optimal model structure and parameters. Thereafter, this procedure is applied to the PVA detection and classification algorithm. Finally, an analysis is done to determine how this model can be further improved in the future.

To obtain the optimal model order and parameters, an optimizer is used to minimize a loss function for varying model orders. This gives models of different orders with optimal parameters. Using the training and validation accuracy it is determined which order of these model is optimal. The model order should be high enough to achieve a good detection and classification accuracy. However, it should not be too high, because this can cause overfitting of the training data. Furthermore, an excessively high order model requires more memory and computation power in the final implementation. To determine the optimal model order, the following steps are followed (note that in all steps a k-fold cross-validation is used):

- minimize the loss function for varying model complexities;
- compute the training and validation accuracy, i.e., the percentage of correctly classified samples, for every model;
- determine the optimal order of the model using the accuracies, i.e., trade-off between validation accuracy and complexity.

This method to find the optimal model is applied to the PVA detection and classification use-case. Throughout this example a five-fold cross validation is used in every step. First, the cost function in (9.14) is minimized for varying model complexities. In this case, the number of LSTM cells $l = [1, 3, 5, 10, 30, 50, 100]$ is varied. Second, the resulting mean of the training and validation accuracies and two times their standard deviation are computed and shown in Fig. 9.8. Third, this figure is used to determine the optimal order of the model. From Fig. 9.8, it is concluded that $l = 50$ gives the optimal model complexity. Smaller values for l give a lower performance and larger values of l cause overfitting of the training data.

Fig. 9.8 shows a significant gap between the training and validation accuracy. This is an indication that the model is not excellently equipped for detecting and classifying data that it has not seen during training. Two potential causes of this are identified, namely; the mapping between x and y cannot be captured by the particular network

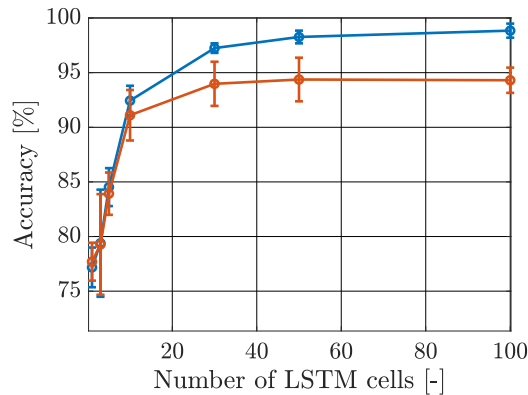


Fig. 9.8. Training (—) and validation (—) accuracy against the number of hidden units using the ground-truth labels. The figure shows that the model is overfitting the training data for 100 LSTM cells.

structure, or a lack of richness in the training data, i.e., the training set and validation set are significantly different.

To verify that this gap between the training and validation accuracy is not caused by the particular network structure choice, the following steps can be followed:

- generate new ‘ground-truth’ labels with a network that is captured by the model structure, such that it is guaranteed that the network structure does describe the mapping from x to y ;
- minimize the cost function for varying model complexities;
- compute the training and validation accuracy, i.e., the percentage of correctly classified samples, for every model;
- if the training and validation accuracy are significantly smaller than 100 % and a significant gap remains, it is likely caused by the fact that the dataset is not rich enough.

These steps are applied to the PVA detection and classification use-case. First, the ground-truth labels are replaced by the output of a trained network with $l = 50$ LSTM cells. Hence, we know that the model structure with $l = 50$ LSTM cells can map the inputs x to the outputs y perfectly. Next, the cost function is minimized for varying model complexities and the training and validation accuracy are computed. These results are visualized in Fig. 9.9. In this figure, a similar gap remains and similar accuracy levels are achieved as with the original ground-truth labels. Therefore, we can conclude that it is likely that the dataset is not rich enough, i.e., the validation set contains data that is significantly different from the training data. Therefore, for further

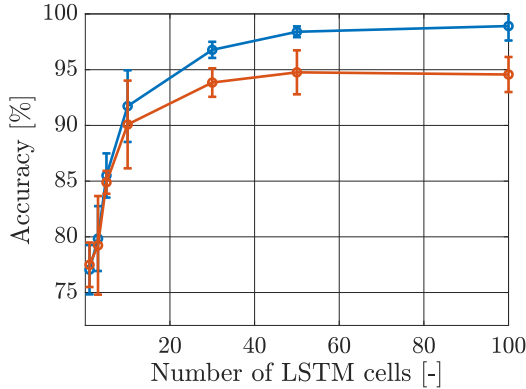


Fig. 9.9. Training (—) and validation (—) accuracy of the number of hidden units using the predicted labels of a model with 50 LSTM cells as ground-truth labels.

improvements of the algorithm it is advised to create a larger dataset, such that the training and validation data set are larger and contain more similar data.

Concluding, a model structure with $l = 50$ LSTM cells is used in the remainder of this chapter. This results in a training and validation accuracy of 98.3 % and 94.3 %, respectively. The performance of this algorithm is evaluated in Section 9.6 on a test set with simulation and experimental data.

9.6 Performance evaluation

In this section, the performance of the final algorithm is evaluated, which is the third sub-contribution of this chapter. First, the considered performance evaluation criterion is explained in Section 9.6.1. Thereafter, in Section 9.6.2, the performance on simulation data from Section 9.4 is evaluated. Then, in Section 9.6.3, an experimental ventilation dataset is generated in a lab environment. Finally, performance of the algorithm on this experimentally obtained dataset is evaluated in Section 9.6.4.

9.6.1 Performance evaluation criterion

For training of the algorithm and optimization of the model structure, a sample-based loss and accuracy measure of the algorithms output is used in Section 9.5. However, this performance measure does not translate well to clinical practice. In practice a clinician wants to know per breath, or on a sequence of breaths, which type of PVA is present. Furthermore, the time-series data contains about 75-80 % labels where no PVA is defined, i.e., the zero label in $y(t)$ is one. This results in an accuracy level of

75-80 % when only classifying zero labels, i.e., $\hat{y}(t)$ with the zero label one at every t . Therefore, a breath-by-breath performance measure is proposed to properly analyze the performance of the algorithm.

To translate the predicted sample-based labels $\hat{y}(t)$ to breath-by-breath labels and a breath-by-breath performance evaluation criterion, the one-hot output vector $\hat{y}(t)$ of the algorithm is first filtered to eliminate instances where a certain label is classified very briefly. This is achieved by counting which class is classified the most in a predefined window and defining this as the new output $\hat{y}_f(t)$. Thereafter, these filtered labels $\hat{y}_f(t)$ are connected to a breath in the breath-domain based on timing. Eventually, these predicted breath-domain labels are used to compute an accuracy, i.e., percentage of correctly classified labels, for the inspiration, cycling, and severe asynchronies. The procedure to obtain the breath-domain accuracy from the predicted time-domain labels $\hat{y}(t)$ is summarized as follows:

Procedure 9.1.

1. The one-hot output vector of the algorithm $\hat{y}(t)$ is filtered with a moving counting filter (MCF) as follows:

$$a(t) := \left(\sum_{\tau=t-w_s/2}^{t+w_s/2} \hat{y}(\tau) \right), \quad (9.15)$$

where $a(t)$ is the sum of all vectors in the specified window around sample t with w_s the window size in samples. The output vector of the filter is computed from $a(t)$ with:

$$\hat{y}_f^c(t) := \begin{cases} 1 & \text{if } a^c(t) \geq a^m(t) \forall m \in \{1, \dots, n_c\}, \\ 0 & \text{otherwise,} \end{cases}$$

where $\hat{y}_f^c(t)$ is the output of the filter at index $c \in \{1, 2, \dots, n_c\}$ and time sample t , such that $\hat{y}_f(t) = [\hat{y}_f^1(t) \dots \hat{y}_f^{n_c}(t)]^T$.

2. The labels $\hat{y}_f(t)$ at a specific time step t are connected to the closest breath. This gives new breath domain labels \hat{Y} . These labels indicate per breath phase which PVA type is detected.
3. Using these new labels, an accuracy, i.e., percentage of correctly classified labels, is computed for the inspiration asynchronies, the cycling asynchronies, and the severe asynchronies.

9.6.2 Performance on simulation data

Using the test set which is generated in Section 9.4, the classification accuracy of the proposed algorithm is analyzed. For this analysis, first some time-domain results are

analyzed and thereafter the breath-by-breath performance evaluation criterion is used. The main results are visualized in Fig. 9.6, 9.10, and 9.11.

Fig. 9.6 shows the time-domain data, the ground-truth labels $y(t)$, and the predicted labels $\hat{y}(t)$ for four scenarios. The figure clearly shows that PVA is correctly detected and classified in the first three scenarios. In the last scenario, only the delayed cycling is incorrectly classified as a normal expiration. Note that the time-domain signals, i.e., airway pressure p_{aw} and patient flow Q_{pat} , for both breaths in the fourth scenario are very similar. Therefore, it is very challenging to detect this asynchrony. Probably, a clinician would also not classify this as an asynchrony.

The classification results of the timing asynchronies are visualized in Fig. 9.10. Every marker in this figure represents a single breath. The location of the marker is defined by the true inspiration Δt_{insp} and expiration delay Δt_{exp} . The background colors of the figure represent the true PVA label, which is the combination of an inspiration and cycling asynchrony (true) label. The marker colors represent the PVA combination as classified (predicted) by the developed algorithm. This means that if a marker has the same color as its background, both the inspiration and expiration are correctly classified. Otherwise, at least one of those two is incorrectly classified. Note that there are no breaths with reverse triggering and delayed cycling, i.e., in the top left area. A patient that is susceptible to reverse triggers is typically not susceptible for delayed cycling. Therefore, this combination is unrealistic and challenging to generate.

In Fig. 9.10, it is shown that most breaths are correctly classified. Most of the incorrect classifications are close to the borders of different PVA types. This is expected because it is more challenging to classify the asynchronies close to these borders, i.e., the artifacts in the signals, induced by the asynchrony, are less prominently present.

The classification accuracy of the severe asynchronies, i.e., auto triggering (AT), double triggering (DbT), and ineffective efforts (IE), is visualized in Fig. 9.11. The figure shows the number of correctly (green) and incorrectly (black) classified severe asynchronies. Also for the severe asynchronies we can conclude that most breaths are classified correctly.

Finally, the accuracy for the different asynchrony classes are computed. The computed classification accuracies are 94.6 %, 91.9 %, and 83.2 % for the inspiration, cycling, and severe asynchronies, respectively. Which is combined to an overall detection and classification accuracy of 92.9 %. These levels of performance are a significant improvement over current clinical practice, where PVA typically remains undetected.

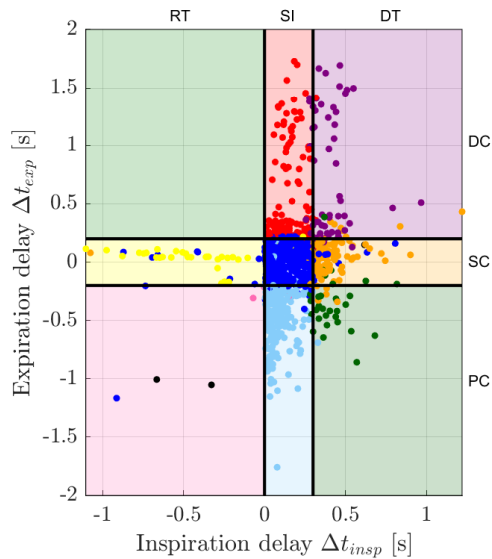


Fig. 9.10. Simulation classification results of the timing asynchronies. Every marker in this figure represents a single breath; the location of a marker is defined by the true inspiration and expiration delay. The PVA labels are indicated by the abbreviations on the top and right axis. The color of the marker indicates the PVA type as determined by the developed algorithm, i.e., if the color of a marker corresponds to its background it is correctly classified. The algorithm has classified 94.6 % of the inspirations and 91.9 % expirations correctly.

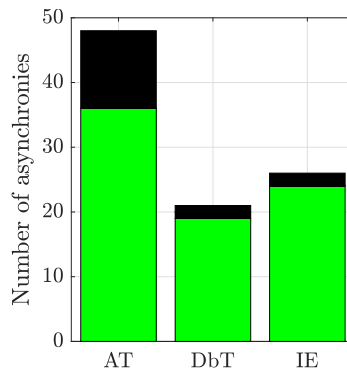


Fig. 9.11. Simulation-based classification results of the severe asynchronies, i.e., auto triggering (AT), double triggering (DbT), and ineffective efforts (IE). The green areas indicate the correctly classified breaths and the black areas indicate the breaths that are incorrectly classified.

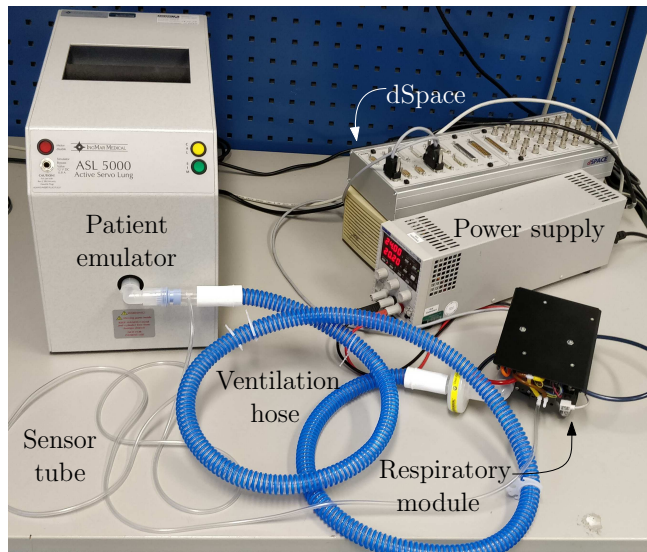


Fig. 9.12. The experimental set-up consisting of the blower driven ventilator, the ASL 5000 breathing simulator, a dSpace, and the ventilation hose.

9.6.3 Experimental setup and dataset

The experimental setup that is used to generate the experimental test set is depicted in Fig. 9.12. The figure shows a Macawi blower-driven mechanical ventilation module (DEMCON macawi respiratory systems, Best, The Netherlands). Furthermore, the ASL 5000™ Breathing Simulator (IngMar Medical, Pittsburgh, PA) is shown. This breathing simulator is used to emulate the different patient types. Furthermore, a typical hose-filter system for ventilation of a patient in a hospital setting is shown. The control and ventilation algorithms are implemented in a dSPACE system (dSPACE GmbH, Paderborn, Germany) with a sampling frequency of 500 Hz. The collected data for the PVA detection and classification algorithm is desampled to a frequency of 50 Hz to reduce the amount of data and to make it compatible with the developed algorithm. Using this setup, labeled experimental data, i.e., p_{aw} , Q_{pat} , V_{pat} , and $y(t)$, of several ventilation use-cases is generated. Fig. 9.13 shows the measured airway pressure p_{aw} and patient flow Q_{pat} for four different scenario's. The total experimental dataset contains 10 ventilation use-cases with approximately 60 seconds of data per use-case, containing 175 breaths. Note that this data set is only used as a test set, it is not used for training of the algorithm.

9.6.4 Performance on experimental data

The algorithm's performance on the experimental dataset is analyzed to evaluate whether the developed PVA detection and classification algorithm based on simulation data works on experimentally obtained data from an actual ventilator. The same analysis as for the simulation results is performed. The main results are visualized in Fig. 9.13, 9.14, and 9.15.

Fig. 9.13 shows the time-domain data, the ground-truth labels $y(t)$, and the resulting filtered predicted labels $\hat{y}(t)$ for four scenarios. It clearly shows that PVA is correctly detected and classified in the first three scenarios. In the fourth scenario it shows that the first breath is identified as a synchronous breath, however, the ground truth labels show a delayed trigger with a premature cycle. Furthermore, the expiration of the second breath is also classified incorrectly. However, the measured data shows no clear artifacts that indicate asynchrony. Therefore, a clinician would likely classify these breaths as synchronous breaths as well.

The breath-domain results are shown in Fig. 9.14 and 9.15. The results of the timing asynchronies are visualized in Fig. 9.14. Note that four of the different timing asynchrony combinations are not present in the experimental data set. However, it is still possible to obtain a good first indication of the performance of the algorithm on experimental lab data. The figure clearly shows that the majority of the breaths are correctly classified, i.e., the marker color is the same as the background color. However, performance is reduced compared to the simulation-based performance analysis. The results for the severe asynchronies, in Fig. 9.15, show that the algorithm is correctly classifying most of the auto triggers (AT) and ineffective efforts (IE). However, the algorithm has problems with classifying double triggering (DbT). Finally, the detection and classification accuracy for the different asynchrony classes are computed. The computed accuracies are 86.7 %, 64.2 %, and 72.7 % for the inspiration, cycling, and severe asynchronies, respectively. Which is combined to an overall accuracy of 75.3 %. These results show that the performance is significantly lower than for the simulation data. However, it is significantly better than clinical practice, where asynchrony typically remains undetected. Furthermore, it shows that this framework is able to detect and classify PVA. In future work, this framework can be developed further to improve performance, for example, by choosing a different model structure and using clinical data.

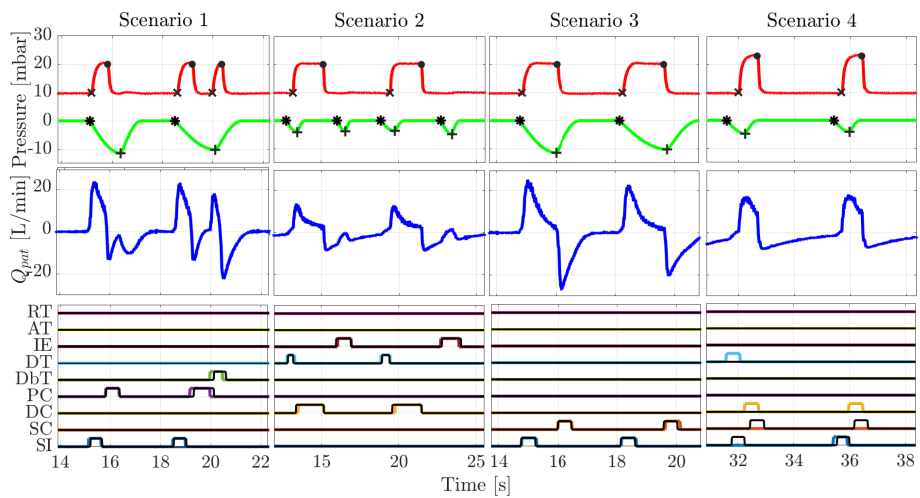


Fig. 9.13. An example of four different experimental scenarios of a ventilation use case, where the airway pressure (—), patient effort (—), patient flow (—), the ground-truth labels $y(t)$ (the colored lines in the bottom plots), and the one-hot output of the developed algorithm $\hat{y}(t)$ (—) are shown. It is shown that in the first three scenarios every breath phase is detected and classified correctly. In the last scenario the first breath and the second expiration are classified incorrectly.

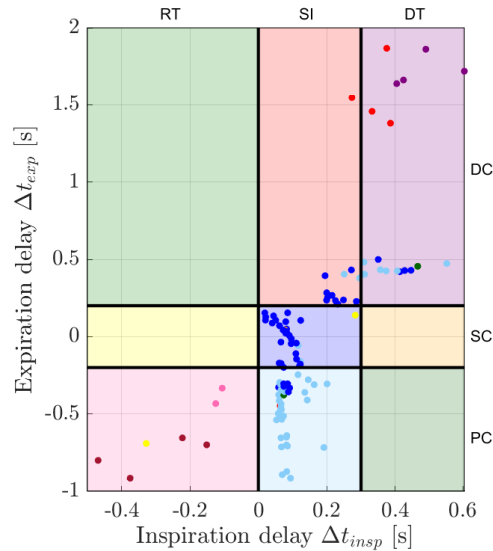


Fig. 9.14. Experimental classification results of the timing asynchronies. Every marker in this figure represents a single breath, the location of a marker is defined by the true inspiration and expiration delay. The PVA labels are indicated by the abbreviations on the top and right axis. The color of the marker indicates the PVA type as determined by the developed algorithm, i.e., if the color of a marker corresponds to its background it is correctly classified. The algorithm has classified 86.7 % of the inspirations and 64.2% expirations correctly.

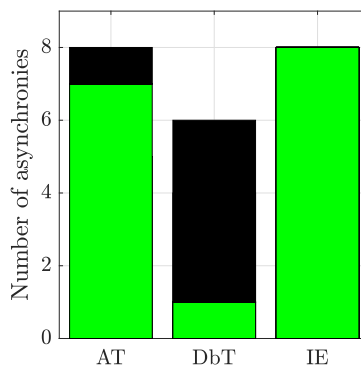


Fig. 9.15. Experimental classification results of the severe asynchronies, i.e., auto triggering (AT), double triggering (DbT), and ineffective efforts (IE). The green areas indicate the correctly classified breaths and the black areas indicate the breaths that are incorrectly classified.

9.7 Conclusions and recommendations

The developed Patient-Ventilator Asynchrony (PVA) detection and classification framework enables real-time detection and classification of the relevant types of asynchrony between a patient and the mechanical ventilator using measured data that is currently available on commercial ventilators. This information about PVA can be used by the clinician to prevent/mitigate PVA and therewith reduce ventilation times.

In simulations, it is shown that the developed algorithm can detect and classify inspiration, expiration, and severe asynchronies with an accuracy of 94.6%, 91.9%, and 83.2%, respectively. In experiments, the same algorithm detects and classifies inspiration, expiration, and severe asynchronies with an accuracy of 86.7%, 64.2%, and 72.7%, respectively. This shows that the algorithm can successfully detect and classify asynchronies. Therewith, the current clinical practice can be improved significantly, where asynchronies typically remain undetected.

It is shown that the algorithm can successfully detect and classify asynchronies. However, several recommendations for future improvements are considered. First, more knowledge should be used in the current PVA definition, e.g., if the patient's spontaneous breathing effort is small it is more important to achieve the desired tidal volume than to prevent asynchrony. Second, the algorithm should be further improved by using a larger and richer dataset, such that the validation and test accuracy get closer to the training accuracy. Third, the classification algorithm should be evaluated on actual patient data. Fourth, performance in practice could be improved by expanding the current algorithm with actual patient data. Transfer learning of the current algorithm can potentially reduce the need for data significantly. Fifth, the algorithm should be implemented in an actual ventilation system, such that it can be used in practice. Finally, we foresee a future system that automatically adapts the ventilator settings to prevent PVA on the basis of the PVA detection results obtained by the proposed algorithm.

Conclusions and recommendations

10.1 Conclusions

The results presented in this thesis are a significant step towards autonomous mechanical ventilation, which, in turn, is envisaged to be a big step towards better treatment and a better scalable Intensive Care Unit (ICU) capacity. Therewith, the algorithms developed in this thesis are addressing the overall Research Challenge formulated in Section 1.4. To tackle the overall Research Challenge, two distinct research goals were formulated in the introduction of this thesis, see Section 1.5. In view of these two research goals the following two main achievements have been obtained.

First, in view of Research Goal I, two distinct learning control approaches have been developed, in Chapters 2 - 7. These control strategies utilize measured data to automatically adapt the control signal to achieve the optimal pressure tracking performance for mechanical ventilators. Thorough analysis, simulations, and experiments with these strategies have shown that they significantly outperform commonly used control strategies for ventilation in terms of pressure tracking performance. Therewith, Research Goal I has been successfully fulfilled.

Second, in view of Research Goal II, two monitoring algorithms have been developed, in Chapters 8 and 9. These algorithms enable a clinician to make a better informed choice for the optimal treatment and/or ventilator settings. These monitoring algorithms use measured data to estimate the patient's spontaneous breathing effort and to detect and classify Patient-Ventilator Asynchrony (PVA). Therewith, Research Goal II has been successfully fulfilled as well.

In the remainder of this concluding section, the main contributions in view of both research goals are further detailed below.

10.1.1 Control systems for ventilation

The motivation for improving the control systems for ventilation is to improve the pressure tracking performance of the mechanical ventilators. This ensures that the pressure profile that is set by the clinician, or is set autonomously in future ventilators, is tracked as accurately as possible. Accurate pressure tracking avoids overshoot and oscillations in both pressure and flow. Avoiding these overshoots and oscillations prevents potentially harmful pressure peaks and improves the patient's comfort during ventilation. Therewith, the patient's treatment can be improved through improved pressure control.

The specific contributions of this thesis in the direction of control systems for ventilation, i.e., Research Goal I, are summed up in terms of the adaptive hose-compensation control strategy in Chapters 2 and 3, and the repetitive control strategies for mechanical ventilation in Chapters 4 - 7.

- *Adaptive hose-compensation control* is a control strategy that estimates the parameters of a hose model during ventilation and uses this model in the control loop to compensate the pressure drop over the hose. In Chapter 2, this method is presented, analyzed, and implemented using a linear hose model. Thereafter, in Chapter 3, a different adaptive hose-compensation control method is developed and implemented. This method uses a nonlinear hose model, which describes the true hose characteristics more accurately. In experiments and simulations it is shown that adaptive hose-compensation control for ventilation can significantly improve pressure tracking performance of mechanical ventilators.

Concluding, the developed adaptive hose-compensation controller is an effective and intuitive control strategy for ventilation that is robust for many system variations, e.g., patients, leaks, and hoses, which has shown to significantly improve the pressure tracking performance.

- *Repetitive control* strategies have been developed to achieve near perfect pressure tracking performance for ventilated patients. Repetitive control is a control strategy suitable for systems that perform repetitive tasks. The repetitive controller utilizes data from previous tasks to learn the optimal input for the next task. This enables repetitive control to achieve tracking errors close to the system's measurement noise levels. In Chapter 4, a design approach for discrete-time repetitive control for ventilation of fully sedated patients in pressure-controlled Continuous Mandatory Ventilation (CMV) is presented. In experiments, it is shown that one single repetitive controller can achieve near zero tracking errors for a variety of patients, from babies to adults. Then, in Chapters 5 and 6, the stability properties of repetitive control for ventilation have been revisited. In Chapter 5, stability of the closed-loop system with discrete-time repetitive control is guaranteed by using feedback linearization to linearize the plant with nonlinear hose characteristics. Thereafter, in Chapter 6, a continuous-time repetitive control strategy based on a finite number of oscillators at the harmonics of the breathing frequency is proposed. Then, using the (incremental version of the) circle criterion,

stability of the closed-loop nonlinear system is guaranteed for nonlinear hose-characteristics. Finally, in Chapter 7, a novel (discrete-time) triggered repetitive control framework is developed that allows the timing inbetween repetitive tasks to be unknown and varying. Using this triggered repetitive control framework, the learning property of standard repetitive control can be used in triggered modes of ventilation for spontaneously breathing patients, or in other application fields with similar control problems. In experiments, this framework has been applied in scenarios with Pressure Controlled - Assist Control Ventilation (PC-ACV), and it has shown that the tracking performance could be improved by almost a factor five compared to a state-of-the-art control strategy for ventilation.

Concluding, repetitive control achieves superior tracking performance in case of sedated patients, with significant robustness for plant variations. Furthermore, the newly developed triggered repetitive control framework has shown that a significant improvement in tracking performance can be achieved for spontaneously breathing patients.

10.1.2 Monitoring for ventilation

The main motivation for improved monitoring algorithms for ventilation is to assist the clinician in choosing the optimal treatment and/or ventilator settings, e.g., the desired pressure profile. This can help to significantly improve ventilation quality and therewith reduce the duration of ventilation for a patient. In the future, the outcome of these algorithms can be used by a supervisory controller to automatically choose the optimal treatment and ventilator settings.

The specific contributions of this thesis in the direction of monitoring algorithms for ventilation, i.e., Research Goal II, are summed up in terms of the patient effort and lung mechanics estimation algorithm of Chapter 8, and the patient-ventilator asynchrony detection and classification algorithm of Chapter 9.

- *Patient effort and lung mechanics estimation* can help the clinician to choose the appropriate treatment and ventilator settings for a specific patient. In Chapter 8, a non-invasive method for estimation of spontaneous breathing effort and lung mechanics of ventilated patients is presented. The developed algorithm uses sparsity properties of a patient's breathing effort to estimate the effort and lung parameters without requiring additional (invasive) sensors and/or interruptions of the treatment. In simulations and experiments, in a lab environment with a mechanical lung emulator it is shown that the algorithm retrieves useful estimates of the lung mechanics parameters and the patient's spontaneous breathing effort.

Concluding, the developed estimation algorithm is able to retrieve useful estimates of the patient effort and lung mechanics. These estimates can help the clinician to accurately diagnose a patient and consequently choose the optimal treatment and ventilator settings.

- *Patient-ventilator asynchrony detection and classification* is essential to overcome one of the largest challenges during ventilation. Therefore, in Chapter 9, a supervised learning framework to detect and classify different types of patient-ventilator asynchrony in real time is presented. Using this framework, a Recurrent Neural Network (RNN) is developed to detect and classify patient-ventilator asynchrony in real time. In simulations, it is shown that the developed algorithm can detect and classify inspiration, expiration, and severe asynchronies with an accuracy of about 94.6%, 91.9%, and 83.2%, respectively. In experiments, the same algorithm detects and classifies inspiration, expiration, and severe asynchronies with an accuracy of 86.7%, 64.2%, and 72.7%, respectively. These results show that the algorithm can effectively detect different types of asynchronies using data that is already available in conventional ventilation systems.

Concluding, the presented framework for patient-ventilator asynchrony detection and classification can be used to develop accurate detection and classification algorithms for bedside monitoring in real time. This can help the clinicians to improve their diagnoses for patient-ventilator asynchrony, and therewith improve the treatment.

10.2 Recommendations

The algorithms developed in this thesis have been shown to significantly improve pressure tracking performance and monitoring capabilities of mechanical ventilators in simulations and on an experimental laboratory setup. Eventually, these algorithms should be implemented in actual ventilators and validated in an actual ICU. Therefore, the recommendations in this section mainly focus on achieving this next step in the algorithm development process. Furthermore, relevant extensions of the current algorithms and the development of additional algorithms are discussed.

In the remainder of this section, the main recommendations for future developments related to the specific research goals in this thesis are presented first. Thereafter, the author's vision in a broader perspective of the overall Research Challenge and the development of smart mechanical ventilators is presented.

10.2.1 Control systems for ventilation

The learning control algorithms in this thesis have shown a significant improvement in pressure tracking performance of mechanical ventilators. Still, several research directions for future work on this topic are identified. Next, the most important directions for future research directions for control systems for ventilation are summed up, focusing on the algorithms in this thesis. Thereafter, a general remark is made on further developments of control systems for ventilation.

- *Extension to dual-hose ventilation systems*: The control strategies presented in this thesis have been developed using a single-hose ventilation setup with a pas-

sive expiration valve. This is the preferred platform for initial development, because analysis of this platform is fairly simple. However, in practice, mostly dual-hose ventilation systems with an active expiration valve are used in the ICU. Therefore, the different control strategies developed in this thesis should be extended, implemented, and analyzed for the dual-hose ventilation system with an active expiration valve. This will complicate control, because the system becomes a Multi-Input Multi-Output (MIMO) system and additional nonlinearities are introduced in the system. This requires some modifications to the developed algorithms.

- *Extension to volume-controlled ventilation modes:* In this thesis, pressure controlled ventilation is considered. However, in practice also many volume controlled modes are used. In these modes, a flow profile instead of a pressure profile is to be tracked by the controller. Therefore, it is recommended to extend the developed algorithms to allow for such volume-controlled modes or even develop other control strategies for these modes.
- *Validation on actual patients:* All control strategies in this thesis have been tested extensively in a laboratory setting with a lung simulator. A next step is to ensure that the performance is also improved in practice with actual patients. Therefore, the control strategies should be implemented in an actual ventilator and tested in an actual ICU environment with actual patients.
- *Reduce memory requirement for repetitive control:* The implementation of repetitive control that is considered in this thesis requires a large amount of memory, which is typically not available on mechanical ventilators. Therefore, implementations that are more efficient in terms of memory should be considered in future work. An example of such implementation is repetitive control using basis functions.
- *Triggered expiration in triggered repetitive control:* The current implementation of triggered repetitive control for ventilation in Chapter 7 does not allow for a patient-triggered expiration. Therefore, this control strategy should be extended to allow further synchronization of the patient and the ventilator. This can be achieved by using separate repetitive controllers for the inspiration and the expiration which are alternated.
- *General remark for controller design:* Future research in control for ventilation should consider the trade-off between complexity, computational burden, memory requirements, and clinical relevance of the performance gain. For example, the triggered repetitive control framework is fairly complex and requires a relatively large amount of memory, which is typically not available on commercially available ventilators. Furthermore, the strategy might introduce artifacts in the flow and pressure curves that might be interpreted by the clinician as spontaneous patient breaths, such artifacts are highly undesired. Besides these disadvantages, no research has been devoted to analyze whether these high levels of

tracking performance actually improve the treatment of the patient. Therefore, it is recommended to investigate whether the performance gains outweigh the added complexity of newly developed control strategies before investing a lot of time in the development of more complex control strategies.

10.2.2 Monitoring for ventilation

The monitoring algorithms presented in this thesis have the potential to significantly improve the treatment of a ventilated patient. However, several research directions to further improve monitoring for ventilation are identified. Furthermore, other monitoring capabilities are briefly considered to further improve ventilation.

- *Actual patient data:* The monitoring algorithms in this thesis have been developed and analyzed using data from a simulation environment and an experimental lab setup. To validate whether the algorithms are of added value in practice, they should be validated using patient data from an actual ICU environment. This will likely lead to new challenges requiring further improvements of the algorithms. Therefore, the algorithms should be further developed using this data.
- *Extension to dual-hose ventilation systems:* Both algorithms have been developed and analyzed using a single-hose ventilation setup with a passive expiration leak. Implementing them in the ICU with the commonly used dual-hose ventilation system will likely lead to complications. For example, the expiration valve typically causes some artifacts in the measured flow. This might deteriorate the performance of the developed algorithms. Therefore, this influence should be analyzed and the algorithms should be adapted accordingly. In theory, this should not affect the estimation algorithm of Chapter 8, because it only uses the relation between flow and pressure measured at the patient. Theoretically this relation is independent of the ventilation system. Furthermore, the PVA detection and classification framework of Chapter 9 is able to handle these dual-hose ventilation systems. However, the dataset should be enriched to contain data from a dual-hose ventilation system.
- *Extension to volume-controlled ventilation modes:* In this thesis, only pressure-controlled ventilation is considered. Therefore, the algorithms should be extended such that they can handle volume-controlled ventilation modes. Again, theoretically this change should not affect the estimation algorithm of Chapter 8. However, this should be analyzed more extensively. For the PVA detection and classification framework of Chapter 9 the same recommendation as above holds; the dataset should be enriched with data of volume-controlled ventilation modes.
- *Effort estimation for Spontaneous Breathing Trials (SBTs):* Especially during an SBT it would be valuable to have accurate real-time information about the patient's spontaneous breathing effort and the variation of this effort over time.

During an SBT, the patient is detached from the ventilation hose while the endotracheal tube is left inside the patient. Then, over a time span of approximately 30 - 60 minutes the patient is monitored. After this SBT, it is determined whether the endotracheal tube should be removed from the patient, or whether the patient should be reattached to the ventilator. Currently, the estimation algorithm is not able to obtain useful estimates during such SBT, mainly because there is no external (known) excitation of the system, i.e., the system is only excited by the patient's effort. It might be possible to include additional assumptions during these SBTs, e.g., that the patient's spontaneous effort is rather large, such that useful estimates of the patient effort can still be obtained using the strategy of Chapter 8.

- *Improved definition of Patient-Ventilator Asynchrony:* Currently, the PVA definition, in the PVA detection and classification framework of Chapter 9, is solely based on the start times of the patient's and ventilator's inspiration and expiration. However, in practice it is relevant to include other information, such as, breath depth. Therefore, the PVA definition should be further extended to include other clinically relevant parameters. To achieve this, a close collaboration with (expert) clinicians in this field is required.
- *Additional sensing and monitoring:* Additional (noninvasive) sensing could help to obtain better monitoring algorithms. Examples of such additional sensing are surface Electromyography (sEMG) and the oxygen saturation level of the blood. More specifically, sEMG gives valuable information about the diaphragm activity of a patient. This could prove to be a helpful input for both monitoring algorithms presented in this thesis. Furthermore, sEMG can potentially improve ventilation in several other ways, e.g., faster and more accurate triggering. The oxygen saturation level of the blood can be used to determine whether the patient's oxygen intake is sufficient and whether a higher or lower oxygen level is required. Note that it is very important to keep the trade-off between additional cost and improved quality in mind. Additional sensing is expensive in terms of money and labor. Therefore, additional sensors should only be considered if the added benefits outweigh the added costs.
- *Use of data-driven algorithms in mechanical ventilation:* Eventually, monitoring algorithms should be integrated in closed-loop ventilators to determine the optimal ventilation strategy. To achieve this, many different parameters about the patient's state should be determined and combined. Therefore, algorithms should be able to interpret the measured data in a similar way as clinician is currently doing. It is essential that the separate algorithms, that will be developed in the future, have clear outcomes that can be integrated in an overall supervisory controller. Eventually, this supervisory controller can determine the full clinical picture of the patient, which it then uses to determine the optimal ventilation strategy.

10.2.3 Towards smart mechanical ventilators: the author's vision

The overall research challenge in the introduction of this thesis is formulated as:

Research Challenge: *Reduce the mechanical ventilation-related workload and costs, while simultaneously improving the treatment for the ventilated patient.*

The algorithms presented throughout this thesis are a significant step towards this research challenge. However, the algorithms in this thesis mainly focus on the second part of the challenge, i.e., improvement of the patient's treatment.

The specific research goals, and therewith the research focus, of this thesis were formulated in 2018, before the current COVID-19 pandemic, when hospital staffing levels were not as big of an issue as it currently is. During this pandemic, it has become more clear that the shortage of nursing staff is a major bottleneck in the current western healthcare system. Especially during a worldwide pandemic, such as the current COVID-19 pandemic, it is vital to have a more scalable ICU capacity. Therewith, it has been clearly exposed that the research focus should shift to fully autonomous mechanical ventilators. A fully autonomous ventilator reduces the required number of ventilated related actions by the nursing staff. Therewith, it allows a higher patient to nurse ratio, resulting in an increased ICU capacity with the same nursing staff. Furthermore, an autonomous ventilator has the potential of significantly improving the treatment, e.g., reducing the risk of complications and reducing the length of stay of a patient.

Therefore, it is of the utmost importance, that the insights during this pandemic lead to an acceleration of the development and acceptance of autonomous ventilators. Because the question is not whether the next pandemic will happen, but when it will happen and it will once again put high levels of strain on the healthcare system. Besides the technical challenges regarding closed-loop ventilation, several other challenges, such as, clinical acceptance, clinical validation, and liability, should be addressed to effectively achieve this goal. Therefore, this research challenge should not be tackled by clinicians, engineers, and researchers alone, also governing bodies should be included to develop workable regulations for such devices.

From a technical point of view, algorithms should eventually replace the hospital staff's translation from measured data to mitigating actions. To achieve this, the closed-loop ventilator should contain algorithms that interpret the available waveforms and other measured signals and parameters, such as, the algorithms in the second part of this thesis. Then, another algorithm uses the output of these algorithms to determine the patient's clinical picture and the current quality of the treatment. Thereafter, a supervisory controller determines whether an action is required, e.g., adjusting ventilator settings or administer medication to the patient. The ventilator settings are in turn used to compute the reference profiles for the low-level controllers as presented in the first part of this thesis. Such an autonomous ventilator is considered to be a realistic solution to the overall Research Challenge, and therewith a significant step towards the scalable ICU of the future.

Bibliography

- Adams, J. Y., Lieng, M. K., Kuhn, B. T., Rehm, G. B., Guo, E. C., Taylor, S. L., Delplanque, J. P., and Anderson, N. R. (2017). Development and validation of a multi-algorithm analytic platform to detect off-target mechanical ventilation. *Scientific Reports*, 7:14980.
- Aiken, L., Clarke, S., Sloane, D., Sochalski, J., and Silber, J. (2002). Hospital nurse staffing and patient mortality, nurse burnout, and job dissatisfaction. *JAMA*, 288(16):1987–1993.
- Amato, M. B., Meade, M. O., Slutsky, A. S., Brochard, L., Costa, E. L., Schoenfeld, D. A., Stewart, T. E., Briel, M., Talmor, D., Mercat, A., Richard, J.-C. M., Carvalho, C. R., and Brower, R. G. (2015). Driving pressure and survival in the acute respiratory distress syndrome. *New England Journal of Medicine*, 372(8):747–755.
- Amato, M. B. P., Barbas, C. S. V., Medeiros, D. M., Magaldi, R. B., Schettino, G. P., Lorenzi-Filho, G., Kairalla, R. A., Deheinzelin, D., Munoz, C., Oliveira, R., Takagaki, T. Y., and Carvalho, C. R. R. (1998). Effect of a protective-ventilation strategy on mortality in the acute respiratory distress syndrome. *New England Journal of Medicine*, 338(6):347–354.
- Andersen, R. S., Peimankar, A., and Puthusserypady, S. (2019). A deep learning approach for real-time detection of atrial fibrillation. *Expert Systems with Applications*, 115:465–473.
- Angus, D. C., Kelley, M. A., Schmitz, R. J., White, A., and Popovich, J. (2000). Current and projected workforce requirements for care of the critically ill and patients with pulmonary disease. *JAMA*, 284(21):2762–2770.
- Arimoto, S., Kawamura, S., and Miyazaki, F. (1984). Bettering operation of robots by learning. *Journal of Robotic Systems*, 1(2):123–140.

- Arnal, J.-M., Garnero, A., Novonti, D., Demory, D., Ducros, L., Berric, A., Donati, S., Corno, G., Jaber, S., and Durand-Gasselín, J. (2013). Feasibility study on full closed-loop control ventilation (IntelliVent-ASV™) in ICU patients with acute respiratory failure: a prospective observational comparative study. *Critical Care*, 17(5):R196.
- Arnal, J.-M., Wysocki, M., Novotni, D., Demory, D., Lopez, R., Donati, S., Granier, I., Corno, G., and Durand-Gasselín, J. (2012). Safety and efficacy of a fully closed-loop control ventilation (IntelliVent-ASV®) in sedated ICU patients with acute respiratory failure: a prospective randomized crossover study. *Intensive care medicine*, 38(5):781–787.
- Astolfi, D., Marx, S., and van de Wouw, N. (2021a). Repetitive control design based on forwarding for nonlinear minimum-phase systems. *Automatica*, 129:109671.
- Astolfi, D., Praly, L., and Marconi, L. (2015). Approximate regulation for nonlinear systems in presence of periodic disturbances. In *Conference on Decision and Control*, pages 7665–7670, Osaka, Japan.
- Astolfi, D., Praly, L., and Marconi, L. (2021b). Nonlinear robust periodic output regulation of minimum phase systems. *Mathematics of Control, Signals, and Systems*, pages 1–56.
- Avanzolini, G., Barbini, P., Cappello, A., Cevenini, G., and Chiari, L. (1997). A new approach for tracking respiratory mechanical parameters in real-time. *Annals of Biomedical Engineering*, 25(1):154–163.
- Bakkes, T., Montree, R., Mischi, M., Mojoli, F., and Turco, S. (2020). A machine learning method for automatic detection and classification of patient-ventilator asynchrony. In *Annual International Conference of the Engineering in Medicine & Biology Society (EMBS)*, pages 150–153.
- Ball, J. E., Bruyneel, L., Aiken, L. H., Sermeus, W., Sloane, D. M., Rafferty, A. M., Lindqvist, R., Tishelman, C., and Griffiths, P. (2018). Post-operative mortality, missed care and nurse staffing in nine countries: A cross-sectional study. *International Journal of Nursing Studies*, 78:10–15.
- Bates, J. (2009). *Lung Mechanics: An Inverse Modeling Approach*. Cambridge University Press.
- Beijers, A. J. R., Roos, A. N., and Bindels, A. J. G. H. (2014). Fully automated closed-loop ventilation is safe and effective in post-cardiac surgery patients. *Intensive care medicine*, 40(5):752–753.
- Bellman, R. E. and Cooke, K. L. (1963). *Differential-Difference Equations*. Santa Monica, CA: RAND Corporation.
- Bin, M., Astolfi, D., and Marconi, L. (2020). About robustness of control systems embedding an internal model. *arXiv preprint arXiv:2010.08794*.

- Bishop, C. M. (1995). *Neural Networks for Pattern Recognition*. In *Neural Networks for Pattern Recognition*. Oxford University Press Inc., New York.
- Bjorklund, S. and Ljung, L. (2003). A review of time-delay estimation techniques. In *Proceedings of the Conference on Decision and Control (CDC)*, pages 2502–2507. Maui, HI, USA.
- Blanch, L., Sales, B., Montanya, J., Lucangelo, U., Garcia-Esquirol, O., Villagra, A., Chacon, E., Estruga, A., Borelli, M., Burgueño, M. J., Oliva, J. C., Fernandez, R., Villar, J., Kacmarek, R., and Murias, G. (2012). Validation of the better care® system to detect ineffective efforts during expiration in mechanically ventilated patients: a pilot study. *Intensive Care Medicine*, 38(5):772–780.
- Blanch, L., Villagra, A., Sales, B., Montanya, J., Lucangelo, U., Luján, M., García-Esquirol, O., Chacón, E., Estruga, A., Oliva, J. C., Hernández-Abadía, A., Albaiceta, G. M., Fernández-Mondejar, E., Fernández, R., Lopez-Aguilar, J., Villar, J., Murias, G., and Kacmarek, R. M. (2015). Asynchronies during mechanical ventilation are associated with mortality. *Intensive Care Medicine*, 41(4):633–641.
- Blanken, L., Koekebakker, S., and Oomen, T. (2020). Multivariable repetitive control: Decentralized designs with application to continuous media flow printing. *Transactions on Mechatronics*, 25(1):294–304.
- Borrello, M. (2001). Adaptive inverse model control of pressure based ventilation. In *Proceedings of the American Control Conference*, pages 1286–1291. Arlington, VA, USA.
- Borrello, M. (2002). Positive feedback in flow controller reduces ventilator imposed work of breathing for critical care patients. In *Proceedings of the American Control Conference*, pages 4050–4055. Anchorage, AK, USA.
- Borrello, M. (2005). Adaptive control of a proportional flow valve for critical care ventilators. In *Proceedings of the American Control Conference*, pages 2166–2180. Portland, OR, USA.
- Borrello, M. (2018). Modeling and control of systems for critical care ventilation. In *Proceedings of the American Control Conference*, pages 104–109. Milwaukee, WI, USA.
- Bouadma, L., Lellouche, F., Cabello, B., Taillé, S., Mancebo, J., Dojat, M., and Brochard, L. (2005). Computer-driven management of prolonged mechanical ventilation and weaning: a pilot study. *Intensive care medicine*, 31(10):1446–1450.
- Bristow, D., Tharayil, M., and Alleyne, A. (2006). A survey of iterative learning control. *Control Systems Magazine*, 26(3):96–114.

- Brochard, L., Roudot-Thoraval, F., Roupie, E., Delclaux, C., Chastre, J., Fernandez-Mondéjar, E., Clémenti, E., Mancebo, J., Factor, P., Matamis, D., Ranieri, M., Blanch, L., Rodi, G., Mentec, H., Dreyfuss, D., Ferrer, M., Brun-Buisson, C., Tobin, M., and Lemaire, F. (1998). Tidal volume reduction for prevention of ventilator-induced lung injury in acute respiratory distress syndrome. *American Journal of Respiratory and Critical Care Medicine*, 158(6):1831–1838.
- Buchan, J. and Aiken, L. (2008). Solving nursing shortages: a common priority. *Journal of Clinical Nursing*, 17(24):3262–3268.
- Byrnes, C. I. and Isidori, A. (2004). Nonlinear internal models for output regulation. *Transactions on Automatic Control*, 49(12):2244–2247.
- Califano, F., Bin, M., Macchelli, A., and Melchiorri, C. (2018). Stability analysis of nonlinear repetitive control schemes. *Control Systems Letters*, 2(4):773–778.
- Candes, E. J. and Tao, T. (2005). Decoding by linear programming. *Transactions on Information Theory*, 51(12):4203–4215.
- Candès, E. J., Wakin, M. B., and Boyd, S. P. (2008). Enhancing sparsity by reweighted ℓ_1 minimization. *Journal of Fourier Analysis and Applications*, 14:877–905.
- Chatburn, R. L. (2004). Computer control of mechanical ventilation. *Respiratory care*, 49(5):507–517.
- Chellaboina, V., Haddad, W. M., Li, H., and Bailey, J. M. (2010). Limit cycle stability analysis and adaptive control of a multi-compartment model for a pressure-limited respirator and lung mechanics system. *International Journal of Control*, 83(5):940–955.
- Chen, C.-W., Wu, C.-P., Dai, Y.-L., Perng, W.-C., Chian, C.-F., Su, W.-L., and Huang, Y.-C. T. (2011). Effects of implementing adaptive support ventilation in a medical intensive care unit. *Respiratory care*, 56(7):976–983.
- Chiew, Y. S., Pretty, C., Docherty, P. D., Lambermont, B., Shaw, G. M., Desaive, T., and Chase, J. G. (2015). Time-varying respiratory system elastance: A physiological model for patients who are spontaneously breathing. *PLoS ONE*, 10(1):e0114847.
- Colombo, D., Cammarota, G., Alemani, M., Carenzo, L., Barra, F. L., Vaschetto, R., Slutsky, A. S., Della Corte, F., and Navalesi, P. (2011). Efficacy of ventilator waveforms observation in detecting patient-ventilator asynchrony. *Critical care medicine*, 39(11):2452–2457.
- Costa-Castelló, R. and Grinó, R. (2006). A repetitive controller for discrete-time passive systems. *Automatica*, 42(9):1605–1610.

- Cox, C. E., Carson, S. S., Govert, J. A., Chelluri, L., and Sanders, G. D. (2007). An economic evaluation of prolonged mechanical ventilation. *Critical care medicine*, 35(8):1918–1927.
- Dasta, J. F., McLaughlin, T. P., Mody, S. H., and Piech, C. T. (2005). Daily cost of an intensive care unit day: the contribution of mechanical ventilation. *Critical care medicine*, 33(6):1266–1271.
- de Castro, A. F. and Tôrres, L. A. B. (2019). Iterative learning control applied to a recently proposed mechanical ventilator topology. *IFAC-PapersOnLine (IFAC Symposium on Dynamics and Control of Process Systems, including Biosystems DYCOPS)*, 52(1):154–159.
- de Magalhães, A. M. M., da Costa, D. G., de Oliveira Riboldi, C., Mergen, T., da Silveira Barbosa, A., and de Moura, G. M. S. S. (2017). Association between workload of the nursing staff and patient safety outcomes. *Revista da Escola de Enfermagem da USP*, 51:e03255.
- de Roover, D. and Bosgra, O. H. (2000). Synthesis of robust multivariable iterative learning controllers with application to a wafer stage motion system. *International Journal of Control*, 73(10):968–979.
- DEMCON macawi respiratory systems (2021). Macawi Respiratory Module: disruptive by design. Available: <https://macawi.demcon.com/product/respiratory-module/>. Accessed: 8-December-2021.
- Determann, R. M., Royakkers, A., Wolthuis, E. K., Vlaar, A. P., Choi, G., Paulus, F., Hofstra, J.-J., de Graaff, M. J., Korevaar, J. C., and Schultz, M. J. (2010). Ventilation with lower tidal volumes as compared with conventional tidal volumes for patients without acute lung injury: a preventive randomized controlled trial. *Critical Care*, 14(1):R1.
- Dietz, F., Schloßer, A., and Abel, D. (2003). Flow controlled non-invasive ventilation considering mask leakage and spontaneous breathing. *IFAC Proceedings Volumes (Symposium on System Identification (SYSID))*, 36(16):151–156.
- Doorduyn, J., van Hees, H. W. H., van der Hoeven, J. G., and Heunks, L. M. A. (2013). Monitoring of the respiratory muscles in the critically ill. *American Journal of Respiratory and Critical Care Medicine*, 187(1):20–27.
- Drinker, P. and Shaw, L. (1929). An apparatus for the prolonged administration of artificial respiration: A design for adults and children. *Journal of Clinical Investigations*, 7(2):229–247.
- Drumond, R. R., Marques, B. A., Vasconcelos, C. N., and Clua, E. (2018). PEEK: An LSTM recurrent network for motion classification from sparse data. *Proceedings of the International Joint Conference on Computer Vision, Imaging and Computer Graphics Theory and Applications*, 1:215–222.

- Duffield, C. and O'Brien-Pallas, L. (2003). The causes and consequences of nursing shortages: a helicopter view of the research. *Australian Health Review*, 26(1):186–193.
- Epstein, S. K. (2011). How often does patient-ventilator asynchrony occur and what are the consequences? *Respiratory care*, 56(1):25–38.
- Filho, F., da Silva, A., Lopes, J., Lam, Z., Simões, V., and Dos Santos, A. (2011). Staff workload and adverse events during mechanical ventilation in neonatal intensive care units. *Jornal de Pediatria*, 87(6):478–492.
- Fot, E. V., Izotova, N. N., Yudina, A. S., Smetkin, A. A., Kuzkov, V. V., and Kirov, M. Y. (2017). Automated weaning from mechanical ventilation after off-pump coronary artery bypass grafting. *Frontiers in medicine*, 4:31.
- Francis, B. A. and Wonham, W. M. (1975). The internal model principle for linear multivariable regulators. *Applied Mathematics & Optimization*, 2(2):170–194.
- Freeman, C. T., Rogers, E., Hughes, A.-M., Burridge, J. H., and Meadmore, K. L. (2012). Iterative learning control in health care: Electrical stimulation and robotic-assisted upper-limb stroke rehabilitation. *Control Systems Magazine*, 32(1):18–43.
- Fresnel, E., Muir, J.-F., and Letellier, C. (2014). Realistic human muscle pressure for driving a mechanical lung. *EPJ Nonlinear Biomedical Physics*, 2:7.
- Gholami, B., Phan, T. S., Haddad, W. M., Cason, A., Mullis, J., Price, L., and Bailey, J. M. (2018). Replicating human expertise of mechanical ventilation waveform analysis in detecting patient-ventilator cycling asynchrony using machine learning. *Computers in Biology and Medicine*, 97:137–144.
- Ghosh, J. and Paden, B. (2000). Nonlinear repetitive control. *Transactions on Automatic Control*, 45(5):949–954.
- Giaccagli, M., Astolfi, D., Andrieu, V., and Marconi, L. (2020). Sufficient conditions for output reference tracking for nonlinear systems: a contractive approach. In *Conference on Decision and Control*, pages 4580–4585, Jeju Island, Republic of Korea.
- Giaccagli, M., Astolfi, D., Andrieu, V., and Marconi, L. (2022). Sufficient conditions for global integral action via incremental forwarding for input-affine nonlinear systems. *Transactions on Automatic Control*.
- Goligher, E. C., Fan, E., Herridge, M. S., Murray, A., Vorona, S., Brace, D., Rittayamai, N., Lanys, A., Tomlinson, G., Singh, J. M., Bolz, S.-S., Rubenfeld, G. D., Kavanagh, B. P., Brochard, L. J., and Ferguson, N. D. (2015). Evolution of diaphragm thickness during mechanical ventilation. impact of inspiratory effort. *American Journal of Respiratory and Critical Care Medicine*, 192(9):1080–1088.

- Goodfellow, I., Bengio, Y., and Courville, A. (2016). *Deep Learning*. MIT Press, Cambridge, Massachusetts.
- Grant, M. and Boyd, S. (2008). Graph implementations for nonsmooth convex programs. In Blondel, V., Boyd, S., and Kimura, H., editors, *Recent Advances in Learning and Control*, Lecture Notes in Control and Information Sciences, pages 95–110. Springer-Verlag Limited. http://stanford.edu/~boyd/graph_dcp.html.
- Grant, M. and Boyd, S. (2014). CVX: Matlab software for disciplined convex programming, version 2.1. <http://cvxr.com/cvx>.
- Grasso, S. and Ranieri, V. M. (2001). Proportional assist ventilation. *Respiratory care clinics of North America*, 7(3):465–473.
- Graves, A., Liwicki, M., Fernández, S., Bertolami, R., Bunke, H., and Schmidhuber, J. (2009). A novel connectionist system for unconstrained handwriting recognition. *Transactions on Pattern Analysis and Machine Intelligence*, 31(5):855–868.
- Gruber, P. C., Gomersall, C. D., Leung, P., Joynt, G. M., Ng, S. K., Ho, K.-M., and Underwood, M. J. (2008). Randomized controlled trial comparing adaptive-support ventilation with pressure-regulated volume-controlled ventilation with automode in weaning patients after cardiac surgery. *Anesthesiology*, 109(1):81–87.
- Hara, S., Yamamoto, Y., Omata, T., and Nakano, M. (1988). Repetitive control system: a new type servo system for periodic exogenous signals. *STransactions on Automatic Control*, 33(7):659–668.
- Hazarika, H. and Swarup, A. (2020). Improved performance of flow rate tracking in a ventilator using iterative learning control. In *International Conference on Electrical and Electronics Engineering (ICE3)*, pages 446–451, London, UK.
- Hespanha, J. (2009). *Linear Systems Theory*. Princeton University Press.
- Holanda, M. A., Vasconcelos, R. D. S., Ferreira, J. C., and Pinheiro, B. V. (2018). Patient-ventilator asynchrony. *Jornal brasileiro de pneumologia*, 44(4):321–333.
- Holden, R., Scanlon, M., Patel, N., Kaushal, R., Escoto, K. H., Brown, R., Alper, S., Arnold, J., Shalaby, T., Murkowski, K., and Karsh, B. (2011). A human factors framework and study of the effect of nursing workload on patient safety and employee quality of working life. *BMJ Quality & Safety*, 20(1):15–24.
- Hunnekens, B., Kamps, S., and van de Wouw, N. (2020). Variable-gain control for respiratory systems. *Transactions on Control Systems Technology*, 28(1):163–171.
- Inoue, T., Nakano, M., Kubo, T., Matsumoto, S., and Baba, H. (1981). High accuracy control of a proton synchrotron magnet power supply. *IFAC Proceedings Volumes*, 14(2):3137–3142.

- Ioannou, P. A. and Sun, J. (1996). *Robust Adaptive Control*. Upper Saddle River, NJ: Prentice-Hall.
- Isidori, A. (1995). *Nonlinear control systems*. Springer.
- Jakob, S. M. and Rothen, H. U. (1997). Intensive care 1980–1995: change in patient characteristics, nursing workload and outcome. *Intensive Care Medicine*, 23(11):1165–1170.
- Jone, A. F. (1864). Improvement in vacuum apparatus for treating diseases. U.S. patent 44,198.
- Kacmarek, R. M., Villar, J., Parrilla, D., Alba, F., Solano, R., Liu, S., Montiel, R., Rico-Feijoo, J., Vidal, A., Ferrando, C., Murcia, I., Corpas, R., González-Higueras, E., Sun, Q., Pinedo, C. E., Pestaña, D., Martínez, D., Aldecoa, C., Añón, J. M., Soro, M., González-Martín, J. M., Fernández, C., Fernández, R. L., and NAVa In Acute respiraTORy failure (NAVIATOR) Network, N. I. A. (2020). Neurally adjusted ventilatory assist in acute respiratory failure: a randomized controlled trial. *Intensive care medicine*, 46(12):2327–2337.
- Kallio, M., Peltoniemi, O., Anttila, E., Pokka, T., and Kontiokari, T. (2015). Neurally adjusted ventilatory assist (NAVA) in pediatric intensive care—a randomized controlled trial. *Pediatric pulmonology*, 50(1):55–62.
- Khalil, H. (2002). *Nonlinear systems*. Prentice Hall, Upper Saddle River, New Jersey.
- Kharitonov, V. L. (2013). *Time-Delay Systems: Lyapunov Functionals and Matrices*. Birkhäuser Boston.
- Kim, K. T., Redmond, D. P., Morton, S. E., Howe, S. L., Chiew, Y. S., and Chase, J. G. (2017). Quantifying patient effort in spontaneously breathing patient using negative component of dynamic elastance. *IFAC-PapersOnLine (IFAC World Congress)*, 50(1):5486–5491.
- Kingma, D. P. and Ba, J. L. (2015). Adam: A method for stochastic optimization. *3rd International Conference on Learning Representations, ICLR 2015 - Conference Track Proceedings*, pages 1–15.
- Kirakli, C., Ozdemir, I., Ucar, Z. Z., Cimen, P., Kepil, S., and Ozkan, S. A. (2011). Adaptive support ventilation for faster weaning in COPD: a randomised controlled trial. *The European respiratory journal*, 38(4):774–780.
- Lachmann, B. (1992). Open up the lung and keep the lung open. *Intensive Care Medicine*, 18(6):319–321.
- Lassen, H. (1953). A preliminary report on the 1952 epidemic of poliomyelitis in Copenhagen with special reference to the treatment of acuterespiratory insufficiency. *The Lancet*, 1(6749):37–41.

- Leiter, M. and Maslach, C. (2005). *Research companion to Organizational Health Psychology*, chapter A mediation model of job burnout, pages 544–564. Edward Elgar, UK.
- Lellouche, F., Bouchard, P.-A., Simard, S., L’Her, E., and Wysocki, M. (2013). Evaluation of fully automated ventilation: a randomized controlled study in post-cardiac surgery patients. *Intensive care medicine*, 39:463–471.
- Lellouche, F. and Brochard, L. (2009). Advanced closed loops during mechanical ventilation (PAV, NAVA, ASV, SmartCare). *Best practice & research. Clinical anaesthesiology*, 23(1):81–93.
- Lellouche, F., Mancebo, J., Jolliet, P., Roeseler, J., Schortgen, F., Dojat, M., Cabello, B., Bouadma, L., Rodriguez, P., Maggiore, S., Reynaert, M., Mersmann, S., and Brochard, L. (2006). A multicenter randomized trial of computer-driven protocolized weaning from mechanical ventilation. *American journal of respiratory and critical care medicine*, 174(8):894–900.
- Li, H. and Haddad, W. M. (2012). Model predictive control for a multi-compartment respiratory system. In *Proceedings of the American Control Conference*, pages 5574–5579. Montréal, Canada.
- Li, H. and Haddad, W. M. (2013). Model predictive control for a multicompartiment respiratory system. *Transactions on Control Systems Technology*, 21(5):1988–1995.
- Liu, L., Xu, X., Sun, Q., Yu, Y., Xia, F., Xie, J., Yang, Y., Heunks, L., and Qiu, H. (2020). Neurally adjusted ventilatory assist versus pressure support ventilation in difficult weaning: A randomized trial. *Anesthesiology*, 132(6):1482–1493.
- Ljung, L. (1999). *System Identification: Theory for the User (2nd Edition)*. Prentice Hall, Upper Saddle River, NJ, USA.
- Longman, R. W. (2010). On the theory and design of linear repetitive control systems. *European Journal of Control*, 16(5):447–496.
- Loo, N., Chiew, Y., Tan, C., Arunachalam, G., Ralib, A., and Mat-Nor, M.-B. (2018). A machine learning model for real-time asynchronous breathing monitoring. *IFAC-PapersOnLine (Symposium on Biological and Medical Systems (BMS))*, 51(27):378–383.
- Lord, P. and Lord, M. V. (1908). Respiration apparatus. U.S. patent 899225.
- Maes, H., Vandersteen, G., Muehlebach, M., and Ionescu, C. (2014). A fan-based, low-frequency, forced oscillation technique apparatus. *Transactions on Instrumentation and Measurement*, 63(3):603–611.

- Maes, H., Zivanovic, M., Schoukens, J., and Vandersteen, G. (2017). Estimating respiratory impedance at breathing frequencies using regularized least squares on forced oscillation technique measurements. *Transactions on Instrumentation and Measurement*, 66(3):479–491.
- Marconi, L., Praly, L., and Isidori, A. (2007). Output stabilization via nonlinear luenberger observers. *Journal on Control and Optimization*, 45(6):2277–2298.
- Mattavelli, P. and Marafao, F. P. (2004). Repetitive-based control for selective harmonic compensation in active power filters. *Transactions on Industrial Electronics*, 51(5):1018–1024.
- Mauri, T., Cambiaghi, B., Spinelli, E., Langer, T., and Grasselli, G. (2017). Spontaneous breathing: a double-edged sword to handle with care. *Annals of Translational Medicine*, 5(14):292–292.
- Michiels, W. and Niculescu, S.-I., editors (2014). *Stability, Control, and Computation for Time-Delay Systems*. Society for Industrial and Applied Mathematics.
- Moore, K. L. (1993). *Iterative learning control for deterministic systems*. Springer-Verlag, London, UK.
- Mulqueeny, Q., Redmond, S., Tassaux, D., Vignaux, L., Jolliet, P., Ceriana, P., Nava, S., Schindhelm, K., and Lovell, N. (2009). Automated detection of asynchrony in patient-ventilator interaction. In *Conference of the Engineering in Medicine and Biology Society*, pages 5324–5327, Minneapolis, MN, USA.
- Murphy, K. P. (2012). *Machine learning: A Probabilistic Perspective*. MIT Press, Cambridge, Massachusetts.
- Mushin, W., Rendell-Baker, L., Thompson, P., and Mapleson, W. (1980). *Automatic ventilation of the lungs*. Oxford: Blackwell Scientific.
- Natarajan, B. K. (1995). Sparse approximate solutions to linear systems. *SIAM Journal on Computing*, 24(2):227–234.
- Navajas, D., Alcaraz, J., Peslin, R., Roca, J., and Farré, R. (2000). Evaluation of a method for assessing respiratory mechanics during noninvasive ventilation. *The European respiratory journal*, 16:704–709.
- Navalesi, P. and Costa, R. (2003). New modes of mechanical ventilation: proportional assist ventilation, neurally adjusted ventilatory assist, and fractal ventilation. *Current Opinion in Critical Care*, 9(1):51–58.
- Needham, D. M., Bronskill, S. E., Calinawan, J. R., Sibbald, W. J., Pronovost, P. J., and Laupacis, A. (2005). Projected incidence of mechanical ventilation in ontario to 2026: Preparing for the aging baby boomers. *Critical Care Medicine*, 33(3):574–579.

- Neuraz, A., Guérin, C., Payet, C., Polazzi, S., Aubrun, F., Dailler, F., Lehot, J.-J., Piriou, V., Neidecker, J., Rimmelé, T., Schott, A.-M., and Duclos, A. (2015). Patient mortality is associated with staff resources and workload in the ICU. *Critical Care Medicine*, 43(8):1587–1594.
- Ohlsson, H., Ljung, L., and Boyd, S. (2010). Segmentation of ARX-models using sum-of-norms regularization. *Automatica*, 46(6):1107–1111.
- Olivieri, C., Costa, R., Conti, G., and Navalesi, P. (2011). Bench studies evaluating devices for non-invasive ventilation: critical analysis and future perspectives. *Intensive Care Medicine*, 38(1):160–167.
- Onuki, Y. and Ishioka, H. (2001). Compensation for repeatable tracking errors in hard drives using discrete-time repetitive controllers. *Transactions on Mechatronics*, 6(2):132–136.
- Oomen, T. and Rojas, C. R. (2017). Sparse iterative learning control with application to a wafer stage: Achieving performance, resource efficiency, and task flexibility. *Mechatronics*, 47:134–147.
- Otis, A. B. (1954). The work of breathing. *Physiological Reviews*, 34(3):449–458.
- Pan, Q., Zhang, L., Jia, M., Pan, J., Gong, Q., Lu, Y., Zhang, Z., Ge, H., and Fang, L. (2021). An interpretable 1D convolutional neural network for detecting patient-ventilator asynchrony in mechanical ventilation. *Computer Methods and Programs in Biomedicine*, 204:106057.
- Pascanu, R., Mikolov, T., and Bengio, Y. (2013). On the difficulty of training recurrent neural networks. In *Proceedings of the International Conference on Machine Learning*, pages 1310–1318, Atlanta, GA, USA.
- Pavlov, A. and Marconi, L. (2008). Incremental passivity and output regulation. *Systems & Control Letters*, 57(5):400–409.
- Pavlov, A. and van de Wouw, N. (2017). Convergent systems: nonlinear simplicity. In *Nonlinear Systems*, pages 51–77. Springer.
- Pavlov, A., van de Wouw, N., and Nijmeijer, H. (2007a). Frequency response functions for nonlinear convergent systems. *Transactions on Automatic Control*, 52(6):1159–1165.
- Pavlov, A., van de Wouw, N., and Nijmeijer, H. (2007b). Global nonlinear output regulation: Convergence-based controller design. *Automatica*, 43(3):456–463.
- Pavlov, A. V., van De Wouw, N., and Nijmeijer, H. (2005). Convergent systems: analysis and synthesis. In *Control and observer design for nonlinear finite and infinite dimensional systems*, pages 131–146. Springer.

- Pavlov, A. V., van De Wouw, N., and Nijmeijer, H. (2006). *Uniform output regulation of nonlinear systems: a convergent dynamics approach*. Springer Science & Business Media.
- Petersen, E., Graßhoff, J., Eger, M., and Rostalski, P. (2020). Surface EMG-based estimation of breathing effort for neurally adjusted ventilation control. *IFAC-PapersOnLine (IFAC World Congress)*, 53(2):16323–16328.
- Petter, A. H., Chioléro, R. L., Cassina, T., Chassot, P.-G., Müller, X. M., and Revelly, J.-P. (2003). Automatic "respirator/weaning" with adaptive support ventilation: the effect on duration of endotracheal intubation and patient management. *Anesthesia and analgesia*, 97(6):1743–1750.
- Pham, T., Teliás, I., Piraino, T., Yoshida, T., and Brochard, L. J. (2018). Asynchrony consequences and management. *Critical Care Clinics*, 34(3):325–341.
- Pintelon, R. and Schoukens, J. (2012). *System Identification: a frequency domain approach*. John Wiley & Sons, Hoboken, NJ, USA.
- Pipeleers, G., Demeulenaere, B., and Swevers, J. (2009). *Optimal Linear Controller Design for Periodic Inputs*, volume 394. Springer London.
- Piquilloud, L., Vignaux, L., Bialais, E., Roeseler, J., Sottiaux, T., Laterre, P.-F., Jolliet, P., and Tassaux, D. (2011). Neurally adjusted ventilatory assist improves patient-ventilator interaction. *Intensive care medicine*, 37(2):263–271.
- Pomprapa, A., Weyer, S., Leonhardt, S., Walter, M., and Misgeld, B. (2015). Periodic funnel-based control for peak inspiratory pressure. In *Proceedings of the Conference on Decision and Control*, pages 5617–5622. Osaka, Japan.
- Portoghese, I., Galletta, M., Copolla, R., Finco, G., and Campagna, M. (2014). Burnout and workload among health care workers: the moderating role of job control. *Safety and Health at work*, 5(3):152–157.
- Rafferty, A. M., Clarke, S. P., Coles, J., Ball, J., James, P., McKee, M., and Aiken, L. H. (2007). Outcomes of variation in hospital nurse staffing in english hospitals: cross-sectional analysis of survey data and discharge records. *International journal of nursing studies*, 44(2):175–182.
- Rehm, G., Han, J., Kuhn, B., Delplanque, J.-P., Anderson, N., Adams, J., and Chuah, C.-N. (2018). Creation of a robust and generalizable machine learning classifier for patient ventilator asynchrony. *Methods of Information in Medicine*, 57(04):208–219.
- Reinders, J., Ciaccagli, M., Hunnekens, B., Astolfi, D., Oomen, T., and van de Wouw, N. (2022a). Repetitive control for Lur'e-type systems: application to mechanical ventilation. *submitted for journal publication (under review)*.

- Reinders, J., Elshove, D., Hunnekens, B., van de Wouw, N., and Oomen, T. (2022b). Triggered repetitive control: application to mechanically ventilated patients. *submitted for journal publication (under review)*.
- Reinders, J., Heck, F., Hunnekens, B., Oomen, T., and van de Wouw, N. (2019). Online hose calibration for pressure control in mechanical ventilation. In *Proceedings of the American Control Conference*, pages 5414–5419. Philadelphia, PA, USA.
- Reinders, J., Hunnekens, B., Heck, F., Oomen, T., and van de Wouw, N. (2021a). Accurate pressure tracking to support mechanically ventilated patients using an estimated nonlinear hose model and delay compensation. *Control Engineering Practice*, 106:104660.
- Reinders, J., Hunnekens, B., Heck, F., Oomen, T., and van de Wouw, N. (2021b). Adaptive control for mechanical ventilation for improved pressure support. *Transactions on Control Systems Technology*, 29(1):180–193.
- Reinders, J., Hunnekens, B., Oomen, T., and van de Wouw, N. (2021c). Linear repetitive control for a nonlinear mechanical ventilation system using feedback linearization. In *Conference on Control Technology and Applications*. San Diego, CA, USA.
- Reinders, J., Hunnekens, B., van de Wouw, N., and Oomen, T. (2022c). Noninvasive breathing effort estimation of mechanically ventilated patients using sparse optimization. *submitted for journal publication (under review)*.
- Reinders, J., van de Kamp, L., Hunnekens, B., Oomen, T., and van de Wouw, N. (2021d). Flipped halfwave: improved modeling of spontaneous breathing effort. *IFAC-PapersOnline (Symposium on Biomedical and Medical Systems (BMS))*.
- Reinders, J., van de Kamp, L., Hunnekens, B., Oomen, T., and van de Wouw, N. (2022d). Automatic patient-ventilator asynchrony detection and classification framework using objective asynchrony definitions. *submitted for journal publication (under review)*.
- Reinders, J., Verkade, R., Hunnekens, B., van de Wouw, N., and Oomen, T. (2020). Improving mechanical ventilation for patient care through repetitive control. In *IFAC-PapersOnline (IFAC World Congress)*, pages 1441–1446. Berlin, Germany.
- Rittayamai, N. and Brochard, L. (2015). Recent advances in mechanical ventilation in patients with acute respiratory distress syndrome. *European Respiratory Review*, 24(135):132–140.
- Rojas, C. R. and Hjalmarsson, H. (2011). Sparse estimation based on a validation criterion. In *Proceedings of the Conference on Decision and Control and European Control Conference*, pages 2825–2830. Orlando, FL, USA.

- Ronneberger, O., Fischer, P., and Brox, T. (2015). U-net: Convolutional networks for biomedical image segmentation. In *Lecture Notes in Computer Science*, pages 234–241. Springer International Publishing.
- Rose, L., Presneill, J. J., Johnston, L., and Cade, J. F. (2008). A randomised, controlled trial of conventional versus automated weaning from mechanical ventilation using smartcare/ps. *Intensive care medicine*, 34(10):1788–1795.
- Rouby, J., Lu, Q., and Goldstein, I. (2002). Selecting the right level of positive end-expiratory pressure in patients with acute respiratory distress syndrome. *American Journal of Respiratory and Critical Care Medicine*, 165(8):1182–1186.
- Rüffer, B. S., van De Wouw, N., and Mueller, M. (2013). Convergent systems vs. incremental stability. *Systems & Control Letters*, 62(3):277–285.
- Scheel, M., Berndt, A., and Simanski, O. (2015). Iterative learning control: An example for mechanical ventilated patients. *IFAC-PapersOnLine (Symposium on Biological and Medical Systems (BMS))*, 48(20):523–527.
- Scheel, M., Schauer, T., Berndt, A., and Simanski, O. (2017). Model-based control approach for a CPAP-device considering patient’s breathing effort. *IFAC-PapersOnLine (IFAC World Congress)*, 50(1):9948–9953.
- Schranz, C., Knöbel, C., Kretschmer, J., Zhao, Z., and Möller, K. (2011). Hierarchical parameter identification in models of respiratory mechanics. *Transactions on Biomedical Engineering*, 58(11):3234–3241.
- Schwake, W. (1927). Pneumatische kammer. German patent DE 449,304.
- Simard, P. Y., Steinkraus, D., and Platt, J. C. (2003). Best practices for convolutional neural networks applied to visual document analysis. In *Proceedings of the International Conference on Document Analysis and Recognition*, pages 958–963. Edinburgh, UK.
- Sinderby, C. and Beck, J. (2008). Proportional assist ventilation and neurally adjusted ventilatory assist—better approaches to patient ventilator synchrony? *Clinics in Chest Medicine*, 29(2):329–342.
- Sinderby, C., Navalesi, P., Beck, J., Skrobik, Y., Comtois, N., Friberg, S., Gottfried, S. B., and Lindström, L. (1999). Neural control of mechanical ventilation in respiratory failure. *Nature Medicine*, 5(12):1433–1436.
- Slutsky, A. S. (2015). History of mechanical ventilation from vesalius to ventilator-induced lung injury. *American Journal of Respiratory and Critical Care Medicine*, 191(10):1106–1115.
- Slutsky, A. S. and Ranieri, V. M. (2013). Ventilator-induced lung injury. *New England Journal of Medicine*, 369(22):2126–2136.

- Sottile, P. D., Albers, D., Higgins, C., Mckeehan, J., and Moss, M. M. (2018). The association between ventilator dyssynchrony, delivered tidal volume, and sedation using a novel automated ventilator dyssynchrony detection algorithm. *Critical care medicine*, 46(2):e151–e157.
- Soydancer, D. (2020). A Comparison of Optimization Algorithms for Deep Learning. *International Journal of Pattern Recognition and Artificial Intelligence*, 34(13).
- Steinbuch, M. (2002). Repetitive control for systems with uncertain period-time. *Automatica*, 38(12):2103–2109.
- Tarnow-Mordi, W., Hau, C., Warden, A., and Shearer, A. (2000). Hospital mortality in relation to staff workload: a 4-year study in an adult intensive-care unit. *The Lancet*, 356(9225):185–189.
- Tassaux, D., Dalmas, E., Gratadour, P., and Jolliet, P. (2002). Patient-ventilator interactions during partial ventilatory support: a preliminary study comparing the effects of adaptive support ventilation with synchronized intermittent mandatory ventilation plus inspiratory pressure support. *Critical care medicine*, 30(4):801–807.
- Thille, A. W., Rodriguez, P., Cabello, B., Lellouche, F., and Brochard, L. (2006). Patient-ventilator asynchrony during assisted mechanical ventilation. *Intensive Care Medicine*, 32(10):1515–1522.
- Tibshirani, R. (1996). Regression shrinkage and selection via the lasso. *Journal of the Royal Statistical Society: Series B (Methodological)*, 58(1):267–288.
- Tibshirani, R., Saunders, M., Rosset, S., Zhu, J., and Knight, K. (2005). Sparsity and smoothness via the fused lasso. *Journal of the Royal Statistical Society: Series B (Statistical Methodology)*, 67(1):91–108.
- Tobin, M. J. (2013). *Principles And Practice of Mechanical Ventilation, Third Edition*. McGraw-Hill Education.
- Tomizuka, M. (1987). Zero phase error tracking algorithm for digital control. *Journal of Dynamic Systems, Measurement, and Control*, 109(1):65–68.
- Tomizuka, M., Tsao, T., and Chew, K. (1988). Discrete-time domain analysis and synthesis of repetitive controllers. In *American Control Conference*, pages 860–866, Atlanta, GA, USA. IEEE.
- Tomizuka, M., Tsao, T.-C., and Chew, K.-K. (1989). Analysis and synthesis of discrete-time repetitive controllers. *Journal of Dynamic Systems, Measurement, and Control*, 111(3):353–358.
- van de Wouw, N., Hunnekens, B., and Kamps, S. (2018). Switching control of medical ventilation systems. In *Proceedings of the American Control Conference*, pages 532–538. Milwaukee, WI, USA.

- van Diepen, A., Bakkes, T. H. G. F., De Bie, A. J. R., Turco, S., Bouwman, R. A., Woerlee, P. H., and Mischi, M. (2021). A model-based approach to synthetic data set generation for patient-ventilator waveforms for machine learning and educational use. *arXiv:2103.15684*.
- van Drunen, E. J., Chiew, Y. S., Pretty, C., Shaw, G. M., Lambermont, B., Janssen, N., Chase, J. G., and Desaive, T. (2014). Visualisation of time-varying respiratory system elastance in experimental ARDS animal models. *BMC Pulmonary Medicine*, 14(1).
- van Zundert, J., Bolder, J., Koekebakker, S., and Oomen, T. (2016). Resource-efficient ILC for LTI/LTV systems through LQ tracking and stable inversion: Enabling large feedforward tasks on a position-dependent printer. *Mechatronics*, 38:76–90.
- Verdon, M., Merlani, P., Perneger, T., and Ricou, B. (2008). Burnout in a surgical ICU team. *Intensive care medicine*, 34(1):152–156.
- Vesalius, A. (1543). *De Humani Corporis Fabrica Libri Septem*. School of medicine, Padua.
- Vicario, F., Albanese, A., Karamolegkos, N., Wang, D., Seiver, A., and Chbat, N. (2015). Noninvasive estimation of respiratory mechanics in spontaneously breathing ventilated patients: A constrained optimization approach. *Transactions on Biomedical Engineering*, 63(4):775–787.
- Vignaux, L., Vargas, F., Roeseler, J., Tassaux, D., Thille, A. W., Kossowsky, M. P., Brochard, L., and Jolliet, P. (2009). Patient–ventilator asynchrony during non-invasive ventilation for acute respiratory failure: a multicenter study. *Intensive Care Medicine*, 35(5):840–846.
- Warner, M. A. and Patel, B. (2013). Mechanical ventilation. In *Benumof and Hagberg’s Airway Management*, pages 981–997. Elsevier.
- Wells, C. R., Fitzpatrick, M. C., Sah, P., Shoukat, A., Pandey, A., El-Sayed, A. M., Singer, B. H., Moghadas, S. M., and Galvani, A. P. (2020). Projecting the demand for ventilators at the peak of the COVID-19 outbreak in the USA. *The Lancet Infectious Diseases*, 20(10):1123–1125.
- Wunsch, H., Linde-Zwirble, W. T., Angus, D. C., Hartman, M. E., Milbrandt, E. B., and Kahn, J. M. (2010). The epidemiology of mechanical ventilation use in the united states. *Critical Care Medicine*, 38(10):1947–1953.
- Wysocki, M., Jouviet, P., and Jaber, S. (2013). Closed loop mechanical ventilation. *Journal of Clinical Monitoring and Computing*, 28(1):49–56.
- Yakubovich, V. (1964). Matrix inequalities method in stability theory for nonlinear control systems: I. absolute stability of forced vibrations. *Automation and remote control*, 7(905-917):202.

- Yonis, H., Crognier, L., Conil, J.-M., Serres, I., Rouget, A., Virtos, M., Cougot, P., Minville, V., Fourcade, O., and Georges, B. (2015). Patient-ventilator synchrony in neurally adjusted ventilatory assist (NAVA) and pressure support ventilation (PSV): a prospective observational study. *BMC anesthesiology*, 15:117.
- Yoshida, T., Uchiyama, A., Matsuura, N., Mashimo, T., and Fujino, Y. (2012). Spontaneous breathing during lung-protective ventilation in an experimental acute lung injury model. *Critical Care Medicine*, 40(5):1578–1585.
- Younes, M. (2003). Proportional assist ventilation. In *Mechanical Ventilation and Weaning*, pages 39–73. Springer Berlin Heidelberg.
- Younes, M., Puddy, A., Roberts, D., Light, R. B., Quesada, A., Taylor, K., Oppenheimer, L., and Cramp, H. (1992). Proportional assist ventilation. results of an initial clinical trial. *The American review of respiratory disease*, 145(1):121–129.
- Zhang, L., Mao, K., Duan, K., Fang, S., Lu, Y., Gong, Q., Lu, F., Jiang, Y., Jiang, L., Fang, W., Zhou, X., Wang, J., Fang, L., Ge, H., and Pan, Q. (2020). Detection of patient-ventilator asynchrony from mechanical ventilation waveforms using a two-layer long short-term memory neural network. *Computers in Biology and Medicine*, 120:103721.

Summary

Technological development of medical equipment has improved the quality and outcome of care over the past decades. At the same time, pressure on the healthcare system and the workload for health workers has been rising over the past decades as well. Therefore, technological advancements of medical equipment are needed to reduce the length of stay in the hospital and/or the number of medical staff interventions. In this thesis, technological advancements of a vital piece of medical equipment, namely, the mechanical ventilator, are presented. Mechanical ventilators are a life-saving piece of equipment commonly used in Intensive Care Units (ICUs) to sustain the life of patients that are unable to breathe on their own.

To further improve mechanical ventilation treatment outcomes and to reduce the ventilation-related workload, a data-driven approach to ventilation is envisaged. In this thesis, two challenges to improve mechanical ventilation are tackled. The first challenge is to improve pressure tracking control to enhance safety, comfort, and consistency of the treatment. The second challenge is to improve monitoring capabilities of mechanical ventilators. The use of data is considered to be essential to tackle these challenges and therewith to reduce the length of stay in the hospital and to reduce the required medical staff interventions.

Sensors in modern mechanical ventilators already collect a vast amount of data, while this data is currently not used to its full potential. Therefore, novel data-driven (learning) algorithms that use this data are developed in this thesis to address both challenges.

To improve the pressure tracking control of mechanical ventilators two different learning control strategies for ventilation are developed. The goal of these control strategies is to reduce the pressure tracking error, i.e., the generated pressure should follow the desired time-varying pressure profile, as set by the clinician, as closely as possible. The main challenge in control for mechanical ventilation is the wide variety and uncertainty on the plant that has to be controlled, e.g., the wide variety of patients. Therefore, learning control techniques, that automatically learn the optimal control signal, are considered to be a solution to this challenging control problem.

The first control strategy developed in this thesis is an adaptive hose-compensation control strategy. This control strategy automatically estimates the parameters of a hose model using a recursive least squares estimator. This hose model is used in a feedback loop to compensate the pressure drop over the hose. To achieve the best performance with this method, different hose models are considered, and a measurement delay compensation method for the estimator is developed. This control strategy has proven to be robust for varying patient and hose characteristics.

The second control strategy developed in this thesis is repetitive control for mechanical ventilation. Repetitive control is a control strategy that utilizes the repetitive nature of the desired pressure profile, resulting in near zero tracking errors. This thesis contains a systematic repetitive control design procedure for ventilation of fully sedated patients, for which the desired pressure profile is indeed periodic. Furthermore, a triggered repetitive control framework is developed for spontaneously breathing patients in triggered ventilation modes. For these patients the desired pressure profile is no longer periodic, thereby obstructing the use of conventional repetitive control. The developed triggered repetitive control strategy only requires the ventilator-induced breath itself to be repetitive, the timing in between breaths is allowed to vary. This enables the application of triggered repetitive control to triggered ventilation modes.

All control strategies developed in this thesis have been implemented in simulations and lab experiments and have shown to significantly outperform traditional pressure feedback control for ventilation.

To improve the monitoring capabilities of ventilators and help the clinician in choosing the appropriate treatment and ventilator settings, two data-driven monitoring algorithms are developed. The first algorithm aims at estimating the patient's lung parameters and spontaneous breathing effort. The developed estimation algorithm uses a sparse optimization method to retrieve valuable information about the lung parameters and the breathing effort of spontaneously breathing patients on ventilator support. The second algorithm aims at detecting and classifying timing asynchrony between the patient effort and the ventilator support. This is achieved by using a recurrent neural network that is trained to detect and classify different types of asynchrony. Both algorithms have shown their potential on data from simulations and experiments in a lab environment. Eventually, the outcome of these algorithms can help to determine the optimal ventilator settings.

The results in this thesis are a significant step towards autonomous closed-loop mechanical ventilators. The presented control techniques allow such system to automatically adjust its control signal to optimally match the patient. Furthermore, the outcome of the presented monitoring algorithms can be used in the future to automatically choose the appropriate ventilator settings for that specific patient.

Samenvatting

Technologische ontwikkelingen van medische apparatuur hebben in de afgelopen decennia de kwaliteit van de zorg sterk verbeterd. Parallel aan deze ontwikkeling is de druk op het zorgsysteem en de werkdruk op het zorgpersoneel in de westerse wereld ook significant toegenomen. Om deze trend te keren zijn ontwikkelingen nodig die de tijdsduur van ziekenhuiszorg en het aantal interventies door het personeel drastisch terug kunnen brengen. In dit proefschrift zijn datagedreven technologieën voor beademingsapparatuur ontwikkeld die daaraan bijdragen.

Beademingsapparaten zijn levensreddende medische apparaten die op de Intensive Care (IC) worden gebruikt om de ademhaling van patiënten te ondersteunen of over te nemen wanneer zij zelfstandig niet (voldoende) kunnen ademen. In dit proefschrift, wordt een datagedreven aanpak van beademing ontwikkeld om de behandeling van beademing te verbeteren en de aan beademing gerelateerde werkdruk te verlagen. Hierbij worden twee specifieke uitdagingen in beademing aangepakt. De eerste uitdaging is het verbeteren van de drukregeling in beademing om zo de veiligheid, het comfort, en de consistentie van de behandeling te verbeteren. De tweede uitdaging is het verbeteren van de mogelijkheden voor monitoring tijdens beademing. Het gebruik van data is essentieel om deze uitdagingen op te lossen en daarmee de behandelingsduur en het aantal interventies door het personeel te reduceren.

Sensoren in moderne beademingsapparatuur verzamelen al grote hoeveelheden data, maar deze data wordt momenteel nog niet optimaal benut. Daarom zijn er in dit proefschrift datagedreven (lerende) algoritmes ontwikkeld die gebruik maken van deze data. Deze algoritmes zijn een significante stap naar het oplossen van de gepresenteerde uitdagingen.

De eerste uitdaging, het verbeteren van de drukregeling in beademing, is aangepakt met twee lerende technieken uit de regeltechniek. Het doel van deze regelstrategieën is het verminderen van de druk volgfout. In andere woorden, de gegenereerde druk door de ventilator moet het door de arts ingestelde tijdsvariërende drukprofiel zo nauwkeurig mogelijk volgen. De grootste uitdaging hierbij is de grote variabiliteit in de dynamica van het regelsysteem, zoals de variatie in patiënten. Om dit uitdagende regelprobleem

op te lossen, zijn lerende regelstrategieën ontwikkeld, die automatisch het optimale regelsignaal leren uit de gemeten data.

De eerste in dit proefschrift behandelde oplossing is een adaptieve slangweerstand-compensatie regelstrategie. Deze regelstrategie schat de parameters van een slangmodel met behulp van een recursief schattings algoritme. Het slangmodel met de geschatte parameters wordt in de regellus gebruikt om de drukval over de slang te compenseren. Om met dit algoritme de best mogelijke regelprestaties te behalen zijn er verschillende slang modellen geanalyseerd en is er een methode ontwikkeld om meetvertraging in de schatter te compenseren. In dit proefschrift is bewezen dat deze regelstrategie robuust is voor variaties in patiënt en slangkarakteristieken.

De tweede regelstrategie in dit proefschrift is een strategie die het repeterende karakter van de ademhaling gebruikt; deze strategie wordt 'Repetitive Control' (RC) genoemd. Door te leren van de regelfout tijdens eerdere ademhalingen kan een regelfout van nagenoeg nul gerealiseerd worden. Dit proefschrift bevat een systematische procedure om een RC regelaar te ontwerpen voor beademing van volledig geseedeerde patiënten. Specifiek voor deze patiëntgroep is RC geschikt omdat hen een exact periodiek drukprofiel wordt opgelegd. Daarnaast is er een getriggerde RC strategie ontwikkeld die geschikt is voor de toepassing op spontaan ademende patiënten in getriggerde beademingsmodi. Voor deze patiënten is het opgelegde drukprofiel niet meer exact periodiek. Daardoor is het niet meer mogelijk om conventionele RC toe te passen. De ontwikkelde getriggerde RC strategie maakt gebruik van het feit dat de opgelegde ademhaling door de ventilator exact repetitief is, maar de timing tussen opvolgende ademhalingen mag variëren. Dit maakt de toepassing van RC mogelijk bij getriggerde beademingsmodi.

Alle regelstrategieën die zijn ontwikkeld in dit proefschrift zijn geïmplementeerd in computersimulaties en een experimentele laboratoriumopstelling. Hier hebben ze laten zien dat ze de drukregeling van bestaande beademingsapparatuur significant kunnen verbeteren.

Om de monitoringsmogelijkheden van beademingsapparatuur te verbeteren, en zo de arts te helpen om de juiste behandelstrategie en beademingsinstellingen te kiezen, zijn er in dit proefschrift twee datagedreven monitoringsalgoritmes ontwikkeld. Het eerste algoritme maakt een schatting van longparameters en de spontane ademactiviteit van de patiënt. Het ontwikkelde algoritme maakt gebruik van een schattingsmethode om waardevolle informatie over de longparameters en spontane ademactiviteit van beademde patiënten te bepalen. Het tweede monitoringsalgoritme in dit proefschrift is ontwikkeld om patiënt-ventilator asynchronie te detecteren en classificeren. Dit wordt gedaan met behulp van een neuraal netwerk dat getraind is om patiënt-ventilator asynchronie te herkennen. Beide algoritmes zijn succesvol getest in computersimulaties en op een experimentele laboratoriumopstelling. Uiteindelijk kunnen de uitkomsten van deze algoritmes helpen bij het bepalen van de optimale behandeling en ventilatorinstellingen.

De resultaten in dit proefschrift zijn een significante stap naar volledig autonome beademingsapparatuur. De ontwikkelde regelstrategieën maken het mogelijk om het regelsignaal automatisch aan te passen zodat de ingestelde drukprofielen zeer nauwkeurig

worden gevolgd. Daarnaast kan de uitkomst van de ontwikkelde monitoringsalgoritmes gebruikt worden om automatisch de optimale beademingsinstellingen te kiezen.

Dankwoord

Hier zit ik dan, schrijvend aan het dankwoord van mijn proefschrift, ongeveer vier-en-een-half jaar nadat ik voor het laatst riep: “ik ga nooit promoveren, ik ga de industrie in!”. Nu, vier-en-een-half jaar na deze uitspraak, kijk ik met veel trots en een goed gevoel terug op deze periode, waarbij ik heb kunnen promoveren in de industrie. Deze afsluitende pagina's van mijn proefschrift wil ik wijden aan iedereen die aan dit resultaat heeft bijgedragen.

Ten eerste, wil ik mijn promotoren Nathan, Tom en Bram bedanken. Jullie hebben mij de juiste sturing, maar ook de vrijheid gegeven om mijn onderzoek uit te voeren. Terugkijkend was het niet altijd even makkelijk om jullie (sterk) verschillende invalshoeken te managen, maar ik denk dat juist deze verscheidenheid in input heeft geleid tot een erg mooi eindresultaat.

Nathan, tijdens mijn afstuderen heb jij gepeild wat ik na mijn master wilde gaan doen en heb je mij uiteindelijk deze promotieopdracht voorgelegd. De aard van deze opdracht en de fijne samenwerking tijdens het afstuderen hebben mij uiteindelijk over de streep getrokken om deze uitdaging aan te gaan. Jouw scherpe en constructieve feedback zijn van grote invloed geweest op mijn werk, maar ook zeker op mijn ontwikkeling als onderzoeker. Dit zal mij zeker helpen in mijn verdere carrière. Nathan bedankt!

Tom, ook jouw bijdrage aan dit traject kan niet overschat worden. Ten eerste heeft ook jouw (af en toe onleesbare) constructieve feedback op mijn werk geleid tot het resultaat dat er nu ligt en heeft het mijn ontwikkeling grote stappen vooruit geholpen. Daarnaast heeft jouw aanstekelijke enthousiasme voor het onderzoek gezorgd voor mooie nieuwe onderzoeksrichtingen en resultaten. Tom bedankt!

Bram, ook jouw bijdrage en sturing aan mijn onderzoek zijn van grote waarde geweest. Onze bijna dagelijkse discussies (in 't 'Kepèls') hebben de lijnen van dit proefschrift gevormd. Ook jouw inhoudelijke bijdrage zijn in ieder hoofdstuk van dit proefschrift duidelijk aanwezig. Daarnaast wil ik je bedanken voor de gesprekken en het lachen tijdens de carpoolritjes (als niet iedereen lag te slapen), koffie in de ochtend, of onder het genot van een bucket chicken wings en/of een biertje. Bram bedankt!

Next, I would like to thank the other members of my defense committee: Professor

Diederik Gommers, Professor Ying Tan, and Professor Paul Van den Hof. Thank you for evaluating and approving my concept thesis and for participating in my defense.

Daarnaast wil ik iedereen binnen Demcon bedanken die bij heeft gedragen aan mijn onderzoek en de fantastische sfeer op de werkvloer. Ook wil ik mijn dank aan Demcon uitspreken voor het aan mij toevertrouwen van deze promotieopdracht en voor deze kans. Specifiek wil ik het Macawi team bedanken, dat ze mij geadopteerd hebben als onderdeel van het team. Van de woensdagmiddag lunchmeeting tot het mountainbike weekendje, het was altijd gezellig en dit heeft zeker op een goede manier bijgedragen aan het positieve gevoel op de werkvloer. Verder wil ik enkele personen nog in het bijzonder bedanken. Geert, jouw kennis over beademing (en alles hieromheen) is een grote bron van inspiratie en heeft sterk bijgedragen aan het positioneren van mijn onderzoek. Frank, ten eerste heeft het resultaat van jouw afstudeerwerk de basis gelegd voor twee hoofdstukken in dit proefschrift. Daarnaast was jij altijd bereid om mij te helpen als ik weer eens ‘ruzie’ had met de experimentele setup.

Verder wil ik ook iedereen van de D&C en CST groep aan de universiteit bedanken. Jullie hebben deze laatste vier jaar aan de universiteit gemaakt tot de mooie tijd die het geweest is. Van de gezellige koffiemomenten, de uitjes met de D&C groep, de conferentie (helaas door de reisbeperkingen enkelvoud) en de Benelux Meetings, met de befaamde TU/e kamerfeestjes. Uiteraard zijn er nog een aantal collega’s aan de universiteit die ik in het bijzonder wil bedanken.

Camiel en Fahim, mijn kamergenoten in -1.137, ik vind het prachtig dat wij dit avontuur tegelijkertijd zijn begonnen en met z’n drieën de afgelopen vier jaar misschien wel het kleinste kantoor op de universiteit hebben gedeeld. Ook al was ik maar parttime op kantoor, ik voelde me toch een volwaardige kamergenoot van jullie. Bedankt voor het lachen, de vele potjes curvefever (en GeoGuessr), de prachtige verjaardagscadeaus en uiteraard de af en toe serieuze gesprekken. Daarnaast wil ik uiteraard ook onze burens in kantoor -1.138 (Nard, Noud, Nic en Max) bedanken. Ook jullie hebben sterk bijgedragen bij het werkplezier op de universiteit. Van de punctualiteit van onze koffiemomenten kan de NS nog veel leren.

Dan zijn er nog de studenten die ik heb mogen begeleiden tijdens hun BEP, stage, of afstuderen, namelijk: Ruben, Mas, David, Lars, Joyce en Anita. Het begeleiden van studenten was een van de leukste werkzaamheden tijdens mijn promotie, ik hoop oprecht dat jullie ook positief op jullie afstudeerperiode terugkijken. Jullie bijdragen heeft niet alleen tot mooie afstudeerscripties geleid, het heeft ook de basis gelegd voor meerdere hoofdstukken in dit proefschrift, bedankt hiervoor!

Daniele and Mattia, during the last period of my PhD I had the pleasure to collaborate with the both of you. I think this was a very enjoyable collaboration with very nice results, which are also presented in this dissertation. Thank you very much!

Niet geheel onbelangrijk, “Kiët aan ’t Rendje” (tegenwoordig: “Andre Fanclub”). Bedankt voor alles, van de serieuze gesprekken tot de onnozele gesprekken en van de gezellige avonden (en nachten) tot de weekenden en vakanties. Samengevat: gae ziet fantastisch en ik hoop det we nog veul sjoene momente moge belaeve samen.

Tot slot wil ik pap, mam, Imke, Stan en Juul bedanken. Ten eerste voor de altijd

gezellige momenten samen. Maar zeker ook voor de stabiele basis waar ik altijd op terug kan vallen. Ik weet dat ik altijd bij jullie terecht kan om de mooie momenten te delen, voor (soms ongevraagd) advies en hulp, maar zeker ook voor steun tijdens moeilijkere periodes. Bedankt veur alles, ik haaj van uch!

Joey Reinders
Panningen, december 2021

List of publications

Peer-reviewed journal articles

- Reinders, J., Hunnekens, B., Heck, F., Oomen., T., van de Wouw, N. (2021), Accurate pressure tracking to support mechanically ventilated patients using an estimated nonlinear hose model and delay compensation, *Control Engineering Practice*, Vol. 116, pp. 104660.
- Reinders, J., Hunnekens, B., Heck, F., Oomen, T., van de Wouw, N. (2020), Adaptive control for mechanical ventilation for improved pressure support, *IEEE Transactions on Control Systems Technology*, Vol. 29, No. 1, pp. 180-193.

Peer-reviewed articles in conference proceedings

- Reinders, J., van de Kamp, L., Hunnekens, B., Oomen., T., van de Wouw, N. (2021), Flipped halfwave: Improved modeling of spontaneous breathing effort, in *11th IFAC Symposium on Biological and Medical Systems*, Ghent, Belgium.
- Reinders, J., Hunnekens, B., Oomen., T., van de Wouw, N. (2021), Linear repetitive control for a nonlinear mechanical ventilation system using feedback linearization, in *5th IEEE Conference on Control Technology and Applications*, San Diego, California, USA.
- Reinders, J., Verkade, R., Hunnekens, B., van de Wouw, N., Oomen., T. (2020), Improving mechanical ventilation for patient care through repetitive control, in *Proceedings of the IFAC 21st Triennial World Congress*, pp. 1441-1446, Berlin, Germany.
- Reinders, J., Heck, F., Hunnekens, B, Oomen., T., van de Wouw, N. (2019), Online hose calibration for pressure control in mechanical ventilation, in *IEEE American Control Conference*, pp. 5414-5419, Philadelphia, Pennsylvania, USA.

Journal articles, submitted and in preparation

- Reinders, J., Hunnekens, B., van de Wouw, N., Oomen, T., Noninvasive estimation

of the breathing effort of a mechanically ventilated patient using sparse optimization, *submitted for journal publication (under review)*.

- Reinders, J., Elshove, D., Hunnekens, B., van de Wouw, N., Oomen, T., Triggered repetitive control: Application to mechanically ventilated patient, *submitted for journal publication (under review)*.
- Reinders, J., van de Kamp, L., Hunnekens, B., Oomen, T., van de Wouw, N., Automatic patient-ventilator asynchrony detection and classification framework using objective asynchrony definitions, *submitted for journal publication (under review)*.
- Reinders, J., Giaccagli, M., Hunnekens, B., Astolfi, D., Oomen, T., van de Wouw, N., Repetitive control for Lur'e systems: application to mechanical ventilation, *submitted for journal publication (under review)*.

Patent applications

- Reinders, J.M.F., Hunnekens, B.G.B., Oomen, T.A.E., van de Wouw, N., Method and system of determining at least a first respiratory system parameter, *NL patent application under application nr. 2028456*.

Curriculum vitae

Joey Reinders is born on June 6, 1994 in Helden, The Netherlands. In 2012 he finished his secondary education at the Bouwens van der Boijecollege in Panningen, The Netherlands. Subsequently, he studied Mechanical Engineering at the Eindhoven University of Technology, The Netherlands, where he obtained his Bachelor of Science degree and Master of Science degree (with great appreciation) in 2015 and 2017, respectively. As part of his curriculum he did an internship at the University of Stuttgart, Germany, in 2016, where he worked on an experimental setup to measure anisotropic friction. The work in his master's thesis, entitled 'String Stability Analysis of MPC-based Heterogeneous Platooning', was conducted in cooperation with Nederlandse Organisatie voor Toegepast Natuurwetenschappelijk Onderzoek (TNO) under the supervision of Nathan van de Wouw.



Since January 2018, Joey has been working at Demcon Advanced Mechatronics, Best, The Netherlands, and in the Dynamics and Control group at the Eindhoven University of Technology, as a Ph.D. student, under the supervision of Nathan van de Wouw, Tom Oomen, and Bram Hunnekens. The focus of his research is on improving the quality of mechanical ventilation in intensive care units. This is achieved by developing learning control algorithms and data-driven algorithms that enhance the estimation of a patient's clinical conditions. The main results of his research are presented in this thesis.